# Determining the mechanisms behind the mesenchymal stem cell response to strontium apatite-wollastonite glass ceramic

**Sam Hollings**

**PhD**

**University of York**

**Biology**

**September 2018**

## Abstract

The aim of this project was to determine the effects of strontium addition to Apatite Wollastonite Glass-Ceramic (SrAWGC) on human mesenchymal stem/stromal cells (MSCs), and to identify through which mechanisms these effects operated. SrAWGC has a molar composition of $35.4SiO_2$-$7.1P_2O_5$-$0.4CaF_2$-7.1MgO-(49.9-x)CaO-xSrO, where x = 0, 6.2, 12.5, 18.7, 24.9, 37.4. Neutron diffraction, Magic Angle Spinning Nuclear Magnetic Resonance and Raman spectroscopy found that Sr substitution did not alter the short-range order, but at the medium range the percentage of $Q^3$ silicate decreased, alongside a significant increase in the density of the glass. The glass compositions were heat treated into SrAWGC discs using a polymer slurry casting method, with high strontium compositions showing altered surface topographies.

SrAW glasses released strontium linearly with increasing strontium content, whereas the SrAWGC discs released both increasing concentrations of strontium and silicon with strontium content, suggesting increased glass-ceramic dissolution with Sr substitution. The 12.5 Mol% SrAW glass conditioned media and 6.2 mol% SrAWGC discs induced an increase in MSC cell number.

The 0 and 12.5 mol% SrAWGC discs significantly raised the expression of genes associated with inflammatory response (determined with RNA sequencing), compared with cells exposed only to the ionic release products of the material. The addition of strontium to the material was found to have a relatively small effect, but did slightly increase the inflammatory gene expression induced by the discs. An *in vivo* study found that the MSCs conditioned to have raised inflammatory gene expression by the discs did not promote a sustained inflammatory response. The discs and ionic dissolution products (with 12.5 mol% Sr) were found to increase the expression of proliferative and survival-oriented gene groupings, such as K-Ras signalling. A K-Ras inhibitor abrogated the previously described SrAW glass associated rise in cell number.

# Table of contents

# List of Figures

# List of Tables

## Acknowledgement

I could not have done this PhD without the help and support of a great number of people. I would like to thank Prof. Paul Genever, Prof. David Wood and Dr Yvette Hancock for giving me the chance to work in this fascinating field and for providing supervision and assistance over the years.

Without the support of my friends in each department the pressure of learning three new sciences could have been overwhelming. Specifically, I'd like to thank my cohort of the DTCTERM, my colleagues in the Genever Laboratory (such as Dr Amanda Barnes, David Kuntin, Andy Stone and Alice Carstairs, who taught me all the cell culture I know and with whom I played many board games!), in the University of Leeds School of Oral Biology (particularly Dr Maria Katsikiogianni and Dr Chris Serna for teaching me glass making, Dr Lucia Pontiroli, my number 1 star glass making partner, and Sam Whitworth who helped with glass making a fair few times!), in the Hancock Laboratory (Drs Raquel and Andre Ponzoni for teaching me Raman and being great friends!) and finally Dr Richard Martin for his help with the Neutron Diffraction. I'd also like to thank the staff in the York Technology Facility for all of their help with the SEM and RNA sequencing (particularly Dr Sally James) and the staff in the Wellcome Trust Brenner Building for help with the *in vivo* (and Kenny Man and Dr Xuebin Yang for doing the surgery!).

A PhD is tough, and perhaps even tougher when it's in three subjects that are new to you split between three departments in two different cities. However, I need to thank my friends yet again for their help and support. Without them I couldn't have made it. I'd like to also thank my family for their pride in me, continued support and cheerleading (particularly you twin bro: the competition is still on!) and perhaps most of all Lucia Pontiroli, with whom I've shared the most challenging moments of our PhDs, and who has always been there for me. Grazie mille, Tesoro!

Finally, I’d like to dedicate this thesis to my late grandfather, Keith Hollings. Though not a scholar in the formal sense, he taught me the value of hard work at an early age, and filled my life with love and support.

## Author's Declaration

I declare that this thesis is a presentation of original work and I am the sole author. This work has not previously been presented for an award at this, or any other, University. All sources are acknowledged as References. Preparation of SEM samples was performed by Meg Stark and Karen Hodgkinson at the University of York, Department of Biology, Technology Facility. Pre-extracted RNA samples were prepared and sent for sequencing by Sally James of the University of York, Department of Biology, Technology Facility. RNA sequencing data was processed into differentially expressed genes by Katherine Newling of the University of York, Department of Biology Technology Facility. The collagen used in the *in vivo* was extracted by Dr Amanda Barnes, whilst the *In vivo* animal care and surgery was performed by Dr Xuebin Yang and Kenny Man (University of Leeds, School of Dentistry) and the staff at the animal house in the Wellcome Trust Brenner Building, University of Leeds. *In vivo* tissue sample processing was performed by Mike Shires and Filomena Esteves in the Wellcome Trust Brenner Building. The staff at the ISIS Spallation Source installed the samples in the General Materials Diffractometer (GEM) and provided me with the data, whilst the staff at the Durham Solid-state NMR service collected the NMR data presented in this work.

# Chapter 1 – The Introduction

Bone is effective at repairing itself, and in healthy adults regularly does so throughout life. However, trauma, infection and cancer surgery can result in large bone defects which will not repair naturally, requiring further intervention. In the USA alone, there are over 100,000 non-union fractures a year, which are defined by the FDA as those which present no visible healing after 3 months (1,2). Smoking, age and poor control of diabetes can increase the incidence of non-unions (2,3), as can osteoporosis which contributes to the fact that in the United Kingdom it is predicted that half of women and 20% of men over 45 will suffer from a fracture within their lifetimes (4,5).This will worsen as the population ages.. The gold standard treatment for larger bone defects and non-union fractures is the autograft (3), where spongiosa is taken from elsewhere in the body to repair the defect. However, this requires further surgery, causes donor site morbidity and may suffer from a lack of suitable tissue (6). Allografts offer an alternative, however there is the potential of disease transmission and a detrimental immune response leading to rejection (6,7). A more elegant solution would be to restore the damaged tissues by providing a suitable scaffold, a source of appropriate cells and the correct chemical and biological cues, and with this in mind there has been considerable research since the 1970s into synthetic bone regeneration scaffolds (8).

Strontium-doped Apatite-Wollastonite Glass-Ceramic (AWGC) presents a promising tissue engineering scaffold for the treatment of larger bone defects, particularly in load bearing sites. This is due to AWGC having high compressive strength and fracture toughness comparable to human bone and other bioactive glasses and glass-ceramics (9). AWGC has already been used successfully in 60,000 patients as a bone substitute, such as in artificial vertebrae and iliac crests (10). However, it can be improved further as a bone regeneration scaffold through doping with strontium, which is itself an established treatment for osteoporosis (11). The work presented in this thesis concerns determining what effects strontium substitution into AWGC has on human MSCs, with the intention of improving SrAWGC as a bone

regeneration scaffold. This chapter provides an introduction to the work presented in this thesis, first discussing bone biology and disease and the need for improved bone regeneration strategies (Section 1.1), before moving onto discussing tissue engineering as a solution to this and describing the material AWGC in more detail (Section 1.2). Finally, the thesis aims and objects are discussed (Section 1.3).

## 1.1 Bone biology and disease

### 1.1.1 The anatomy of bone

Bone is a dynamic composite tissue which has the primary function of supporting the body and directing muscle force mechanically. However, it is not simply an inert framework, as the bone mineral itself finds secondary use as a store of various ions, primarily calcium but also strontium, boron, copper, fluorine, magnesium, zinc and manganese, all of which have essential functions in the human body (12). Finally, bone also plays host to blood production, with haematopoietic stem cells being responsible for the production of erythrocytes (red blood cells), various types of white blood cells and also osteoclasts (13).

Bone manifests in two types of structure: cortical and trabecular (also called cancellous) bone. These two types of bone and associated structures are shown in Figure 1. The trabecular bone is the core of the larger bones and is composed of a network of struts (trabeculae). Within this porous structure resides the bone marrow with associated haematopoietic and bone marrow stromal cell populations and functions. The cortical bone is much denser, forming in cylindrical structures called osteons, with central Haversian canals that act as the main channels through the bone mineral (14). Within this dense network there is a distributed population of osteocytes, located in lacunae throughout the bone, and dormant osteoblasts resident on the bone surfaces (14).

The bone material itself is a composite of organic and mineral components. This consists primarily of mineralised collagen type I and collagen forms 90% (w/w) of the organic component of the bone (15). Other non-

collagenous proteins are also present such as fibronectin and bone-specific proteins such as osteocalcin , osteonectin and osteopontin, whose role is not fully understood, but appears associated in part with bone turn over (15–17).

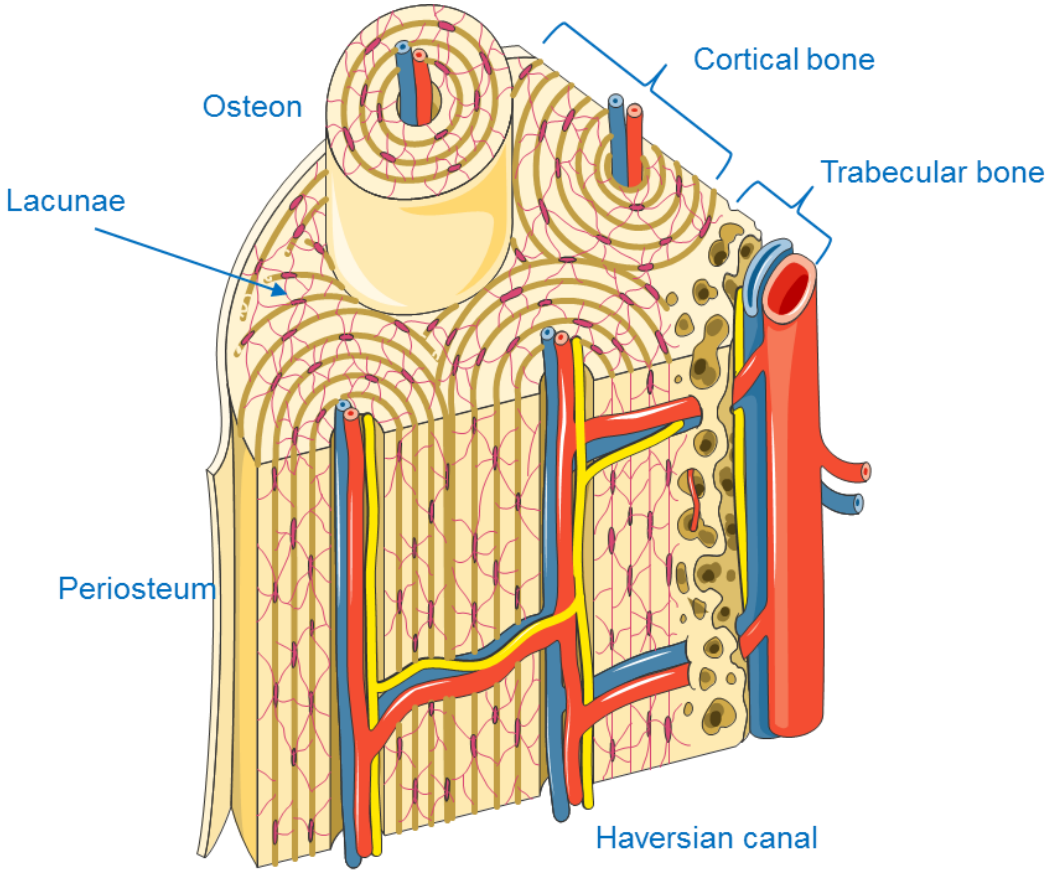


**Figure 1: Schematic of the anatomy of cortical and trabecular bone. The trabecular bone is composed of cylindrical osteons through which run Haversian canals and a network of lacunae occupied by osteocytes. The trabecular bone is at the centre of the bone, and is composed of network of struts which are well vascularised. adapted from Servier Medical Art (Creative Commons)(18).**

The mineral component of the bone is composed of hydroxyapatite (HA), $Ca_{10}(PO_4)_6(OH)_2$ (50% to 70% (w/w))(16). The process by which this forms is not fully understood, however osteoblasts release alkaline phosphatase into the extracellular environment to raise the surrounding phosphate content (15), whilst the bone specific proteins (osteocalcin, osteopontin and osteonectin) draw $Ca^{2+}$ and $PO_4^{3-}$ ions to themselves, and studies suggest

that osteocalcin and osteopontin can form tethers between the collagen matrix and the crystals further strengthening the material (19–21).

### 1.1.2 Bone remodelling

Bone is a complex vascularised tissue undergoing a process of constant resorption and formation, known as bone remodelling. This is facilitated primarily by cells arising from two different lineages, osteoclasts, which descend from haematopoietic stem cells, and osteoblasts, which differentiate from mesenchymal stem cells. It is useful to describe the functions of the various cells in bone in the context of bone remodelling. A schematic of this process can be seen in Figure 2.

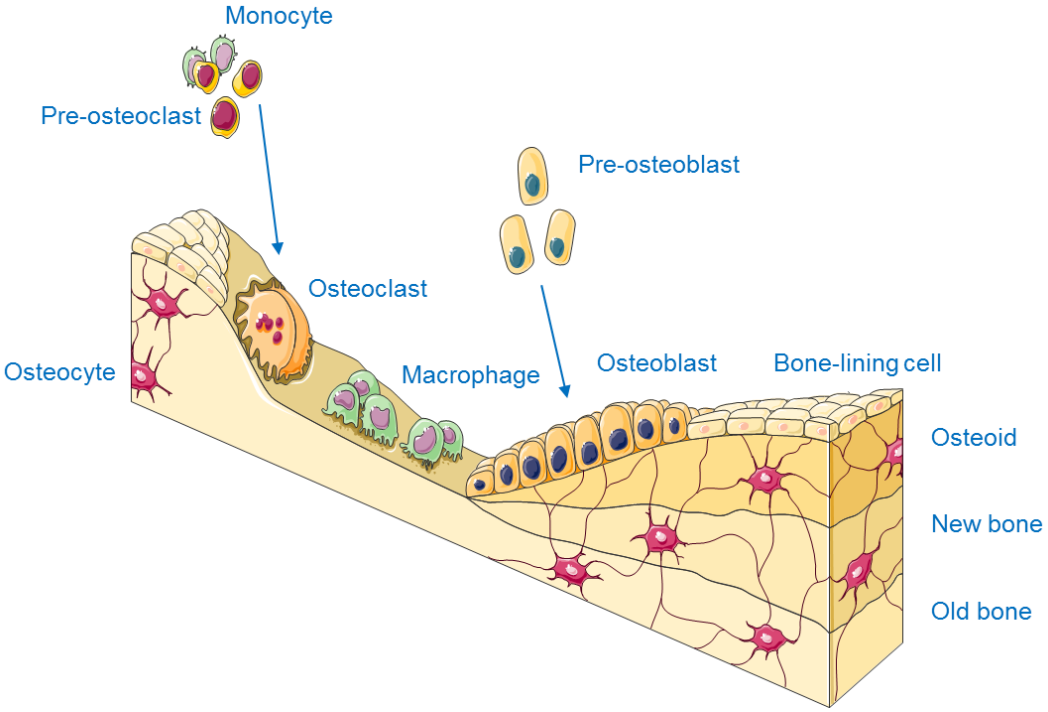


**Figure 2: Schematic of the bone remodelling process, showing how osteoclasts form, resorb the bone then vacate, and are followed by osteoblast formation, bone production and subsequent entombment/dormancy of the osteoblasts. Adapted from Servier Medical Art (Creative Commons) (18).**

The bone structure described previously experiences micro-fractures during the normal bending and stressing of the bone (22). Osteocytes entombed within the bone sense the fracture with their processes, causing them to apoptose resulting in the release of factors which will induce osteoclastic

bone absorption whilst also ending the release of factors which would have inhibited the bone healing response (23).

#### 1.1.2.1 Osteoclasts

Osteoclasts are terminally differentiated cells whose function is to break down the bone matrix, facilitating bone turnover and repair, in combination with osteoblasts as part of a basic multicellular unit (BMU) (24). They are formed in response to stimuli from osteocytes (such as during bone injury or micro-fracture), and also from osteoblasts, both of which release RANKL (receptor activator of nuclear factor κ-B ligand), the primary activator of osteoclastogenesis, which is also critical for osteoclast precursor survival and expansion (15,24). A number of other cytokines such as Tumour Necrosis Factor Alpha (TNFα) and Interleukin 6 (IL6) can promote RANKL expression and subsequent bone resorption (25). Osteoclastogenesis is the process by which the mononuclear osteoclast precursor cells fuse together forming osteoclasts (15,26). Osteoprotegerin (OPG), which is also produced by osteoblasts can inhibit the formation of osteoclasts by binding to RANKL preventing it reaching its receptor (27). The bone remodelling process occurs with the osteoclasts working at the front of the BMU, and adhering to the surface of the bone mineral (24). The osteoclasts then proceed to break down the hydroxyapatite by lowering the pH through flooding the site with $H^+$ ions and enzymes, such as matrix matelloproteinase-9 (MMP-9) and tartrate-resistant acid phosphatase (TRAP)(26). Together, these degrade the bone matrix, forming a Howship lacuna in the bone(26). The bone resorption phase is followed by bone formation, which is mediated by osteoblasts. The remodelling process is different in the two bone types. In trabecular bone, the osteoclasts work across the surface of the trabeculae making a resorption lacuna which is later filled by the osteoblasts (23,25). In cortical bone, the osteoclasts form “cutting tunnels”, followed by osteoblasts which then fill this in causing “closing cones”, and resulting in new osteons forming as the tunnels near-fully close (23,25).

#### 1.1.2.2 Osteoblasts

The other main components of the BMUs are osteoblasts. These differentiate from bone marrow mesenchymal stem cells (MSCs) and work in concert with osteoclasts to remodel and repair bone. Osteoblasts produce both RANKL and OPG which promote and inhibit osteoclast activity, respectively, demonstrating that although osteoblasts themselves are responsible for bone production, they indirectly regulate bone resorption (15,24,27). Similarly, osteoclasts release Transforming Growth Factor Beta (TGFβ) from the bone matrix which can promote MSC migration to the site (26,28,29).

MSCs undergoing osteogenic differentiation go through a series of transit amplifying stages to proliferate and sequentially differentiate to become mature osteoblasts. These then facilitate the repair of the lacunae formed by the osteoclasts, by depositing primarily Collagen I along with non-collagenous matrix elements (osteocalcin, osteopontin, osteonectin and others) (24,26). The osteoblasts also release alkaline phosphatase (ALP) to free up phosphate ions, in addition to vesicles containing many negatively charged proteoglycans, encouraging increased $Ca^{2+}$ concentrations, and facilitating the mineralisation of nano-hydroxyapatite (24,26). This mineralises the collagen network, forming new bone. Once the mature osteoblasts have finished forming bone they either apoptose (85% of the cells), become osteocytes, or become quiescent bone lining cells (26).

The differentiation of osteoblasts is a key element of bone biology. Initially, MSCs produce daughter cells which are induced towards an osteogenic lineage through a series of steps brought on by stimulatory factors such as bone morphogenic protein (BMP) and Wnt (an acronym for Wingless/Integrated) (26,30). This begins with raised expression of Runt-related transcription factor 2 (Runx2) which commits the daughter cell to the osteogenic line, and results in raised ALP and osterix expression (30). Next the cells progress through transit amplifying stages before becoming osteoblasts, indicated through expression of the late stage osteogenic differentiation markers osteocalcin, osteonectin and osteopontin (30). These cells will then begin to repair bone cavities as described previously.

#### 1.1.2.3 Osteocytes

Osteocytes are the most abundant cell type in the bone, making up between 90 to 95% of the adult bone cell population (31,32). They are the result osteoblasts entombing themselves in bone matrix during the formation of bone (32), after which they continue to play some part in bone turn over (25). The osteocytes are located within lacunae, small spaces in the bone matrix, with thin filopodia extending down caniliculi to interact with other osteocytes and cells on the bone surface, whilst releasing various proteins related to mineralisation (24). In particular, osteocytes are the primary source of sclerostin, a major regulator of the remodelling process (33). Sclerostin downregulates bone formation in the vicinity of the osteocyte by inhibiting Wnt signalling through binding to the LRP5/6 Wnt co-receptors expressed by osteoblasts (34). Mechanical stimulation of bone can increase osteocyte viability (35), however loading sufficient to induce micro-fractures has been associated with osteocyte apoptosis, halting the production of sclerostin and allowing nearby osteoblasts to commence bone formation (23). In addition osteocytes are an important regulator of bone resorption as they produce TGF-β, which has been shown to act as an inhibitor to osteoclastogenesis (24,32,36), and recently it has been discovered that osteocytes are an important source of RANKL, the primary activator of osteoclasts(32,33).

#### 1.1.2.4 Mesenchymal Stem Cells

MSCs are a heterogeneous multipotent stromal cell population, that are capable of dividing asymmetrically and which are often defined as having tri-lineage differentiation potential, acting as the progenitor cells for bone (osteoblasts), fat (adipocytes) and cartilage (chondrocytes)(37). Though mainly taken from the bone marrow for tissue engineering purposes, MSCs have been found throughout the body, such as in the brain, liver, kidney, lungs, and muscles(38). They have been extensively studied and could most likely represent a heterogeneous population of stromal cells with varying characteristics and purposes (39). Typically MSCs are defined as being adherent to culture plastic, of a fibroblastic morphology, and expressing surface markers such as CD29, CD44, CD73, CD90, CD105, CD166 and

STRO-1 (40). MSCs are also typically defined as not expressing the following haematopoietic cell surface markers: CD14, CD34, CD45 and HLA-DR (40). The definition of an MSC is still open to debate however, and some groups choose to use different methods of isolation and identification, in addition to numerous other names (Mesenchymal Stromal Cells, Bone Marrow Stromal/Stem Cells and others).

MSCs are encouraged down an osteochondral lineage by activation of Runx2 gene expression. This can occur in response to many paracrine, autocrine and endocrine signals, such as growth factors (Fibroblast Growth Factor, FGF, and Transforming Growth Factor Beta, TGF-β), glycoproteins (Wnt) and Bone Morphogenetic Proteins (BMPs), amongst others (30,41). A schematic describing key events in the osteogenic differentiation of MSCs is shown in Figure 3.

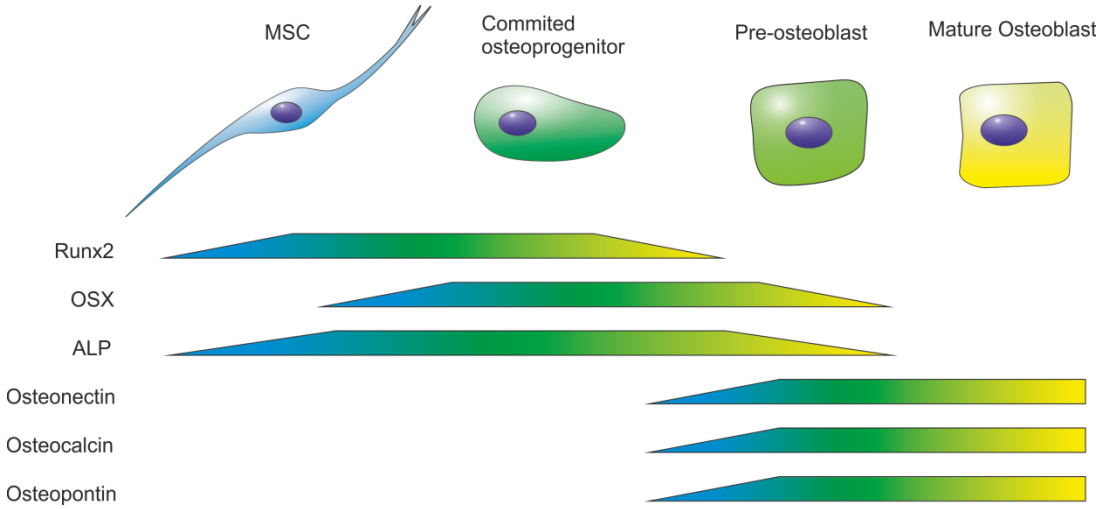


**Figure 3: The stages of osteogenic differentiation of Mesenchymal Stem Cells into Osteoblasts along with the expression of the Runx2 and OSX transcription factors and ALP, Osteonectin, Osteocalcin and Osteopontin proteins. Adapted from (30).**

During the differentiation of MSCs into osteoblasts, Runx2 expression is raised, the key transcription factor of this process, which commits the MSCs to an osteochondral lineage and raises the expression of many osteoblast related genes such as Col1 and ALP (26,30). Osterix (OSX) then acts to further restrict the cell to an osteogenic lineage hence becoming a committed osteoprogenitor whilst also enhancing the proliferation of the

cells. Further transcription factors are then upregulated (Msx2, Dlx3 and Dlx5/6) which carry the cell onto maturation into an osteoblast and associated bone matrix protein production (30).

MSCs also perform an immune-suppressive function, as they have been seen to inhibit stimulated peripheral blood mononuclear cells (PBMCs) and produce immune-suppressive factors (TGFβ1, IDO1 and CD274) in response to inflammatory cytokines such as combined Tumour Necrosis Factor Alpha (TNFα) and Interferon Gamma (IFNγ)(39). However, MSCs are a varied population of cells, and are not all multipotent. Instead, some present a more immunomodulatory phenotype, potentially exhibiting raised IL-7 expression (39) and TGFβ, though the cytokines the MSCs release and the effects these have on surrounding cells vary greatly depending on the tissue and the other cells present (42).

#### 1.1.2.5 Bone Healing

Alongside the near constant process of bone remodelling, bone healing occurs when the bone suffers more significant damage and can allow the original structure of the bone to be reformed without scar formation (17). This occurs in two different forms, with primary healing taking place when the fracture consists of two surfaces in close proximity or contact (43), whilst secondary healing occurs when the fracture site is more fragmented (17,44). In primary healing the osteoclasts activated by the osteocyte network form cutting cones through the fracture surfaces, which mature into new bone “bio-pins” which stabilise the fracture (17,43). These bio-pins and the surrounding bone then undergo normal bone remodelling, erasing the fracture completely. Secondary healing is a more involved process akin to normal wound healing, with an initial inflammation stage followed by formation of granulation tissue which then mineralises and is remodelled to form bone (17,43). The inflammation stage sees an influx of white blood cells which then begin releasing cytokines such as TNFα and IL-6 (45). These orchestrate the wound healing response, as TNFα is chemotactic, drawing MSCs and fibroblasts (which form the granulation tissue) to the wound site (45), and controlled exposure has been associated with MSC

osteogenic differentiation (46), whilst IL-6 promotes MSC migration and survival (47) and there is some evidence to suggest it is associated with improved mineralisation of the wound site (48).

### 1.1.3 Repairing large bone defects

Despite the ability of bone to repair itself, trauma, infection and cancer surgery can result in large bone defects which will not repair naturally, requiring further intervention. Defining a defect which will not heal itself is difficult as the dimensions and nature of the defect can vary between patients, depending on their age, smoking status and management of diabetes (2,3). However, a number of factors can increase the probability of a defect not healing, such as the defect being above a critical size (~2 cm) and there being more than 50% of full thickness bone loss (49,50). Once this leads to no visible healing of the defect for 3 months, this is defined by the FDA as a non-union fracture (1,2). Additionally, these will become more common due the aging population and the susceptibility of humans to decreasing bone density with age (51). Eventually, the bones may weaken sufficiently that is at greatly increased risk of fracture after which the defect may not heal sufficiently; a condition called osteoporosis (52).Whatever the cause, the need for repairing large bone defects is on the increase and there are already 100,000 non-union fractures in the USA (1,2), and 1 million bone reconstructions in Europe every year (53).

Autografts (using the patient's own tissue from another site in the body) are the current gold standard treatment in this area, however they are expensive, damaging to the patient and there is sometimes insufficient autologous bone (54). The alternative would be an allograft, where foreign tissue (from a donor or a recently deceased person) is used to repair the damage, however these are also in relatively short supply and the tissue processing required for the graft to not induce a huge immune response can render it non-osteoinductive (54,55).

## 1.2 Tissue engineering

### 1.2.1 The pillars of tissue engineering

There is an increasing demand for bone regeneration, and the currently established methods for treating bone defects are both expensive and have a series of associated drawbacks. Hence there is a need for improved bone regeneration strategies. Tissue engineering aims to solve these problems by regenerating the damaged tissue, resulting in the damaged or lost tissue being repaired or replaced, and ultimately restoring functionality. Langer and Vacanti (1993) further defined it as “the application of engineering and life sciences principles towards the development of biological substitutes that restore, maintain or improve tissue function” (56).

The crux of tissue engineering, is the combination of a scaffold to support the wound site and fill in the damaged tissue, a source of cells to populate the scaffold and to create and maintain the new tissue, and finally the appropriate environment (a combination of forces, chemical and biological signals) that will encourage correct cell function and result in the formation of a functional and viable tissue (57).

To break this down, it is important to consider carefully what is required of each of these elements.

#### 1.2.1.1 Tissue Engineering Scaffold

The scaffold is the core element of the tissue engineering construct, and at its simplest it supports the cells within the wound site providing the matrix upon which growth can take place. The scaffold must be biocompatible, meaning that it should not induce a prolonged inflammatory response or damage resident cells as this would clearly cause the implant to fail (58). A material for bone tissue engineering needs to have mechanical properties similar to bone, as bone cells respond to mechanical signals and the stress-shielding of very hard materials can result in bone resorption (58). Ideally, the material should be biodegradable, such that it temporarily performs the role of a scaffold whilst the new tissue is forming and subsequently maturing

in its place (58). The rate of degradation is important, to ensure that the mechanical properties of the material are not compromised (particularly if load bearing). The material should have interconnected porosity to allow cell infiltration and nutrient/waste transfer throughout the tissue engineering construct, with macropores of at least 100μm diameter to allow bone ingrowth (59,60). To be effective as a bone tissue engineering scaffold, the material ideally needs to possess the properties of osteoconductivity and osteoinductivity. Osteoconductivity is the ability of bone to bond to and form on the surface of the material, and has also been associated more specifically with the ability for bone cells to adhere to, proliferate and form bone on the material surface (58,61,62). Osteoinductivity, takes this further, as it describes a material which not only permits bone growth, but which actively induces MSCs to differentiate down an osteogenic lineage, in a non-osseous environment (62–64). As the tissue engineering scaffold is intrinsically a non-osseous environment, this property is required for bone to form beyond the periphery of the material. Osteoinduction has been shown to have been caused by both the ions released from materials (such as in the case of Bioglass 45S5)(65,66) and also the material surface properties, such as nanotopography (67–69) or the ability to adsorb certain types of proteins to its surface (62).

Scaffolds are typically made of biodegradable materials, such as polymers. Natural polymers which are abundant in the body have also proven to be useful as tissue engineering scaffolds, with collagen and hyaluronic acid (both components of the extracellular matrix) having been used to make scaffolds for softer tissues, though depending on the degree of processing, these materials risk transferring disease (70). There are also a range of alternative natural polymers, such as alginate and chitosan, in addition to synthetic polymers such as poly(ethylene glycol) (PEG) and polycaprolactone (PCL), which have found some success in tissue engineering (70).

Various bioactive glasses are better suited to hard tissue engineering due to their strength and ability to form hydroxyapatite mineral, however there has been much work on combining the favourable properties of both polymer

scaffolds, with those of bioactive glasses (and ceramics) to produce a new generation of bone tissue engineering scaffolds (71).

#### 1.2.1.2 Cells for Tissue Engineering

The next components required in a tissue engineering therapy are suitable cells, which can facilitate repair. MSCs are the obvious choice for bone tissue engineering, as they possess the ability to differentiate into osteoblasts (and hence produce bone) in response to well established stimuli, such as growth factors, steroids such as Dexamethasone, or even surface topography (67–69) and dissolution products (72). However, acquiring sufficient cells to produce an autologous tissue engineered bone substitute can be challenging in older patients, or patients who have suffered trauma or major surgery to excise large areas of bone. Additionally, MSCs change with the age of the patient, losing potency (73), however, Pennock *et al.* (2015) found that initiating autophagy (through 3D cell culture) in MSCs from aged donors (56-79 years old) was seen to raise the expression of Oct4, Nanog and Sox2, which are associated with raised potency. This potentially describes a route by which older cells could be used for tissue engineering purposes (74).

#### 1.2.1.3 Environment for correct tissue growth and function

This is a very broad requirement for tissue engineering constructs and covers almost everything not included in cells and scaffolds. The cells on the scaffolds need to be instructed to form the correct tissue through appropriate cues, in addition to adequate vascularisation taking place to ensure the viability of the construct. For bone tissue engineering some concerns might be mechanical loading of the scaffolds (62,75,76), or addition of growth factors to encourage osteogenic differentiation of the cells into osteoblasts. So called “therapeutic ions” have been found to be a relatively simple way to induce osteogenic differentiation as they will be released as part of the material’s normal degradation, when incorporated into the material(72,77). For the bioactive glass “Bioglass 45S5” this has been shown to be an important part of its innate osteoinductivity (78,79), most likely associated

with the high amounts of silicon and calcium released, for which there is substantial evidence that they promote osteogenesis (72,80). There is also evidence that other ions influence gene expression in bone cells, and hence could prove useful in bone tissue engineering. Zinc has been shown to improve cell viability in combination with strontium (81,82), whilst there is substantial evidence that strontium raises osteoblast and MSC proliferation and osteogenic differentiation (83–87). Magnesium has also been utilised as a dopant in biomaterials, but has instead has been shown to alter MSC and osteoblast adhesion to the material (88,89), whilst there is evidence that copper both promotes osteogenic differentiation and the release of angiogenic factors (90,91).

### 1.2.2 Ceramic scaffolds

Bioactive glasses and ceramics are an attractive hard tissue scaffold due to their biocompatibility, ability to form hydroxyapatite and strength, potentially allowing their use in load-bearing bone tissue engineering (92). The basis of most bioactive glasses and ceramics is calcium phosphate, as this is the family of materials to which hydroxyapatite belongs. However, synthetic (monolithic or sintered) hydroxyapatite (HA) itself is not optimum for bone tissue engineering as the large crystal size and low porosity results in it being relatively insoluble (even by osteoclasts), greatly reducing its osteoconductivity (93–96). Another calcium phosphate bioactive glass is β-tricalcium phosphate, which has improved solubility over HA, showing improved bone growth onto and over the material *in vivo*, and which can be combined with HA to tune the mechanical properties and dissolution rate (97). Bioglass 45S5 is perhaps the most commercially successful of the bioactive glasses and possesses innate osteoinductivity, shown to be associated with its dissolution products (78,79). It is a calcium-silicate glass with significant sodium content, which not only rapidly forms a hydroxyapatite layer on its surface, but also induces raised osteogenic gene expression in MSCs (98). Bioglass 45S5 has already been used in the clinic to repair bone defects of more than a million patients, particularly in the jaw and in orthopaedics (71). Additionally, it has found significant commercial success in the toothpaste NovaMin® (GlaxoSmithKline), where it is the

active ingredient responsible for mineralising dentine holes, reducing tooth sensitivity (71). There are also other particulate based Bioglass 45S5 products, such as PerioGlas® (used in 35 countries), NovaBone and Biogran® which can be made into a putty through interaction with bodily fluids and then used to facilitate bone repair (71). Despite these successes, it is arguable that Bioglass 45S5 is not being fully exploited, considering its potential as a bone regeneration scaffold. A limitation of Bioglass 45S5 is that it has relatively poor mechanical properties (99). Another commercially successful bioactive glass is BonAlive (with an S53P4 composition)(71). This is also used in a granular form and has shown much clinical success such as a sinus and maxilla orthopaedic bone-graft (100). However, early attempts to sinter both Bioglass 45S5 and BonAlive into scaffolds resulted in a significant drop in the bioactivity (due to crystallisation), though recent advancements have allowed Bioglass 45S5 scaffolds to be formed into scaffolds (101).

Bioactive glass-ceramics are similar to bioactive glasses but their mechanical properties have been improved by controlled partial crystallisation. Apatite-wollastonite Glass-Ceramic (AWGC) is an example of these, and is amongst the strongest of bioactive glasses (99). Additionally, the production method of glass-ceramics is easily adapted into scaffold production as the glass is made, formed into the scaffold shape and then is sintered into the glass-ceramic, with this having been carried out extensively at the University of Leeds (102,103). AWGC scaffolds can also be 3D printed using selective laser sintering, allowing bespoke or complex designs to be fabricated (104). For these reasons, AWGC offers the potential to act as a bone tissue engineering scaffold for load bearing defects, something which currently commercially successful bioactive glasses (such as Bioglass 45S5) cannot fulfil. AWGC has already been used successfully in 60,000 patients as a bone substitute, such as in artificial vertebrae and iliac crests (10). However, AWGC can still be improved as a scaffold by altering it so that it interacts with the cells growing on it in a way which encourages bone growth and repair. Within the context of this thesis, it is important to understand what glasses and glass ceramics are and how they are designed to function in the body as a background to future discussion.

### 1.2.3 Glass theory

Glasses are fundamentally disorganised networks of oxides. This is easiest to envisage when compared with crystals, and whilst considering a common glass $SiO_2$. In a silica crystal (such as quartz) the silicon and oxygen atoms form tetrahedra which then form a network. Because the arrangement and form of the silicon and oxygen is repeated regularly throughout the material it is said to have long range order. A silica glass is made from the same basic tetrahedral units as a silica crystal, and as these units will be present throughout the material a glass is said to have short range order. However the tetrahedral units do not form a repeated extended network, and instead connect to each other in a disorganised manner, resulting in the amorphous silica having no long-range order. Schematics of the different forms of silica can be seen in Figure 4.

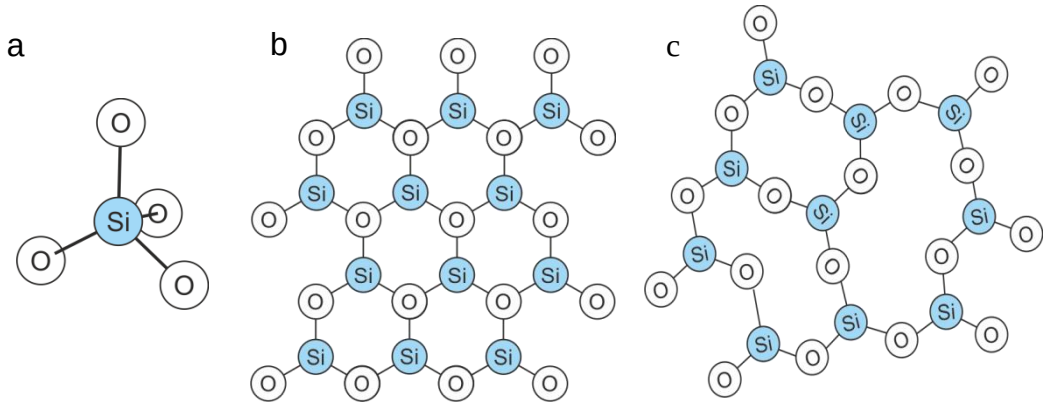


**Figure 4: Silica tetrahedron (a), ordered crystal (b) and disordered glass (c). The crystal and glass schematics do not show the 4th oxygen which would be out of the plane of the page.**

Although silicon and oxygen are common glass components, they are not required to form a glass. Goldschmidt 1926 determined that physically only certain combinations of atoms could form glass, as the ratio in size between the cation (network former) and anion (for example oxygen) must allow the atoms to arrange themselves such that the cations do not repulse each other too much (105,106). Building on this, and through studying silica glasses, Zachariasen developed four rules to describe whether an oxide was able to form a glass (105,106):

- The oxygens must not be linked to more than two cations
- The coordination number of the oxygen atoms to the cation (the number of oxygens connected) must be generally four (tetrahedral) or lower.
- The polyhedral anion-cation units must bond at the vertices
- Each polyhedron must bond to at least three other polyhedra

These rules describe the so-called network formers, the atomic combinations that form the backbone of a glass, and consist of (amongst others) $SiO_2$ and $P_2O_5$. It is beneficial for some applications to break this glass network up, altering its mechanical properties, the way it responds to heat and its rate of degradation. This is done through the addition of so-called network modifiers, such as Ca, Sr, Mg (107). These atoms have very low electronegativity, forming strong ionic bonds with the oxygen and do not function as network formers, effectively removing oxygen atoms from the glass network (making them non-bridging oxygens, NBOs) (108). The network is usually composed of the network formers linked by bridging oxygens (BOs); however the presence of network modifiers turns these into NBOs, breaking the network up, and reducing the number of other network forming tetrahedra each tetrahedron is connected to. This is referred to as lowering the network connectivity (NC), where the NC is defined as the number of other tetrahedra that a tetrahedra is connected to.

### 1.2.4 Bioactive glasses

Bioactive glasses are glasses designed to be useful in a medical or tissue engineering context. Between 1969 and 1971 it was found that various compositions of glass bonded strongly to the surrounding bone, and could not be dislodged, in comparison to the controls which slid out easily (109). The bond formed was found to be due to the formation of a hydroxyapatite layer on the surface of the material which fused with bone mineral, however, only a subset of compositions were able to do this (see Figure 5). Both the silicon and phosphorus content seemed key in the response, and although sodium did affect the ability of the bioactive glasses to bond to human tissue, it was not required for them bond to bone, as apatite wollastonite glass-

ceramic (AWGC, which has no sodium) was found to also possess this ability (110). The formation mechanism of this hydroxyapatite layer for both Bioglass and AWGC is essentially the same, beginning with $Ca^{2+}$ ion exchange from the glass for $H^+$ or $H_3O^+$ ions in the solution, also raising the pH of the solution (110). This hydrolyses the silica in the glass, making silanols (Si-OH), whilst the increase in pH results in the silica network being broken down (110,111). This leads to a silica rich gel forming on the surface of the material, on top of which a calcium and phosphate rich layer forms, which then crystallises into hydroxyapatite (110).

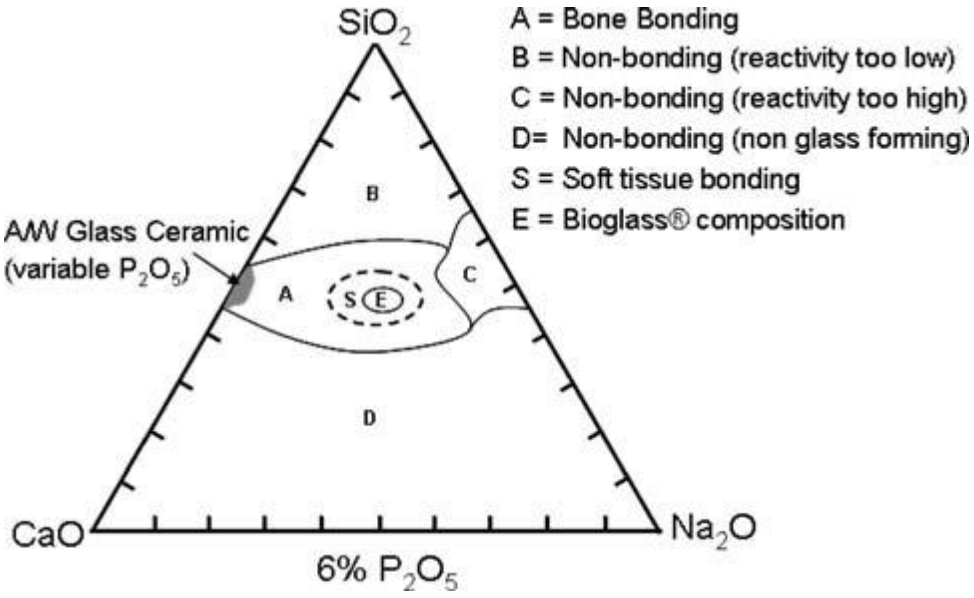


**Figure 5: Ternary phase diagram of the CaO-$SiO_2$-$NaO_2$ glass system with regions indicating compositions which showed bioactivity, and more specifically the ability of the material to bind to living tissue (A, S and E). Reproduced with permission** (109)**.**

The formation of the hydroxyapatite layer is a key element of the bioactivity of bioactive glasses, and Hill and Brauer (2011) proposed it was associated with, and could be predicted using, the network connectivity of the bioactive glass (112). As said previously, the network connectivity describes how many other tetrahedra are connected to each silicon tetrahedra. For the purposes of bioactivity, if the connectivity is too high, the material is too robust and will not break down sufficiently to proceed through the stages towards HA formation. An NC in the range between 2 and 2.6 (average connections per tetrahedra) appears optimum (depending on the glass),

however there is a lower range because it is also possible for the material to be too disrupted (112–114). Once the network connectivity drops sufficiently, the network is so disrupted that the Si-O-Si bonds in the material can dissolve without the need for the hydrolysis step described previously, preventing the Si-OH gel from forming on the surface and thus inhibiting HA formation (112). The phosphorus content also plays an important role. Phosphorus is a network former, however in calcium silicate bioactive glasses the phosphorus manifests in the form of orthophosphate ($PO_4^{3-}$), which is essentially a network modifier (112). The orthophosphate is essentially a second glass phase dispersed at the nano-scale throughout the material (112). For glass compositions with the same NC but different phosphorus content, the higher phosphorus content compositions showed greater bioactivity (112,113). This was not associated solely with increased dissolution of the material generally, but the increased phosphate ions released by the material were implicated in the improved bioactivity (112,115).

A large range of bioactive glasses have been designed despite the limitations to glass composition described previously (section 1.2.3), with the greater understanding of the importance of the hydroxyapatite layer, and the method and factors involved in its formation having most likely contributed to this. However, despite there being a close relationship between bioactive glass bioactivity and network connectivity (and phosphorus content) and this often being associated with raised dissolution rates over glasses with high network connectivity (and low P content), a high dissolution rate will not necessarily result in HA formation as many of the atoms released by the materials aren't utilised in those processes and those that are need to be exchanged with the surrounding fluid according to the Hench paradigm for HA formation described previously (110,112).

### 1.2.5 Glass-ceramic theory

Bioactive glasses have many useful properties; however partial crystallisation into glass ceramics has been explored as a means of improving the mechanical properties of bioactive glass. The most widely

used clinically is AWGC (which consists of approximately one third each $MgO\text{-}CaO\text{-}SiO_2\text{-}P_2O_5$ glass, apatite and wollastonite crystals), however there are other examples, with glass-ceramics having been made of Bioglass 45S5 (though initially presenting reduced bioactivity)(71), Ceravital® (apatite crystals in a $Na_2O–K_2O–MgO–CaO–SiO_2–P_2O_5$ glass), Bioverit® (apatite and phlogopite crystals in a $Na_2O–MgO–CaO–Al_2O_3–SiO_2–P_2O_5–F$ glass) and Biosilicate ($23.75Na_2O–23.75CaO–48.5SiO_2–4P_2O_5$) to name a few (93,111).

To form a glass ceramic, the base glass is exposed to a heat treatment, designed to provide the glass network with the energy to reorganise itself (in a controlled manner) into the desired crystal structures. The result is essentially a glass interwoven with crystalline phases which can alter the solubility of the material, deflect cracks and make the material more resistant to bending and crushing.

Bioactive glass is transformed into a glass-ceramic through a process of controlled crystallisation, which utilises a heating regime that leads to the nucleation and growth of the crystal phases. These do not always happen at similar temperatures, potentially requiring a stepped heat treatment. However, for AW glass, Kokubo *et al.* (1986) found that a heat treatment of 1050°C at 5°C/min was sufficient to induce the required crystal nucleation and growth (116). However with bulk AW material it was found that cracks formed upon heating, which was attributed to the wollastonite phase forming just below the surface and inducing a directional volume change leading to the material to cracking (116). However, they found grinding the glass into a fine powder with grains below 44μm size, forming this into a compact, then applying the heat treatment resulted in the formation of a robust glass-ceramic, as instead of forming along the surface of each grain the wollastonite crystals nucleated throughout each grain evenly (116). More generally, this process of crushing the glass into powder and heating it to form a new glass/glass-ceramic/ceramic structure, is called sintering, and is a useful methods for producing tissue engineering scaffolds.

### 1.2.6 Glass-ceramic scaffolds

A relatively simple way to form a scaffold of a desired shape is to form a compact in that shape composed of some binding material and the glass particles. This can then be heat treated causing the binder to burn off, whilst the glass particles sinter together to form the final structure. The heat treatment used to form the glass-ceramic also causes the glass particles to fuse, in a process called sintering. When the material is heated, the glass particles in contact with each other stick, then connect forming a neck, which progresses until the two glass particles are one particle (117). For compacts of glass powder, this results in particles sticking to each other and then fusing with the material densifying until it is a completely solid material with next to no pores between what used to be the glass particles. Furthermore, this process can occur at temperatures well below the glass melting temperature.

The compact to be sintered can be made through various techniques, though perhaps the most simple is to just pour the glass powder into a mould without a binder, though this clearly limits the structures that can be made. Another technique is to mix the glass powder with a polymer (such as poly-vinyl alcohol), which than then be extruded into a mould to form a green body of a particular shape, or could be impregnated into a polymer foam in a method called foam replication (99,101). These glass powder-binder constructs are referred to as green bodies and during the heat-treatment (to sinter the glass and induce the transformation to glass-ceramic) the binding substance burns off whilst the glass particles fuse, producing the scaffold in the required format (99,101). Another method is a type of 3D printing, called selective laser sintering (SLS), where a laser is used to selectively adhere a bed of glass powder (mixed with an acrylic binder) according to some design, which is then stepped through layer by layer (with more glass powder being added at each step), eventually producing the final 3D design (118). This green body is then sintered to produce the final scaffold.

### 1.2.6.1 Apatite-Wollastonite Glass-Ceramic as a scaffold material

AWGC (35.4$SiO_2$-7.1$P_2O_5$-0.4$CaF_2$-7.1MgO- 49.9CaO) is a MgO–CaO–$SiO_2$–$P_2O_5$ glass in which forms two crystalline phases: a fibrous wollastonite phase, woven around apatite crystals (93). Due to the production method (glass formation, followed by crushing and sintering of these glass particles) the crystals are distributed evenly throughout the material, and this is considered to play an important role in the material's impressive mechanical properties (which are even higher than sintered hydroxyapatite) as cracks are prevented from propagating through the glass as they are deflected by the apatite crystals (116,119). This leads to AWGC having bending strength and fracture toughness comparable to human bone and greatly improved compared with AW glass, AW glass treated to have an apatite phase or hydroxyapatite alone (see Figure 6) (93),

AWGC also possesses higher compressive strength than hydroxyapatite and human bone, higher Young's modulus than Bioglass 45S5 and human bone (119) and higher hardness than Bioglass 45S5 and hydroxyapatite (see Table 1). Additionally, after 8 weeks implantation the failure load of AWGC was seen to exceed that of hydroxyapatite, Bioglass 45S5 and an alumina ceramic (120)

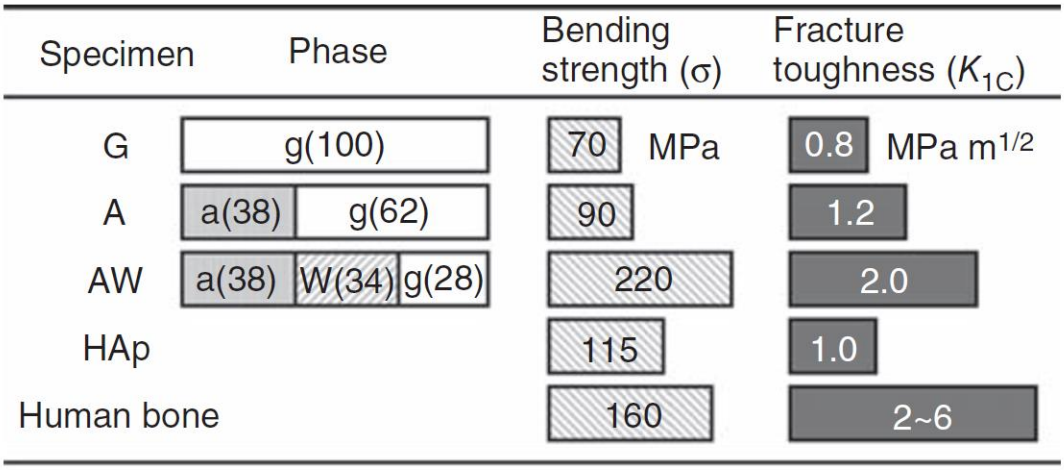


**Figure 6: A comparison of the bending strength and fracture toughness of AWGC (AW), its parent AW glass (G), AW glass treated to have apatite crystals (A), sintered hydroxyapatite (HAp) and human bone** (93) **(reproduced with permission).**

| Property | AWGC | Bioglass 45S5 | HAp | Bone |
|---|---|---|---|---|
| Density (g/cm$^3$) | 3.07 | 2.66 | 3.16 | 1.6-2.1 |
| Flexural strength (MPa) | 157-220 | 42 (tensile) | 115-200 | 50-160 |
| Compressive Strength (MPa) | 1060 | | 500-1000 | 100-230 |
| Young's modulus (GPa) | 103-118 | 35 | 74-110 | 7-30 |
| Hardness (Vickers) | 680 | 458 | 600 | |
| Fracture toughness (MPa.m$^{1/2}$) | 2.0 | | 1.0 | 2-6 |

**Table 1: A comparison of the mechanical properties of AWGC, Bioglass 45S5, hydroxyapatite (HAp) and cortical human bone** (119,121)**.**

In addition to its preferable mechanical properties, the material has very high bioactivity, readily forming a surface hydroxyapatite layer in biological fluids and having been shown to bind firmly to bone in numerous *in vivo* experiments (93). Additionally, it has been shown to be able to be fashioned into porous scaffolds with macro and microporosity, either through foam replication or selective laser sintering, and to support MSC growth (103,104). Although it's commercial production has now finished, between 1990 and 2000, AWGC was used successfully in 60,000 patients as a bone substitute, such as in artificial vertebrae and iliac crests (10).

### 1.2.7 The addition of strontium to biomaterials

Despite its favourable mechanical properties, clinical success and bioactivity, apatite wollastonite is not osteoinductive, and hence its use as a tissue engineering scaffold should be limited to smaller defect sizes. However, the addition of strontium to AWGC presents a potential solution to this problem as it is well known to induce osteogenic differentiation and is chemically similar to calcium allowing for relatively easy incorporation into the material. Before discussing the addition of Sr to AWGC further, it important to understand the effects that Sr has on bone cells. The methods

by which strontium influences cells have been studied for some time, though primarily in its ionic form as part of studies into the osteoporosis drug strontium Ranelate (122).

#### 1.2.7.1 The effect of strontium on bone cells

There is a wealth of information on how strontium influences bone cells, gathered as part of studies into the effects of strontium ranelate, an osteoporosis treatment. Given the very close similarities between strontium and calcium (5% larger ionic radius, divalent cation) it is perhaps unsurprising that the Calcium Sensor Receptor (CaSR) has been established as a method by which strontium affects MSCs, although it is not yet understood in what manner (or even if) this receptor can distinguish Ca from Sr, as it can also sense other divalent and trivalent cations (122). In Fromigue *et al.* (2009) studies on mouse calvarial osteoblasts showed that Sr was found to raise Akt and ERK activation, indicating the involvement of Sr in both the Akt pathway and elements of the mitogen activated protein kinase (MAPK) pathway (see Figure 7) (123). However, they also showed that Sr still induced proliferation in CaSR knockout mouse calvarial osteoblasts via Akt phosphorylation, suggesting that Sr could act on the osteoblasts in a CaSR independent manner, via Akt (123).

Further work has confirmed the role of CaSR, as a study on MC3T3-E1 osteoblastic cells found that a CaSR inhibitor strongly abrogated Sr-induced proliferation and matrix mineralisation (122), whilst Rybchyn *et al.* (2011) showed that a CaSR inhibitor reduced Sr-induced Akt phosphorylation (124). Rybchyn *et al.* (2011) also determined that the CaSR mediated strontium response was potentially routed via PI3K, as Wortmannin (a PI3K inhibitor) was seen to greatly lower the presence of Thr308 phosphorylated Akt (124). Interestingly, the strontium-induced phosphorylation of Akt at Ser473 was not abrogated by Wortmannin, potentially confirming the results of Fromigue *et al.* (2009) that Akt can be activated by Sr in a CaSR independent manner (123,124) (see Figure 7).

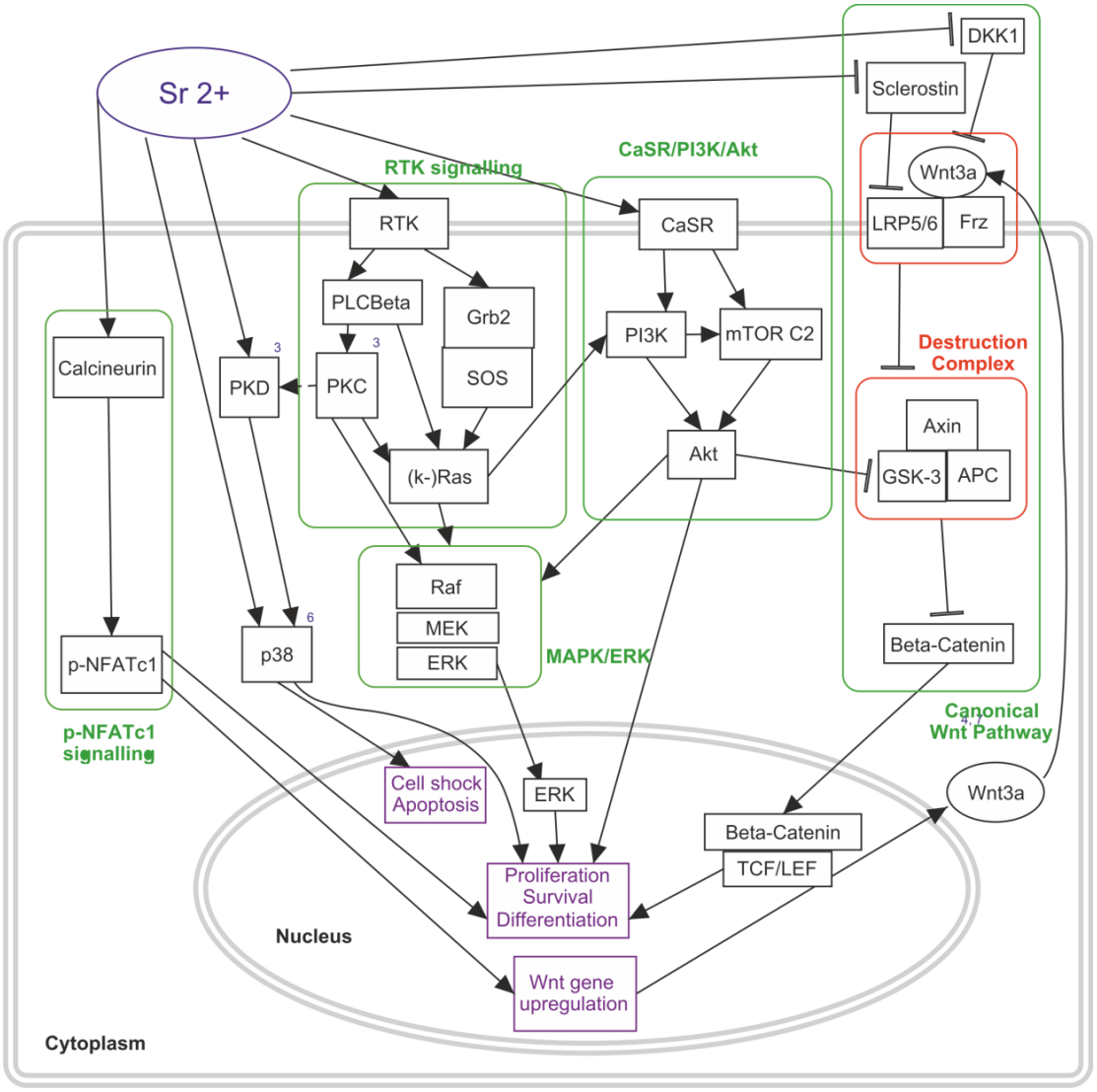


**Figure 7: The osteogenic and proliferative signalling pathways in human MSC lineage cells affected by Sr. Studies have found Sr acts through the Wnt pathway mediated by the CaSR signalling response. MAPK/ERK mediated RTK signalling has also been implicated, potentially associated with the PI3K/Akt cascade associated with the CaSR signalling. Sr has also been found to activate p-NFATc1 signalling through a yet not understood means. These culminate in proliferative, survival and osteogenic gene expression.** (122,124–128)

Additionally, Rybchyn *et al.* (2011) also found that the application of an Akt inhibitor (AKT-XI) reduced the strontium induced amount of Ser9 phosphorylated GSKβ3, an element of the Wnt pathway, and also both phosphorylated and nuclear translocated β-catenin (124)(see Figure 7).

A study by Yang *et al.* (2011) complemented this work by showing that Sr raised the gene expression of osteogenic genes Col1a1, ALP and OPN,

whilst also increasing the expression of β-catenin *in vitro* and *in vivo* (129). The Wnt signalling pathway is known to be important in osteoblast differentiation and has been linked with the response of osteoblasts to calcium. The canonical Wnt signalling pathway begins with Wnt ligand interacting with its pair receptors, LRP5/6 and Frizzled. These then cause the breakup of the GSK3/Axin/APC destruction complex, which would otherwise facilitate the degradation of cytosolic β-catenin (130). The Wnt signalling then culminates in β-catenin translocation to the nucleus, which activates TCF/LEF leading to osteogenic gene expression. Further studies have indicated the importance of Wnt signalling in the Sr response of osteoblastic cells, as it has been shown that the Wnt inhibitors DKK1 and sFRP1 abrogate Sr induced osteogenic gene expression (125), whilst it has also been shown that Sr reduces sclerostin expression and production in human osteoblasts (124). These clearly show that strontium interacts with the Wnt pathway via at least two mechanisms, one of which is CaSR mediated.

Other studies have implicated other pathways in the osteoblast Sr response (previously suggested in Fromigue *et al.* (2009) which found CaSR knockouts still responded to Sr). The calcium activated, calcineurin mediated NFATc1 pathway has been associated with strontium (122,123). Nuclear factors of activated T-cells c1 (NFATc1) are normally phosphorylated in the cytoplasm, however when calcineurin is activated by sufficient $Ca^{2+}$, it dephosphorylates NFATc1, which then translocates to the nucleus raising osteogenic gene expression, and perhaps working more specifically through the transcription factor Maf (122). Fromigue *et al.* (2010) found that Strontium Ranelate induced NFATc1 translocation to the nucleus of MC3T3-E1 osteoblastic cells and mouse calvarial osteoblasts, as did calcium (125). Interestingly, dexamethasone, a commonly used *in vitro* osteogenic steroid, did not induce NFATc1 nuclear translocation, and NFATc1 transcriptional activity, which were abrogated using calcineurin inhibitors (see Figure 7). Saidak *et al.* (2012) described how the Wnt response to strontium potentially occurs downstream of the NFATc1 response, due to NFATc1 induced Wnt5a production (122).

Strontium has also been implicated in receptor tyrosine kinase (RTK) mediated signalling, such as FGF (122) (see Figure 7). As seen in Figure 7, this typically takes the form of a growth factor interacting with a receptor resulting in a signalling cascade of Ras to Raf and then through a series of mitogen activated protein kinases (MAPKs) and extracellular signal regulated kinases (ERKs) leading to altered gene expression. Caverzasio and Thouverey (2011) found that a selective FGF inhibitor abrogated the Sr-induced raise in cell number and phosphorylation of PLCγ and ERK, both elements of the RTK mediated MAPK/ERK pathway (127). This confirmed the earlier work by Caverzasio (2008) that found that Sr phosphorylated ERK (126). Peng *et al.* (2009) further established that Ras siRNA abrogated the Sr induced ALP activity, OCN expression and ERK phosphorylation (128). This suggests that in some manner, the Sr mediated cell osteogenic gene expression is dependent on the ERK/MAPK signalling cascade. Interestingly, it was also found that the FGFR inhibitor lowered the Sr induced phosphorylation of Akt (suggesting that any effects on the Wnt pathway could be down stream of effects on the RTK pathways). It was also found that inhibition of FGFR and H-Ras (with siRNA) also abrogated the strontium induced activation of p38 MAPK (127,128), which has been found to play a role in Wnt3a signalling, and in the associated ERK mediated osteogenic differentiation of MSCs (131,132).

In summary, Sr has been found to induce proliferation and osteogenic differentiation in MSCs and to support the osteogenic activity of osteoblasts, potentially acting though a number of mechanisms, but with RTK mediated MAPK signalling, Akt associated Wnt signalling and p38 signalling playing key roles. However, many aspects of this have not been fully elaborated. Although it has been shown strontium can induce Wnt signalling there are a number of questions remaining around how the CaSR can distinguish between $Sr^{2+}$ and $Ca^{2+}$, or the mechanism around how strontium induces MAPK/ERK signalling. Furthermore, there is a lack of research into the broader effects of strontium on human cells and tissues, with most studies concentrating on genes and pathways directly associated with MSC growth and osteogenic differentiation. However, some recent studies have begun to broaden the understanding of strontium’s effects. Hench (2009) conducted a

review of Bioglass 45S5 ion release studies and found, genes associated with cell cycle regulation, DNA synthesis and repair, apoptosis, growth factors cell surface antigens and receptors and signal transduction molecules were affected in osteoblasts and primary MSCs (78,80,133). Another study by Autefage *et al.* (2015) found strontium substituted Bioglass 45S5 ion release upregulated the usual collection of osteogenic genes in human bone MSCs, but that the greatest change in gene expression was associated with sterol/steroid production, which was previously not associated with strontium (87).

Strontium has been found to not only improve osteoblast bone production, it also inhibits the production and function of osteoclasts (122). Studies have shown that strontium (like calcium) acts to prevent osteoclast formation, seeming to inhibit RANKL induced osteoclast differentiation (134–136). Additionally strontium was found to reduce the demineralisation caused by the osteoclasts (134–136), and caused them to apoptose (135,137). Using siRNA, Caudrillier *et al.* (2010) found that Sr was acting through the CaSR, and that this worked to inhibit the RANKL induced translocation of NFκB to the nucleus, which would otherwise raise osteoclastogenic gene expression (134). CaSR was also found to be responsible for the Sr induced apoptosis of the osteoclasts, however, unlike Ca induced cell death in osteoclasts, this acted via PKCβII suggesting slightly different signalling pathways (137). Additionally, it was found that the combination of both Sr and Ca induced yet more apoptosis in the osteoclasts (137). NFκB was also seen to play an important role in the apoptosis of the osteoclasts, however in Hurtel-Lemaire *et al.* (2009) they found that Sr induced apoptosis of osteoclasts was abrogated using NFκB inhibitors (137).

Usually, osteoclast activity is regulated by osteoblasts through the use of both RANKL, acting to increase osteoclast formation and activity, and OPG, which binds to RANKL and hence inhibits osteoclast formation and activity. In Peng et al (2011) and Atkins *et al.* (2009) they found that Sr raises the ratio of the expression and protein secretion of OPG to RANKL in osteoblastic cells (136,138). This means that Sr causes the osteoblasts to swing the balance of these two factors in favour of down-regulating osteoclast activity (136).

As mentioned previously, Sr was also found to inhibit the osteoclasts ability to break down minerals. In the body, the Sr-induced apoptosis and Osteoclastogenesis inhibition would both contribute to an effective reduction in the ability of osteoclasts to resorb bone mineral, however studies have shown that Sr also works to prevent osteoclasts from forming the sealing ring (potentially through disruption of the formation of the actin cytoskeleton in this area)(135).

In summary, Sr works to change the normal balance of bone creation and resorption by altering the factors that osteoblasts release, resulting in less pro-osteoclastic RANKL and more OPG, which inhibits osteoclasts. This leads to less osteoclast formation, and osteoclast activity. However, Sr also works to interfere with the effects that RANKL has on osteoclasts and their precursors via CaSR and NFκB, and obfuscates the formation of the actin sealing ring making it more difficult for the osteoclast to begin the process of demineralisation.

#### 1.2.7.2 The effects of strontium addition to AWGC

AWGC is a very promising load bearing tissue engineering scaffold due to its favourable mechanical properties, however its inability to direct cell function (and in particular MSC osteogenic differentiation) limits its use in this arena. However, the osteoinductive effects of other bioactive glasses have been shown to be greatly influenced by the ions released by the material (72,79), therefore if the ions released by AWGC could be altered, this could result in the material becoming more osteoinductive. AWGC contains $Ca^{2+}$, $Si^{4+}$ and $Mg^{2+}$, all of which are known to have osteogenic effects on cells, in addition to phosphorus which is essential for bone mineralisation (72,139). As they of similar size, and both divalent cations, some of the Ca in the material could be substituted for Sr to enhance the osteoinductivity of the material. In previous work from our laboratory, Sr was successfully incorporated into a mesoporous AWGC without adversely impairing its mechanical properties (102). Additionally, MSCs grown on the surface of the mesoporous strontium AWGC showed improved ALP activity and cell number compared with AWGC without strontium. However, the mechanisms behind this response

were not explored. This previous work found strontium was taken into the glass and wollastonite phases, and so it can be assumed that it would be released into the material's surroundings as part of its normal degradation, where it would then come into contact with T-cells. This is important, as had the strontium been taken primarily into the apatite phase of the AWGC phase could have impaired its release as the apatite phase is relatively insoluble.

## 1.3 Thesis aims and objectives

Strontium is established as an osteoporosis drug in the form of strontium ranelate, and as an osteoinductive dopant for tissue engineering scaffolds. However, much of the work on the effects of strontium scaffolds on cells is narrow, focussing on confirming the already established osteogenic effects without further exploring the mechanisms behind these responses. Although it has been established in previous work that strontium can be substituted into mesoporous AWGC to produce a viable material, there is still much that remains unknown about this alteration of AWGC and the cause behind the cell response.

Therefore, this thesis will study how the substitution of strontium into AWGC alters the MSC response to the material and the mechanisms by which this acts. The thesis hypothesis is that the substitution of strontium into Apatite-Wollastonite Glass-Ceramic is beneficial to human MSCs, bone tissue engineering and acts primarily through the release of ions.

In challenging this hypothesis, the first aim was to determine how the substitution of strontium into Apatite-Wollastonite Glass-Ceramic affected the material's ability to break down and release ions. This is because the way in which the material breaks down is fundamental to the cell response, as it will significantly change the stimuli the cells experience. However, doping the material with strontium could alter the glass network structure potentially making the material too weak (or too strong) for tissue engineering purposes. To achieve this aim, the following objectives were set, and are covered in Chapter 2:

- Establish how Sr substitution into AW glass alters its short and medium range order
- Establish whether Sr substitution into AWGC alters formation of glass ceramic discs

The short range order will be determined using Neutron Diffraction as this technique has sufficient resolution to resolve the atomic separations and an empirical contrast mechanism which allows elements with similar atomic masses to be more easily distinguish. Nuclear Magnetic Resonance and Raman spectroscopy will be used to determine the medium range order and will provide complimentary information necessary for completion of the analysis of the Neutron Diffraction data. This will focus on the AW glass as this is a model for the most reactive part of the glass ceramic, the amorphous phase, and the crystalline phases in the glass-ceramic would completely obscure the amorphous phase spectra.

The ability of the material to form glass ceramic discs, and whether the Sr alters this, will be confirmed, and Scanning Electron Microscopy used to determine the material has sintered as seen in previous work (102).

The second aim for the project would then be to determine the mesenchymal stem cell response to the SrAWGC, and whether this would change with Sr content. To meet this aim, the following objectives were set and are covered in Chapters 3 and 4:

- Establish whether Sr substitution into AWGC changes the rate of ion release from the material
- Determine MSC growth response to Sr, SrAW ions and SrAWGC
- Determine Gene expression changes of MSCs induced by the material, and whether this is caused by dissolution products or the material itself
- Determine what cellular mechanisms could be responsible for these effects

Prior to establishing how the cells respond to the material, first the ions released by both the SrAW glass and the SrAWGC discs, and whether the substitution of Sr into the material alters them, will be measured using Inductively Coupled Plasma Optical Emission Spectroscopy. Studying the

MSC growth in response to SrAWGC and how this is altered by its strontium content, will use cell number and proliferation assays. The growth response of the MSCs to the ions released by the material (modelled using SrAW glass) will be studied to determine whether these dissolution products alone can produce the same effects as the material itself. Additionally, the response of MSCs to Sr ions will be determined using Strontium Chloride, to establish whether the strontium released by the material was capable of inducing any observed response.

The global gene expression changes induced by the SrAWGC will be studied using RNA sequencing and will determine those changes caused by the Sr content, the material itself and its ionic dissolution products by cross comparing SrAWGC samples, and SrAW ionic dissolution products, with and without strontium. Finally, inhibitors will be used to interrogate pathways responsible for the MSC growth response to the material (modelled with SrAW dissolution ions)

# Chapter 2 – The effect of strontium on the short and medium range order of SrAW and on SrAWGC disc formation

## 2.1 Introduction

As described previously, bioactive glasses in general are promising avenues of research in tissue engineering, because of their versatility, high biocompatibility and bioactivity (71,109,140–142). Apatite-Wollastonite glass-ceramic (AWGC) in particular it is of great interest because compared to other bioactive glass ceramics it is physically strong, can be fashioned into hard scaffolds and can bind to the surrounding bone with greater affinity than bone binds to itself (116,119,120). AWGC is bioactive, and so over time undergoes a chemical process where the material turns into hydroxyapatite, also enriching the fluid around the material with ions such as Si and Mg which are known to have positive effects on cell growth and development (72,77,143). Substituting some of the calcium for strontium within AWGC could improve the material as a tissue engineering scaffold as localised release of strontium around the tissue engineering construct could aid in bone tissue regeneration by improving cell growth, osteogenic differentiation and microbial resistance (11,72,77,86).

This chapter will cover the manufacture of the SrAW glass, the precursor material to SrAWGC, and then it will move on to using neutron diffraction, MAS-NMR and Raman spectroscopy to study how short (and medium) range order of the SrAW glass with 0, 6.2, 12.5, 18.7, 24.9 and 37.4 mol% Sr are affected by the increasing Sr content of the material. These percentages of Sr represent 0, 12.5, 25, 37.5, 50 and 75% substitution of Ca for Sr in the material and so will allow both minimal and near full Sr substitution to be studied. Finally, the SrAW glass will be heat treated to form the SrAWGC discs, with the heat treatment binding the glass powder and making it partially crystallise to ensure the material has the correct mechanical properties and bioactivity.

### 2.1.1 The short range order of glasses and ceramics

A major component of the bioactivity of SrAWGC is the way in which the material breaks down and releases ions, to which cells sense and respond (79,114). Changing the strontium content of SrAWGC could alter the way in which the material breaks down and therefore could change the biological response of the human MSCs exposed to SrAWGC. Determining the short range order of the material and how this changed with strontium substitution would indicate how the substitution of strontium for calcium could affect the way in which the material breaks down, and could help understand any differences in cell response with the strontium content of SrAWGC.

The short range order describes the immediate environment of the atoms in a material, only out to about one or two atoms distance (107,144). Glasses and even liquids possess a short range order, as there is a predictable, repeated and measurable arrangement and interaction between each single atom in the substance and the atoms in its immediate vicinity. Crystals have a long range order, as the regular ordering of the atoms in the material extends far beyond one or two atoms to macroscopic scales, producing crystalline planes (107). However, for glass, there is no long range order as it is composed of a disordered network (section 1.2.3 in Chapter 1). Understanding the short range order is instrumental in designing bioactive glasses as the changes at this level can have significant effects on glass bioactivity and degradation time, potentially altering the rate or concentration of ions released and hence potentially how cells respond to the material (72,79,114,145).

As atomic separations are only a couple of Angstroms (Å) in width they fall within the short range order regime, and as such there should be a relatively conserved distribution of these separations across a material. Therefore measuring the distances between atoms, and hence short range order, in the material is one way of determining whether the short range order of the SrAWGC would change with substitution of Ca for Sr. Neutrons are useful for probing these atomic separations. However, neutron diffraction cannot be used to study the atomic separations within the glass-ceramic itself as the contributions from the crystalline phases would completely obscure the

relatively weak contributions from the amorphous phase. This is concerning because the amorphous phase of bioactive glass-ceramics is considered to be the most bioactive component, due to its relatively high dissolution rate (72,146,147). It is not possible to extract the amorphous phase from the SrAWGC to study the short ranger order; however it can be modelled with the SrAW glass (the glass which is heat treated into SrAWGC). Therefore, the short range order of the SrAW glass with increasing strontium substitution will be studied in this section as a model for the SrAWGC.

#### 2.1.1.1 Introduction to neutron diffraction

Neutron diffraction measures the inter-atomic spacings by diffracting a stream of neutrons through these spacings, and subsequently measuring and analysing their angular distribution. This is possible because thermal neutrons have a de Broglie wavelength in the range of Angstroms (Å), which is similar to that of the interatomic spacings in glasses (148). The technique is functionally quite similar to X-ray diffraction; however there are several differences which are advantageous. X-rays are scattered by the electrons in atoms hence the scattering of X-rays (and the penetration depth of the x-rays into a material) is related to the atomic number of that element. Elements with a high atomic number, and hence a high electron density, more strongly scatter X-rays and so produce a stronger diffraction signal. Neutrons interact primarily with nuclei, and the intensity of the diffracted neutrons is not related to the atomic number (it varies empirically). This allows neutron diffraction to more easily detect lighter elements, and in particular to resolve the atomic spacings between a heavier and a much lighter element (with X-rays the brighter heavier elements would obscure the lighter ones). Strontium is quite heavy in comparison to the other constituents of AW glass; hence this is a useful trait. Finally, neutrons are generally more weakly scattering than X-rays, and as such can penetrate far deeper into a sample. This means that a larger volume of sample can be probed, and that the resulting measurement will be an average across the whole sample, rather than just a surface measurement (148,149). The main disadvantage of neutron diffraction is the expense of the technique. Thermal

neutron sources are expensive and large; hence this inevitably leads to fewer experimental repeats as time on the instrument is limited.

#### 2.1.1.2 Neutron diffraction theory

The theory behind neutron scattering is well established, and so only the key points will be presented here, which will be useful in later analysis and discussion (148,149)

During a neutron diffraction measurement the sample is placed into the path of a collimated beam of neutrons which then scatter off the atoms in the sample though an angle $2\theta$. This is represented by the vector $Q$., and these scattered neutrons then interfere with each other. The way in which these scattered neutrons interfere is dependent on their phase difference, which is related to the physical separation of the atoms from which they originally scattered. The resulting scattered neutron waves then produce diffraction fringes, with either constructive (with raised intensity) or destructive (lowered intensity, potentially reduced to zero) fringes appearing at particular scattering angles, or vectors $Q$, depending on how the atomic separation compared with the wavelength of the neutron. If a neutron of known wavelength is used, the atomic separation through which the neutrons scattered can be determined using the angle at which the scattered neutron was detected. Therefore, neutrons are scattered by the inter-atomic separations in the sample, producing a strong signal at particular angles (related to the separation) and these are detected by neutron detectors in an array around the sample. The total of all (coherently) neutrons scattered by the sample across the whole angular space is the coherent scattering intensity, $\mathrm{i}(\mathrm{Q})$, given by (150):

**Equation 1:**

$$\boldsymbol{i(Q)} = \sum_{\boldsymbol{i}} \sum_{\boldsymbol{j}} \boldsymbol{c_i c_j b_i b_j} \left[\boldsymbol{p_{ij}(Q)} - \mathbf{1}\right]$$

This equation describes how the scattering intensity is given by the sum over all pairs of atoms "*i*" and "*j*", and these atoms have concentrations of $c_{\mathrm{i}}$ and $c_{\mathrm{j}}$ (within the material) and a coherent scattering lengths of $b_{\mathrm{i}}$ and $b_{\mathrm{j}}$. This is

equation is in Q-space, or reciprocal space, and uses units of inverse distance (Å$^{-1}$). The pair correlation function, $p_{ij}(Q)$, relates to the relationship between the atomic pair scattering of the neutrons. It is described by the following (150):

**Equation 2:**

$$\boldsymbol{p_{ij}(Q)_{ij} = \frac{N_{ij} w_{ij}}{c_j} \frac{sin(Q r_{ij})}{Q r} exp\left[\frac{-Q^2 \sigma_{ij}^2}{2}\right]}$$

Again this function is in reciprocal $Q$-space, where $N_{ij}$, $r_{ij}$ and $\sigma_{ij}$ represent the coordination number, atomic separation and disorder parameters respectively. The coordination number represents the number of other atoms connected to an atom in a material, the atomic separation is simply the distance between the two atoms in this pairing, and the disorder parameter is a measure of disorder in that separation (a higher disorder results in a broader distribution of atomic separations). The weighting factor $w_{ij}$ is given by (150):

**Equation 3:**

$$\boldsymbol{w_{ij} = 2 c_i c_j b_i b_j \quad \text{if } i \neq j}$$

$$\boldsymbol{w_{ij} = c_i^2 b_i^2 \quad \text{if } i = j}$$

This is because atomic pairs with low concentrations of either of the atoms in the pair, or where either of the atoms is weakly scattering, will scatter fewer neutrons and produce a lower scattering intensity.

To get the final total correlation function ($T(r)$), describing the quantity of neutron scattering events at particular atomic separations, a Fourier transform is needed to move the data from reciprocal $Q$-space to real space. $T(r)$, given by (150):

**Equation 4:**

$$\boldsymbol{T(r) = T_0 \ (r) + \frac{2}{\pi} \int_0^\infty Q.\mathrm{i}(Q) M(Q) sin(Q r) dQ}$$

where $M(Q)$ is a Lorch window function, that corrects the result to accommodate the finite maximum experimentally attainable value of $Q$. $T_0(r)$ is the average density term for the material, given by:

**Equation 5:**

$$\boldsymbol{T_0(r) = 4\pi r \rho_0 \left(\sum_i c_i b_i\right)^2}$$

where $r$ is the distance from an arbitrary atom at the origin and $\rho_0$ is the number density of atoms. In other words, the scattering intensity is determined by considering the number of neutrons scattered from every combination of pairs of atoms in the material (weighted based on how abundant they are, and how much they tend to scatter neutrons), per square angle around the sample. When this is then Fourier transformed it becomes the $T(r)$, which represents the number of neutrons scattered for each atomic separation.

Ceramics and crystals, due to their highly organised nature, produce very sharp neutron diffractions peaks associated with the tightly ordered atomic separations found in atomic network within the crystals. In contrast, glasses produce broad and shallow peaks, as the disorganised nature of the glass network produces a relatively large distribution of atomic separations for each pairing, compared with crystals. In a glass-ceramic, this results in the peaks from the ceramic phases of the material masking the peaks from the glass phase. To get around this, the neutron diffraction can be performed on the SrAW glass (the material made during the glass making process which has not yet been heat treated to form the SrAWGC). The SrAW glass is essentially the same material which forms the glass phase of SrAWGC and understanding its short-range order would contribute greatly to understanding how SrAWGC responds to strontium substitution. This is because the glassy phase of bioactive glass-ceramics is considered to be the most bioactive component, due to its relatively high dissolution rate (72,146,147).

#### 2.1.1.3 MAS-NMR

Another technique useful in exploring the short-range order of SrAW glass, and also determining the medium range order (and how it changes with the substitution of calcium for strontium) is utilising magic angle spinning nuclear magnetic resonance (MAS-NMR). MAS-NMR utilises the concept that the

magnetic resonance of a nucleus is altered by its chemical environment, and so it can be used to identify different chemical structures inside glasses and ceramics (151). The sample is placed in a magnetic field then excited with radio-waves until its nuclei enter nuclear magnetic resonance. Sensitive radiofrequency receivers are then used to detect this resonance. This varies between elements, but importantly varies significantly when the same element is put in different intramolecular environments (chemical shift-anisotropy), allowing the measurement of the NMR resonance frequency to be used to identify particular molecules, with the use of known standards. However, the peaks are usually very broad for solid samples, but spinning the sample at an angle of 54.74° (with respect to the magnetic field) causes the non-chemical-shift anisotropy to cancel out, leaving only the shift to the resonance frequency caused by the chemical environment (151,152). The technique is most easily performed on isotopes with spin ½ nuclei (such as $^{29}$Si and $^{31}$P) as these have no quadrupolar component to their magnetic moment (153,154). Isotopes with nuclei with half-integer spin greater than ½ require more advanced analysis and more expensive techniques to get high resolution spectra (154). However, fortunately the main elements in AW glass have relatively abundant spin ½ isotopes and so can be studied without the need of these techniques. The most common isotope of phosphorus ($^{31}$P) has spin ½, hence that will produce a strong signal. For silicon only the second most common isotope $^{29}$S has a spin ½ nucleus. However, this only makes up ~4.67% of silicon and so this will reduce the signal as only a fraction of the material is being probed.

#### 2.1.1.4 Glass network connectivity

As mentioned previously, glass is composed of a network, and for SrAW this network will primarily be composed of Si (a network former), O and P (which could potentially act as a network modifier, based on studies of Bioglass 45S5 (150,155,156)). MAS-NMR can be used to determine the nature of the phosphorus-oxygen and silicon-oxygen environment within the SrAW glass, and thus determine whether and how strontium has influenced the glass network. Knowledge of the P and Si environments can be used to determine the network connectivity (NC) of phospho-silicate bioactive glasses, such as

AWGC, which can then be used as a measure of bioactivity (112,114). The NC describes the number of network forming tetrahedra (such as silica, $SiO_4$) each tetrahedra within the glass is connected to. Crystalline silica (such as quartz) has a network with a high NC, as each oxygen in the silica tetrahedra bridges to another silicon atom (bridging oxygens, $O_B$), resulting in a highly interconnected, and durable, ceramic network. This can be seen in Figure 8e as the $Q^4$ silica. Network modifiers (such as phosphate, $PO_4^{3-}$, Mg, Ca and Sr) can be added to the glass precursor, so that when the glass is made this silica network is broken up, becoming disorganised and resulting in a less durable and more easily broken down glass (see Figure 9) (157). The presence of these network modifiers utilises oxygens that would otherwise have bridged to neighbouring silicon atoms (making them become non-bridging oxygens, $O_{NB}$), changing the speciation of the silica tetrahedrons down from $Q^4$ to $Q^3$, or $Q^2$ (see Figure 8) and resulting in the silicon and oxygen forming branching chains throughout the glass structure (Figure 9) (157,158).

Exactly which speciations form in the final glass depends on the stoichiometry of the precursor and the nature of the phosphate ions in the network. The lower the $Q^n$ of the phosphate, the more Si-O-Si bonds it will disrupt and hence will push the $Q^n$ of the silicate lower, lowering the NC and disrupting the Si network (150,157,159,160). This notation can also be used to describe other glass network formers, such as phosphorus (156). However, if the $Q^n$ drops to $Q^0$, then the tetrahedra no longer connect to any other and are isolated from the network, instead functioning as a kind of network modifier.

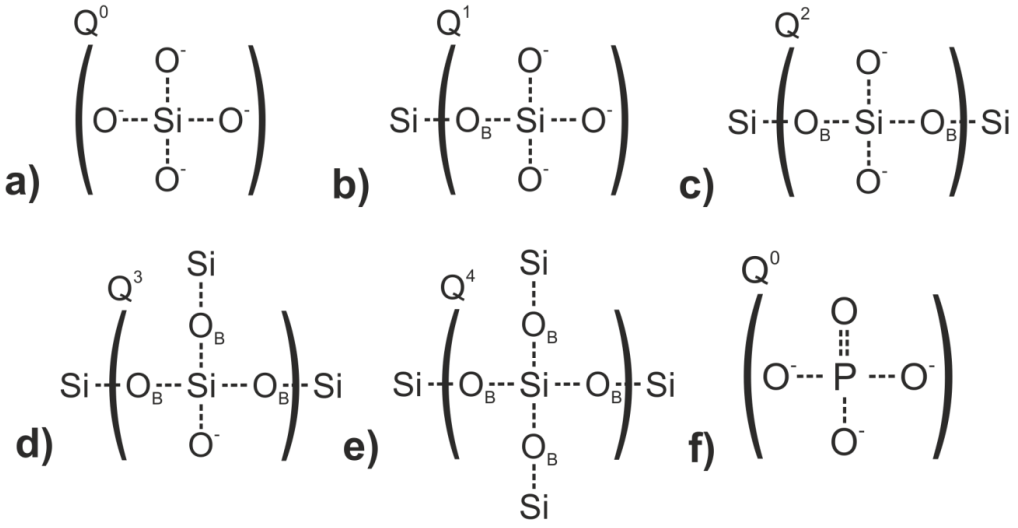


**Figure 8: Schematics describing Q-speciation, where $Q^n$ describes the number of non-binding oxygens in the tetrahedron. a-e) describe the different $Q^n$ speciations of $SiO_4$, f) describes the form of orthophosphate ($Q^0$ $PO_4^{3-}$). Adapted from Martin *et al* (2012)** (157)

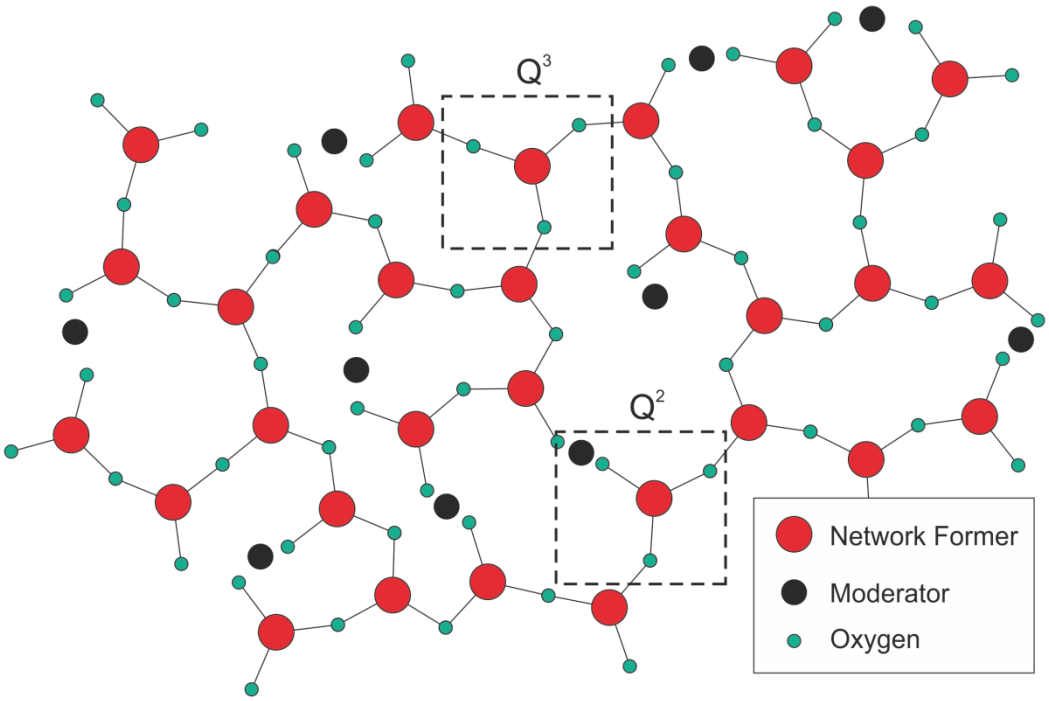


**Figure 9: A two-dimensional schematic of a theoretical glass network. The white circles represent network formers (such as Si), which form the backbone of the glass. The grey circles the network modifiers, breaking up the network. $Q^2$ and $Q^3$ speciations of silica tetrahedra are indicated.**

The $Q^0$ form of phosphate ($PO_4^{3-}$), orthophosphate, can be seen in Figure 8f. Si and P MAS-NMR measurements can then be used to determine which form (or speciation) of the silica and phosphorus tetrahedra are present, allowing more detail on the short range and medium range order of the material to be determined.

### 2.1.1.5 Bond coordination number

When discussing the short-range order within the glass network, an essential concept is the coordination number of the bond. This describes the abundance of the bond, and hence will contribute to the intensity of that atomic separation in the neutron diffraction. Silicon to oxygen bonds (Si-O) make up a large part of the network of phospho-silicate bioactive glasses (150,160). As described previously the silicon and oxygen form tetrahedra which connect in different manners depending on the $Q^n$. These different $Q^n$ speciations have different O-Si-O bond coordination numbers, because in each of these environments each oxygen atom is able to interact with different numbers of other oxygen atoms via a silicon atom. This relates to the number of $O_B$ and $O_{NB}$, as the $O_B$, by definition, bridge two different silicon atoms and so are able to interact with more oxygen atoms via a silicon atom. In Figure 8 it can be seen that the $O_{NB}$ can only interact with three other oxygen atoms via a silicon atom, whilst the $O_B$ is able to interact with six. However, when calculating the coordination number for a unit cell (*i.e.* around one Si), the contributions from these $O_B$ must be halved, as the $O_B$ is shared between two unit cells. The final coordination number of the O-Si-O bond is then determined by making a weighted average across the $O_B$ and $O_{NB}$ in the $Q^n$ unit cell. This leads to:

**Equation 6:**

$$\boldsymbol{N_Q = \frac{3.n_{O_{NB}} + \frac{6.n_{O_B}}{2}}{n_{O_{NB}} + \frac{n_{O_B}}{2}}}$$

Where for tetrahedra (such silicon and phosphorus with oxygen) $n_{O_B} = Q^n$ and $n_{O_{NB}} = 4 - n_{OB}$. This can be applied to phosphorus as well, and leads to

$Q^0$ having an O-P-O (or O-Si-O) coordination number N = 3, whilst $Q^2$ has N = 4 and $Q^3$ has N = 4.8 (150).

### 2.1.2 Raman spectroscopy for studying changes to medium range order of SrAW with increasing Sr content

In addition to neutron diffraction and MAS-NMR, Raman spectroscopy can be used to provide further information on the short and medium range order of the SrAW glasses. Raman spectroscopy uses visible light to measure the vibrational states within a material, and these can be characteristic of certain speciations of Si, or other chemical arrangements.

The theory and practice of Raman spectroscopy are well established, hence only the key points will be covered here (for more information see (161)). The technique is based on subjecting the sample to visible light from a high powered laser. This induces a Raman transition causing the sample's molecules to move into a vibrational state. When they relax from the virtual state down into the vibrational state, a photon is released, which is then detected. The difference in the energy of this photon and the initial energy level provide the characteristic energy level of the vibrational state. When the measurement is taking place, the laser scans through a segment of the visible spectrum, and hence will excite a sequence of different vibrational states, which can then be measured to form a spectrum. The resulting spectra then describe the counts at particular wavelength differences, which can be interpreted as the counts of particular vibrational states and hence particular atomic arrangements or chemical bonds. These vibrational states typically belong to either symmetric or asymmetric stretching, rocking or bending modes, and are well studied over a variety of glasses and ceramics (162,163), with the main modes found for silicon or phosphorus to oxygen bonds described in Figure 10.

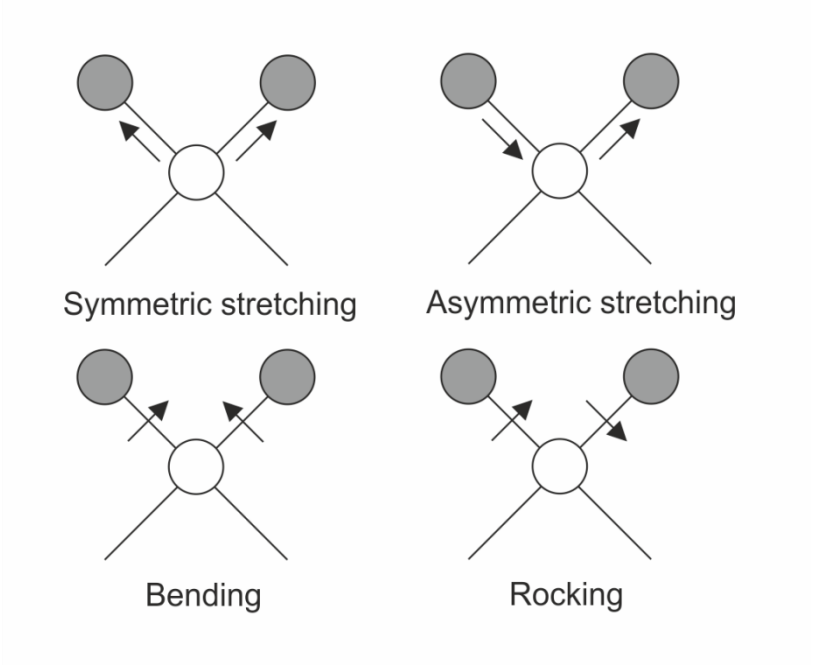


**Figure 10: Schematic of the main Raman modes found in silicon and phosphorus to oxygen bonds. The grey circles are O, whilst the white circles indicate P or Si. The arrows indicate the direction of movement for that vibrational mode. Adapted from** (162)**.**

## 2.2 Methods

### 2.2.1 Glass manufacture

The Strontium Apatite Wollastonite (SrAW) glass compositions used in this work are based on the same basic recipe as first reported by Kokubo in 1991 (9) and more recently used by Lee *et al.* (2015) (118), however they have been altered following work in the David Wood Laboratory(102), to have a gradual substitution of calcium for strontium in the material. The molar contents of the different compositions of SrAW with increasing strontium content are described by:

**Equation 7: $(SiO_2)_{35.4}$, $(MgO)_{7.1}$, $(CaF)_{0.4}$, $(P_2O_5)_{7.1}$, $(CaO)_{49.9}$, $(SrO)_{x-49.9}$ ,**

**where x = 0, 6.2, 12.5, 18.7, 24.9 or 37.4 mol%**

The values for this can be seen in Table 2, along with the molecular weight of each composition.

During the production process CaO and SrO were not used as they are not stable in air, spontaneously taking on $CO_2$ to form $CaCO_3$ and $SrCO_3$. $CaCO_3$ and $SrCO_3$ are stable at room temperature (defined as 20°C) in air (undergoing no further spontaneous reactions) and can there before used instead of CaO and SrO in glass precursor The additional $CO_2$ contained in the carbonates is released at temperatures above 825°C as the carbonates thermally decompose. Furthermore, as both CaO and $CaCO_3$ (and SrO and $SrCO_3$) both contain only one calcium atom, the molar ratios are unaffected, although as $CaCO_3$ has a higher molecular weight this would affect the actual mass of precursors used.

The mass of each reagent used in the precursors of the different compositions is calculated using the molar ratios in Table 2, along with the molecular weights of each composition. The specific products used, and the molecular weights of those substances can be found in Table 3.

| Molar percentage of each precursor (Mol%) | | | | | | Molecular weight (g/Mol) |
|---|---|---|---|---|---|---|
| SrO | $SiO_2$ | MgO | CaF | $P_2O_5$ | CaO | |
| 0 | 35.4 | 4.6 | 0.4 | 7.1 | 49.9 | 62.6 |
| 6.2 | 35.4 | 4.6 | 0.4 | 7.1 | 43.7 | 65.5 |
| 12.5 | 35.4 | 4.6 | 0.4 | 7.1 | 37.4 | 68.5 |
| 18.7 | 35.4 | 4.6 | 0.4 | 7.1 | 31.2 | 71.5 |
| 24.9 | 35.4 | 4.6 | 0.4 | 7.1 | 25.0 | 74.4 |
| 37.4 | 35.4 | 4.6 | 0.4 | 7.1 | 12.5 | 80.3 |

**Table 2: Molar ratios of SrO, $SiO_2$, MgO, CaF, $P_2O_5$ and CaO in the six different compositions of SrAWGC, and the molecular weights of the final compositions.**

| Reagent | Supplier and Product | $W_{mol}$ (g/Mol) |
|---|---|---|
| $SiO_2$ | Tilcon Sands | 60.08 |
| MgO | Sigma | 40.30 |
| $CaF_2$ | GPR, 275944X | 78.07 |
| $P_2O_5$ | Fisher, P/2960/50 | 141.94 |
| $SrCO_3$ | Fisher, >98% purity | 147.63 |
| $CaCO_3$ | Fisher, 99+% purity | 100.09 |

**Table 3: The reagents used in making the SrAWGC precursors and their molecular weights ($W_{mol}$).**

To make a batch of 400g of SrAW glass, the mass of each reagent required can be determined by working backwards. First, the moles of each reagent required are determined, such that the total of all of the reagents used is 400g. This is given by:

**Equation 8:**

$$\boldsymbol{W_t = \sum_{reagent} W_{reagent} = \sum_{reagent} W_{mol} . N_{mol} = 400g}$$

The number of moles for each reagent, $N_{mol}$, is then related back to the formula for the molar ratios of the SrAW glass (Equation 7), using the total number of moles required ($N_{mol_{total}}$):

**Equation 9:**

$$\boldsymbol{Mol\%_{reagent} = \frac{N_{mol}}{N_{mol_{total}}} = \frac{N_{mol}}{\sum_{reagent}(N_{mol})}}$$

It is more straightforward to do this calculation for SrO and CaO, and then use the ratio of $W_{mol}$ between $SrCO_3$/SrO and $CaCO_3$/CaO to adjust the expected weight of reagent from that of the oxide to the carbonate. Hence:

**Equation 10:**

$$W_{CaCO_3} = W_{CaO} \cdot \frac{W_{mol_{CaCO_3}}}{W_{mol_{CaO}}}$$

$$W_{SrCO_3} = W_{SrO} \cdot \frac{W_{mol_{SrCO_3}}}{W_{mol_{SrO}}}$$

The molecular weight ($W_{mol}$) of SrO and CaO are 103.62 g/mol and 56.08 respectively. The mass of each reagent used in a 400g batch was then calculated and is displayed in Table 4. Note that the total is higher than 400g as it includes the $CO_2$ from the carbonates which is released during the glass making process.

| | Weight of reagent (g) for 400g of glass | | | | | | Total Weight (g) |
|---|---|---|---|---|---|---|---|
| Composition (Mol% Sr) | $SiO_2$ | MgO | $CaF_2$ | $CaCO_3$ | $SrCO_3$ | $P_2O_5$ | |
| 0 | 136.37 | 18.30 | 2.00 | 319.31 | 0.00 | 64.43 | 540.40 |
| 6.2 | 130.23 | 17.47 | 1.91 | 267.05 | 55.89 | 61.53 | 534.09 |
| 12.5 | 124.54 | 16.71 | 1.82 | 218.56 | 107.75 | 58.84 | 528.23 |
| 18.7 | 119.40 | 16.02 | 1.75 | 174.81 | 154.54 | 56.42 | 522.94 |
| 24.9 | 114.67 | 15.38 | 1.68 | 134.52 | 197.63 | 54.18 | 518.07 |
| 37.4 | 106.19 | 14.25 | 1.55 | 62.29 | 274.88 | 50.17 | 509.33 |

**Table 4: The weights of each reagent needed to make 400g of composition of SrAW glass, with increasing strontium content. The total weight of the precursor mixture for each composition is also provided.**

The reagents were weighed to the nearest 0.1g using a Sartorius Roughing Balance (PT3100) into a mixing bottle. Prior to mixing the $SrCO_3$ and $CaCO_3$, they were calcined (*i.e.,* held at 200°C for at least 3 hours) to remove moisture, and the $P_2O_5$ was added last to the precursors and the mixing container sealed directly after addition to minimise water content in precursor. The precursor had to be as dry as possible as the $P_2O_5$ rapidly heats up in contact with any moisture. This was made in 400g batches, and

then mixed in a sealed bottle with a clean and dry agitation bar for one hour using a bottle roller.

### 2.2.2 SrAW glass for general use

The glass for use in every experiment in this work, except the neutron diffraction experiment, was made in bulk using alumina crucibles. This allowed the glass to be made in larger quantities approaching a commercial scale.

After mixing, the precursor for each composition was packed into separate slip-cast alumina crucibles (thick-walled speckle-finished CL70 from Almath), approximately 180g per crucible, utilising a plastic bar to compress the powder and ensure it was fully compacted (as air in trapped in the precursor would cause an explosion when heated later). The packed crucible was then placed into a larger Mullite crucible (Magma ceramics), already one quarter full with alumina powder (see Figure 11). The larger crucible's purpose was to catch any molten glass should the inner crucible fail during the glass making process. Two mullite crucibles were placed into the furnaces at the same time to allow more material to be made at once. Two furnaces were used in the procedure, allowing a cooler furnace to raise the temperature initially from room temperature to an intermediate temperature, followed by transfer to a second furnace, which due to its design could not be generally lowered below 800°C without damage to the furnace interior. The two mullite crucibles containing the packed glass precursor were initially heated at 10°C/min from 0 to 500°C (Elite BCF13/12 furnace, Eurotherm 2416 controller), then held for 30 minutes to ensure the crucibles and their contents were fully heated. The mullite crucibles were then transferred to a second furnace, pre-heated to 1450°C (Pyrotherm furnace, Eurotherm 2416 controller), and then held at this temperature for 2 hours. During this time the glass precursor would react and melt to form the SrAW glass, and the carbon dioxide could be released from the carbonates.

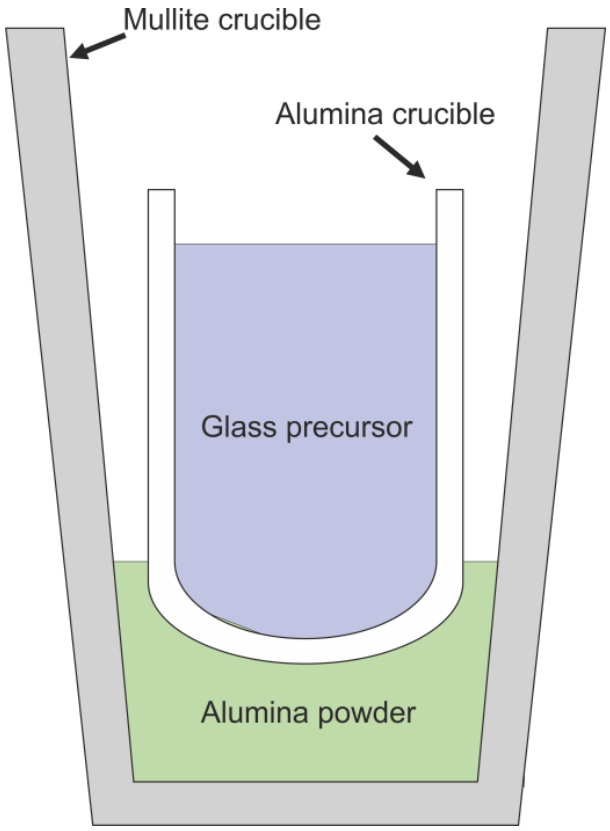


**Figure 11: A section of the crucible set-up for glass production. The glass powder is packed within an alumina crucible, resting on a bed of alumina powder, within a mullite crucible.**

The crucibles were then extracted from the Pyrotherm furnace and placed on a sand surface, after which the inner crucible was removed and poured into a quenching tank filled with tap water at 4°C. The molten glass hitting the water rapidly cooled to form glass frits which collected at the bottom of the tank. The quenching tank was then drained using a bespoke pump (Clarke CPE 110) and sieve mechanism (using Fisher Scientific BSI410/1986 certified sieves, 90µm) and the glass frit placed in a drying cabinet overnight.

### 2.2.3 SrAW glass for neutron diffraction

The glass for use in neutron diffraction was made using platinum crucibles, following the procedure in Martin *et al.* (2012) (150), to avoid ion leeching from the crucible into the glass melt which occurs when using alumina crucibles (102,164,165). However, the platinum crucible production method had a low yield and was relatively expensive preventing its more extensive

use throughout the other experiments in this project. As a slightly different method was utilised to produce the glass for neutron diffraction than that used in section 2.2.2 (for the other experiments) it was possible this would induce slight differences into the glass. However, the expense and difficulty of securing time on the neutron diffraction instrument justified changing the process to reduce the impurities in the glass. After mixing, the precursor mixes for each composition (described in section 2.2.1) were packed into platinum crucibles, which were then then heated to 1450°C in an electric furnace (EHF 17/3, Lenton, Hope Valley, UK) and held at this temperature for two hours. The molten glass was then poured into pre-heated graphite moulds (350°C) and annealed at this temperature overnight before being allowed to cool slowly to room temperature.

### 2.2.4 Grinding and sieving of the glass frit to acquire glass particles of known size range

The glass frit samples for each composition were ground using a Gyromill Puck Mill, where 20g of the glass was distributed evenly around the puck. The ground SrAW glass powder was then sieved in an Octagon Digital (Endacotts) Sieve Stack (using Fisher Scientific BSI410/1986 certified sieves, 2mm, 1mm, 125µm, 90µm, 45µm) set at amplitude 9 for 30 minutes on intermittent mode. The sieve stack was then separated into the different size fractions of ground SrAW glass (<45µm, 45-90µm, 90-125µm, 125µm-1mm, 1-2mm and >2mm), labelled and bagged.

For the purposes of the neutron diffraction, the glass samples were crushed using a percussion mill, then ground into a course powder using pestle and mortar.

### 2.2.5 Solid state MAS-NMR on SrAW glass

$^{31}P$ and $^{29}Si$ MAS-NMR were used to provide more information about the nature of the Si and P components of the SrAW glass compositions, and whether they changed with strontium substitution. This was only performed on the SrAW glass (and not the SrAWGC) as this would give insight into the amorphous phase of the SrAWGC, which was predicted to be the

component most associated with the cell response. $^{31}P$ and $^{29}Si$ were chosen as they are predicted to be major components of the SrAW glass network and they are also the most abundant spin ½ nuclei in the glass. This is important because MAS-NMR cannot be performed on isotopes with integer spin and isotopes with nuclei with half-integer spin greater than ½ require more advanced analysis and more expensive techniques to get high resolution spectra (153,154)(154).

One-dimensional $^{31}P$ and $^{29}Si$ MAS NMR were performed on the six different compositions of crushed SrAW glass (0, 6.2, 12.5, 18.7, 24.9 and 37.4 Mol% Sr) made for the neutron diffraction experiments. Measurement were taken from a single batch of glass for each composition (the same used for the neutron diffraction), with 40, 32, 44, 16, 28 and 28 technical repetitions for 0, 6.2, 12.5, 18.7, 24.9 and 37.4 Mol% Sr, respectively. This was done by the Durham University NMR service, using 250mg of sample and using the parameters and reference samples shown in Table 5. The resulting spectral peaks were fit using IGOR Pro. The fittings utilised a single peak for the $^{31}P$ MAS NMR and a two peak fit for the $^{29}Si$ MAS NMR (changed to three peak fit for the 37.4 Mol% SrAW as this produced a superior fit and more closely aligned with the data).

| | Sr Mol% (x=...) | Field (T) | Frequency (MHz) | MAS (kHz) | Probe | Reference |
|---|---|---|---|---|---|---|
| $^{31}P$ | 0, 6.2, 12.5, 18.7, 37.4 | 9.4 | 79.44 | 6.8 | VNMRS | Phosphorus, 85% $H_3PO_4$ |
| $^{31}P$ | 24.9 | 9.4 | 79.43 | 6.4 | VNMRS | Phosphorus, 85% $H_3PO_4$ |
| $^{29}Si$ | 0, 6.2, 12.5, 18.7 24.9, 37.4 | 9.4 | 161.87 | 6.8 | VNMRS | Silicon, tetramethylsilane |

**Table 5: Experimental parameters for the one-dimensional solid state NMR experiments**

### 2.2.6 Determining the how the short-range order of the SrAW glass changes with strontium substitution for calcium

Neutron diffraction was performed on the different SrAW glass compositions to determine whether the substitution of strontium into the material had significant effects on the short-range order of the AW glass produced in Section 2.2.3. Neutron diffraction detects the short-range order by bombarding the samples with neutrons of a known energy. The way in which the neutrons are scattered by the atoms in the material can then be analysed to determine the distances between the atoms in the sample. This was only performed on the SrAW glass because the crystalline phases in the SrAWGC would completely obscure the relatively weak contributions from the amorphous phase. This was concerning because the amorphous phase of bioactive glass-ceramics is considered to be the most bioactive component, due to its relatively high dissolution rate (72,146,147). It is not possible to extract the amorphous phase from the SrAWGC to study the short ranger order; however it can be modelled with the SrAW glass (the glass which is heat treated into SrAWGC). Therefore, the short-range order of the SrAW glass with increasing strontium substitution will be studied in this section as a model for the SrAWGC.

#### 2.2.6.1 Determining the change in SrAW glass density with strontium content using helium pycnometry

For certain sections of the neutron diffraction analysis, it was important to know the density of the material. The macroscopic densities of the six different glass samples (with increasing strontium content) were determined using helium pycnometry using a Quantachrome micro-pycnometer, utilising the manufacturer's instructions. The pycnometer was calibrated using steel spheres using the manufacturer's instructions. First a small quantity of the glass was weighed to get the sample mass, $M_s$, and then this was placed in the pycnometer chamber. The chambers were initially purged with helium gas then zeroed. Helium was then introduced to the sample chamber up to 17 psi. Once this was stabilised, the pressure was recorded as $P_1$. A valve

was then opened to allow the helium gas to expand into the empty reference chamber after which the pressure was allowed to stabilise again. This was then recorded as $P_2$. This was repeated until the $P_1/P_2$ ratio ceased fluctuating. The volume could then be calculated using the following equation,

**Equation 11:**

$$V_s = V_c + \frac{V_r}{1 - \frac{P_1}{P_2}}$$

Where $V_s$ is the volume of the sample, $V_c$ is the volume of the sample chamber and $V_r$ is the volume of the reference chamber (166). The density of the sample was then determined by dividing the measured mass of the sample, $M_s$, with the measured volume, $V_s$. All measurements were taken from samples from a single batch of each of the glass compositions (the same used for the neutron diffraction experiment). A Dunn-Holland-Wolfe test was used to compare the data, as the conditions had different numbers of repeats (5 repeats for 0 and 6.2 Mol% Sr, 4 for 12.5, 18.7 and 24.9 Mol% Sr and 6 repeats for 37.4 Mol%)

#### 2.2.6.2 Acquiring, cleaning and processing the Neutron Diffraction data

Neutron diffraction was performed on the different glass compositions to determine whether the substitution of strontium into the material had significant effects on the short-range order of the AW glass produced in Section 2.2.3. Neutron diffraction detects the short-range order by bombarding the samples with neutrons of a known energy. The way in which the neutrons are scattered by the atoms in the material can then be analysed to determine the distances between the atoms in the sample.

The coarsely ground glass powder for each composition was loaded into cylindrical vanadium cans (as described in Figure 12) of 8.3 mm internal diameter and 0.025 mm wall thickness, with the height of the glass in each can being measured for use in determining the packing density of the

material in the cans. Cans were prepared for each of the six compositions of SrAW with increasing strontium content, then one further empty can. The filled vanadium cans were placed into an automated sample changer, along with the empty vanadium can, a vanadium rod of 8mm diameter, and one further chamber being left empty.

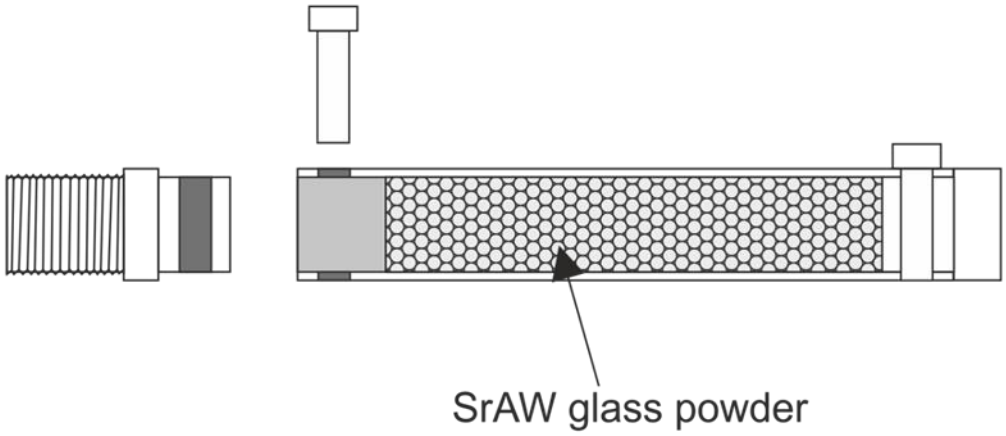


**Figure 12: Schematic of the vanadium cans used to hold the SrAW glass powder. The threaded end (left) screwed into the sample changer of General Materials Diffractometer (GEM). The top and bottom lids were held in place with pins.**

The empty can, the vanadium rod and the empty chamber were necessary for later corrections. The sample changer was in turn placed into the neutron diffraction instrument, the General Materials Diffractometer (GEM, ISIS, Rutherford Appleton Laboratory,(167)).

The neutron diffraction measurements were taken over 48 hours, with each sample being measured three times in technical repeats. Each composition of SrAW glass had a single sample measured. The raw data from GEM (the differential cross section, DCS) contained numerous terms which needed removing to leave behind only the signal from the samples, i(Q). Gudrun (GudrunGUI_2)(167) was used for this purpose, to clean the data by normalising, adjusting the baseline and removing the background scattering terms. Gudrun also corrected for absorption, inelastic and multiple scattering effects (167). As part of its processing, Gudrun calculates the theoretical packing density of the different glass compositions within the vanadium can,

however an adjustment factor was used so that the DCS (the quantity measured by GEM) from the measurements was 100% of the expected (theoretical) DCS. This adjustment factor altered the theoretical density of the samples to account for the suboptimal packing of the sample in the cans, as there will be air gaps and space between the glass particles. The density adjustment was compared with the density calculated from the mass and quantity of glass in the can (previously measured using a plunger when filling the can), and any adjustments were kept within 7% of the measured value. Xsect (168) was then used to the determine the sample cross-sections from the abundance of each element in the samples (see Table 6). “Open GENIE V2.3” (169) was then used to calculate the self-scattering terms for each sample using the output from Gudrun and the sample cross-sections from Xsect.

| | Mol% Sr | 0 | 6.2 | 12.5 | 18.7 | 24.9 | 37.4 |
|---|---|---|---|---|---|---|---|
| Elemental abundance (%) | Si | 13.06 | 13.06 | 13.06 | 13.06 | 13.06 | 13.06 |
| | P | 5.24 | 5.24 | 5.24 | 5.24 | 5.24 | 5.24 |
| | Ca | 18.55 | 16.27 | 13.94 | 11.66 | 9.37 | 4.76 |
| | Mg | 2.62 | 2.62 | 2.62 | 2.62 | 2.62 | 2.62 |
| | O | 60.24 | 60.24 | 60.24 | 60.24 | 60.24 | 60.24 |
| | F | 0.30 | 0.30 | 0.30 | 0.30 | 0.30 | 0.30 |
| | Sr | 0 | 2.29 | 4.61 | 6.90 | 9.18 | 13.80 |

**Table 6: The elemental abundances of Si, P, Ca, Mg, O, F and Sr within the six different compositions of SrAW glass.**

The data from different detector banks in GEM needed to be combined so that the neutron diffraction data from across the whole sphere around the sample could be considered together, rather than in discrete angular slices. The GEM2O_v3 Matlab software (170) was then used to combine the data from the different detection banks into one total signal for each composition. This process involved sequentially adding the contributions from each detector bank, adjusting the “self-factor” such that the signal oscillated around the self-scattering level (computed using Open GENIE). The signal

from each bank was truncated outside of its optimal angular range, and this was adjusted to minimise the noise in the final merged signal. Bank 0 was excluded as this tended to both increase the noise in the signal and cause the low Q region to drop un-physically.

The merged neutron diffraction signal was in reciprocal space units ($i(Q)$, in units of atoms barn$^{-1}$ steradian$^{-1}$), however interpreting this was not intuitive. The Fourier transform described in Equation 4 was used to move the neutron diffraction data from reciprocal space, $i(Q)$, into real space, $T(r)$ (counts per Å$^{-2}$), which is then more intuitive to interpret. This was done in Matlab, using programs written by Alex Hannon for the Rutherford Laboratory and the GEM instrument (170). This Fourier transform requires an estimate of the number density and theoretical cross-sections of the elements in the material, and this was calculated by Xsect (168).

To determine how the substitution of strontium into the SrAW glass altered the short range order, the real-space neutron diffraction signals $T(r)$ were fit using NXFit in Matlab (171). NXFit parametrises the $T(r)$ signal by fitting the expected atomic separations to the data, based on the atomic content of the sample and using estimations of the coordination numbers and disorder terms (see Equation 4). Fitting the whole $T(r)$ was a complex process, as multiple atomic separations were predicted to be present (Si-O, P-O, O-Si-O, O-P-O, Mg-O, Ca-O and Sr-O) based on the elements in the material and in consultation with the literature (150,159,160,172). Additionally, due to limitations in NXFit, the O-P-O and O-Si-O peaks had to be combined together and fit as one O…O peak, which could then be split based on the proportion of the Si and P in the material. Hence, a methodical approach was used to break the neutron diffraction signal up and determine as much information about each component of the signal, allowing better initial predictions of the parameters in the final fit and the number of free parameters to be reduced. The steps were:

1. The Si-O/P-O peak was fit in isolation
2. Estimation of O…O bond separation though MAS-NMR, Si-O and P-O allowing the prediction of the O-Si-O and O-P-O separations.

3. An isomorphic substitution approach was used to determine the Sr-O and Ca-O correlations.
4. With the Si-O, P-O, O-Si-O, O-P-O, Sr-O and Ca-O peak parameters determined separately, this information was fed into the final fit of the $T(r)$, allowing the Mg-O to be determined.

#### 2.2.6.3 O…O bond estimation for Silicon and Phosphorus

The $T(r)$ for each composition of SrAW glass contains overlapping contributions from all of the different elements within the material, making analysis of the neutron diffraction data, and determination of the effects of Sr substitution on the material's short range order, incredibly challenging. To make the fitting of the final $T(r)$ more manageable, some of the contributions can be determined using other techniques, such as the O…O separations. The neutrons diffract between not only the Si-O and P-O separations, but also between O-Si-O and O-P-O (referred to as the O…O separations) found in the glass $SiO_4$ and $PO_3^{4-}$ tetrahedra (150). The lengths of the O-Si-O and O-P-O bonds ($r_{O-x-O}$, where x = Si or P) can be mathematically determined using geometry, resulting in the following relationship (150):

**Equation 12:**

$$\boldsymbol{r_{O-x-O} = r_{x-O} \cdot \sqrt{\frac{8}{3}}}$$

where $r_{x-O}$ is the length of the Si-O or P-O bonds. These bonds can then be combined to form an average of the two types of O…O bond, where each bond is weighted on the relative abundance of the two elements in the glass compositions (see Table 6). This gives the average O…O bond length as:

**Equation 13:**

$$\boldsymbol{r_{O\ldots O} = \frac{c_{Si}}{c_{Si} + c_P} r_{Si-O} + \frac{c_P}{c_{Si} + c_P} r_{P-O}}$$

where $c_{Si}$ and $c_P$ describe the concentration (or abundance) of Si and P in the SrAW glass compositions (constant between all samples).

The coordination number, related to the quantity of this bond type (see Equation 2), of the O…O peak, $N_{O\ldots O}$, and can be determined using the $Q^n$ ($Q^0$, $Q^2$ and $Q^3$ have coordination 3, 4 and 4.8, respectively, described previously in Section 2.1.1.5) and then taking a weighted average of the $N_{O-Si-O}$ and the $N_{O-P-O}$, as in Equation 13, but for "N" rather than "r". Hence, the O…O distances and coordination numbers would be known and could be used to simplify the fitting of the $T(r)$ for each glass composition.

#### 2.2.6.4 Isomorphic substitution of Sr for Ca to simplify the neutron diffraction signals

As described previously, the $T(r)$ neutron diffraction signal for each composition of SrAW glass will be composed of the overlapping peaks of many different atomic separations, and hence establishing precise values for the atomic separations could be difficult without first de-convoluting the $T(r)$. Isomorphic substitution is an approach which can be used to extract just part of this signal, simplifying what needs to be deconvoluted, and then reducing what is unknown about the whole $T(r)$ for each composition (150,159,160,173). This is a well-established technique for analysing neutron diffraction data, having been used by Martin *et al.* (2012) to deconvolute the neutron diffraction signal for Bioglass 45S5 where Ca was substituted with Sr (150), and also for numerous other glass systems and substitutions, such lanthanum for cerium, dysprosium for holmium and nickel for cobalt (160,173–176). As strontium is slightly larger than calcium when they are substituted one for the other the section of the neutron diffraction signal containing Sr and Ca components will alter, due to the Sr-O and Ca-O distances being slightly different. Assuming the short range order of the other elements in the material aren't significantly affected by this small alteration, the neutron diffraction signal for a glass without strontium could then be subtracted from that of one with strontium, eliminating all non-Sr and non-Ca components. The $i(Q)$ structure factors for each composition of SrAW were subtracted from one another where the scattering lengths were $b_{x=37.4} > b_{x=24.9} > b_{x=18.7} > b_{x=12.5} > b_{x=6.2} > b_{x=0}$ (where $x$ is the Mol% Sr in the SrAW glass). This gave difference functions of the form:

**Equation 14:** $$^{x-y}\Delta \boldsymbol{i}(\boldsymbol{Q}) = {}^{x}\boldsymbol{i}(\boldsymbol{Q}) - {}^{y}\boldsymbol{i}(\boldsymbol{Q})$$

where "*x*" and "*y*" represented the different compositions of SrAW glass (37.4, 24.9, 18.7, 12.5, 6.2 or 0 Mol% Sr) and the scattering lengths corresponded to the definition above. The assumption of isomorphism is valid over the short and medium range order in SrAW as it should be dominated by the Si-O and P-O tetrahedra which are not expected to be altered by the substitution of Ca for Sr (150,160). However, in the more extended range order (beyond 3Å) the assumption of isomorphism breaks down as this range would include the interaction between Si or P and Sr or Ca, in the form of Si-O-Ca or P-O-Sr bonds, which could be affected by the size difference between the Ca and Sr ions (150).

Again, to make the data more intuitive, the Q-space difference functions, $\Delta i(Q)$, were then Fourier transformed into real space difference functions, $\Delta T(r)$ using Equation 4 in Matlab (170) as described Section 2.1.1.1, and the higher frequency counts (Q > 0.2 $Å^{-1}$) were set to zero to reduce noise as described in Section 2.2.6.1. The $\Delta T(r)$ were then fit using NXFit (171) in Matlab, utilising two Sr-O and Ca-O peaks (as in Martin (2012) (150)), as initial attempts to fit with only one Sr-O and Ca-O peak gave fits that did not adequately represent the data. This was established through visual comparison of the $\Delta T(r)$ with the fit, and the fitting parameter, $R^2$, indicating lowering towards one with the additional peaks, indicating an improved fit. The region beyond 3Å was ignored for the purposes of the fitting as the assumption of isomorphism breaks down as discussed previously. The parameters of the Ca-O and Sr-O separations could then be used in the fit of the whole $T(r)$ for each composition.

### 2.2.7 Raman spectroscopy for studying the medium range order of SrAW with increasing Sr content

Raman spectroscopy was used to further explore the short and medium range order of the SrAW glass, to provide complementary data to that collected in the neutron diffraction and NMR experiments. This is because the Raman spectral peaks could be used to determine the speciation of the

Si and P tetrahedral present in the SrAW glass, and whether these changed with the substitution of Sr into the material.

Powdered samples of each of the six glass compositions were placed on silica slides. A HORIBA XploRA instrument with 532 nm laser wavelength and 100×/0.75 NA objective in confocal mode was used for Raman spectroscopy and 15 spectra were obtained for each of the glass compositions. Spectra were obtained using the HORIBA LabSpec software set at 15 second laser exposure and resulting in ~7 mW power at the sample with each measurement averaged over 6 spectral acquisitions (technical repeats). Acquired spectra were background corrected with a $4^{th}$ degree polynomial using RamanToolSet (177), before being analysed using IGOR Pro. A series of averages of 2 spectra, 3 spectra, etc. up to all 15 being averages was made, randomly for each of the glass compositions. These averages were then fit over the 772-1240$cm^{-2}$ region, utilising four peaks at: 864, 950, 960, 1039$cm^{-2}$ , assigned to $Q^0$ Si-O-Si asymmetric stretch, $Q^0$ $PO^{-1}$ $v_1$, $Q^2$ Si-O-Si asymmetric stretch and a high wavenumber band (HWB) region (consisting of $Q^1$, $Q^2$ and $Q^3$ Si contributions), respectively (85,178–183). The position of the 1039$cm^{-2}$ peak was fixed to reduce the variation in the fittings of the other peaks and to allow for the fitting to complete, as otherwise this relatively broad and poorly defined shoulder peak caused the fittings to fail. An uncertainty in the fitting parameters was estimated by fitting the averages of 15 spectra plus or minus the standard error of the average. This gave an upper and lower estimate of the fitting parameters.

Due to the way in which the Raman spectra are produced the ordinate axis in Raman spectra is described in “arbitrary units” and so this must be considered during analyses. This is because although this is related to the intensity of photons scattered by the material, the value can change depending on the intensity of the laser and the angle of the sample to the incoming laser (183). When using a powdered sample (where the laser will be interacting with a number of arbitrarily oriented samples) this will result in arbitrary intensities.

### 2.2.8 SrAWGC disc production

The SrAW glass powder must be heat treated for it to fuse and partially crystallise into SrAWGC, where it forms a single body with vastly improved mechanical properties (102,119). The SrAWGC discs were produced using a polymer slurry method developed in the David Wood Laboratory for AWGC, described in Serna (2016) (103), whilst the heating regime also utilised work from the David Wood Laboratory, described in Vickers (2013) (102). First "green bodies" (constructs of the right form but not heat treated) were produced, by mixing the glass powder with PVA in water to form a "glass slurry" and then applying a known quantity of this to moulds. The molar ratios of the slurry can be seen in Table 7. Once dry, the green bodies were then heat treated in a furnace to produce the finished SrAWGC discs. The polymer for making the slurry was composed of 5.34% (w/w) of poly-vinyl-acetate (PVA) diluted with water (this can be determined from Table 7) and was made in 500ml batches.

| | water | PVA | glass |
|---|---|---|---|
| weight % | 54.3 | 2.9 | 42.8 |
| mol % | 81.5017 | 0.0004 | 18.4979 |

**Table 7: Weight and molar percentage ratios of the components of the glass-PVA slurry used in the creation of the 0 mol% SrAWGC discs**

First, 500ml of ultrapure water was placed in a glass beaker. The ultrapure water was produced by a Purite Ondeo IS machine with resistivity between 17.6 and 18.2 MΩ. The beaker was then covered with foil and heated using a magnetically stirred heating plate to 91°C. 26.7g of high molecular weight polyvinyl alcohol (PVA, Mowiol® 56-98, Mw~195000, Aldrich) was weighed out on a Sartorious Roughing Balance (to the nearest 0.1g) then gradually added to the stirring water over the course of an hour. The PVA could not be added all at once as it would clump and fail to dissolve fully.

The green bodies were made in batches, using 5g of 0 Mol% SrAW glass powder, however to ensure there was a fixed molar ratio of the different

glass compositions the mass of the strontium SrAW glass compositions had to be adjusted to account for their higher molecular weights, due to Sr being more massive than Ca. The altered molecular weights of each composition (see Table 2) were used to calculate new weight percentages using the molar percentages in Table 7. These could then be re-normalised into new weight percentages for each composition of SrAW, seen in Table 8.

| Mol% Sr | weight % | | |
|---|---|---|---|
| | water | PVA | Glass |
| 0 | 54.3 | 2.9 | 42.8 |
| 6.2 | 53.2 | 2.8 | 43.9 |
| 12.5 | 52.2 | 2.8 | 45.0 |
| 18.7 | 51.2 | 2.7 | 46.1 |
| 24.9 | 50.2 | 2.7 | 47.1 |
| 37.4 | 48.4 | 2.6 | 49.0 |

**Table 8: Adjusted weight percentage ratios for the components of the glass-PVA slurry used in the creation of the six compositions of discs within increasing Sr content.**

The appropriate amount of PVA-water solution was measured out using a weighing scale (due to the viscosity) into a separate beaker and placed on a magnetic stirrer. Whilst continually stirring, the appropriate amount of <45μm glass powder (according to Table 8) was added gradually to ensure thorough mixing. This was repeated for each glass composition. These were mixed for 1 hour to fully homogenise the PVA-glass slurry.

Once homogenised the glass slurry was dispensed with a pipette onto multi-well plate lids (clear 96 and 24 well plates, Corning). These had been greased with paraffin wax to prevent adhesion of the slurry to the well plate lid. Discs were made of varying sizes with corresponding volumes of slurry

per well, however all retained the same ratio of “area of well” to “volume of slurry” based on 96-well plate (0.32cm$^2$ area) using 83µl of slurry. For example, 48 well-plates with an area of 1cm$^2$ used 166µl per well. The slurry was then left to dry in the well-plate lid “moulds” for 24 hours.

Once dried, the disc green bodies were carefully detached from the greased well-plate lids. These were then distributed onto plates of carbon free investment material (which acted as a support) which were then placed into the furnace. The discs were placed round side down on the investment material, to ensure as much of the disc was exposed to the air inside the furnace as possible. The furnace was then set to undergo a heat treatment in three stages:

1. Room temperature up to 1050°C at 10°C/min
2. Hold at 1050°C for 2 hours
3. Cool at 10°C/min.

The initial step facilitated the burnout of the polymer binder. The second stage sintered and partially crystallised the SrAW into SrAWGC. Once cool the discs were then ready to be used in further experiments. The discs were autoclaved prior to use in any biological experiments.

A scanning electron microscope (SEM) was used to take pictures of the disc surface to determine whether there were any obvious morphological changes resulting from the substitution of strontium into the SrAW. The samples were then mounted onto aluminium SEM stubs with adhesive pads and silver dag (a viscous conductive silver paint from Agar Scientific, see (184) page 43) was applied to ensure conduction between the surface of the discs and the stub. These were then sputter coated with approximately 20nm thick layer of Au (gold) using an Agar Auto Sputter Coater to form a conducting layer across the sample. Images were taken of the centre of three discs for each compositions, for two 2 different batches, using an accelerating voltage of 20V and probe current of 60µA in a Hitachi S3400N variable pressure SEM. Secondary electron mode was used as it provides increased edge detection, which would be useful for analysing the disc surface morphology.

## 2.3 Results

### 2.3.1 Glass manufacture

Initially, the SrAW glass was produced in six different compositions with increasing strontium content, from 0 to 37.4 Mol%. This was made using two different methods, with a more general bulk method used for the majority of the work in this thesis, and a method specifically for the neutron diffraction experiment, which utilised platinum crucibles to avoid ions leaching from the crucibles into the glass.

The glass produced by the more general bulk melt-quench method (see section 2.2.1) came out as a glassy frit without apparent phase separation. The dry frit for every composition of SrAW glass was successfully ground using the puck mill. The 15 minute grinding regime resulted in 50% (w/w) of the SrAW glass being ground to <45 µm diameter. This was determined using a sieve stack.

The glass production for the neutron diffraction (utilising platinum crucibles) yielded glass beads that were transparent for all compositions described. These glass beads could be readily crushed with a percussion mill and ground with a pestle and mortar into a fine powder for use in the neutron diffraction experiment.

### 2.3.2 Solid state MAS-NMR on SrAW glass

$^{31}P$ and $^{29}S$ MAS-NMR was performed on the SrAW glass compositions to determine whether the substitution of strontium into the material altered the P and Si environments within the glass. The $^{31}P$ and $^{29}S$ MAS-NMR spectra can be seen in Figure 13 and Figure 14 respectively, whilst the chemical shifts for each composition can be seen in Table 9. For all of the glass compositions the $^{31}P$ spectra appeared very similar, displaying a single main peak at ~2.5ppm, assigned to orthophosphate ($PO_4^{3-}$, $Q^0$) (150,157,159,160,185,186), however the peak was seen to move with strontium content of the SrAW glass, starting at 2.26ppm for 0 Mol% Sr and rising monotonically to 2.79ppm for 37.4 Mol% Sr (see Figure 13). The

addition of a second smaller peak (at ~-5ppm) improved the fits to the $^{31}P$ MAS-NMR spectra for every composition, due to the slight asymmetry in the lower part of the peak, potentially suggesting a small amount of a second species. The identity of this species is potentially $Q^1$ phosphate, however it could also be another peak of $Q^0$ phosphate as it remains in the region in which this species has been measured (187,188) However, these secondary peaks accounted for only ~2% of the total area and the spectra lacked noticeable sidebands and hence did not suggest the presence of other forms of phosphate within the material.

| Nucleus | $^{29}Si$ | | | | | | $^{31}P$ | |
|---|---|---|---|---|---|---|---|---|
| Glass (mol% SrO) | Environment (area %) | $\delta_{iso}$ (ppm) | Width (ppm) | Environment (area %) | $\delta_{iso}$ (ppm) | Width (ppm) | $\delta_{iso}$ (ppm) | Width (ppm) |
| 0 | $Q^2$/72 | -80.4 | 12.4 | $Q^3$/28 | -88.11 | 17.44 | 2.26 | 7.05 |
| 6.2 | $Q^2$/72 | -80.94 | 12.34 | $Q^3$/28 | -88.41 | 16.96 | 2.36 | 7.07 |
| 12.5 | $Q^2$/76 | -80.84 | 12.2 | $Q^3$/24 | -88.39 | 16.28 | 2.43 | 7.01 |
| 18.7 | $Q^2$/78 | -80.92 | 12.33 | $Q^3$/22 | -88.6 | 15.04 | 2.49 | 6.92 |
| 24.9 | $Q^2$/69 | -81.17 | 11.8 | $Q^3$/31 | -88.29 | 16.41 | 2.69 | 6.93 |
| 37.4 | $Q^2$/89 | -80.01 | 12.64 | $Q^3$/11 | -88.84 | 17.17 | 2.79 | 6.71 |

**Table 9: Solid state $^{29}Si$ and $^{31}P$ MAS-NMR parametrisation for each of the compositions of SrAW glass (with 0, 6.2, 12.5, 18.7, 24.9 and 37.4 Mol% Sr). The position and width of the two main silicon peaks and the main phosphorus peak are displayed. The area percentage and $SiO_4$ speciation of each main peak is also shown for the silicon. Measurements were taken of a single batch of each composition.**

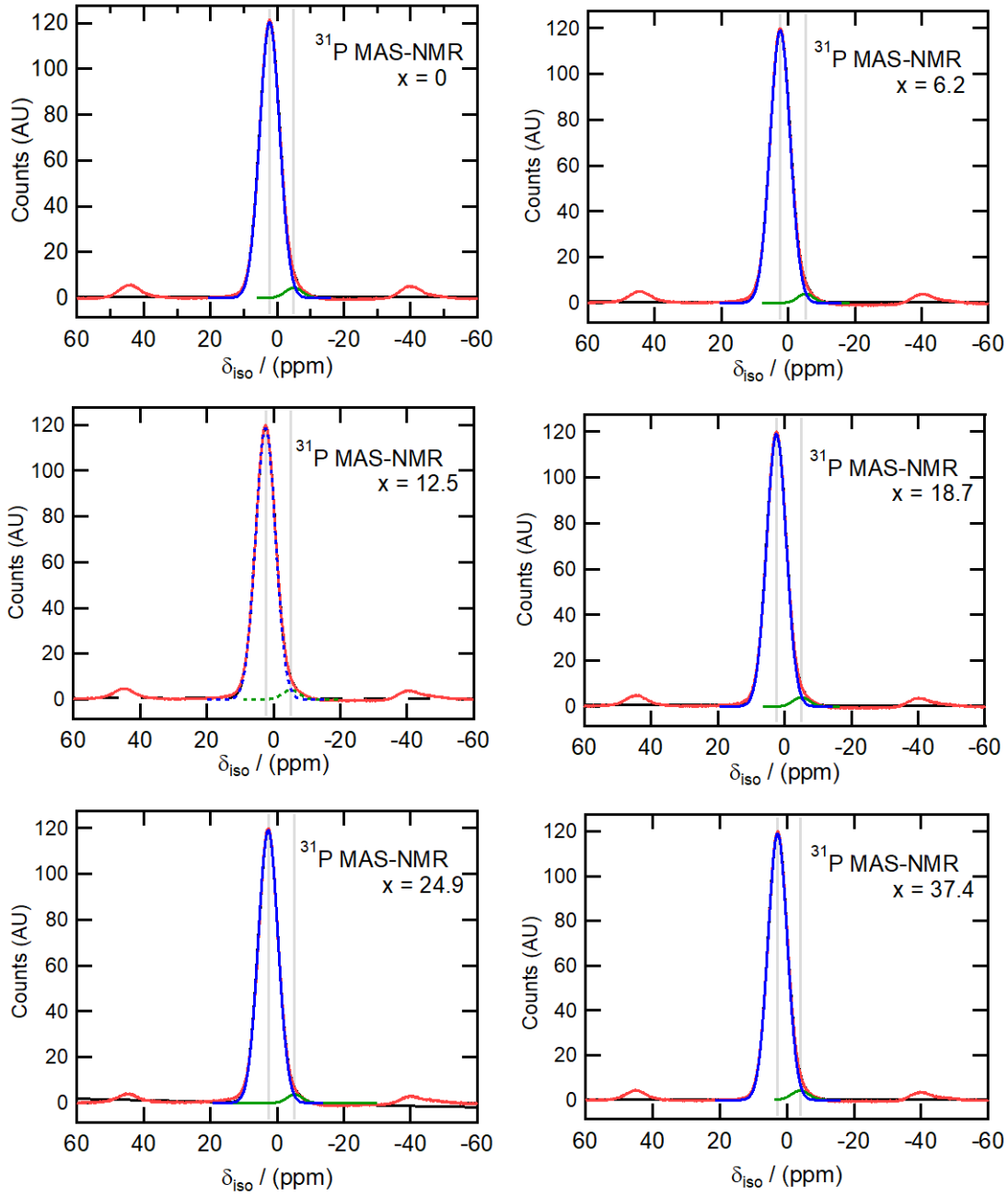


**Figure 13: Solid state $^{31}$P MAS-NMR for the SrAW glass compositions, with x=0, 6.2, 12.5, 18.7, 24.9 and 37.4 Mol% Sr. The traces are: red, the original data; blue, the main peak fit; green, the ancillary peak fit; black, the total fit. Measurements were taken of a single batch of each composition.**

The $^{29}$Si MAS-NMR signals displayed a broad asymmetric peak for all of the SrAW glass compositions at ~ -82 ppm, with only the 37.4 Mol% Sr compositions having an additional side peak (see Figure 14).

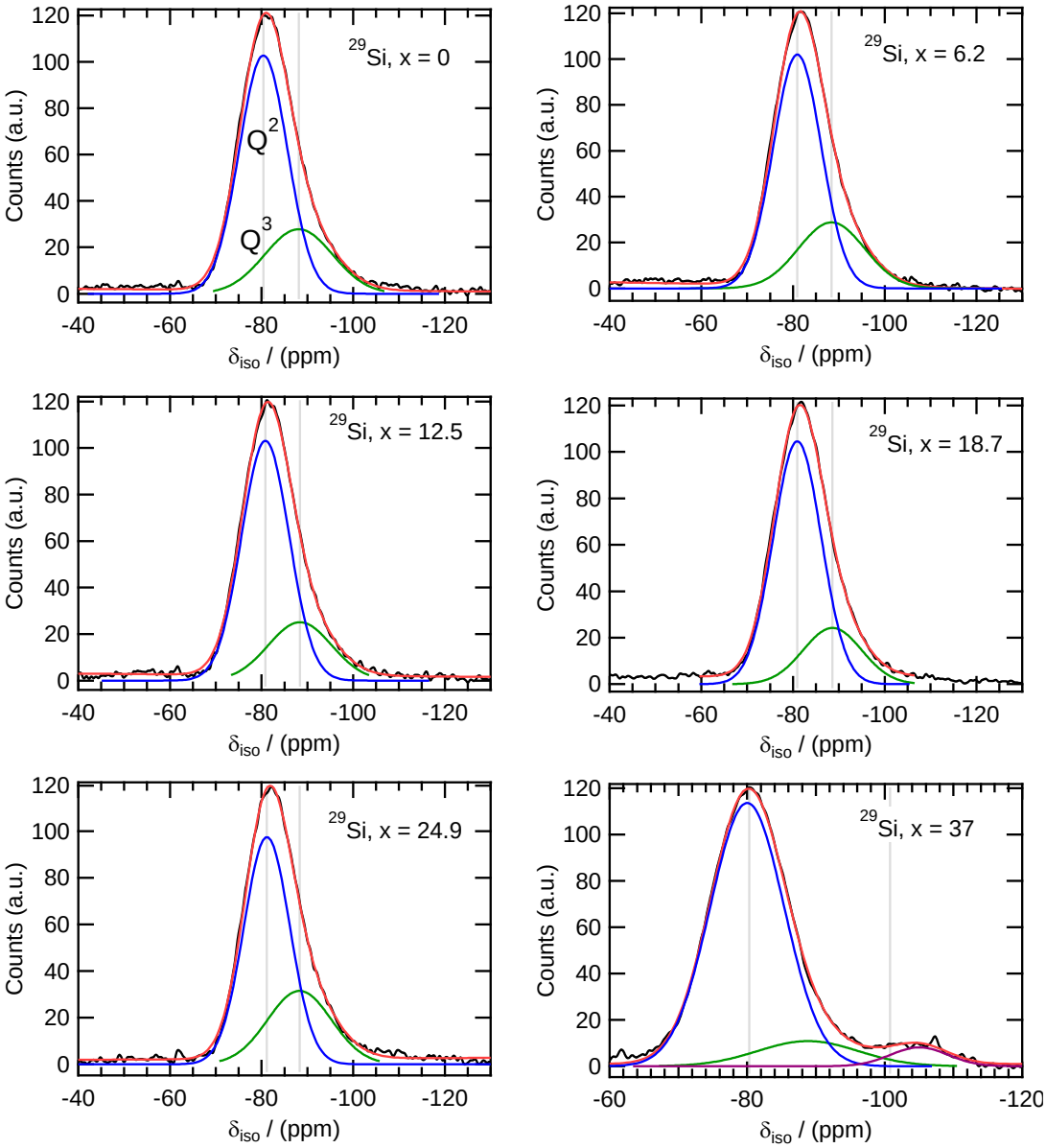


**Figure 14: Solid state $^{29}$Si MAS-NMR for the SrAW compositions, with x=0, 6.2, 12.5, 18.7, 24.9 and 37.4 Mol% Sr. The data is shown in black, with the deconvolutions shown in blue ($SiO_4$ $Q^2$) and green ($SiO_4$ $Q^3$). The 37.4 Mol% showed an additional peak which is in purple. The final fit to the data is in red. Measurements were taken of a single batch of each composition.**

To accommodate the asymmetry of the peaks, two peaks were used for the fittings with one at ~ -81ppm and another at ~ -88ppm, which were associated with the $Q^2$ and $Q^3$ Si tetrahedra, respectively (see Table 9)(150,186,189,190). The ~88ppm ($SiO_4$ $Q^3$) peak was seen to be between

11 and 28% of total area of the two peaks across the glass compositions, with the percentage decreasing with strontium content, excepting the 24.9 Mol% Sr composition which showed an increase to 31% $Q^3$. These peaks were relatively unchanged between the different compositions, with the exception of the 37.4 Mol% Sr composition, which required a third peak to accommodate the more pronounced shoulder peak of the NMR signal. This additional 37.4 Mol% Sr peak was at -105.03ppm (width of 9.87ppm), was 5.5% of the area of the ~81ppm $Q^2$ peak and was associated with $Q^4$ $SiO_4$ (190–192).

### 2.3.3 Density of the SrAW glass compositions with increasing Sr content

The density of the different glass compositions was measured to determine whether the substitution of strontium into the SrAW altered its density. Determining how the density changed with strontium content was important for establishing the way in which the different compositions can be used to make scaffolds (such as discs) and was also a critical factor when filtering, analysing and interpreting the neutron diffraction data. The density was measured using a helium pycnometer, which measures the volume of a sample, from which the density can be calculated using the sample weight. The density of the SrAW glass compositions were found to increase linearly and monotonically with strontium content (Figure 15). A Dunn-Holland-Wolfe test was used to compare the data, as the conditions had different numbers of repeats (5 for 0 and 6.2 Mol% Sr, 4 for 12.5, 18.7 and 24.9 Mol% Sr and 6 for 37.4 Mol%), finding that 24.9 and 37.4 were significantly increased above the 0 Mol% composition ($p < 0.05$).

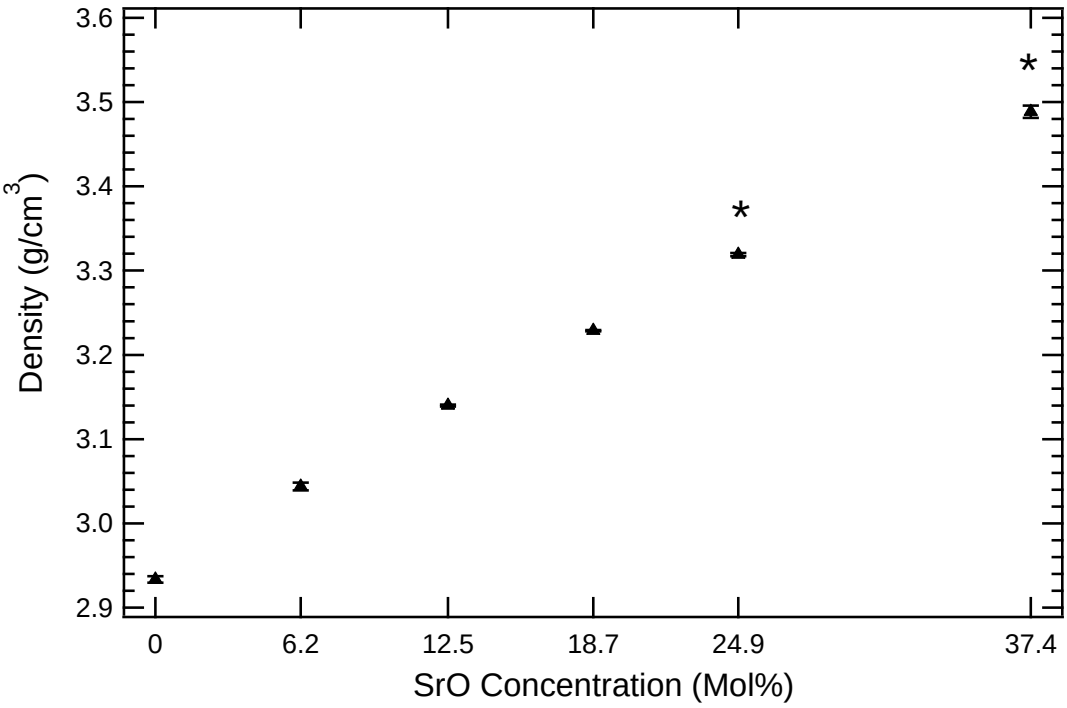


**Figure 15: The density of the different SrAW compositions against their Mol% Sr content. The * indicate a significant difference ($p<0.05$) from the 0 Mol% Sr composition (n=4 to 6 technical repeats). Measurements were taken of a single batch of each composition.**

### 2.3.4 Neutron diffraction of SrAW glass to determine the effect of Sr content on short range order

#### 2.3.4.1 Neutron diffraction data acquisition and cleaning

Neutron diffraction was performed on the different glass compositions to determine whether the substitution of strontium into the SrAW glass had significant effects on its short-range order. The glass powder for each SrAW composition produced in Section 2.3.1 was loaded into vanadium cans and then placed into the GEM detector. The neutron diffraction measurements were successfully taken (the DCS) for all samples, and GUDRUN was successfully used to the clean the data (see section 2.2.6.1). The scattering weighting factors for the total correctional functions, T(r), were calculated (using Xsect, Equation 3) which can be seen in Table 10.

| | Neutron weighting factors (mbarns) | | | | | |
|---|---|---|---|---|---|---|
| | $^{x=0}i(Q)$ | $^{x=6.2}i(Q)$ | $^{x=12.5}i(Q)$ | $^{x=18.7}i(Q)$ | $^{x=24.9}i(Q)$ | $^{x=37.4}i(Q)$ |
| $p_{Si-Si}(Q)$ | 22.53 | 22.53 | 22.53 | 22.53 | 22.53 | 22.53 |
| $p_{P-P}(Q)$ | 13.78 | 13.78 | 13.78 | 13.78 | 13.78 | 13.78 |
| $p_{Ca-Ca}(Q)$ | 42.04 | 36.86 | 31.59 | 26.41 | 21.23 | 10.78 |
| $p_{Mg-Mg}(Q)$ | 7.57 | 7.57 | 7.57 | 7.57 | 7.57 | 7.57 |
| $p_{O-O}(Q)$ | 202.84 | 202.84 | 202.84 | 202.84 | 202.84 | 202.84 |
| $p_{F-F}(Q)$ | 0.94 | 0.94 | 0.94 | 0.94 | 0.94 | 0.94 |
| $p_{Sr-Sr}(Q)$ | N/A | 11.27 | 22.72 | 33.99 | 45.26 | 67.99 |
| $p_{Si-P}(Q)$ | 55.64 | 55.64 | 55.64 | 55.64 | 55.64 | 55.64 |
| $p_{Si-Ca}(Q)$ | 51.63 | 51.63 | 51.63 | 51.63 | 51.63 | 51.63 |
| $p_{Si-Mg}(Q)$ | 58.30 | 58.30 | 58.30 | 58.30 | 58.30 | 58.30 |
| $p_{Si-O}(Q)$ | 62.94 | 62.94 | 62.94 | 62.94 | 62.94 | 62.94 |
| $p_{Si-F}(Q)$ | 61.33 | 61.33 | 61.33 | 61.33 | 61.33 | 61.33 |
| $p_{Si-Sr}(Q)$ | N/A | 76.15 | 76.15 | 76.15 | 76.15 | 76.15 |
| $p_{P-Ca}(Q)$ | 25.58 | 25.58 | 25.58 | 25.58 | 25.58 | 25.58 |
| $p_{P-Mg}(Q)$ | 28.89 | 28.89 | 28.89 | 28.89 | 28.89 | 28.89 |
| $p_{P-O}(Q)$ | 31.19 | 31.19 | 31.19 | 31.19 | 31.19 | 31.19 |
| $p_{P-F}(Q)$ | 30.39 | 30.39 | 30.39 | 30.39 | 30.39 | 30.39 |
| $p_{P-Sr}(Q)$ | N/A | 37.73 | 37.73 | 37.73 | 37.73 | 37.73 |
| $p_{Ca-Mg}(Q)$ | 94.94 | 83.24 | 71.35 | 59.64 | 47.94 | 24.35 |
| $p_{Ca-O}(Q)$ | 102.50 | 89.87 | 77.03 | 64.39 | 51.76 | 26.29 |
| $p_{Ca-F}(Q)$ | 99.87 | 87.56 | 75.05 | 62.74 | 50.43 | 25.61 |
| $p_{Ca-Sr}(Q)$ | N/A | 108.71 | 93.18 | 77.90 | 62.61 | 31.80 |
| $p_{Mg-O}(Q)$ | 16.34 | 16.34 | 16.34 | 16.34 | 16.34 | 16.34 |
| $p_{Mg-F}(Q)$ | 15.92 | 15.92 | 15.92 | 15.92 | 15.92 | 15.92 |
| $p_{Mg-Sr}(Q)$ | N/A | 19.76 | 19.76 | 19.76 | 19.76 | 19.76 |
| $p_{O-F}(Q)$ | 395.27 | 395.27 | 395.27 | 395.27 | 395.27 | 395.27 |
| $p_{O-Sr}(Q)$ | N/A | 490.77 | 490.77 | 490.77 | 490.77 | 490.77 |
| $p_{F-Sr}(Q)$ | N/A | 2.34 | 2.34 | 2.34 | 2.34 | 2.34 |

**Table 10: Weight factors ($w_{ij}$) for each atomic combination calculated for the 0, 6.2, 12.5, 18.7, 24.9 and 37.4 Mol% strontium SrAW composition. These are for the pair correlation functions, $p_{ij}(Q)$, and were determined by Xsect.**

The neutron diffraction signal for each sample is detected by a several detectors in GEM. To form the total correlation function for each composition, $^{x}T(r)$, the signals from the individual banks were combined (see section 2.2.6.1), with the overlaid signals from each detector bank provided in Appendix A (Figure 88 and Figure 89).

Once combined, this produced the neutron diffraction coherent scattering intensity function, $^{x}i(Q)$ for each composition of SrAW, and these can be

seen in Figure 16. There are clear differences between the signals with the Sr content of the SrAW glass for Q < 14Å$^{-1}$ however the meaning of changes are difficult to interpret due to being in reciprocal units.

Putting the reciprocal space neutron diffraction signal, ${}^{x}i(Q)$, through the Fourier transform described in section 2.2.6 converts the signals into real space units (${}^{x}T(r)$) which are then more intuitive to interpret. This Fourier transform requires an estimate of the number density and theoretical cross-sections of the elements in the material, and this was calculated by Xsect.

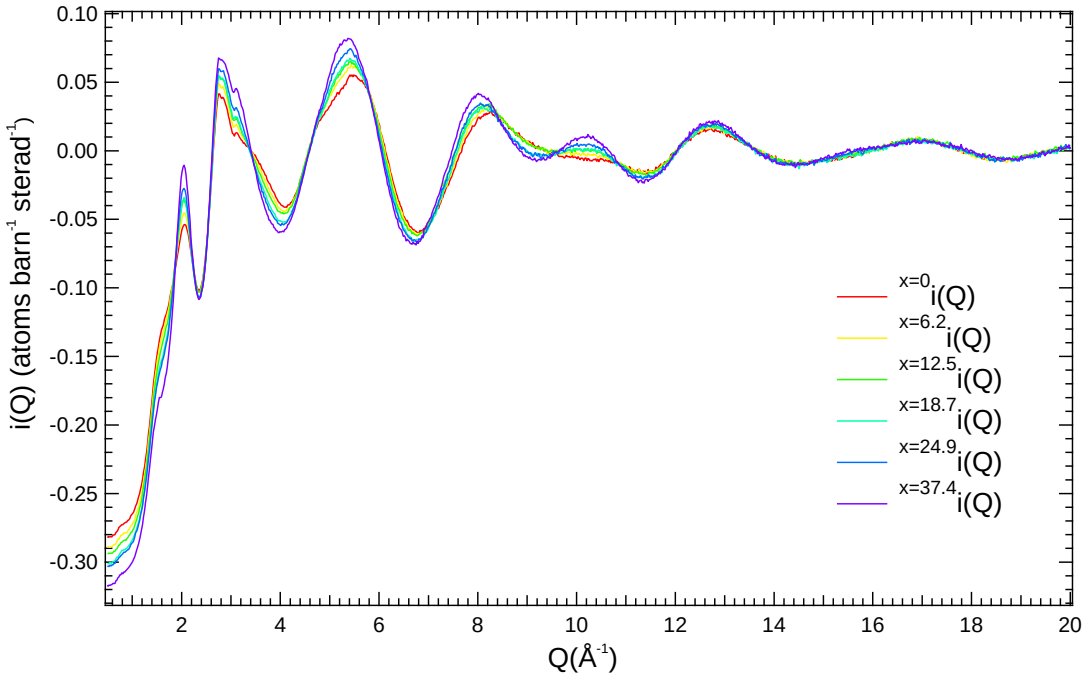


**Figure 16: The final reciprocal space neutron diffraction signal (coherent scattering intensity), $i(Q)$, for SrAW glass with 0, 6.2, 12.5, 18.7, 24.9 and 37.4 Mol% Sr. Measurement was taken of three technical repeats of a single batch of each composition.**

Prior to running the Fourier transform to produce ${}^{x}T(r)$, the signal was set to zero below 0.2Å$^{-1}$, as the lower frequency counts were seen to rise unphysically in the $i(Q)$ below 0.2Å (see Appendix A, Figure 88 and Figure 89), which was an artefact of the detector. ${}^{x}T(r)$ was back-Fourier transformed to give $i(Q)_{low}$ and it was observed that $i(Q)_{low}$ was similar to $i(Q)$. This indicates that removing the <0.2Å$^{-1}$ component did not significantly distort the resulting ${}^{x}T(r)$ (Figure 17 and Figure 18).

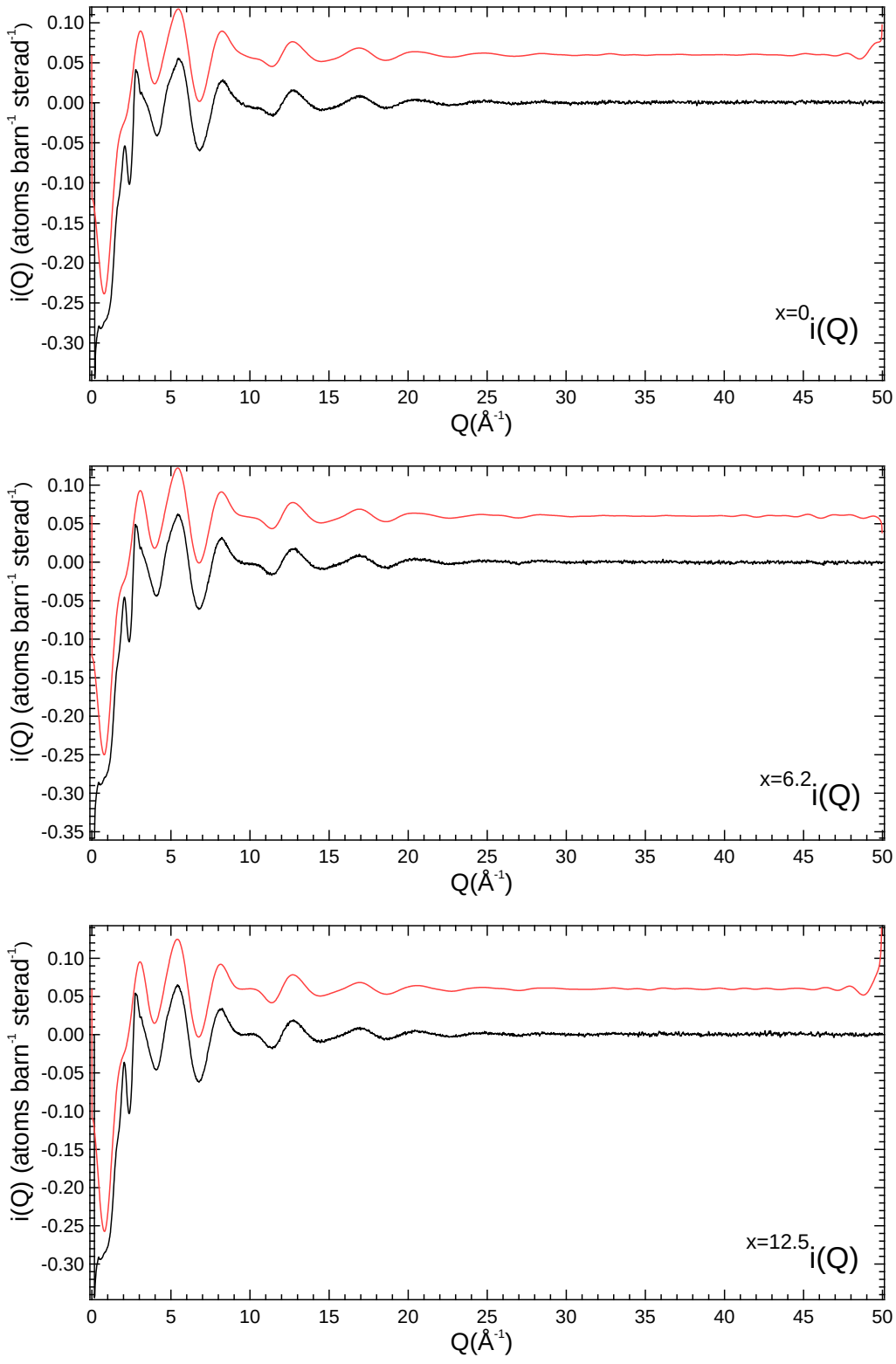


**Figure 17: The coherent scattering intensity, $i(Q)$, for SrAW glass with 0, 6.2, 12.5 Mol% Sr before (black) and after (red) removal of the non-physical low frequency region (<0.2Å$^{-1}$)(and subsequent Fourier transform to $T(r)$ and back Fourier transform to $i(Q)_{low}$). Measurement was taken of three technical repeats of a single batch of each composition.**

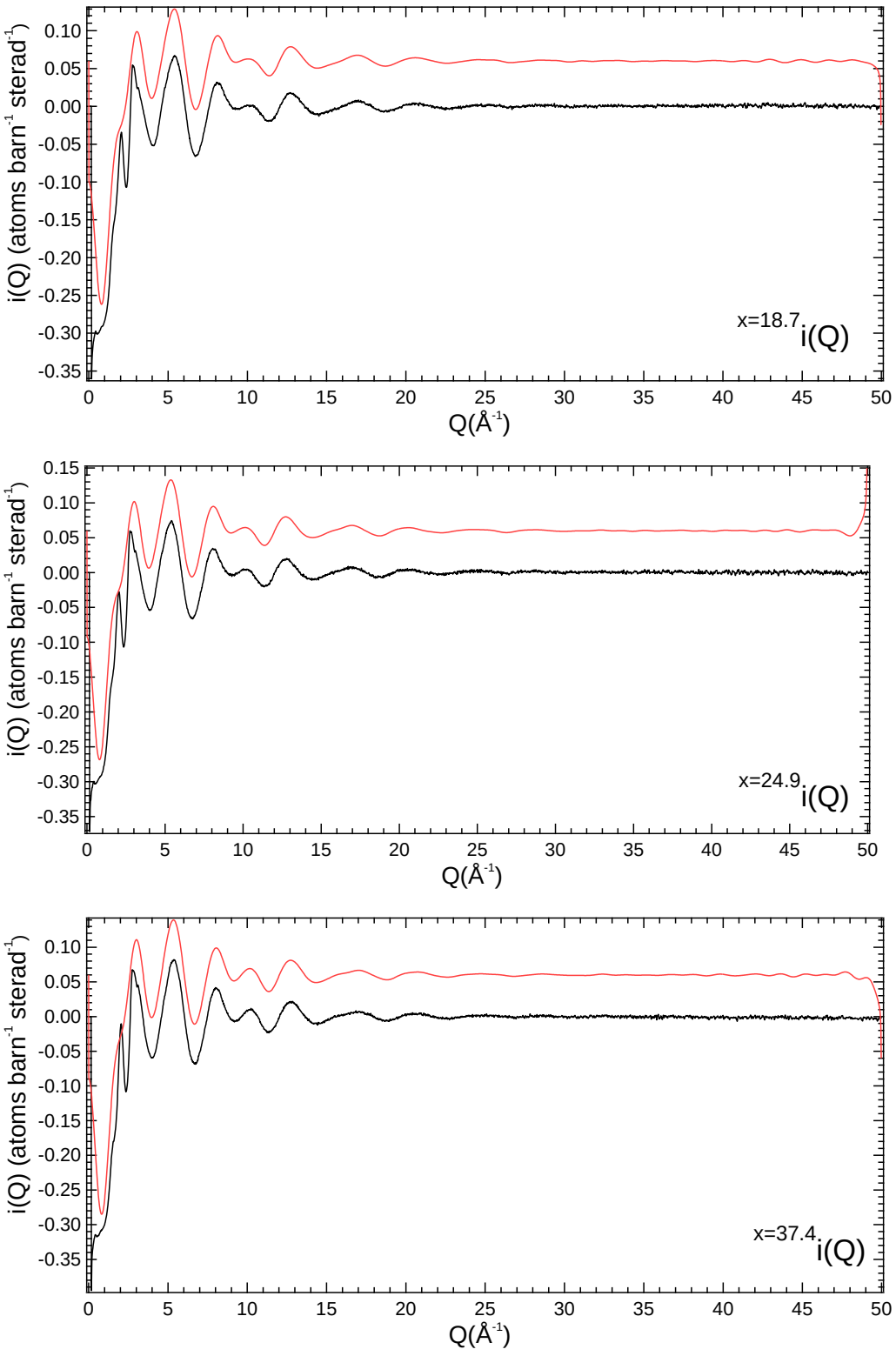


**Figure 18: The coherent scattering intensity, $i(Q)$, for SrAW glass with 18.7, 24.9, 37.4 Mol% Sr before (black) and after (red) removal of the non-physical low frequency region (<0.2Å$^{-1}$)(and subsequent Fourier transform to $T(r)$ and back Fourier transform to $i(Q)_{low}$). Measurement was taken of three technical repeats of a single batch of each composition.**

The total correlation function (real space diffraction pattern), ${}^{x}T(r)$, for each composition can be seen in Figure 19. The ${}^{x}T(r)$ was seen to be composed of three main features for all Sr compositions of SrAW: a peak at ~1.6 Å, a smaller peak at ~1.9 Å and a large feature at 2.6 Å. The region beyond 3 Å was deemed to be a superposition of numerous extended range atomic separations and moves beyond the short-range order. The peak at 1.6Å was determined to be composed of the Si-O and P-O correlations based on previous studies (150,159,160,167,193,194), and was relatively unchanged between the different compositions of SrAW glass. The second smaller peak at 1.9 Å, assigned to Mg-O (172,195,196), was seen to fluctuate slightly but did not have a clear correlation between its changes and strontium content. The third feature was seen to clearly change gradually with strontium content, with a shoulder peak at ~2.2 Å becoming less prominent as the strontium content of the SrAW rose. This third feature was predicted to be composed of a superposition of the longer range O-Si-O and O-P-O separations (O…O), in addition to the Ca-O and Sr-O separations (150,159,160,167,193,194,196,197). Due to the number of peaks convoluted together, determining how these contributions resulted in the observed changes in the ${}^{x}T(r)$ with strontium content of the SrAW glass would require further analysis.

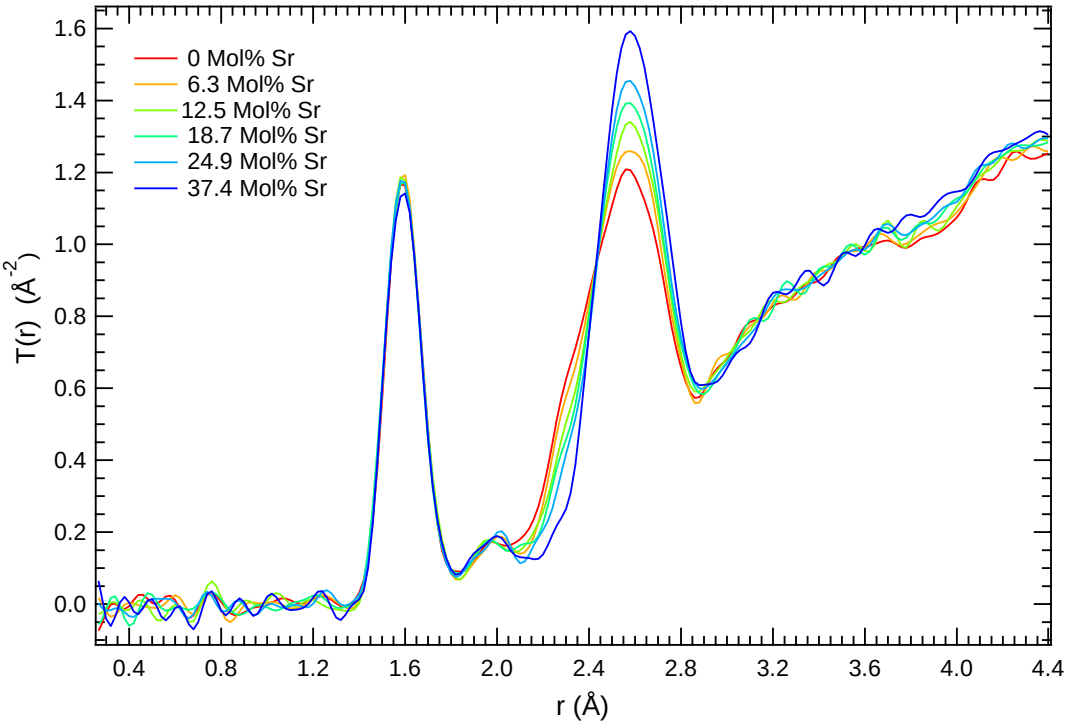


**Figure 19: The real space $T(r)$ neutron diffraction traces (total correlation functions) for the six different SrAW glass compositions with 0, 6.2, 12.5, 18.7, 24.9 and 37.4 Mol% Sr. Measurement was taken of three technical repeats of a single batch of each composition.**

### 2.3.4.2 Isomorphic substitution of neutron diffraction signals to parametrise Strontium and Calcium components

Determining whether the Sr content of SrAW glass affects the short-range order requires the 1.6, 1.9 and 2.6Å features of the $T(r)$ to be deconvoluted for each glass composition. The strontium and calcium components of the $T(r)$ can be studied in isolation by utilising isomorphic substitution (see section 2.2.6.4). By mathematically subtracting the signals from one another, the components associated with Sr and Ca (such as Ca-O and Sr-O) will be left, whilst the components which are unchanged between the compositions (Si, Mg, P), will cancel out. The largest resulting reciprocal-space isomorphic substitution difference functions, $\Delta i(Q)$, between the glass compositions are seen in Figure 20. Smaller differences were not used as they were comparatively weak and hence difficult to fit reliably.

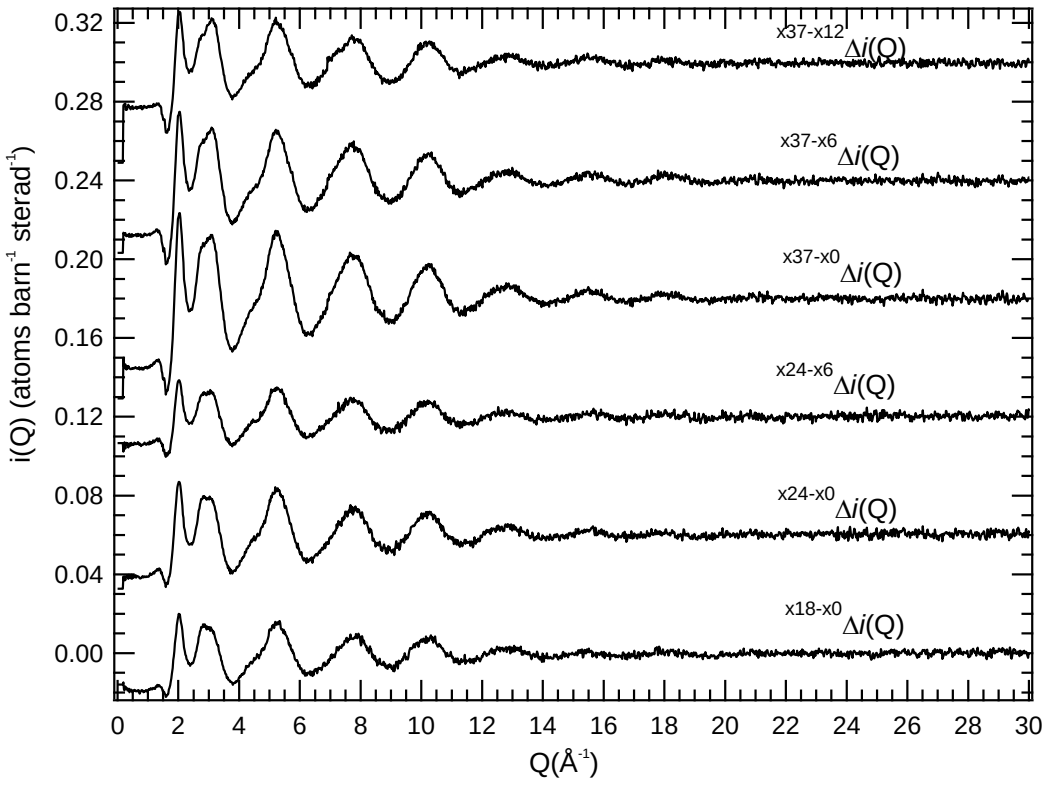


**Figure 20: The reciprocal (Q) space difference functions $\Delta i(Q)$ for the SrAW glass compositions which had the largest residual signal ($^{x37-x12}\Delta i(Q)$, $^{x37-x6}\Delta i(Q)$, $^{x37-x0}\Delta i(Q)$, $^{x24-x6}\Delta i(Q)$, $^{x24-x0}\Delta i(Q)$, $^{x18-x0}\Delta i(Q)$) These are offset, and displayed only shown up to 30Å$^{-1}$ for clarity. Measurement was taken of three technical repeats of a single batch of each composition.**

The corresponding real space difference functions, $\Delta T(r)$, can be seen in Figure 21. The signals have been normalised base on the size of the residual signal, which is the same as the difference in molar Sr content in the compositions. This means $^{x37-x0}\Delta i(Q)$ was divided by 37.4, and $^{x24-x6}\Delta i(Q)$ was divided by 18.7. When comparing the $T(r)$ for the different SrAW compositions (Figure 19) and the $\Delta T(r)$, it is clear that the features at 1.6 Å (Si-O/P-O) and 1.9 Å (Mg-O) have cancelled out in all of the difference functions. There were two prominent peaks remaining in each of the difference functions: a negative amplitude peak at ~2.25 Å and positive amplitude peak ~2.7 Å, both relatively conserved between the difference functions. The difference functions represent the difference in the spectra from substituting in x-y mol% of strontium, for example the $^{x37-x0}\Delta T(r)$ represented the difference induced with 37.4 mol% Sr substituted into the

material, whilst $^{x24-x6}\Delta T(r)$ represented the difference induced substituting 18.7 Mol% of Sr.

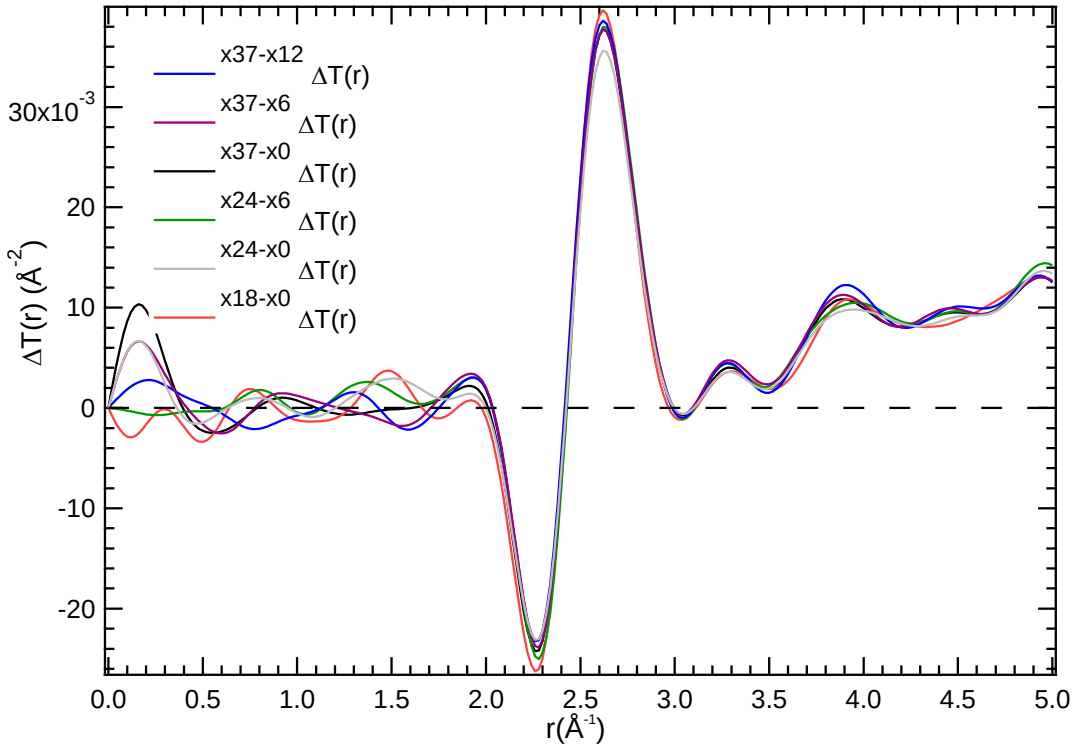


**Figure 21: The real-space difference functions $\Delta T(r)$ for the SrAW glass compositions which had the largest residual signal ($^{x37-x12}\Delta T(r)$, $^{x37-x6}\Delta T(r)$, $^{x37-x0}\Delta T(r)$, $^{x24-x6}\Delta T(r)$, $^{x24-x0}\Delta T(r)$, $^{x18-x0}\Delta T(r)$). These have been overlaid and scaled by the size of the difference for comparison. Measurement was taken of three technical repeats of a single batch of each composition.**

These are seen to overlay in Figure 21 when scaled by the size of the difference, meaning that across the combinations tested, the change in spectra per Mol% Sr substituted for Ca is independent of the Sr content of the material.

As the difference functions were made by subtracting the compositions with less Sr from those with more Sr, the positive amplitude peak will contain the Sr-O correlations, whilst the negative amplitude peak will contain the Ca-O correlations. The features beyond 3 Å cannot be accurately modelled as they fall outside the realm in which isomorphism can be assumed.

NXFit was used to deconvolute the peaks of the $\Delta T(r)$ and describe the Sr-O and Ca-O separations (seen in Figure 22 and Figure 23), with the values for the all of the fits found in Table 11, and the averages across all of the fits found in Table 12. Only Ca-O and Sr-O correlations were fit, as although this region should also contain Ca-F and Sr-F the quantity of fluorine in SrAW is very small. This would make the Ca-F and Sr-F difficult to reliably fit as the signals for these peaks would be two hundred times smaller than those of the Ca-O and Sr-O; due to how much more oxygen there is in the material than fluorine. Additionally, the longer range contributions, such as O-Ca-O or Ca-O-Ca need not be considered as they would be outside the 2-3 Å region being fitted (150). The asymmetric shapes of the Sr (positive) and Ca (negative) peaks suggested two peaks would be required for a good fit. The structural parameters of the fits varied between the $\Delta T(r)$, due to the number of peaks competing during the fitting in NXFit, was within the uncertainty of the technique. The nature of the fit required the 2$^{nd}$ Ca-O and Sr-O peaks to be fit such that they overlapped, essentially cancelling each other out in the total fit, resulting in some variation in the values determined. However, the fitting software, NXFit did take into account the residual strontium content of the different function, and the coordination numbers were restricted so that the values did not become unphysical. The amplitude of the signals in Figure 22 and Figure 23 were also seen to differ between the $\Delta T(r)$, however this was associated with the size of the residual signal.

| $^{x37-x12}\Delta T(r)$ | r (Å) | N | σ (Å) |
|---|---|---|---|
| Ca-O | 2.38 | 4.89 | 0.15 |
| Ca-O (2) | 2.73 | 1.55 | 0.21 |
| Sr-O | 2.52 | 4.34 | 0.16 |
| Sr-O (2) | 2.73 | 1.32 | 0.16 |

| $^{x37-x6}\Delta T(r)$ | r (Å) | N | σ (Å) |
|---|---|---|---|
| Ca-O | 2.38 | 5.00 | 0.14 |
| Ca-O (2) | 2.73 | 1.55 | 0.19 |
| Sr-O | 2.52 | 4.34 | 0.16 |
| Sr-O (2) | 2.73 | 1.36 | 0.16 |

| $^{x37-x0}\Delta T(r)$ | r (Å) | N | σ (Å) |
|---|---|---|---|
| Ca-O | 2.38 | 5.36 | 0.12 |
| Ca-O (2) | 2.73 | 1.89 | 0.12 |
| Sr-O | 2.52 | 4.69 | 0.13 |
| Sr-O (2) | 2.73 | 1.27 | 0.05 |

| $^{x24-x6}\Delta T(r)$ | r (Å) | N | σ (Å) |
|---|---|---|---|
| Ca-O | 2.38 | 5.05 | 0.14 |
| Ca-O (2) | 2.73 | 1.61 | 0.19 |
| Sr-O | 2.52 | 4.34 | 0.16 |
| Sr-O (2) | 2.73 | 1.34 | 0.15 |

| $^{x24-x0}\Delta T(r)$ | r (Å) | N | σ (Å) |
|---|---|---|---|
| Ca-O | 2.38 | 5.25 | 0.15 |
| Ca-O (2) | 2.73 | 1.33 | 0.22 |
| Sr-O | 2.52 | 4.18 | 0.14 |
| Sr-O (2) | 2.73 | 1.36 | 0.12 |

| $^{x18-x0}\Delta T(r)$ | r (Å) | N | σ (Å) |
|---|---|---|---|
| Ca-O | 2.38 | 5.11 | 0.16 |
| Ca-O (2) | 2.73 | 1.47 | 0.20 |
| Sr-O | 2.52 | 4.16 | 0.15 |
| Sr-O (2) | 2.73 | 1.31 | 0.13 |

**Table 11: The structural parameters of the real-space difference functions $^{x37-x12}\Delta T(r)$, $^{x37-x6}\Delta T(r)$, $^{x37-x0}\Delta T(r)$, $^{x24-x6}\Delta T(r)$, $^{x24-x0}\Delta T(r)$ and $^{x18-x0}\Delta T(r)$ of SrAW with varying Sr content, obtained by NXFit. 'r' is the atomic separation, 'N' is the coordination number and 'σ' is the disorder term (describing the thermal and static disorder in the bonds and being related to the widths of the distributions of the atomic separations).**

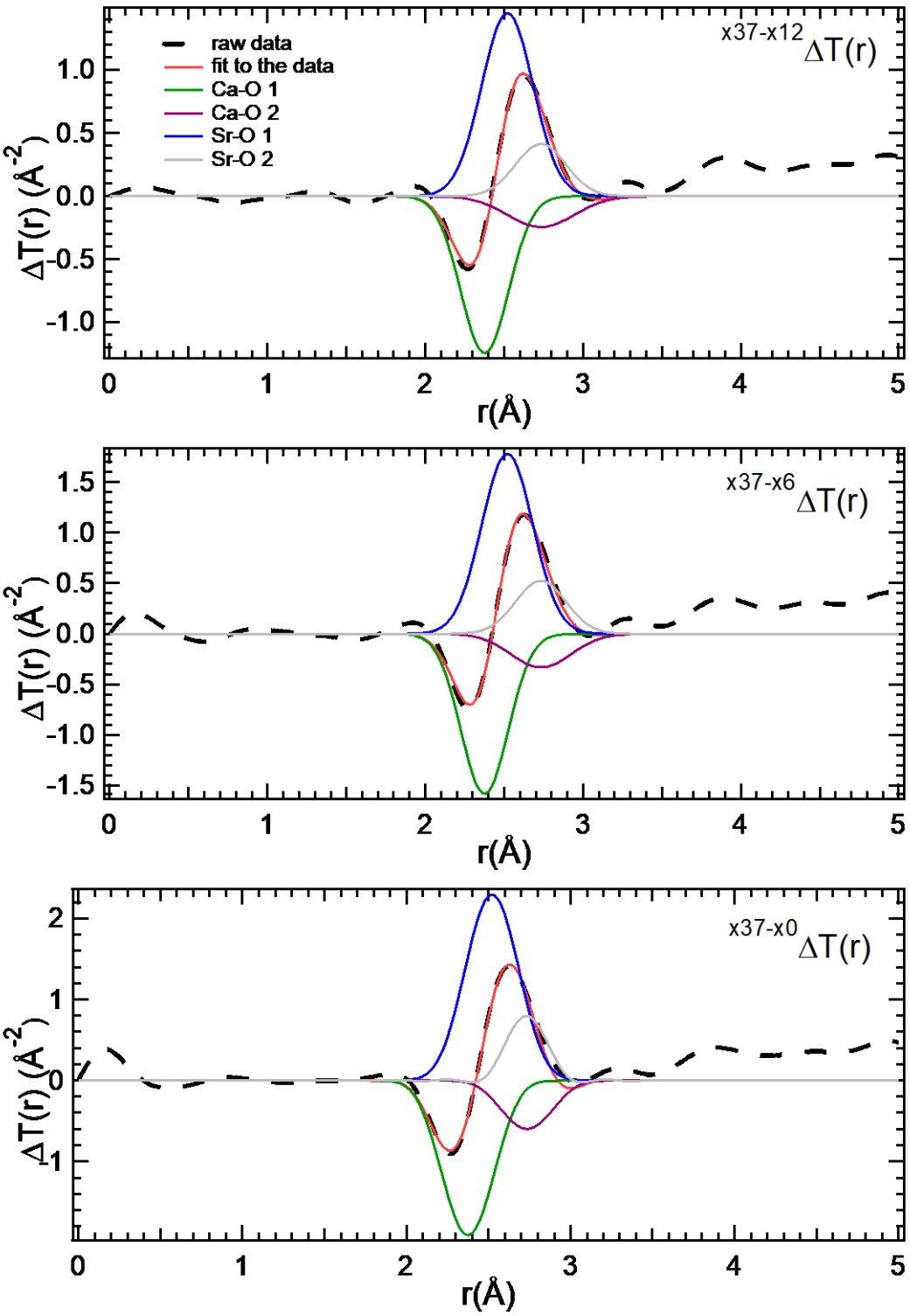


**Figure 22: The NXFit fittings to real-space difference functions $^{x37-x12}\Delta T(r)$, $^{x37-x6}\Delta T(r)$ and $^{x37-x0}\Delta T(r)$ of SrAW with varying Sr content. The curves are described in the key above.**

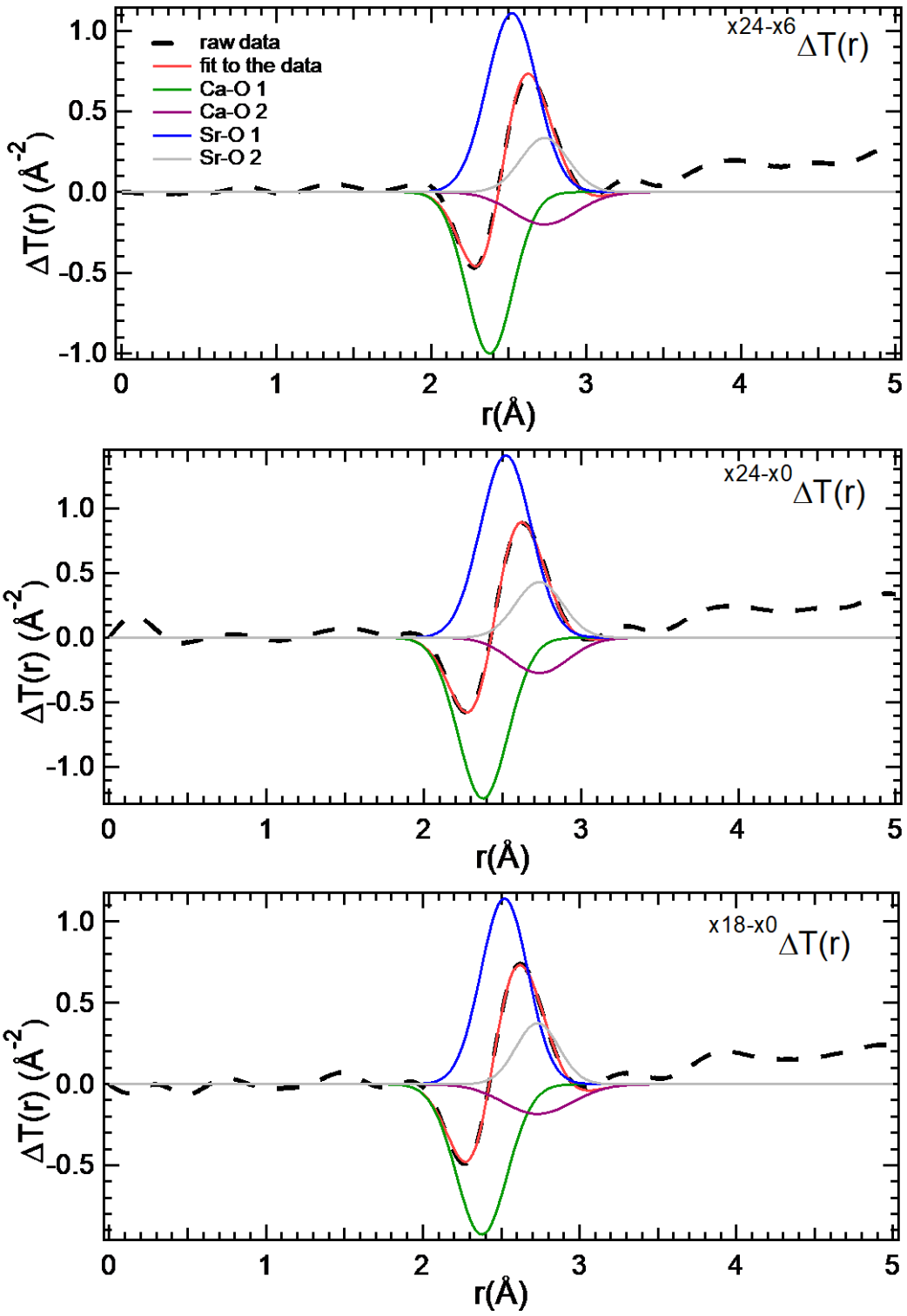


**Figure 23: The NXFit fittings to real-space difference functions $^{x24-x6}\Delta T(r)$, $^{x24-x0}\Delta T(r)$ and $^{x18-x0}\Delta T(r)$ of SrAW with varying Sr content. The curves are described in the key above.**

Finally, the parameters determined for the difference functions across the different compositions of SrAW were averaged to produce an estimate, based on the assumption they did not change significantly between the different compositions (supported by the similarity of the overlapping difference functions in Figure 21). The average of the parameters is seen in Table 12 and was in good agreement with those of strontium doped Bioglass 45S5 studied in (150).

| | SrAW (this study) | | | Sr Bioglass 45S5 | | |
|---|---|---|---|---|---|---|
| | r (Å) | N | σ (Å) | r (Å) | N | σ (Å) |
| Ca-O 1 | 2.38 | 5.11 | 0.14 | 2.33 | 5.4 | 0.1 |
| Ca-O 2 | 2.73 | 1.57 | 0.19 | 2.73 | 1.3 | 0.2 |
| Sr-O 1 | 2.52 | 4.34 | 0.15 | 2.49 | 4.7 | 0.14 |
| Sr-O 2 | 2.73 | 1.33 | 0.13 | 2.75 | 1.3 | 0.14 |

**Table 12: The average of the structural parameters of the real-space difference functions $^{x37-x12}\boldsymbol{\Delta T}(\boldsymbol{r})$, $^{x37-x6}\boldsymbol{\Delta T}(\boldsymbol{r})$, $^{x37-x0}\boldsymbol{\Delta T}(\boldsymbol{r})$, $^{x24-x6}\boldsymbol{\Delta T}(\boldsymbol{r})$, $^{x24-x0}\boldsymbol{\Delta T}(\boldsymbol{r})$ and $^{x18-x0}\boldsymbol{\Delta T}(\boldsymbol{r})$ of SrAW with varying Sr content, obtained by NXFit. 'r' is the atomic separation, 'N' is the coordination number and 'σ' is the disorder term (describing the thermal and static disorder in the bonds and being related to the widths of the atomic separation distributions). The values found by Martin *et al.* 2012 for Sr Bioglass 45S5 are also shown for comparison** (150)**.**

### 2.3.4.3 Parametrising the real-space neutron diffraction signals of SrAW glass with increasing strontium content

The isometric substitution and MAS-NMR results both assist in constraining the potential deconvolutions of the $T(r)$ for the SrAW glass compositions. Once deconvoluted, the $T(r)$ would allow the effect of Sr on the short range order of SrAW to be determined. Stoichiometry and glass theory can be used to further simplify the remaining fitting. To better constrain the initial conditions of the total fit, the ~1.6Å peak in the $T(r)$ of the 0 Mol% strontium SrAW glass was fit independently from the rest of the spectra. This peak was assigned to Si-O and P, based on studies on similar materials (150,159,160,167,193,194). This produced initial Si-O and P-O fitting parameters, seen in Table 13.

| | r (Å) | N | σ (Å) |
|---|---|---|---|
| P-O | 1.54 | 3.92 | 0.03 |
| Si-O | 1.63 | 3.81 | 0.05 |

**Table 13: Si-O and P-O correlations fit in isolation from the rest of the 0 Mol% Sr $T(r)$, for SrAW glass. 'r' is the atomic separation, 'N' is the coordination number and 'σ' is the disorder term (describing the thermal and static disorder in the bonds and being related to the widths of the distributions of the atomic separations).**

These initial estimates of the Si-O and P-O correlations, combined with the MAS-NMR data allow the O…O bond parameters to be estimated. The O-Si-O and O-P-O bond lengths were calculated using the geometry of tetrahedra (as described in section 2.2.6.3), giving values of 2.51Å for O-P-O, 2.66Å for O-Si-O and 2.61Å for the combined O...O separation. The disorder factor, σ (describing the thermal and static disorder in the bonds and being related to the widths of the distributions of the atomic separations), was calculated in the same manner yielding 0.05Å, 0.08Å and 0.07Å for O-P-O, O-Si-O and O…O respectively. The weighted average of the O…O coordination numbers can also be estimated, utilising the MAS-NMR results which found the silicon to be in a mixture of $Q^2$ (~73.4%) and $Q^3$ (~26.6%) environments. The oxygen in a $Q^2$ Si tetrahedron has four nearest neighbour oxygens and whilst those in $Q^3$ Si tetrahedra have 4.8 (see section 2.1.1.4). Hence, the estimated average coordination number of the O-Si-O in the 0 Mol% SrAW glass would be N = 4.22. The phosphorus in the SrAW compositions were all found to be orthophosphate ($Q^0$), which results in a O-P-O coordination number of N = 3. Combining $N_{O\text{-}Si\text{-}O}$ and $N_{O\text{-}P\text{-}O}$ as a weighted average (see section 2.2.6.3) led to the estimate of $N_{O\ldots O}$ = 3.87 for the O…O coordination number.

With the estimates for the Si-O, P-O, O...O, Ca-O and Sr-O established, the fitting process for the $T(r)$ of each SrAW composition was greatly simplified (as only the Mg-O peak was unknown). The fits using NXFit to the whole $T(r)$ for each composition of SrAW glass (with increasing strontium content) are shown together in Figure 24. The total fittings were seen to reflect the data, though clearly the region beyond 3.0Å was not fit and ignored.

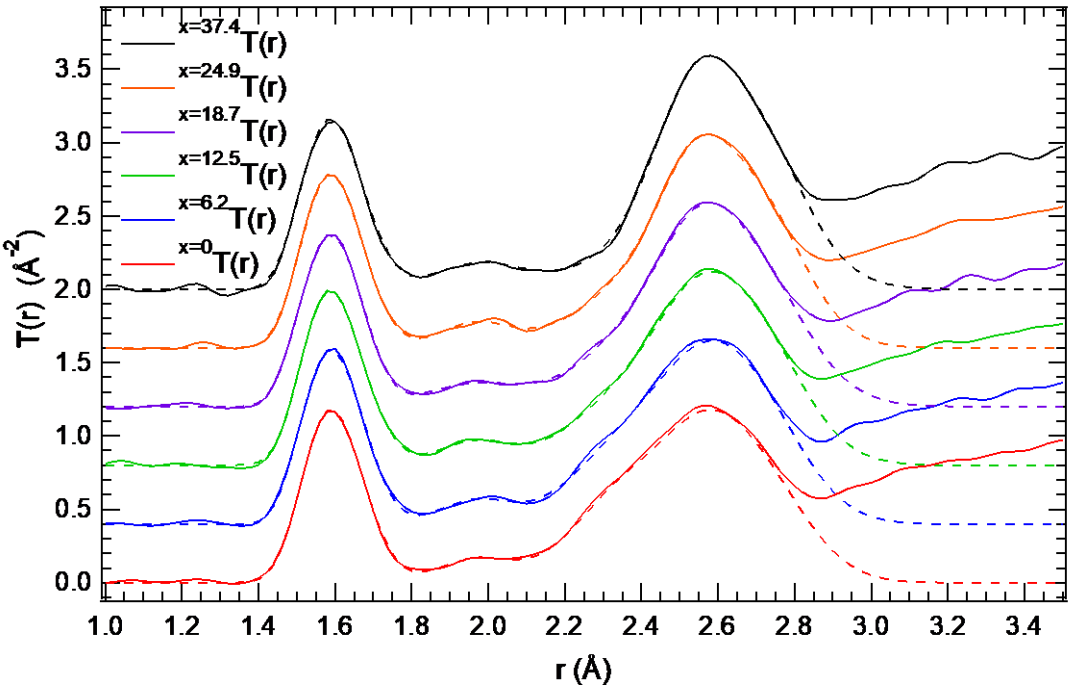


**Figure 24: The fittings to the real space $T(r)$ neutron diffraction traces (total correlation functions) for the six different SrAW glass compositions with 0, 6.2, 12.5, 18.7, 24.9 and 37.4 Mol% Sr, offset for clarity. The region beyond 3Å was ignored during the fitting as this is beyond the short range order and due to the large number of overlapping bonds putting the analysis beyond the scope of this work. Measurement was taken of three technical repeats of a single batch of each composition.**

The individual fittings for the 0 and 6.2 Mol% Sr compositions can be seen in Figure 25, whilst the parameters for these fits are shown in Table 14. The peaks (representing the Si-O, P-O, Mg-O, Ca-O, Sr-O and O…O atomic separations) were not seen to change in position significantly with strontium content, as seen when 6.2 Mol% was added in Figure 25. Despite the 0 Mol% Sr composition being fit in NXFit with Sr-O peaks, these are not visible in Figure 25 as the software set their amplitude to zero based on the elemental abundance in the composition. However, for the 6.2 Mol% Sr composition the Sr-O peaks can be seen, along with a subsequent decrease in the amplitude of the Ca-O peaks (associated with the substitution of Ca for Sr).

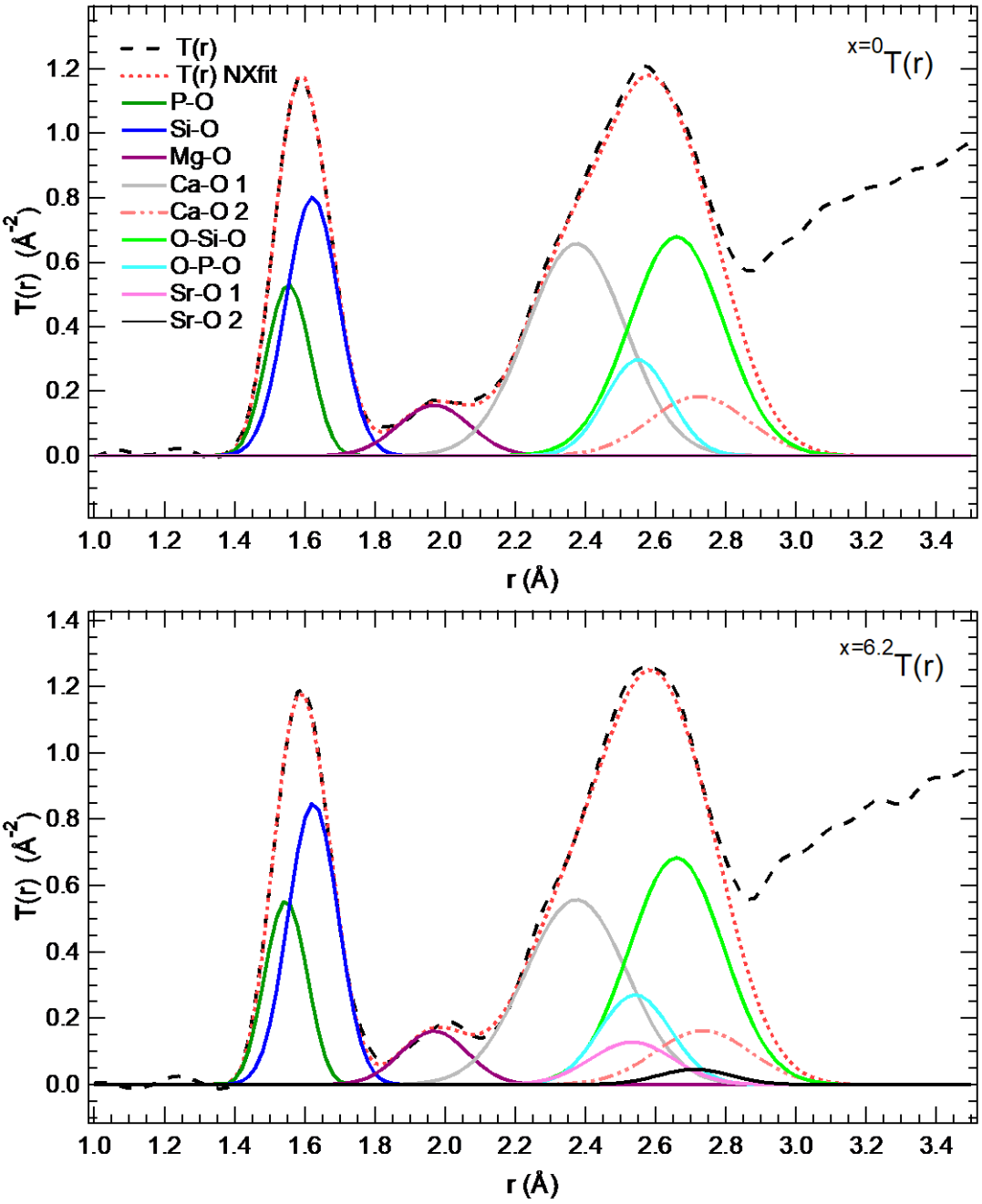


**Figure 25: The full deconvolutions of the real space $T(r)$ neutron diffraction traces (total correlation functions) for the SrAW glass compositions with 0 and 6.2 Mol% Sr, fit using NXFit. The region beyond 3Å was ignored during the fitting as this is beyond the short range order and due to the large number of overlapping bonds putting the analysis beyond the scope of this work. The Sr-O correlations are zeroed in the $^{x=0}T(r)$ as that composition had no Sr.**

This largely explains the change in the shape of the 2.6Å region with SrAW strontium content as the 1st Ca-O peak lies under the shoulder at 2.3Å and so as the Ca is substituted for Sr in the material this shoulder peak disappears. The structural parameters were seen to be relatively unchanged between the 0 and 6.2 Mol% Sr compositions (Table 14).

Figure 26 shows the individual fittings for the 12.5 and 18.7 Mol% Sr compositions, whilst the parameters for the fits are shown in Table 14. The fits were good, producing low goodness-of-fit parameter in NXFit, $R^2$ indicating a good fit) and reflecting the data closely, with the exception of the larger separation region which was not considered by the fit. The peaks (representing the Si-O, P-O, Mg-O, Ca-O, Sr-O and O…O atomic separations) were not seen to change in position significantly with strontium content, being in the same position both compared with each other, and the 0 and 6.2 Mol% Sr compositions. There was a slight increase in the coordination number of the Si-O peak, and subsequent decrease in the coordination number of the P-O peak for the 12.5 Mol% Sr composition, which is also reflected in the O-Si-O and O-P-O peaks. The 1st Ca-O and Sr-O peaks were seen to fall and rise in amplitude, respectively, as strontium was added between the 12.5 and 18.7 Mol% Sr compositions, and when compared with the 0 and 6.2 Mol% compositions. The other peaks were not seen to move in position between the two compositions, and this agreed largely with what was seen in Figure 25; that the addition of strontium does not affect the position of the peaks. The structural parameters in Table 14 were not seen to change between the 12.5 and 18.7 Mol% Sr compositions, with the exception of the slight change in the coordination numbers of the Si and P peaks, however the 18.7 Mol% composition showed general agreement with the parameters for the other compositions.

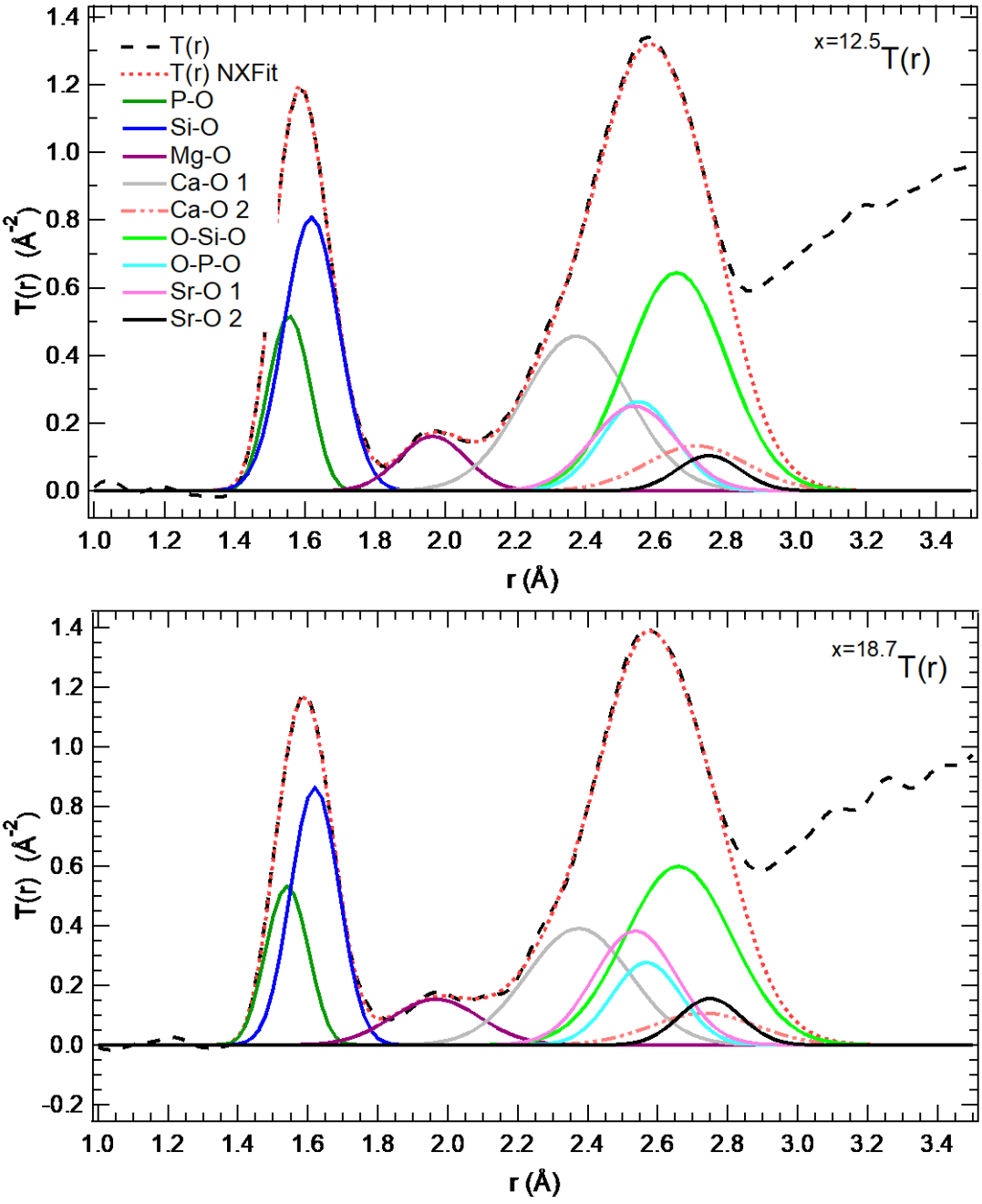


**Figure 26: The full deconvolutions of the real space $T(r)$ neutron diffraction traces (total correlation functions) for the SrAW glass compositions with 12.5 and 18.7 Mol% Sr, fit using NXFit. The region beyond 3Å was ignored during the fitting as this is beyond the short range order and due to the large number of overlapping bonds putting the analysis beyond the scope of this work..**

Finally, Figure 27 shows the individual $T(r)$ fits to the 24.9 and 37.4 Mol% Sr compositions, and their component sub-peaks, with the accompanying fitting parameters found in Table 14. The fits produced low fitting parameters ($R^2$) in NXFit, indicating the fits were good and closely matching the data, again with the exception of the region beyond 2.8Å which was not considered in the fit (as it is beyond the short range order), and for the 24.9 Mol% composition peak at 2Å, where the fit could not fully represent the sharpness of that peak. As more strontium was substituted into the material, the Ca peaks were seen to decrease in amplitude dropping noticeably as Sr increased from 24.9 to 37.4 Mol%, and when compared with the 0 to 18.7 Mol% Sr compositions. At the same time, the additional Sr resulted in an increase in the amplitude of the Sr peaks, however the position of Ca and Sr peaks was not seen to change. Subsequently, for the 37.4 Mol% composition the shoulder peak at 2.3Å has essentially vanished, whilst the amplitude of the $T(r)$ at 2.6Å increased. The Si-O and O-Si-O peaks were seen to be relatively unchanged between the two compositions, and also compared with the 0 to 18.7 Mol% Sr compositions. However, the 37.4 Mol% Sr composition did show a slight decrease in the P-O coordination number compared with the other compositions, similar to that found for the 12.5 Mol% composition. The 1$^{st}$ Sr-O and Ca-O peaks did also show a slightly lower coordination number for the 37.4 Mol% composition compared with the other compositions, whilst the 24.4 Mol% composition showed a 1$^{st}$ Ca-O peak coordination lower than that of the 37.4 Mol% Sr composition. The other parameters were seen to be similar to those found for the other compositions, and were not seen to change in position with strontium content.

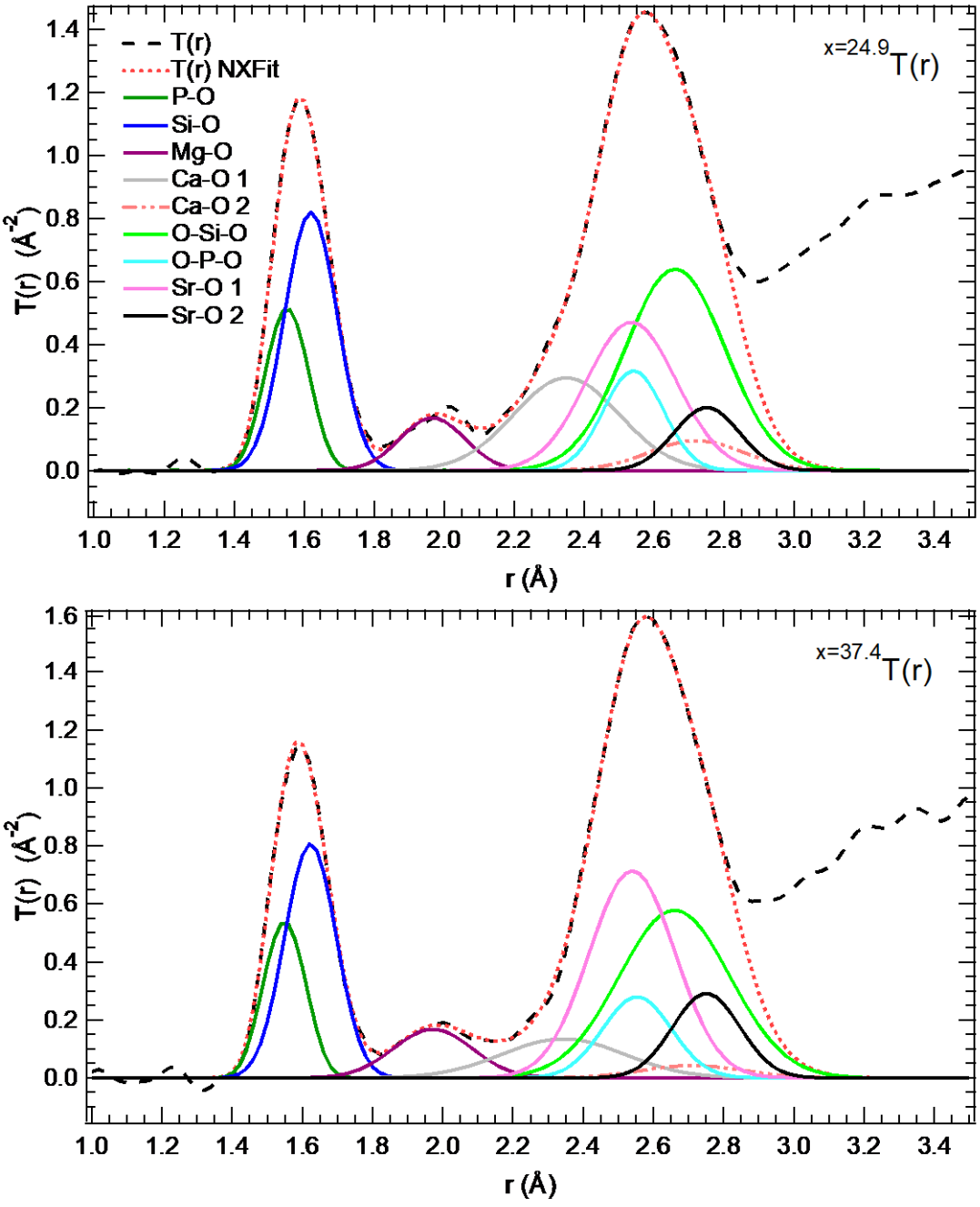


**Figure 27: The full deconvolutions of the real space $T(r)$ neutron diffraction traces (total correlation functions) for the SrAW glass compositions with 24.9 and 37.4Mol% Sr, fit using NXFit. The region beyond 3Å was ignored during the fitting as this is beyond the short range order and due to the large number of overlapping bonds putting the analysis beyond the scope of this work..**

| Si-O | | | |
|---|---|---|---|
| Mol% Sr | r (Å) | N | σ (Å) |
| 0 | 1.62 | 3.82 | 0.06 |
| 6.2 | 1.62 | 3.85 | 0.06 |
| 12.5 | 1.62 | 4.03 | 0.07 |
| 18.7 | 1.62 | 3.80 | 0.06 |
| 24.9 | 1.62 | 3.92 | 0.06 |
| 37.4 | 1.62 | 3.88 | 0.07 |

| Sr-O | | | |
|---|---|---|---|
| Mol% Sr | r (Å) | N | σ (Å) |
| 0 | N/A | N/A | N/A |
| 6.2 | 2.53 | 5.10 | 0.11 |
| 12.5 | 2.54 | 5.10 | 0.11 |
| 18.7 | 2.54 | 5.10 | 0.11 |
| 24.9 | 2.53 | 5.10 | 0.12 |
| 37.40 | 2.54 | 4.87 | 0.12 |

| Sr-O (2) | | | |
|---|---|---|---|
| Mol% Sr | r (Å) | N | σ (Å) |
| 0 | N/A | N/A | N/A |
| 6.2 | 2.71 | 1.69 | 0.09 |
| 12.5 | 2.75 | 1.70 | 0.08 |
| 18.7 | 2.75 | 1.70 | 0.08 |
| 24.9 | 2.75 | 1.70 | 0.08 |
| 37.40 | 2.75 | 1.70 | 0.09 |

| P-O | | | |
|---|---|---|---|
| Mol% Sr | r (Å) | N | σ (Å) |
| 0.0 | 1.55 | 4.04 | 0.05 |
| 6.2 | 1.55 | 4.05 | 0.04 |
| 12.5 | 1.56 | 3.80 | 0.04 |
| 18.7 | 1.55 | 3.99 | 0.05 |
| 24.9 | 1.55 | 3.92 | 0.05 |
| 37.4 | 1.56 | 3.80 | 0.05 |

| Ca-O | | | |
|---|---|---|---|
| Mol% Sr | r (Å) | N | σ (Å) |
| x0 | 2.37 | 5.40 | 0.14 |
| x6 | 2.37 | 5.40 | 0.14 |
| x12 | 2.37 | 5.40 | 0.15 |
| x18 | 2.37 | 5.40 | 0.15 |
| x24 | 2.35 | 5.07 | 0.15 |
| x37 | 2.34 | 5.28 | 0.17 |

| Ca-O (2) | | | |
|---|---|---|---|
| Mol% Sr | r (Å) | N | σ (Å) |
| 0.0 | 2.72 | 1.70 | 0.13 |
| 6.2 | 2.73 | 1.70 | 0.13 |
| 12.5 | 2.72 | 1.70 | 0.14 |
| 18.7 | 2.74 | 1.70 | 0.13 |
| 24.9 | 2.72 | 1.70 | 0.13 |
| 37.4 | 2.73 | 1.70 | 0.13 |

| Mg-O | | | |
|---|---|---|---|
| Glass | r (Å) | N | σ (Å) |
| 0.0 | 1.97 | 4.81 | 0.09 |
| 6.2 | 1.97 | 4.59 | 0.09 |
| 12.5 | 1.96 | 4.60 | 0.09 |
| 18.7 | 1.96 | 4.73 | 0.10 |
| 24.9 | 1.97 | 4.67 | 0.08 |
| 37.4 | 1.97 | 4.73 | 0.09 |

| O-Si-O | | | |
|---|---|---|---|
| Glass | r (Å) | N | σ (Å) |
| 0.0 | 2.66 | 4.22 | 0.13 |
| 6.2 | 2.66 | 4.22 | 0.13 |
| 12.5 | 2.66 | 4.22 | 0.14 |
| 18.7 | 2.66 | 4.22 | 0.14 |
| 24.9 | 2.66 | 4.22 | 0.14 |
| 37.4 | 2.66 | 4.22 | 0.15 |

| O-P-O | | | |
|---|---|---|---|
| Glass | r (Å) | N | σ (Å) |
| 0.0 | 2.55 | 3.08 | 0.08 |
| 6.2 | 2.54 | 3.08 | 0.09 |
| 12.5 | 2.55 | 3.08 | 0.10 |
| 18.7 | 2.54 | 3.08 | 0.09 |
| 24.9 | 2.54 | 3.08 | 0.08 |
| 37.4 | 2.54 | 3.08 | 0.08 |

| O…O | | | |
|---|---|---|---|
| Glass | r (Å) | N | σ (Å) |
| 0.0 | 2.63 | 3.89 | 0.12 |
| 6.2 | 2.63 | 3.89 | 0.12 |
| 12.5 | 2.63 | 3.89 | 0.13 |
| 18.7 | 2.63 | 3.89 | 0.13 |
| 24.9 | 2.63 | 3.89 | 0.12 |
| 37.4 | 2.63 | 3.89 | 0.14 |

**Table 14: The structural parameters for the NXFit fittings to the real space $T(r)$ neutron diffraction traces (total correlation functions) for the six different SrAW glass compositions with 0, 6.2, 12.5, 18.7, 24.9 and 37.4 Mol% Sr. 'r' is the atomic separation, 'N' is the coordination number and 'σ' is the disorder term (describing the thermal and static disorder in the bonds and being related to the widths of the distributions of the atomic separations).**

Comparing all of the compositions against each other, the differences between the fitting parameters for the different compositions displayed in Table 14 are relatively minor, indicating that the addition of Sr to the SrAW glass has no, or only a minor, effect on the short range order of the glass. Largely the position of the peaks was not observed to change with the addition of strontium, though the coordination of the peaks was more variable.

### 2.3.5 Raman Spectroscopy for studying longer range order of SrAW with increasing Sr content

The Raman spectra of the different compositions of SrAW glass were measured to provide complimentary information on the medium range order of the materials, and how these were affected by Sr content. The average Raman spectra for each glass composition (0, 6.2, 12.5, 18.7, 24.9 and 37.4 Mol% Sr) are shown in Figure 28. The spectra all show two main peak regions, the second of which has strong peak shoulders. The asymmetry of the 580-720cm$^{-1}$ peak region suggested the presence of two peaks, which the literature suggests were the $Q^2$ Si-O-Si rocking mode (~620cm$^{-1}$) (85,198) and the $\nu_4$ O-P-O bending mode (~600cm$^{-1}$)(199,200). There was some dependence of this peak on strontium content, however it was not seen to be clearly correlated with strontium content.

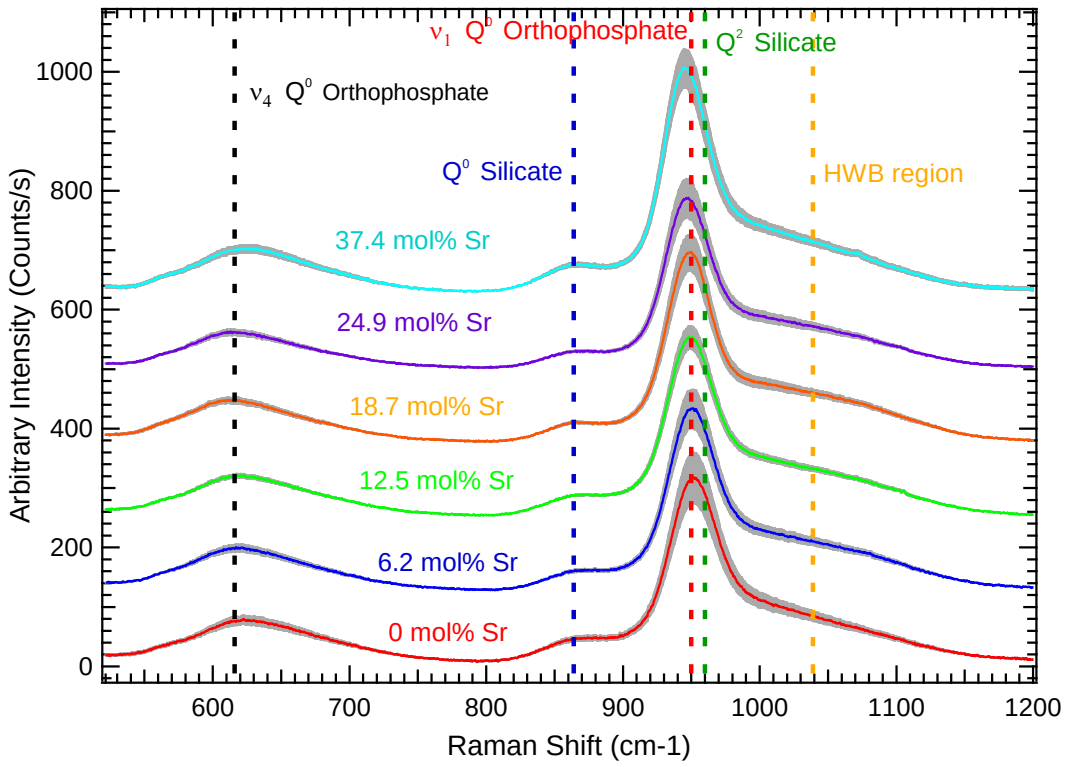


**Figure 28: Raman spectra of the six compositions of SrAW glass (0, 6.2, 12.5, 18.7, 24.9 and 37.4 Mol% Sr). These are an average of 15 spectra, with the standard error displayed as a shaded area. They have been offset for clarity, and the positions of Raman modes of interest are displayed. N=15, taken from a single batch of each composition.**

The higher wave number peak region was fit, as the literature indicated this contained the Si contributions (85,178,179,182,183,201,202). Four Raman peaks were fit to the 800 – 1150 $cm^{-1}$ region for each composition (Figure 30 and Figure 30), with mean peak positions across the SrAW glass compositions found at 865 $cm^{-1}$, 948 $cm^{-1}$ and 959 $cm^{-1}$. The fitting parameters can be seen in Table 15. The first peak was assigned to the stretch vibrations of the $Q^0$ silicate component (85,178,179,182,183,201,202), the second peak to the orthophosphate $PO_4^{3-}$ $\nu_1$ component (85,179,183,201), and the third peak to the $Q^2$ silicate component (85,179,182,183,201,202). The fourth peak, termed the high wavenumber band (HWB), was determined to be a convolution of $Q^1$, $Q^2$ and $Q^3$ silicate units and so was difficult to resolve further (85,178,179,181–183,201,202). To facilitate the fitting, the HWB was kept fixed at 1039 $cm^{-1}$

for all of the compositions (which was determined from the 0 Mol% Sr spectra).

The orthophosphate $PO_4^{3-}$ $v_1$ peak position and FWHM were seen to decrease in wave number as the Sr concentration in the SrAW glass increased, acting in good agreement with the findings in the $^{31}P$ MAS-MNR, and suggesting the phosphate component of the glass becomes more ordered as the strontium concentration is increased. The $Q^0$ silicate component was similar in peak position and FWHM between the different glass compositions, suggesting the substitution of Sr for Ca did not affect this component of the material. However, the $Q^2$ silicate peak did show a decrease of peak FWHM for all of the Sr containing SrAW glass compositions, except for the 18.7 Mol% Sr composition, which showed a $Q^2$ peak more similar to that of the 0 Mol% Sr composition. The HWB did not show any correlations with strontium content, with the exception of a substantially reduced FWHM for the 37.4 Mol% Sr composition, though any changes may have been masked by the peak being a superposition of many $Q^1$, $Q^2$ and $Q^3$ components.

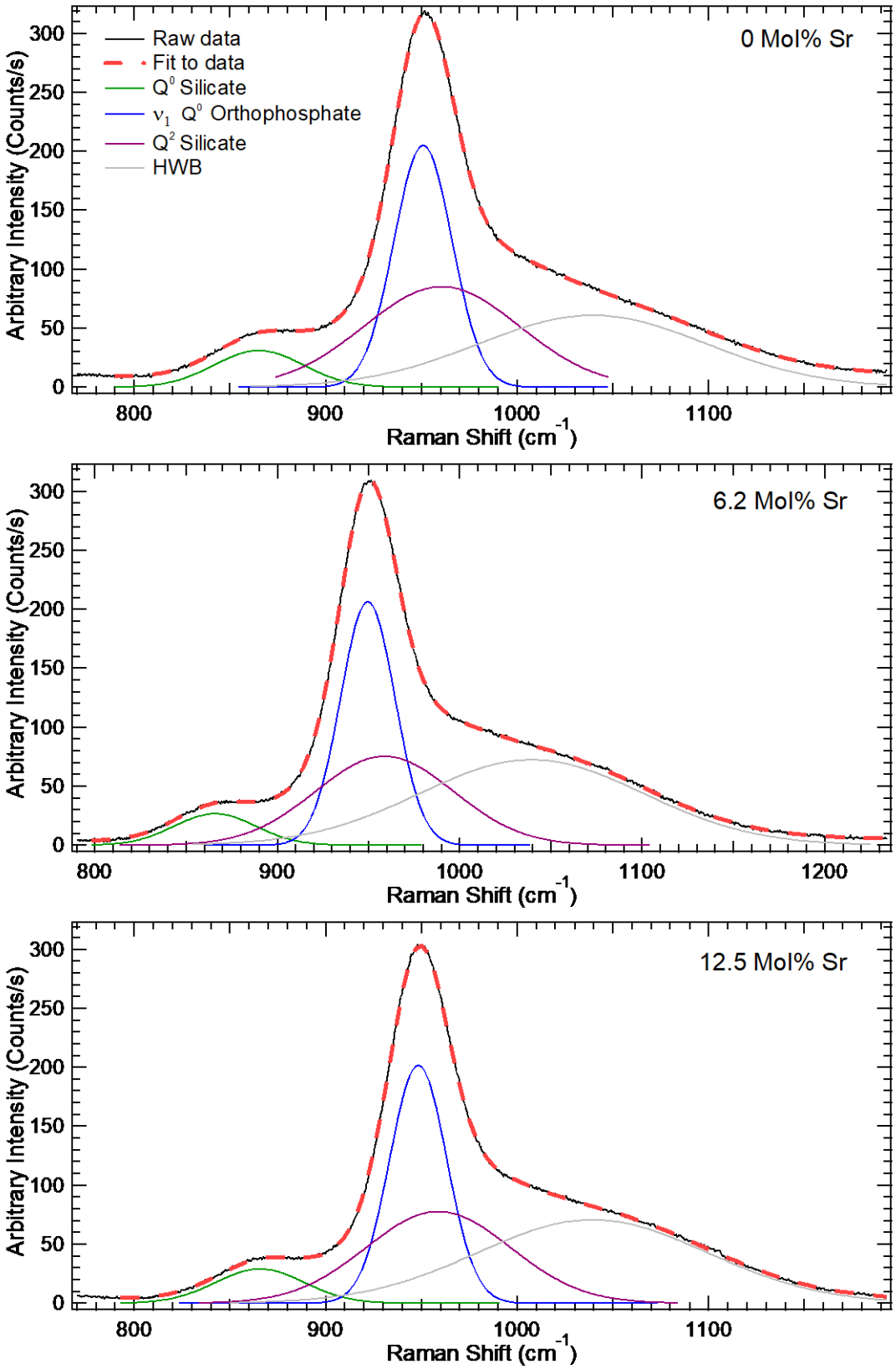


**Figure 29: Deconvolution of the averaged Raman spectrum for the 0, 6.2 and 12.5 Mol% Sr glass compositions, showing the spectral fitting (dashed line) and assigned peaks (see inset key). N=15, taken from a single batch of each composition.**

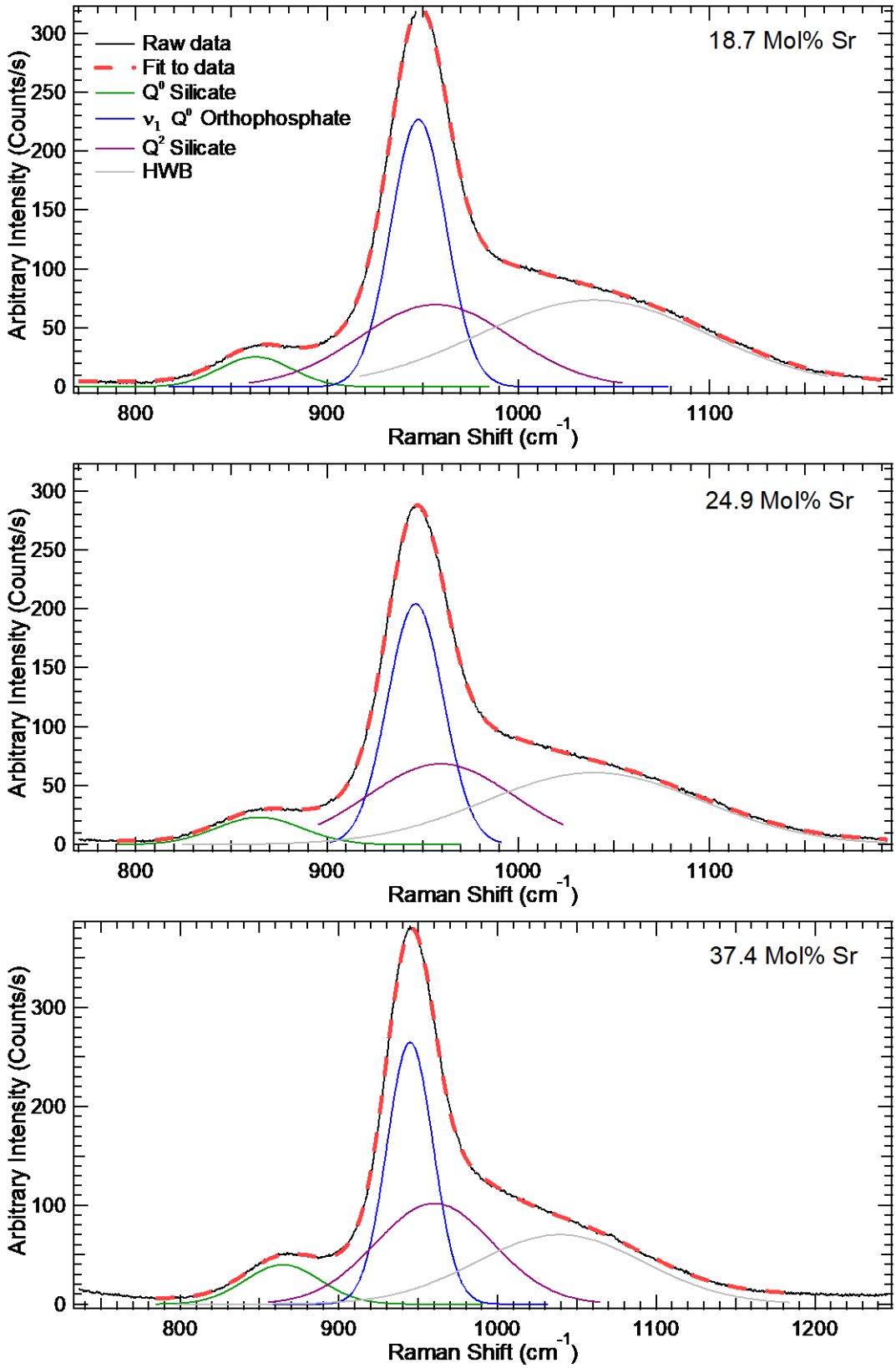


**Figure 30: Deconvolution of the averaged Raman spectrum for the 18.7, 24.9 and 37.4 Mol% Sr glass compositions, showing the spectral fitting (dashed line) and assigned peaks (see inset key). N=15, taken from a single batch of each composition**

| Peak | Mol% Sr | Peak position ($cm^{-1}$) | FWHM ($cm^{-1}$) |
|---|---|---|---|
| Peak 1 | 0 | 865 ± 1 | 54 ± 2 |
| $Q^0$ silicate component | 6.2 | 865.9 ± 0.4 | 52 ± 1 |
| | 12.5 | 865.7 ± 0.3 | 54.4 ± 0.3 |
| | 18.7 | 862.6 ± 0.6 | 46 ± 2 |
| | 24.9 | 865 ± 1 | 52 ± 2 |
| | 37.4 | 865 ± 2 | 55.5 ± 0.3 |
| Av. Value | | 865 ± 2 | 52 ± 2 |
| Peak 2 | 0 | 950.9 ± 0.2 | 35.8 ± 0.2 |
| $PO_4^{3-}$ $v_1$ band | 6.2 | 949.6 ± 0.1 | 35.1 ± 0.3 |
| | 12.5 | 948.4 ± 0.1 | 35.0 ± 0.1 |
| | 18.7 | 947.8 ± 0.2 | 34.1 ± 0.2 |
| | 24.9 | 946.3 ± 0.1 | 34.4 ± 0.3 |
| | 37.4 | 944.9 ± 0.1 | 34.2 ± 0.7 |
| Av. Value | | 948.0 ± 0.2 | 34.8 ± 0.7 |
| Peak 3 | 0 | 961 ± 1 | 95 ± 1 |
| $Q^2$ silicate component | 6.2 | 958.8 ± 0.4 | 88.6 ± 0.3 |
| | 12.5 | 958.8 ± 0.3 | 88.8 ± 0.9 |
| | 18.7 | 957 ± 2 | 94.0 ± 0.8 |
| | 24.9 | 959 ± 2 | 90.0 ± 0.7 |
| | 37.4 | 960 ± 1 | 87 ± 3 |
| Av. value | | 959 ± 2 | 91 ± 3 |
| Peak 4 | 0 | 1039 | 138 ± 5 |
| HWB silicate component | 6.2 | 1039 | 143 ± 4 |
| | 12.5 | 1039 | 140 ± 2 |
| | 18.7 | 1039 | 141 ± 2 |
| | 24.9 | 1039 | 134 ± 7 |
| | 37.4 | 1039 | 126 ± 2 |
| Av. value | | 1039 (fixed) | 137 ± 7 |

**Table 15: Values for the fitted peak positions and full width at half maxima (FWHM) obtained from each of the six strontium-substituted apatite-wollastonite glass compositions corresponding to the stretching vibrations of the orthophosphate $PO_4^{3-}$ $v_1$ band and the tetrahedral silicate components. The latter relate to the $Q^0$ and $Q^2$ silicate components, and the high wavenumber band (HWB) comprising a convolution of $Q^2$, $Q^1$ and $Q^3$ (in increasing wavenumber order). The average values are taken across the sample compositions and the uncertainties are obtained from the standard error of the mean associated with these quantities (N = 15) measured for a single batch of each composition.**

As the intensity of the Raman spectra is given in arbitrary units, it is not possible to directly compare the intensities of the peaks between compositions. Instead, peak ratios must be created. Peak ratios between peak 1 and peaks 2, 3 and 4 were made, and the results are displayed in Table 16. Peak 1 was chosen as it was the least changed between the different compositions. These peak ratios show that there were increases in the orthophosphate $PO_4^{3-}$ $v_1$, $Q^2$ silicate and HWB components, with respect to the $Q^0$ silica component with increasing Sr content in the SrAW glass. These changes were not gradual, however, with the 37.4 Mol% results becoming quite different to the other Sr containing compositions and the area ratios of the peaks changing to be lower than that found for the 0 Mol% peak. Additionally, the 18 Mol% composition peak area ratios differed from the other compositions by more than the standard error, although in part this would have been due to its decreased FWHM for the $Q^0$ Si peak (and thus resulting in a lower peak area for that peak).

| Mol% Sr | $A_{Peak\ 2}/A_{Peak\ 1}$ ($PO_4^{3-}$ $v_1/Q^0Si$) | $A_{Peak\ 3}/A_{Peak\ 1}$ ($Q^2Si/Q^0Si$) | $A_{Peak\ 4}/A_{Peak\ 1}$ ($HWB/Q^0Si$) |
|---|---|---|---|
| 0 | 4.4 ± 0.7 | 4.8 ± 0.7 | 5.0 ± 0.6 |
| 6.2 | 5.2 ± 0.6 | 4.8 ± 0.6 | 7.5 ± 0.7 |
| 12.5 | 4.5 ± 0.4 | 4.4 ± 0.3 | 6.3 ± 0.4 |
| 18.7 | 6.6 ± 0.7 | 5.6 ± 0.6 | 8.8 ± 0.6 |
| 24.9 | 5.8 ± 0.7 | 5.1 ± 0.5 | 6.7 ± 0.4 |
| 37.4 | 4.1 ± 0.5 | 4.0 ± 0.4 | 4.0 ± 0.4 |

**Table 16: Fitted peak area ratios taken relative to the peak area of the $Q^0$ silicate component ($Q^0$ Si) for each of the six different strontium-substituted apatite-wollastonite glass compositions as obtained from the spectral averages. Here, $Q^2$Si refers to the $Q^2$ silicate component and HWB refers to the high wavenumber band comprising a convolution of the $Q^2$, $Q^1$ and $Q^3$ silicate components (in increasing wavenumber order). The uncertainties are determined from the propagated standard errors of the mean associated with the peak area values (N = 15) measured for a single batch of each composition.**

To determine whether sufficient spectra (from different grains of glass powder) were taken to compose the average for each composition, convergence tests were performed. The percentage standard error of the ratio of peak areas for the $Q^0$ silicate (peak 1) to $PO_4^{3-}$ $v_1$ (peak 2) bands was determined as a function of increasing the number of spectra (of different glass grains) in the spectral average, and these can be seen in Appendix B: Figure 90,Figure 91,Figure 92. As more spectra were added to the average, the percentage standard error of the 0 Mol% and 6.2 Mol% Sr peak1/peak2 area ratio was seen to fall, indicating that measurement of this value is converging on the true value as more spectra were added. By 15 spectra the standard error was seen to stabilise (Figure 90).The tests were seen to converge, showing that the addition of the spectra to the average worked to improve the estimates of these averages and that the data were statistically representative of the SrAW glass compositions (Figure 91). This was also found for the 12.5 and 18.7 Mol% Sr spectra in 90 and the 24.9 and 37.4 Mol% spectra in Figure 92. Hence the averages of the spectra used in the analyses in this thesis were found to improve the precision of the measured parameters, and sufficient spectra were taken to significantly reduce the uncertainty in these measurement.

### 2.3.6 Scaffold manufacture

The SrAW is not generally used as a biomaterial because though bioactive, it is not strong enough to make a bioactive scaffold for bone tissue engineering. Heat treatment can cause the grains of SrAW glass to partially crystallise and sinter together making a scaffold of a defined shape with much more favourable mechanical properties.

When the six different compositions of SrAWGC were heat treated (1050°C for 2 hours) they were seen to consistently form discs with a flat upper-side, with a curved underside Figure 31.

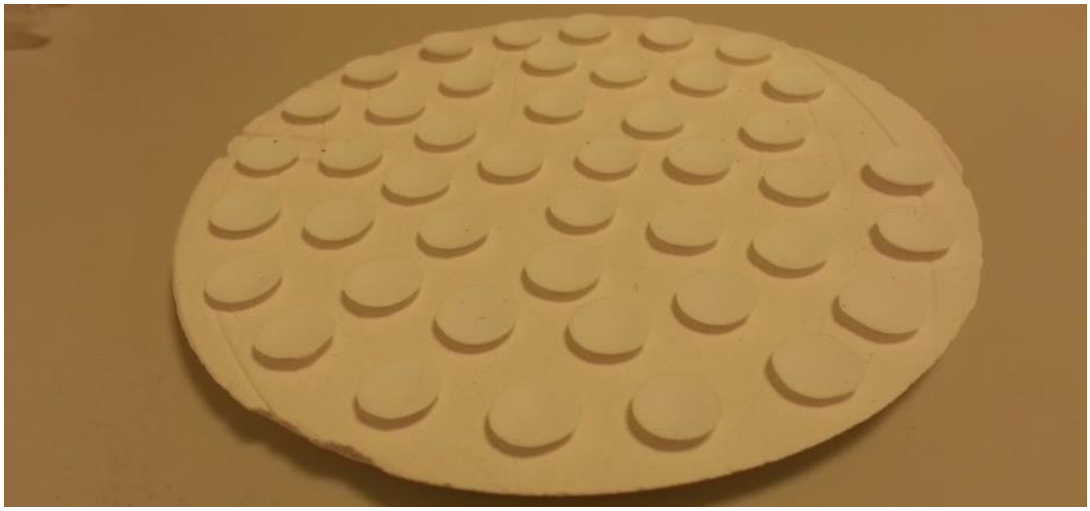

**Figure 31: Top: 12.5 Mol% SrAWGC Discs after firing. Bottom: Representative images of the fired AWGC discs made with 0, 6.2, 12.5, 18.7, 24.9 and 37.4 Mol% Sr.**

When imaged with SEM, the surface of the discs were seen to have sintered and changed from being composed of individual grains to a single material, with the lower strontium compositions showing a very smooth surface, whilst the higher strontium compositions showed progressively rougher surfaces (Figure 32). This roughening with strontium substitution was reproducible between batches, however the extent was quite variable, as was the material surface.

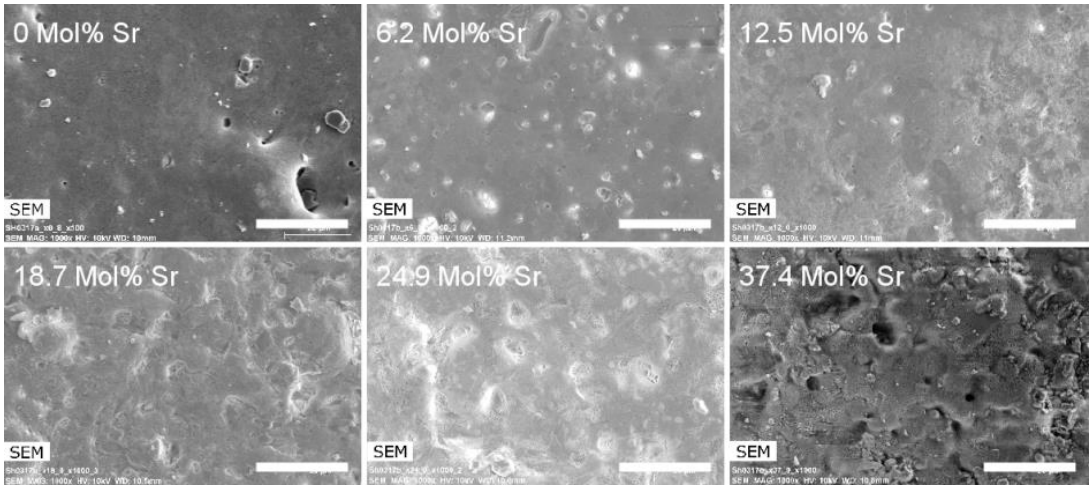


**Figure 32: Scanning electron microscopy images of the surfaces of the six different compositions of Sr Apatite Wollastonite (SrAWGC) disc with 0, 6.2, 12.5, 18.7, 24.9 and 37.4 Mol% Sr, using secondary electron mode. The scale bar displays 20µm. Representative images of the centre of the discs.**

## 2.4 Discussion

The aim of the work described in this chapter was to determine how the substitution of strontium into the AW glass might affect its short and medium range order, and so inform on how strontium could alter the properties of the Apatite-Wollastonite Glass-Ceramic. Initially, the different compositions of Apatite-Wollastonite glass with increasing calcium for strontium substitution were made, and then neutron diffraction was used to study the short range order, whilst NMR and Raman spectroscopy were used to study the medium range order. Finally, the AW glass was used to make scaffolds from the material for later use in determining how MSCs respond to the strontium content in the SrAWGC. Prior to discussing the results it is necessary to comment on the batch to batch variability inherent in glass and ceramic manufacture. Multiple batches of glass were used in this project and there were found to be some batch to batch variability due the intrinsic uncertainty in the operation of the weighing balances, furnaces and quenching tank. Pontiroli assessed the similarity of three batches of SrAW glass made in the same laboratory as in this project and using the same melt-quench method, using EDS to measure the composition of the glass powder. The standard deviation of the Ca, Sr, Si, Mg and P content of the glass powder was less

than 1% and within the uncertainty of the EDS technique (203). Pontiroli also found that the fluorine content was more variable; however, this was near the detection limit of the machine increasing the uncertainty in the measurements. Like the SrAW glass, the SrAWGC has also been found to show variability between batches, with differences arising due to furnace use and green body preparation. Pontiroli performed DSC measurements on three batches of SrAW glass (for each Sr composition) to ensure the thermal treatment would create similar glass-ceramics. The characteristic temperatures (onset temperatures and peak temperatures) were found to have a standard deviation of 1-2%, with the wollastonite peak being the most variable (203). However, these values were within the inherent uncertainty of the DSC machine.

### 2.4.1 SrAW glass manufacture and bulk properties

The six different compositions of SrAW glass were successfully made by substituting Ca for Sr (6.2, 12.5, 18.7, 24.9, 37.4 Mol%) extending work done in the David Wood Laboratory, Vickers (2013) (102), on AW glass. However, full substitution of the Ca for Sr (49.9 Mol%) in this project was seen to cause phase separation, and hence these glasses were not considered in this work. Strontium has been successfully incorporated into other (simpler) glass systems, such as Bioglass 45S5 (87,150,155,204) and through sol-gel synthesis (205). For Bioglass 45S5 it was found that full substitution of strontium into the material was possible, although in Fujikura *et al.* (2012) they did report a small, but growing crystalline component in their Sr Bioglass 45S5 as they increased the Sr content to 100% substitution (155), whilst Hill *et al.* (2004) (206) found that strontium altered the way in which their glass crystallised, suggesting that the substitution of strontium into the material can nucleate the formation of different phases when at a sufficient concentration. The glass density was seen to gradually and linearly rise with strontium substitution into the SrAW. It is important to note the lack discontinuities in the increase in density with Sr content, as any shifts or outlying values for the density could indicate that the substitution of Ca for Sr caused phase separation or some changes in network structure. This is expected, as although strontium is larger than calcium, and hence should

push the network out slightly and thus potentially make it less dense, strontium is more massive proportionate to its size, and hence each strontium atom is denser than each calcium atom. Other studies on simpler soda-lime phosphosilicate bioactive glasses and Bioglass 45S4, have also found that substitution of Ca for Sr increased glass density, but lowered oxygen density and as such resulted in increased ion dissolution rates (207–210). The oxygen density, $\rho_o$, for the different compositions of SrAW glass can be determined using:

**Equation 15:**

$$\boldsymbol{\rho_o = \frac{m_o}{V_{mol}} = \frac{M(O) \times (2x_{SiO2} + 5x_{P2O5} + x_{CaO} + x_{SrO} + x_{MgO})}{m_{mol}/\rho_{exp}}}$$

where $m_O$ is the mass of oxygen present in the glass (which is given by the mass per mole of oxygen M(O), multiplied by the fractions of the different oxygen containing precursors ,e.g. $x_{SiO_2}$, weighted by their oxygen content) and $V_{mol}$ is the molar volume of the glass (given by the mass per mol of the glass divided by the experimental density) (207).

This results in the values given in Table 17:

| Composition (SrO Mol%) | 0 | 6.2 | 12.5 | 18.7 | 24.9 | 37.4 |
|---|---|---|---|---|---|---|
| $\boldsymbol{\rho_O}$ | 1.20 | 1.19 | 1.18 | 1.16 | 1.15 | 1.12 |

**Table 17: The oxygen density of the SrAW glass compositions with increasing Sr content.**

Therefore, in addition to raising the density of the AW glass, the substitution of strontium into the SrAW results in a fall in the oxygen density of the AW glass network. As described earlier, studies on other glass systems that found a rise in glass density with the substitution of strontium also predicted this would lead to an expansion of the glass network, and this could lead to faster dissolution rates (207–210).

### 2.4.2 Determining the short-range order of SrAW glass

The short and medium range order analyses in this chapter were performed on the SrAW glass with the aim of modelling the amorphous component of the SrAWGC. This is because the amorphous phase of glass-ceramics is considered to be the most bioactive component and therefore important in the cell response due to its relatively high dissolution rate (72,146,147). However, it is not possible to measure the short-range order of the amorphous phase directly, as its contribution to the neutron diffraction and Raman spectroscopy would be masked by the crystalline phase. It is also not possible to extract the amorphous phase from the material, so it was modelled using the SrAW glass. The amorphous phase is the residual material left after the SrAW glass is heat treated to form SrAWGC and so should have a similar structure and stoichiometry to the SrAW; however, due to the formation of the crystal phases it also displays some differences. Overall, the SrAW glass has been shown by Pontiroli to have the same composition as the SrAWGC discs (203), however it is not a perfect model. Previous work in the David Wood laboratory found that that the crystal phases (wollastonite and apatite) of the 18.7 and 24.9 Mol% Sr AWGC compositions depleted the amorphous phase of Mg and Si (102). Further work would be needed to determine the nature of the residual amorphous phase in SrAWGC.

To study how the substitution of strontium into the SrAW affected its short and medium range order, first NMR was performed. The $^{31}P$ NMR found a main peak at ~2.5ppm for all of the SrAW glass compositions, suggesting the phosphate was present as $Q^0$ orthophosphate (150,157,159,160,185,186). A small additional peak was measured at ~−5ppm, however this was ignored as it only represented ~2% of the total area of the $^{31}P$ NMR peaks, but also as it still fell within the range for the $Q^0$ and $Q^1$ species, indicating that it could also be orthophosphate (187,188). $Q^1$ or higher would result in bridging oxygens, which could in turn result in Si-O-P linkages, which would produce noticeable side bands in the phosphorus spectra due to the relatively large chemical shift anisotropy such an environment would cause. Therefore, it was determined that the phosphorus

in the SrAW was entirely orthophosphate, and the substitution of Ca for Sr did not alter this. Other bioactive glass systems have also found that the phosphorus is also present as orthophosphate (150,157,159,160,185,186). However, there was movement of the orthophosphate $Q^0$ peak to higher chemical shift with higher strontium content, which was in agreement with the movement of peak 2 ($PO_4^{3-}$ $Q^0$) in the Raman spectroscopy to higher wavenumbers with strontium content of the SrAW glass. In Yang *et al.* (1986) they studied $MgCaSi_2O_6$, $CaSiO_3$, $SrSiO_3$, all with 2 weight percent $P_2O_5$ added, and found that this produced a main peak a 1.5, 2.6 and 3.9 ppm, respectively. From this, we could predict that as the SrAW glass contains both calcium and magnesium, this would draw the peak to a lower chemical shift than expected for $CaSiO_3$. The addition of strontium would then shift this back up to the measured value of ~2.5ppm (188). O'Donnell *et al.* also found a similar trend in their Sr-substituted Bioglass (85,181), attributing the movement of the phosphate peak to the increased mass of the strontium ions, and the expanded glass network due to the larger size of strontium. The increased density of the glass would result in the orthophosphate having lowered bond strength, resulting in the movement of the NMR to higher chemical shifts and the Raman spectral peaks to lower wavenumbers (181). The FWHM of peak 2 in the Raman spectra and of the orthophosphate $Q^0$ peak in the NMR were both found to decrease as strontium was added to the SrAW glass, suggesting that the orthophosphate component of the glass network grew more ordered with strontium content. This has also been observed for Bioglass 45S5 in other studies (85,181), and could be indicative of the orthophosphate beginning to phase separate out from the glass network.

The $^{29}S$ MAS-NMR found that the silicon in the glass composition was split between $Q^2$ and $Q^3$, with the ratio of these two changing with strontium content, going from 11% $Q^3$ with the 37.4 Mol% Sr glass up to 28% $Q^3$ with the 0 Mol% Sr glass (though the 24.9 Mol% Sr composition did not follow this sequence). This suggests the substitution of Ca for Sr effectively made the glass weaker, and would cause the network connectivity to go down as the strontium content increased. The Raman spectra largely confirmed these results, in that they also showed the presence of a $Q^2$ Si peak in every

composition and a HWB region which could potentially contain $Q^3$ (in addition to $Q^2$ and $Q^1$). The Raman spectra were also able to detect a $Q^0$ Si species present in all of the compositions, which did not change with strontium content. This was able to be detected within the Raman spectra, as the $Q^0$ Si stretch mode has a Raman scattering cross-section 3.4 time greater than that observed for $Q^2$ Si, allowing much smaller quantities to be detected (85). Additionally, although $Q^0$ Si is not normally predicted for bioactive glasses (usually composed of $Q^2$ and $Q^3$, as found here and numerous other studies (150,160,189,211)), a numerical simulation by Tilocca *et al* of Bioglass 45S5 have suggested it could be present in small quantities similar to those found here (160,212,213).

Uniquely for the 37.4 Mol% SrAW glass there was an additional peak at -105.03ppm (width of 9.87ppm), which was 5.5% of the area of the ~81ppm $Q^2$ peak. This was attributed to $Q^4$ Si, and potentially represented some very diffuse phase separation throughout the material (190–192). However, simulations by Tilocca *et al.* (2007) found 5.7% of their simulated phosphosilicate glass was $Q^4$ Si. Therefore, although it is possible a small quantity of $Q^4$ Si this could be found normally within the SrAW glass, this would not explain the sudden increase in quantity from 24.9 Mol% to 37.4 Mol%. This indicates some sort of phase separation leading to the sudden step change from un-measurable to noticeable quantities of $Q^4$ Si.

These NMR and Raman spectroscopy results both indicate the substitution of strontium into the SrAW glass altered the medium range order of the material potentially weakening the material, by lowering the bond energy and decreasing the disorder parameter in the orthophosphate phase, and decreasing the ratio of the $Q^3$ to $Q^2$ Si tetrahedra.

To study how the substitution of strontium into the SrAW glass altered its short-range order (which could indicate how the material might degrade and response to heat treatments), neutron diffraction experiments were performed. The neutron diffraction experiment produced total correlation functions, $T(r)$, which consisted of three main features: a peak at 1.6 Å associated with Si-O and P-O, a smaller peak at 1.9 Å attributed to Mg-O and a large broad peak at 2.6Å which was attributed to O…O, Ca-O and Sr-

O. The only feature that clearly changed with strontium content was the broad peak at 2.6 Å, which gradually lost a shoulder peak at ~2.2 Å as Sr was substituted into the material (and Ca was removed). These features correspond well with those seen in other studies on bioactive glasses (150,159,160,167,193,194,210), and in particular with those in which strontium was substituted for calcium (150,210,214). To determine what was responsible for this change in the 2.6 Å $T(r)$ peak with strontium content, the spectra were deconvoluted. The first stage in this was to use isomorphic substitution to extract the Sr and Ca correlations from the total signal. Two peaks for Ca-O and Sr-O each were fit (Ca-O at ~2.38 and ~2.73 Å ,and Sr-O at ~2.52 Å and ~2.73 Å), to accommodate the asymmetric shapes of features in the $\Delta T(r)$ (150). Previous studies have assigned the ~2.3 Å and 2.75 Å peaks to non-bridging (Ca-$O_{NB}$) and bridging (Ca-$O_B$) oxygen bonds, respectively (150,193,215). Newport *et al.* also found a third Ca-O peak at ~2.5 Å in sol-gel glass, which they attributed to the Ca-OH. However this is an artefact of that production process and so it is correct that it would not appear in the melt-quench derived SrAW studied here. The region beyond 3 Å in the difference functions has been suggested to contain Ca-(O)-Ca and Ca-(O)-Si linkages and the equivalent Sr next neighbour correlations, however modelling these was beyond this study due to the complexity of all of these correlations overlapping in the >3 Å region (150,193). The Sr-O separations determined for the SrAW glasses also agree with those found in two crystalline systems, with strontium meta-silicate ($SrSiO_3$) having Sr-O separations of between 2.46 to 2.74 Å, whilst in $Na_2SrSiO_6$ they were primarily 2.46 Å (150,216,217).

It is important to recall that the isometric substitution technique relies on the assumption that the short-range order of the glass is largely unaffected by the substitution of strontium into the SrAW. This is easy to confirm because the Si-O/P-O peak at 1.6 Å and the Mg-O peak at 1.9 Å completely disappear from all of the difference functions, ${}^{x-y}\Delta T(r)$, suggesting that the Si-O, P-O and Mg-O separations were not affected by the substitution of strontium into the material. This is in agreement with the later fittings of the Si-O, P-O and Mg-O correlations in the total neutron diffraction spectra for each composition, ${}^{x}T(r)$, where it was found that the atomic separations,

coordination numbers and disorder terms were unchanged between the different compositions of SrAW glass. In contrast, it is more difficult to determine whether the O…O bonds cancelled each other out in the $\Delta T(r)$, as both the trigonometric calculations and $T(r)$ fits determined the peaks to be at ~2.53 Å for O-P-O and ~2.66 Å for O-Si-O, and therefore potentially overlapping with the Ca-O and Sr-O correlations. Additionally, the MAS-NMR showed there were slight changes in both the $PO_4^{3-}$ and $SiO_4$ environments with the substitution of strontium into the material, most notably that the percentages of $Q^2$ and $Q^3$ Si changed, from ~28 $Q^3$ down to ~11% $Q^3$ as strontium was substituted for Ca. Knowing that N=4 for $Q^2$ Si and N=4.8 for $Q^3$ Si, this could have resulted in the coordination number of the O-Si-O falling from N=4.22 for the 0 Mol% Sr composition, to N=4.09 for the 37.4 Mol% composition. This is only a ~3% change, however it could potentially contribute to any uncertainty in the value of N determined for the Sr-O and Ca-O peaks in the isomorphic substitution analysis.

To continue the analysis of the $T(r)$, and to ultimately determine whether Sr alters the short-range order of SrAW, it was important to predict the O…O bonds, which would then further simplify the subsequent fits. Given the MAS-NMR results, it was possible to determine an estimate of the O-Si-O and O-P-O coordination number as 4.22 and 3, respectively (through knowledge of their Q speciations and using Equation 6). The coordination numbers could also be determined using elemental abundances in the glass and using a suitable network connectivity (NC) model for this material (150). The NC for a silicate glass network is defined by:

**Equation 16:** $$\boldsymbol{NC = 4 - 2Z}$$

where Z represents the number of excess oxygens per $SiO_2$ in the initial glass mix (150). For a purely silicate glass, Z is given by (150):

**Equation 17:** $$\mathbf{Z} = \frac{\mathbf{c_O}}{\mathbf{c_{Si}}} - \mathbf{2}$$

where $c_O$ and $c_{Si}$ are the abunances of oxygen and silicon in the glass, respectively. However, SrAW glass contains phosphorus, which will take oxygens that would otherwise be utilised by the Si tetrahedra in the network.

Phosphorus does not utilise oxygen in the same manner as silicon, hence this potentially complicates the determination of the NC. For example, in a phosphate-based glass the NC is given by $NC = 3 - \left(\frac{2c_O}{c_p} - 5\right)$ (173). This study found (using $^{31}$P MAS-NMR) that the phosphate ions were present as orthophosphate (in agreement with many other studies on bioactive glasses (112,150,185,186)), and therefore would utilise four oxygens per phosphorus that could then no longer be used by the silicate glass network. Hence, the number of excess oxygens per $SiO_2$ would become:

**Equation 18:** $$\mathbf{Z = \frac{C_O - 4C_P}{C_{Si}} - 2}$$

where $c_P$ is the abundance of phosphorus (150).

The contribution of magnesium must also be considered, however although Mg is a divalent cation, like Ca and Sr, its significantly smaller size results in its role in the glass network being more complicated, and less well understood. Calcium and strontium are network modifiers, and due to their size form distorted octohedral (or higher order) environments, meaning that they coordinate with six or more oxygens (150,160). As magnesium is smaller in size, the other atoms (primarily oxygen) can pack more closely around it, allowing 4-fold (such as tetrahedral) geometries as for Si-O and P-O (four oxygens), or higher geometries such as 5-fold or 6-fold (such as octohedral)(172,186). However, the Mg-O environment can vary greatly between different glasses and with the Si/Mg ratio (172). The total $T(r)$ fits for all compositions of SrAW glass found Mg-O coordination numbers of $N_{Mg}$~4.8, potentially suggesting at least some tetrahedral Mg was present, which would act as a network former and increase the network connectivity (186), with the resulting number of excess oxygens being given by:

**Equation 19** $$\mathbf{Z = \frac{C_O - 4C_P}{C_{Si} + RC_{Mg}} - 2}$$

where *R* is the fraction of Mg occupying a tetrahedral environment (and hence acting as a network former). In this study it is difficult to determine with certainty the fraction of Mg in a 4-fold (tetrahedral) environment, however if a binary 4-fold / 5-fold structure is assumed and the Mg-O coordination number of 4.8 taken from the $T(r)$ fit, then it can be estimated

that ~ 30% of the Mg is in a tetrahedral environment based on a weighted average:

**Equation 20:** $\boldsymbol{N_{Mg} = N_{4fold}x_{4fold} + N_{5fold}x_{5fold} = 4x_{4fold} + 5(1 - x_{4fold})}$

where $x_{Nfold}$ is the fraction of that environment and $N_{Nfold}$ is the coordination number of that environment (4 for 4-fold, 5 for 5-fold). There were assumed to be no other Mg environments, therefore $N_{4fold} + N_{5fold} = 1$. Al-Hasni *et al.* found Mg-O distances of ~ 2.00 Å with coordination numbers of 4.5-5.0 for their magnesium silicate glasses (218), in good agreement with that found in the $T(r)$ fits here for SrAW, although it should be noted that the concentration of Mg in this study was somewhat lower than that used in Al-Hasni *et al* (218). Guignard *et al.* found that in their alumina-silicate glasses (again with a relatively high magnesium concentration) the Mg was present principally in five-fold geometries, however it also possessed significant percentages of four and six-fold geometries (37, 50 and 13% $MgO_4$, $MgO_5$ and $MgO_6$, respectively). Furthermore, the ratio of Si to Mg in their glass is comparable to that in the SrAW glass, and also gave a similar Mg-O coordination number of $N_{Mg} = 4.75$. Patel *et al.* found a coordination number of 4.7-5.2 as they substituted strontium into their primarily phosphate glass (219). Finally, Watts *et al.* reported that ~ 14% of the Mg in their Bioglass 45S5 analogue occupied a tetrahedral environment (186). For the SrAW glass studied here, if R for the Mg is taken as 0.3, and utilising the abundances of Si, O, P and Mg of 0.131, 0.602, 0.052 and 0.026, respectively, in the SrAW glass, this results in a $Z_{SrAW} = 0.84$ and $NC_{SrAW} = 2.32$. This theoretically derived value for the network connectivity of the SrAW glass is based off the experimental findings of the neutron diffraction experiment and is in good agreement with the NC = 2.23 produced by solely considering the Q species from the $^{29}$Si MAS-NMR (27% $Q^3$, NC=3 and 73% $Q^2$, NC=2).

The fitting to the $T(r)$ for each composition was performed using the MAS-NMR and isomorphic substitution analyses to defined the Si, P, Ca and Sr components meaning only the Mg-O bond was unknown. The final fits and subsequent values of ‘r’, ‘N’ and σ for the Si-O, P-O, O-Si-O, Ca-O (1 and 2),

Sr-O (1 and 2) and Mg-O were found to be in relatively good agreement across the different compositions. The slight variations in the Si-O, P-O and 1$^{st}$ Sr-O and Ca-O peaks with Sr content were not seen to clearly associate with Sr content. It is possible these variations were an artefact of the fit, resulting from using the same O-Si-O bond coordination for all of the compositions despite the decreasing O-Si-O coordination with Sr shown by the NMR. The slight differences of the Si-O peaks may have then slightly altered how the software fit the other peaks. The deconvolutions reveal that the observed disappearance of the shoulder peak at 2.2Å with increasing Sr content was due to the changing quantities of Sr and Ca in the material. As the Sr content was increased, the Ca was replaced, reducing the intensity of the 1$^{st}$ Ca-O peak at 2.37Å, whilst increasing the intensity of the 1$^{st}$ Sr-O peak at 2.54Å. Other studies in Bioglass 45S5 found there was little change in the fitting parameters (r, N, σ) with Sr substitution into the material, whilst in Patel *et al.* they found only the Mg-O fitting parameters changed with Sr substitution, attributed to the much larger Mg and P content (24 and 40 Mol%, respectively) and the larger size of Sr slightly altering the OPMgCa/Sr$_{1 \text{ or } 2}$ bonding environment (150,219). Therefore, the neutron diffraction experiment has determined that the addition strontium has very little effect on the short-range order of the SrAW glass. The changes in the shape of the spectra that were seen were deemed to vary in a linear manner with strontium content and were determined to be due to the alteration in the abundance of the elements, rather than actual changes in atomic separations, coordination or disorder. Based on these findings, a schematic for the glass network of the SrAW glasses is described in Figure 33.

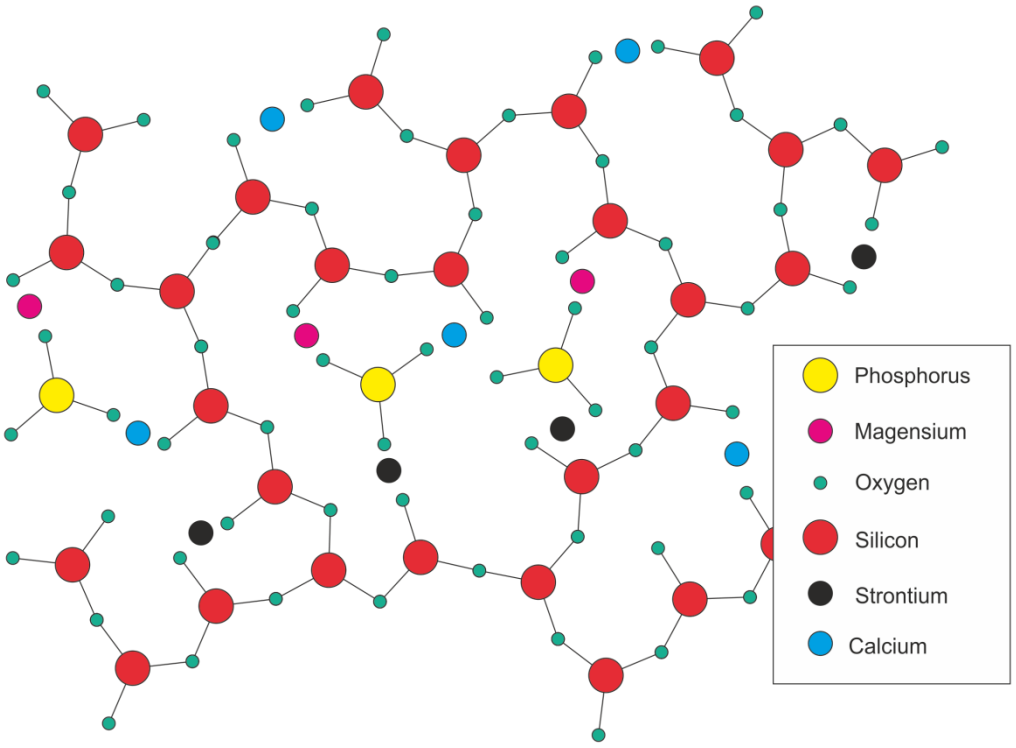


**Figure 33: A proposed two-dimensional schematic of a section of the SrAW glass network based off the neutron diffraction findings. The 4th bond of the Si should extend into, or out of, the page. Note: the atomic separations are not to scale.**

### 2.4.3 Raman Spectroscopic analysis of the SrAW glass

Using Raman spectroscopy, the vibrational spectra of the compositions of SrAW glass were measured, as this would provide complimentary information to the neutron diffraction and NMR on how the Sr content of the material affected the medium range order. The average Raman spectra for each glass composition (0, 6.2, 12.5, 18.7, 24.9 and 37.4 Mol% Sr) were composed of two regions. The lower wavenumber region (580-720cm$^{-1}$) was assigned to the $Q^2$ Si-O-Si rocking mode (~620cm$^{-1}$)(85,198,220) and the $\nu_4$ O-P-O bending mode (~600cm$^{-1}$)(181,199,200), and showed some variation in peak shape and position with strontium content. This region was also seen in the Sr substituted Bioglass 45S5 in O'Donnell *et al.*, and the strontium hydroxyapatite glass of O'Donnell *et al.*, where they attributed the slight movement in the peak position with Sr content to the broader effects of strontium size altering the Si-O and P-O bond angles and lengths (85,181).

The second region in the Raman spectra, between 800 and 1150cm$^{-1}$, was primarily concerned with Si and P, and so was studied in greater detail to complement the neutron diffraction and NMR studies described in this chapter. However, the assignment of the peaks in this region is debated in the literature. The position of peak 3 was seen to fall from 950cm$^{-1}$ to lower wavenumbers, and its FWHM decreased with increasing Sr content, with this also having been reported in O'Donnell *et al.* for a hydroxyapatite glass ($Ca_5(PO_4)_3OH$) substituted with strontium, where they identified it as the $PO_4^{3-}$ $v_1$ symmetric stretch (181). A separate study by O'Donnell *et al.* found Bioglass 45S5 (relatively similar to SrAW glass) substituted with Sr also responded in this manner, again identifying the peak as the $PO_4^{3-}$ $v_1$ symmetric stretch (85). Additionally, this was in complete agreement with the NMR data discussed previously, further suggesting that the 950cm$^{-1}$ peak was that of orthophosphate. However, Si bond vibrations do appear in this region, and this results in seemingly conflicting peak assignments in the literature, with many studies indicating the O-Si-NBO, or $Q^2$ Si-O-Si asymmetric stretch appear between 940-1000cm$^{-1}$ (corresponding with peak 4 in this study, at 960 cm$^{-1}$), and hence potentially overlapping with the phosphorus peak (85,179,181,198,201,220). In González *et al.*, they studied a mainly Si-Na-Ca glass and refused to attribute the peak at 950cm$^{-1}$ to $PO_4^{3-}$ as it wasn't present in their reference phosphate glass (220). However, as their glass is primarily phosphate, the phosphate will be in higher $Q^n$ speciations to form the network and so orthophosphate might not be a major component, which is seen as the peak clearly drops away and disappears as phosphate content in the material falls from 6 to 0.1 weight percent (220). Agathopolous *et al.* acquired spectra from a primarily Si-Ca glass, with a stoichiometry and Raman spectral profile similar to those found in this study on SrAW, and allocated the 956cm$^{-1}$ peak to vibrations derived from both asymmetric $Q^2$ Si $-O^-$ and $PO_4^{3-}$ symmetric stretching vibrations, as this peak was clearly present in the beta tri-calcium phosphate reference glass spectra (179). However, they did not deconvolute the peak, as performed in this study, hence in this project it is possible to model separate orthophosphate and $Q^2$ Si peaks, and assign the higher wavenumber peak to Si (180,183), whilst the 950cm$^{-1}$ peak (due to its close agreement with the

$^{31}$P NMR) shall be attributed to $PO_4^{3-}$ $v_1$ symmetric stretch. The movement of the orthophosphate peak in the SrAW glass with strontium content, seen in both the Raman and the NMR results, was also reported in O'Donnell *et al*. (2008) for strontium hydroxyapatite glass ($Ca_5(PO_4)_3OH$), where the $PO_4^{3-}$ $v_1$ phosphorus peak wavenumber and FWHM decreased linearly with Sr (181). However, they also found that this was inversely correlated with crystal size in the material suggesting that the substitution of Ca for Sr lessened the disorder of their material (181). O'Donnell *et al*. also found for Bioglass 45S5 that principal consequence of strontium substitution was the movement of the $PO_4^{3-}$ $v_1$ phosphorus peak to lower wavenumbers (85). They attributed this in part to the heavier mass of the Sr ion, and partly to the strontium ion's larger size expanding the glass network and consequently distorting the P-O bonds (85).

A feature not identified by the other methods described in this project was the $Q^0$ Si tetrahedra, and alongside the HWB region they represent the other contributions of Si to the medium range order of the SrAW glass. The Raman spectra $Q^0$ Si stretch vibration peak 1 (865 $cm^{-1}$) and HWB peak 4 (1039 $cm^{-1}$) were not observed to change in either position or FWHM maximum with strontium content, except a reduced FWHM in the HWB for the 37.5 Mol% Sr composition. The $Q^2$ Si stretch vibration peak 3 (959 $cm^{-1}$) was also consistent between the different compositions; however the 6.2 and 12.5 Mol% Sr compositions did show a slight shift in peak position and reduction in FWHM. The intensity ratios of the $Q^2$ Si peak 3 (against the $Q^0$ Si peak 1) were consistent (within uncertainty) between the compositions, however the HWB peak 4 showed some significant fluctuation, being seen generally to rise with Sr content in the SrAW glass. Comparing these findings with the NMR is made more challenging, as with the current data it was not possible to deconvolute the HWB region, and so some information on the $Q^3$ and $Q^2$ Si species present was inaccessible in the Raman spectra. Bearing this in mind, and considering that the amplitude of the $Q^2$ Si were with respect to the $Q^0$ Si (rather than the $Q^3$ Si in the NMR), this might explain why the increase in the $Q^2$ Si species (as a share of the total Si species) seen in the NMR, was not clear in the Raman spectra. In Martin *et al*. (150), they also found a slight increase from 83 to 89% $Q^2$ Si (as a total of

the Si speciations) between their 1:0 Ca:Sr and their 1:1 Ca:Sr composition, somewhat agreeing with the results reported in this project. However, their 100% Sr composition then showed a slight fall, or return to, 81% $Q^2$, suggesting that, as seen in the SrAW glass here, the way in which Sr alters the Si network does not simply favour the formation of $Q^2$ Si. In Fujikura *et al*., their NMR found that Bioglass 45S5 experienced a step change in Si chemical shift with more than 50% Sr substitution (155). They attributed this both to a change from $Q^2$ chain to $Q^2$ ring structures, the different sizes and charge shielding of the $Ca^{2+}$ and $Sr^{2+}$ ions, and a change from $Q^3$ to $Q^2$ Si species (155), as seen in this project and reported elsewhere (150). Therefore, it is clear that the substitution of Ca for Sr can potentially increase the disruption of the Si network, lowering network connectivity, which would then predict the material would then lead to the predicted faster breakdown of material in the body (112).

Thus, the Raman spectra determine the presence of a $Q^0$ Si species, along with $Q^2$ Si and $Q^3$ Si species, similar to the NMR. Though the NMR observation that the ratio of $Q^3$ to $Q^2$ changed with Sr was not replicated, this could be due to difficulties in further deconvoluting the peaks. It was also found that (like for the NMR) the phosphorus was present as orthophosphate, and that the peak moved to lower energies and became sharper with substitution of strontium into the material, suggesting that Sr addition made the orthophosphate more ordered. This means that although strontium did not alter the short range order it was seen result in a more disrupted Si-O network, with lower NC. This potential suggests that the substitution of strontium into the SrAW glass could result in faster breakdown of the material, which could have implication for the material-cell interaction.

It is important to note that the neutron diffraction, Raman spectroscopy and NMR were all performed on the same batch of (platinum crucible made) glass to allow for direct comparison between the results of these analyses. However, other work in the David Wood Laboratory on SrAW and SrAWGC has shown there is slight batch to batch variability during the production of these materials (203). Additionally, alterations to the production process, such as using alumina crucibles, or mass-production methods (were the

material to make it to market), could also feasibly result in a slightly altered glass structure. Therefore, it would be prudent for future work to analyse repeat batches of the SrAW glass to determine how variable the short and medium range order is across batches. Furthermore, batches of SrAW glass produced in alumina crucibles could also be analysed to confirm whether this alteration to the production process also had any effect on the glass network.

### 2.4.4 Disc production

The glass powders for each composition were heat treated for 2 hours at 1050°C, a procedure established in the David Wood Laboratory, to make AWGC porous scaffolds with <45μm AW glass particles (103). The SrAW glass compositions were able to sinter into SrAWGC discs, with 0, 6.2, 12.5, 18.7, 24.9 and 37.4 Mol% Sr. This is an important stage in the incorporation of Sr into the base AWGC material as it is the heat treatment of the AW glass into the final AWGC, that causes the apatite and wollastonite crystals to grow (119). This crystalline component is what gives the material more strength (119). Observation of the discs by SEM found that the surface morphology of the material changed noticeably with substitution of Ca for Sr. The 0 Mol% SrAW samples showed a nearly completely sintered smooth surface, which was also the case for the lower strontium compositions, however at 18.7 Mol% Sr and above the surface appeared to be increasingly textured, perhaps suggesting less sintering (as the <45μm glass particles would not have melted and fused so completely). Previous work in the David Wood Laboratory, described in  found that the substitution of strontium into the AW glass (45-90μm particles) altered the way in which the material responded to heat (102). This found that the substitution of Ca for Sr lowered the glass transition temperature, making the glass less viscous during the heating process, whilst also resulting in a shift of temperature at which the apatite crystals formed to a lower value (102). In addition, the temperature of formation for wollastonite, and the size of its exotherm falling, resulted in less wollastonite in the final SrAWGC samples (102). The samples in this project used <45μm SrAW glass, smaller than that used  in previous work (102), which would have caused the glass to be more

susceptible and further move the glass transition temperature downward (102,103,221). Therefore, the alterations in the surface morphology of the SrAWGC discs studied in this chapter potentially arise from an altered response of the material to the 2 hour long 1050°C heat treatment.

These changes could potentially be more than cosmetic. Alterations to the surface morphology could change the way in which the material interacts with biological systems, such as cell culture media, by changing the surface area of the material. Furthermore, if the changes in texture are due to the presence of difference crystal phases either at the surface, or throughout the material, this could also alter the way in which the material breaks down and also alter the ions released, and their final concentrations. Earlier work found that the higher strontium SrAWGC (45-90μm) mesoporous scaffolds took more magnesium into the apatite crystal phases, and that the apatite crystal phases were larger (102). This agrees with the increased apatite crystal size with increased strontium substitution shown elsewhere(222) and is significant because apatite is the least bioactive of the three phases present in AWGC (the others being wollastonite and the glassy phase) (72,146,147). Although these findings do not perfectly predict how the SrAW or SrAWGC studied in this project will respond to Sr substitution, they are important considerations, as the ion release and surface of a material can both have significant effects on cell.

Overall, the findings of, Raman spectroscopy, neutron diffraction and NMR are complimentary, and showed that although there were no differences in the short-range order of SrAW resulting from the substitution of Sr, there were some changes to the medium range order, mediated by changes in bond energy and disorder of the orthophosphate component and a slight drop in the quantity of $Q^3$ Si. It was also observed that there were even larger scale consequences for the SrAW when substituting in Sr, namely a raise in the density of the material, and a fall in oxygen density, which along with the general decrease in the network connectivity could indicate the higher Sr compositions of SrAW glass would experience higher dissolution rates. In addition, the SrAW glass was able to be formed into SrAWGC discs, though at higher Sr substitutions there were noticeable alterations to the surface topography of the discs, which could potentially alter the both the

way in which the SrAWGC discs release ions into solution and how cells respond to the material surface.

# Chapter 3 – MSC responses to strontium apatite wollastonite glass and glass-ceramics

## 3.1 Introduction

The previous chapter has established that the addition of the strontium does have some effects on the material, seen both in the medium-range atomic=level order and microscopically in the surface topography of the materials. Previous work in the laboratory has shown that some compositions of strontium Apatite Wollastonite Glass Ceramic (SrAWGC) raised alkaline phosphatase (ALP) production in primary mesenchymal stem cells (MSCs) when used with osteogenic media (102). When designing a biomaterial, it is important to determine the effects it has on cells and mechanisms through which they act to determine its efficacy as a scaffold. For the material to be a successful bone regeneration scaffold it needs to provide a positive environment for human MSCs, initially allowing attachment, promoting growth and providing (or at least not blocking) osteogenic factors which enable osteogenic differentiation. The ionic degradation products are one of the key ways in which bioactive glasses are thought to affect cells and so determining the identity of these ions, their concentrations and how they change between compositions of the material is essential in understanding both how the material responds to the physiological environment, and how cells respond to them. To test the effects of the released ions further, and to determine whether these are the primary cause of any effects, the MSCs were grown with media conditioned by the glass (and hence containing the ions released by the material). It is important to note, that material will release not only strontium ions into the media, but also potentially any of the other ions in the material (Silicon, Calcium, Phosphorus, Magnesium and Fluorine).

Additionally, it is important to consider the conditions the cells are tested in. Much of the literature uses osteogenic media to determine how cells respond to biomaterials, and how they respond to strontium in the materials

and culture media (85,87,122,204,223). However, dexamethasone, the key component in osteogenic media, is a potent steroid, which does not play a part in physiologic MSC-driven bone regeneration (224,225). Dexamethasone is also not used therapeutically; hence MSCs in a bone tissue engineering scaffold would never be exposed to dexamethasone whilst *in situ*. For this reason, exposing MSCs to dexamethasone and SrAWGC may distort or mask the properties of the material and the effects of the strontium content. As strontium is theorised to be an inducer of osteogenic differentiation it would be useful to determine whether using media without dexamethasone, either normal (basal) culture media, or “mineralisation media” (which still contains the beta-glycerophosphate and L-ascorbic acid necessary for mineralisation, but without the osteoinductive stimulus of dexamethasone) would still elicit any effects.

The biological assessment of the SrAWGC used an established immortalised human mesenchymal stem cell line, referred to as Y201 MSCs (39). These cells have been shown to have tri-lineage potential and have been thoroughly characterised, in terms of their behaviour, appearance, gene expression profiles and reproducibility (39). Initially, it was important to determine whether the cells seed appropriately on the material, and to optimise the seeding of the SrAWGC discs as the experiments were not being conducted on culture plastic (where seeding of the cells is relatively simple because they cannot flow around the surface and they readily adhere).

The majority of the testing of how the cells responded to the SrAWGC took the form of alkaline phosphatase (ALP) and DNA assays to screen the different compositions of SrAWGC discs for their ability to enhance osteogenic differentiation or proliferation. SrAW glass conditioned media and media doped with Sr alone were also screened to determine whether the surface of the material, or simply elements released by the material were responsible for any effects. In addition, further experiments were performed with these conditions, such as Colony Forming Unit assays (to determine whether initial colony formation is affected), metabolic activity assays and proliferation assays (to confirm any increase in cell number).

## 3.2 Materials and methods

### 3.2.1 Immortalised MSC line: Y201

Throughout this work an established immortalised MSC line was utilised, referred to as Y201 MSCs, with their properties well understood (39). In brief, they were positive for CD29, CD44, CD73, CD90, CD105 and CD166 surface markers, whilst not displaying CD34, CD45, CD11b and CD14 (39), and this profile is typical of that displayed by human bone marrow MSCs (226). The Y201 MSCs also have tri-lineage potential which is another marker of human bone marrow MSCs (226). Following established protocols they can be differentiated to display adipogenic markers, such as lipid staining with oil red O and increased LPL and PPRγ expression (39). They can also be differentiated display cartilage markers such as GAG staining with Alcian blue staining, raised total GAG content and Sox9 gene expression (39). Finally, they can present osteogenic differentiation markers such as calcium staining with alizarin red staining and raised ALP and RUNX2 gene expression (39,227) Additionally, Y201 MSC cultures and mineralized matrix produced after 21 days of osteogenic differentiation was found to have Ca/P ratio comparable to femoral trabecular bone when analysed by EDS microscopy (228). There is not yet published work where the Y201 MSCs have been used *in vitro* to grow new bone, however they meet the industry standard of a human bone marrow MSC.

The cells were used preferentially over other MSCs, such as primary MSCs obtained from donated human bone, as they have been characterised in detail and shown to respond in a consistent manner to a range of stimuli. This contrasts with primary cells, which have great variability between lines and cannot be propagated indefinitely. Hence, using Y201 MSCs would greatly reduce the number of variables whilst studying the cell response to SrAWGC, making any cellular response to the material easier to interpret. The method by which the cells were immortalised has been published (39), however in brief they were created from primary human MSCs extracted from the femoral head of routine hip replacement patients which were immortalised before passage 3 using a hTERT (human Telomerase reverse

transcriptase) lentiviral vector. hTERT allows lengthening of the telomeres and subsequent cell immortality. The cells were used in the experiments described in this work between passage 60 and passage 90.

### 3.2.2 General cell culture technique

Y201 hTERT cells were used in all experiments unless otherwise indicated. All reagents were sterile. Cells were typically grown in T175 culture flasks at 37°C, with a 5% $CO_2$ atmosphere. This was to mimic the physiological environment and ensure the buffers used maintained a constant pH. The cells used were between passages 60 and 90 and kept less than 80% confluent by regular passaging (assessed using a phase contrast microscope). Cells were cultured in basal media unless otherwise specified, consisting of Dulbecco's Modified Eagle's Medium (DMEM, Gibco, high glucose 4.5 g/l with pyruvate and L-glutamine, ref no. 41966-029) with 10% (v/v) Foetal Bovine Serum (FBS, Sigma, F7524-500ML) and 1% (w/v, 10mg/ml) Penicillin Streptomycin (Invitrogen, S15140-122). All percentages are volume per volume. Cells were detached for passaging using 0.1% (v/v) trypsin ethylene-diamine-tetra-acetic-acid solution (trypsin-EDTA, Invitrogen, S25300-054) and counted using a haemocytometer.

All previous work on the Y201 cell line has utilised the high glucose, 10% FBS cell culture media described previously (determined through personal correspondence with authors (39,227)), hence this cell culture media was chosen for the experiments described in this work. This means that the Y201 MSCs should respond more predictably and would allow for the results of this study to be more easily compared with the body of work carried out using Y201 MSCs. However, using FBS can induce variability into the experiments as the FBS can vary between batches. FBS was bought in bulk all deriving from the same batch and the same batch was used for the experiments in this study to reduce this variability.

### 3.2.3 SEM and EDX to establish cell attachment and morphology of Y201 MSCs on SrAWGC

Scanning electron microscopy (SEM) and Energy Dispersive X-ray spectroscopy (EDX) were used to establish that the Y201 MSCs attached to the material surface, to observe their morphology, and to determine the quantity of cells needed to achieve confluence.

SrAWGC discs with 0, 6.2, 12.5, 18.7, 24.9 and 37.4 Mol% Sr were made as detailed previously (Chapter 2, Section 2.2.8), autoclaved, then washed in 1 x Phosphate Buffered Saline (PBS) before being placed in 48 well plates, with the curved side facing down (see Figure 34). Curved discs were used as this was the result of the production method employed. Creating and optimising a new production method was outside the scope of the project and would not have improved the experiment. This is because the main challenge resulting from this production method was disc to disc and batch to batch variability and this would have remained even with discs which were flat on both sides. Y201 hTERT MSCs were seeded into the wells with the discs at concentrations of 0, 2, 4 and 8 x $10^4$ cells/$cm^2$. After 24 hours the samples were washed in PBS and fixed in 2.5% (v/v) glutaraldehyde and 4% (v/v) paraformaldehyde in a 0.1M phosphate buffer overnight. These were then washed three times in 0.1M phosphate buffer and a secondary fix of 1% (v/v) osmium tetroxide in 0.1M phosphate buffer was applied for 45 minutes at room temperature. All percentages were volume per volume. The samples were then washed in ultrapure water twice and then dehydrated in a graded series of ethanol solutions (25-100% (v/v) in ultrapure water), with a wait of 30 minutes in each ethanol gradient. Absolute ethanol was then removed and replaced with hexamethyldisilane (HMDS) for 30 minutes after which the samples were transferred to fresh 24 well plates and left in a desiccator to dry overnight. The samples were then mounted onto aluminium SEM stubs with adhesive pads and silver dag (a viscous conductive silver paint from Agar Scientific, see page 43 of reference (184)) was applied to ensure conduction between the surface of the discs and the stub. These were then sputter coated with approximately 20nm thick layer of Au (gold) using an Agar Auto Sputter Coater to form a conducting layer across the

sample. Images were taken using an accelerating voltage of 20V and probe current of 60µA in a Hitachi S3400N variable pressure SEM. There were three discs for each SrAWGC composition and four images were taken of each sample. One picture was taken in the centre of the sample and three more pictures were taken around the centre. The experiment was repeated a second time independently. When identifying whether the cells had attached to the discs, secondary electron mode was used as it provides increased edge detection. For detailed analysis of cell morphology, backscattered electron mode was used to highlight low density cells (as dark areas) compared to the high density (bright) glass ceramic. This was determined by taking pictures of 10 cells per sample at x 800 magnification and then importing these into ImageJ (229). The outline of the cell was then traced by hand in ImageJ and “measure polygon” was used to determine the area and circularity.

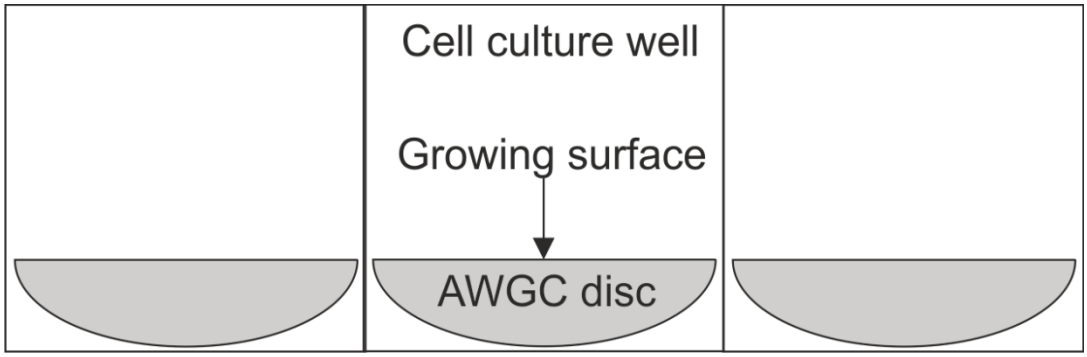


**Figure 34: Description of how the AWGC discs are positioned within the multi-well plates. The curved surface of the disc faces down, whilst the flat surface, on which cells are grown, faces up.**

EDX was also performed on the surface of the scaffolds using a Bruker XFlash detector and analysed with Quantax analysis software (smoothing of 15, 5 minute surface map). This was used to identify the cells against the material surface, however it was not suitable for taking many images for use in quantification of the cell morphology due to the technique being relatively slow, and the number of samples being analysed.

### 3.2.4 Glass and disc conditioned media to establish the effects of ions released by the material on Y201 MSCs

Cell culture media were conditioned with the different compositions of AW glass powder (with increasing Sr content) to screen these different glass compositions, and specifically their ionic degradation products, for any effects they might cause on the Y201 MSCs. The glass conditioned media is a useful model to explore the cell response to the ions released by the glass and can be used as a model for the glass-ceramic, however it is not an exact representation of the ions released by the glass-ceramic itself. This is because the glass-ceramic is composed of multiple phases and the residual amorphous (glassy) phase may have undergone some changes (such as becoming enriched or deprived in elements) during the production process. This could then potentially result in an altered release profile of the AWGC amorphous phase compared with the AW glass itself. However, the glass conditioned media does reduce the number of variables in the experiments, compared with trying to use the amorphous component of the AWGC as the production process is more easily controlled. For these reasons glass conditioned media will be used as a relatively simple model to explore the cell response to SrAW and how the Sr content alters this. Batch to batch variability in the glass is also a consideration as these experiments were performed from a single batch of each composition.

The glass conditioned media was made by mixing 12mg/mL of AW glass powder (<45µm particle size) with high glucose DMEM for 24 hours at room temperature, before filtering to remove the glass powder (method adapted from (87)). The other components of the cell culture media (FBS, Pen/Strep, osteogenic supplements) were added after the media was filtered. This quantity of glass powder per volume was chosen arbitrarily, based on the quantities used in Autefage *et al.* (87). The quantity used was not important to the outcome of future experiments as it was not an exact model of how the SrAWGC released ions. Additionally, the glass conditioned media could be diluted with DMEM to reduce the concentration of ions to an appropriate level if necessary following characterisation of the ions released. The glass powder was autoclaved (121$^{o}$C for 20 minutes) in the mixing bottle prior to

use. The glass conditioned media for the other SrAW compositions was made by adjusting to 12mg/mL according to the different densities of the materials (determined in Chapter 2, Section 2.3.3), to ensure the same molarity of glass is being mixed with the media (see Table 18). A sample of each medium for each glass composition was frozen for later ion content analysis.

| Composition | mg/mL |
|---|---|
| AW | 12.00 |
| SrAW 6.2 Mol% Sr | 12.45 |
| SrAW 12.5 Mol% Sr | 12.86 |
| SrAW 18.7 Mol% Sr | 13.23 |
| SrAW 24.9 Mol% Sr | 13.60 |
| SrAW 37.4 Mol% Sr | 14.29 |

**Table 18: Concentration of <45μm glass powder in DMEM, adjusted for each composition according to their densities, as measured by pycnometry.**

The SrAWGC conditioned media was made by exposing 0.5ml DMEM to 15mm diameter SrAWGC discs (0, 12.5 and 24.9 mol%)(approximately the same size as the wells of a 24 well plate), placed in 24 well plates (as in Figure 34), for 24 hours, before removing and freezing until use.

### 3.2.5 Ion content of glass and disc conditioned media determined using ICP-OES

To understand the effects of the ionic dissolution products of the SrAW glass (and therefore the SrAWGC material), it is necessary to know the ions released by the material, and this was determined using Inductively-Coupled-Plasma Optical-Emission Spectroscopy (ICP-OES). ICP-OES involves a liquid sample being nebulised into a mist which is then fed into a plasma flame. The sample is then disintegrated into its constituent elements, which are repeatedly excited by the flame resulting in the release of radiation that is characteristic of different ions. Diffraction gratings then allow for this light to be split into its component colours and the intensities of these can be

quantified. The concentration of each element in the sample can then be calculated using the ICP-OES spectra of standards with known quantities of each element.

The ionic content of both glass and disc conditioned media were determined using ICP-OES, provided as a service by the Department of Geography at the University of Leeds. The glass conditioned media was made as described in Section 3.2.4. For the disc media, discs were submerged in culture media for 24 hours and the media then extracted. The media samples were then immediately frozen. 1ml of frozen sample was thawed, and diluted 10 times in ultrapure water prior to transport to Leeds and measurement, using a Thermo Scientific iCAP7600 Duo ICP (high solids nebuliser, normal spray chamber). Multiple wavelengths for each element were checked to measure for interference (Mg: 270.553nm and 280.270nm, Ca: 393.366nm and 396.847nm, Sr: 407.771nm and 421.552nm, P: 177.495nm and 178.284nm, Si: 251.611nm and 212.412nm). Yttrium (371.03nm) was used to normalise for slight variations in the volume of each sample. Three independently made batches of glass conditioned media were measured.

### 3.2.6 Determining the effects of SrAW conditioned media on osteogenic differentiation and proliferation utilising different osteogenic supplements

To establish how effective SrAWGC could be as a tissue engineering scaffold, it was important to determine what effects its dissolution products would have on MSCs, and whether the addition of strontium to the material would alter these effects. The ionic dissolution products of the discs were modelled using SrAW conditioned media, made with the different compositions of SrAW glass with increasing strontium content. The glass conditioned media was also made using different base media with increasing content of osteogenic supplements to establish how effective the SrAW conditioning was at assisting osteogenic differentiation. Basal media had no osteogenic supplements, mineralisation media had supplements to induce collagen deposition and provide the required phosphorus, and osteogenic

media contained these same supplements and the osteogenic steroid dexamethasone. As strontium was predicted to be a key factor in the response of the cells to the glass conditioned media, another series of experiments were performed where the MSCs were exposed to media with added Sr, to determine how the MSCs would respond to strontium alone.

Y201 MSCs were encouraged to osteogenically differentiate by being seeding to confluence ($4x10^4$ cells/$cm^2$) then after 24 hours, exposed to the medium of interest for 9 or 21 days. The seeding density was near confluency and as this would result in more consistent cell seeding, reducing variability in the results. Also, in order to differentiate the MSCs needed to reach confluence and so seeding near confluence would reduce the time needed for the MSCs to begin differentiating. At the required time points the ALP activity of the MSCs was measured using a pNPP-Pico Green assay, as described in section 3.2.9.

The media of interest were variations of basal, osteogenic and mineralisation media with additional supplements, such as being conditioned with SrAW glass, or with added strontium chloride (Acros Organics, 99.9% purity, anhydrous).

The basal media was as described above, whilst osteogenic media was basal media supplemented with 50µg/ml L-ascorbic acid-2-phosphate, 5mM β-glycerophosphate and 10nM Dexamethasone. Mineralisation media was osteogenic media without Dexamethasone.

### 3.2.7 Determining the effects of Strontium alone on osteogenic differentiation and proliferation utilising different osteogenic supplements

To determine whether the strontium in the glass conditioned media was solely responsible for any response, the osteogenic response of the MSCs to media containing $SrCl_2$ was investigated. A strontium chloride (prepared using 99.99% purity anhydrous solid, Fisher) solution of 176mM was prepared in ultrapure water (0.14g in 5ml $H_2O$), then filtered sterile. The ultrapure water was produced by a Purite Ondeo IS machine with resistivity between 17.6 and 18.2mΩ. This was then added to mineralisation media

(see Section 3.2.6), on the day when required, to produce media with 0, 0.125, 0.5, 1, 2, 4 and 8mM $SrCl_2$, with sterile ultrapure water being added ensure all media had been diluted with the same volume of ultrapure water (including that in the $SrCl_2$ solution). First, the most appropriate media type was confirmed using basal, mineralisation and osteogenic media with 4mM $SrCl_2$ (based on that used previously and seen to induce raised ALP (230)) and measuring osteogenic response of the MSCs using ALP normalised to DNA (pNPP and PicoGreen, see Section 3.2.9). The results of this lead to mineralisation media being taken forward (as theoretically Sr should play the role of the osteogenic inducer dexamethasone) and then this was supplemented with 0, 0.125, 0.5, 1, 2, 4 and 8mM $SrCl_2$ to determine the optimum concentration of $SrCl_2$ for osteogenic differentiation. These concentrations were selected as they are centred around the concentration of Sr found at bone formation sites in patients taking Strontium ranelate (124). After being exposed to these media for 9 days, ALP activity of the MSCs was measured using a pNPP-PicoGreen assay, as described in section 3.2.9. These assays were run over a short timescale to facilitate rapid screening.

### 3.2.8 Determining the effects of Sr content of SrAWGC discs on MSC proliferation

MSCs were exposed to SrAWGC discs to determine its effectiveness as a tissue engineering scaffold. Initially, the ability of the SrAWGC to support proliferation was measured, and whether the strontium content of the material affected this.

48-well sized SrAWGC Discs were made as detailed previously, autoclaved, then washed in 1 x Phosphate Buffered Saline (PBS) before being placed in 96 well plates, with the curved face down (see Figure 34). Y201 hTERT MSCs were seeded into the wells at concentrations of $4.5 \times 10^4$ cells/$cm^2$ to provide a baseline from which the cells could grow. This was near confluency which prevents the cells entering the “lag phase” of cell growth resulting from having too few cells. After 24 hours, they were encouraged to differentiate by being exposed to the medium of interest for 9, 14 or 21 days.

As with the glass conditioned media studies, media with different supplements were used to determine the limitations of any osteoinductive effects of the SrAWGC discs.

First, to establish how osteogenic media, and media without any osteogenic supplements (basal), compared, the Y201 MSCs were cultured on the SrAWGC discs with or without strontium (0 and 12.5 Mol% Sr) for up to 21 days using basal or osteogenic media. This was then followed by an experiment which compared the Y201 MSCs on all six compositions of SrAWGC discs (0, 6.2, 12.5, 18.7, 24.9 and 37.4 Mol% Sr) for 21 and 14 days whilst growing in only osteogenic media or mineralisation media, respectively, to determine whether it was the dexamethasone within the osteogenic media which was responsible for any effects. The media used have been described in section 3.2.6. At the time point, the samples were prepared for a PicoGreen assay, as described in Section 3.2.9.

### 3.2.9 pNPP-PicoGreen assay for determination of osteogenic differentiation through ALP and DNA quantification

The experiments in Sections 3.2.6, 3.2.7 and 3.2.8 utilised the pNPP-Pico Green assay to determine the ALP activity and cell number at the time points for the conditions studied. The assay is described briefly here. At the chosen time point, the medium was aspirated from the well and washed twice in 0.2M Carbonate Buffer (2:1 volume to volume ratio of 0.2M $Na_2CO_3$ to 0.2M $NaHCO_3$, pH 10.2) after which 0.1% (v/v) Triton X was added to lyse the cells (150µl in a 96 well plate), and then the well plate was frozen. Once all time points had been collected they were freeze thawed three times, after which 50µl from each experimental well was moved respectively to a clear and a black 96-well plate. To the clear well-plate, ALP standards (were added (100µl in triplicate), followed by 50µl of pNPP (10mg pNPP, P4744, Sigma, in 20ml ultrapure water plus 9ml 0.2M carbonate buffer and 1ml 100mM $MgCl_2$). The standards were made through sequential dilution described of 10mM pNPP (cat N7660, Sigma) in 0.2M Carbonate Buffer as described in Table 19. After 1 hour absorbance at 405nm was read using a plate reader (Thermo Scientific Multiskan Go). To the black well-plate, DNA

standards were made from a 10µg/ml stock of salmon sperm (Invitrogen, see Table 20) and added (50µl in triplicate), followed by 50µl of PicoGreen (Invitrogen, P7581) diluted 1:50 in TE Buffer (10mM Tris, 1mM EDTA at pH 7.5). This was agitated to mix, then after 10 minutes under foil this was measured using 485nm excitation and detecting 538nm fluorescence emission on a BMG Labtech POLARstar OPTIMA plate reader.

The ALP activity (pNPP nmol/ml/min) was determined by first using the measurement of the pNPP standards to determine the counts per pNPP concentration, and using a linear fit to interpolate this for the values measured for the experimental conditions. This was then divided by the time over which the pNPP reaction took place (1 hour) to get the pNPP per millilitre per minute. The DNA concentration (µg/ml) was determined by using the DNA standards to interpolate the DNA concentration from the fluorescence measurements (utilising a cubic spline fit in IGOR Pro). The ALP activity was then normalised against DNA content (to produce a final value of (nmol/ml/min)/(µg/ml) to ensure ALP increases were due to a change in cell function and not due to a simple raise in the number of cells producing baseline ALP levels. The DNA measurements were also used to quantify cell proliferation as the quantity of DNA in the experimental conditions is proportional to the number of MSCs present.

| Concentration pNPP (µmol/ml) | pNPP (µl) | 0.2M carbonate buffer (µl) |
|---|---|---|
| 0.5 | 20µl pNPP | 380 |
| 0.3 | 12µl pNPP | 388 |
| 0.2 | 16µl pNPP | 784 |
| Following made by serial dilution of the 0.2 µmol/ml standard | | |
| 0.1 | 400µl of 0.2µmol/ml | 400 |
| 0.05 | 400µl of 0.1µmol/ml | 400 |
| 0.025 | 400µl of 0.05µmol/ml | 400 |
| 0.0125 | 400µl of 0.025µmol/ml | 400 |
| 0 | 0 | 400 |

**Table 19: pNPP standards for use in pNPP-PicoGreen experiments.**

| DNA concentration (µg/ml) | Volume of DNA (µl) | Volume of 0.1% (v/v) Triton X (µl) |
|---|---|---|
| 8 | 80 (µl of 100µg/ml stock) | 920 |
| 4 | 500 of A | 500 |
| 2 | 500 of B | 500 |
| 1 | 500 of C | 500 |
| 0.5 | 500 of D | 500 |
| 0.25 | 500 of E | 500 |
| 0 | 0 | 500 |

**Table 20: DNA standards for use in pNPP-PicoGreen experiments.**

### 3.2.10 Determining the effects of strontium addition to AW and AWGC on MSC proliferation using an EdU assay

It was important to determine whether the ionic dissolution products of the SrAWGC raised cell proliferation and whether the addition of strontium to the material affected this. A proliferation assay (Click-iT EdU) was used to determine this, where the SrAW glass conditioned media were used to model the ionic dissolution products of the material, whilst the SrAWGC discs were used to determine the effects of the intact material. In this assay, EdU (5-ethynyl-2'-deoxyuridine) is taken up into the DNA during S-phase, then this can be measured by utilising a click-chemistry reaction which attaches a fluorescent dye to the EdU, marking cells which are undergoing or have undergone cell cycling. This can then be normalised to the number of cells determined by a DNA counter fluorescent stain (Hoechst). This assay was performed on both MSCs grown on discs and MSCs exposed to glass conditioned media.

Cells were seeded at 50% confluence to ensure they could adequately proliferate (on culture plastic or on SrAWGC discs). The next day these were synchronised bat G0 phase using low serum media (0.5% (v/v) FBS) for 24 hours. The cells seeded on culture plastic were then exposed to the SrAW glass conditioned media with 10μM EdU (Click-iT EdU assay, Sigma, catalogue number C10337), whereas those on SrAWGC discs were exposed to mineralisation medium with 10μM EdU. After 48 hours exposure (to ensure at least one cell cycle was captured, as the cell cycle of Y201 cells is approximately 24 hours) the media was aspirated and the cells fixed with 3% (v/v) paraformaldehyde.

The EdU was stained following the manufacturer's instructions, and the Hoeschst stain added by following the manufacturer's instructions within the Click-It EdU 488 kit. The uptake of EdU was quantified by taking 4 images of each well/ disc using a Leica DM IRB inverted microscope. The cells grown with glass media were imaged with an x10 objective. The discs used an x20 objective as the fluorescence was less intense. ImageJ was then used to analyse the fluorescence images (229). First they were binarised (set to 16 bit) to change the image to be a grey scale going from black (the

background) to white (the nuclei). Next a threshold was employed (threshold (17,255) in ImageJ) to remove noise and make a clear cut-off below which was considered “background”. The nuclei were then counted using the “count particles” function, which counted all contiguous roughly circular white spots on the image. Spots with area between 6 $\mu m^2$ and 600 $\mu m^2$ were counted as nuclei.

### 3.2.11 Determining the effects of strontium addition to AW and AWGC on MSC metabolic activity using a WST-1 assay

To compliment the findings of the proliferation assay, a WST-1 assay was used to determine whether the SrAWGC discs or their ionic dissolution products (modelled using the SrAW glass conditioned media) could alter cell metabolic activity (as a second measure of cell growth), and whether the strontium content of the material also affected this. The WST-1 metabolic activity assay determines cell numbers through a tetrazolium salt being cleaved in the mitochondria during respiratory processes, resulting in a colour change from pink to orange. A higher number of cells results in a higher metabolism of the dye and a stronger colour being produced.

For the cells exposed to glass conditioned media, the cells were seeded confluent ($4x10^4$ cells/$cm^2$) and after 24 hours to attach, were exposed to the glass conditioned media for 9 days before WST-1 media (10% (v/v) in media, Roche) was added and after 1 hour the absorption at 440nm was measured with a Thermo Scientific Multiskan Go plate reader, a 600nm reference frequency.

For the cells grown on glass on glass ceramic discs they were seeded onto the discs at 50% confluence to promote growth ($2.25 x10^4$cells/$cm^2$) and after 24 hours to attach, were exposed to mineralisation media for 7 days. At the time point WST-1 media (10% (v/v) in media, Roche) was added and after 1 hour the absorption at 440nm was read as above.

### 3.2.12 Colony Forming Unit-fibroblastic assay to determine effect of SrAW on colony forming ability of Y201 MSCs

To explore whether the ions released from the glass could affect MSC progenitor cell activity a Colony forming unit fibroblastic (CFU-f) assay was performed. The cells were plated at 10 cells/cm$^2$, and left to grow in cell culture medium conditioned without glass or with the six different glass conditioned media with increasing Sr (as used previously). Once colonies were distinct, defined typically as 50 cells or more (~10 days), they were stained with crystal violet and once dried were scanned using a flatbed scanner. The crystal violet stained colonies were then quantified using ImageJ (229) by scaling the image (using measurements of the multiwell plates the experiment was conducted in) and then manually circling the colonies and using the “measure” function in ImageJ. This created an assessment of the size and circularity of the colonies in all of the experimental conditions.

### 3.2.13 Statistical analysis

Statistical analysis for all experiments was performed using IGOR Pro Version 6.37 software (WaveMetrics). Equality of variance was established utilising Bartlett’s test. Significant differences between conditions were then determined using a Tukey test if the variance was equal between conditions, or a Nemenyi (Tukey type) non-parametric multiple comparison test between the conditions otherwise, with significance being defined as p-value of less than 0.05.

## 3.3 Results

### 3.3.1 SEM and EDX to establish cell attachment and morphology of Y201 MSCs on SrAWGC

Initially, cell attachment to the SrAWGC discs was explored to determine how the MSCs attach and spread, and the effect of different Sr concentrations in the material, using different electron microscopy and associated techniques.

Initially, the cells were seeded on the six different compositions of SrAWGC disc with increasing strontium content (0, 6.2, 12.5, 18.7, 24.9 and 37.4 Mol% Sr) at 4 x $10^4$ cells/$cm^2$ and after 24 hours the samples were prepared and SEM taken. Three discs for each composition were imaged at the centre and three points around the centre, with the whole experiment repeated a second time independently. The discs were seen to support cell attachment, with flattened cells distinguishable from the surface using only SEM in secondary electron mode, and with no rounded cells detected (representative images can be seen in Figure 35). For all of the compositions the cells are spread out with processes extending into the surface features. From these images the addition of strontium to the material was not seen to change the cell attachment. The contrast between the cell and surface was good, although it was not always easy identify the edge of the cell. Additionally, the cells were clearly not in their physiological state having been dried out.

EDS mapping was  then used to establish the elemental content of the surface, allowing the carbon rich cells to be clearly identified against the silicon rich surface. The MSCs were seeded on the discs in increasing concentrations to determine the concentration of cells at which confluence was reached. EDS maps were then taken of the prepared samples after the MSCs had been given 24 hours to attach.

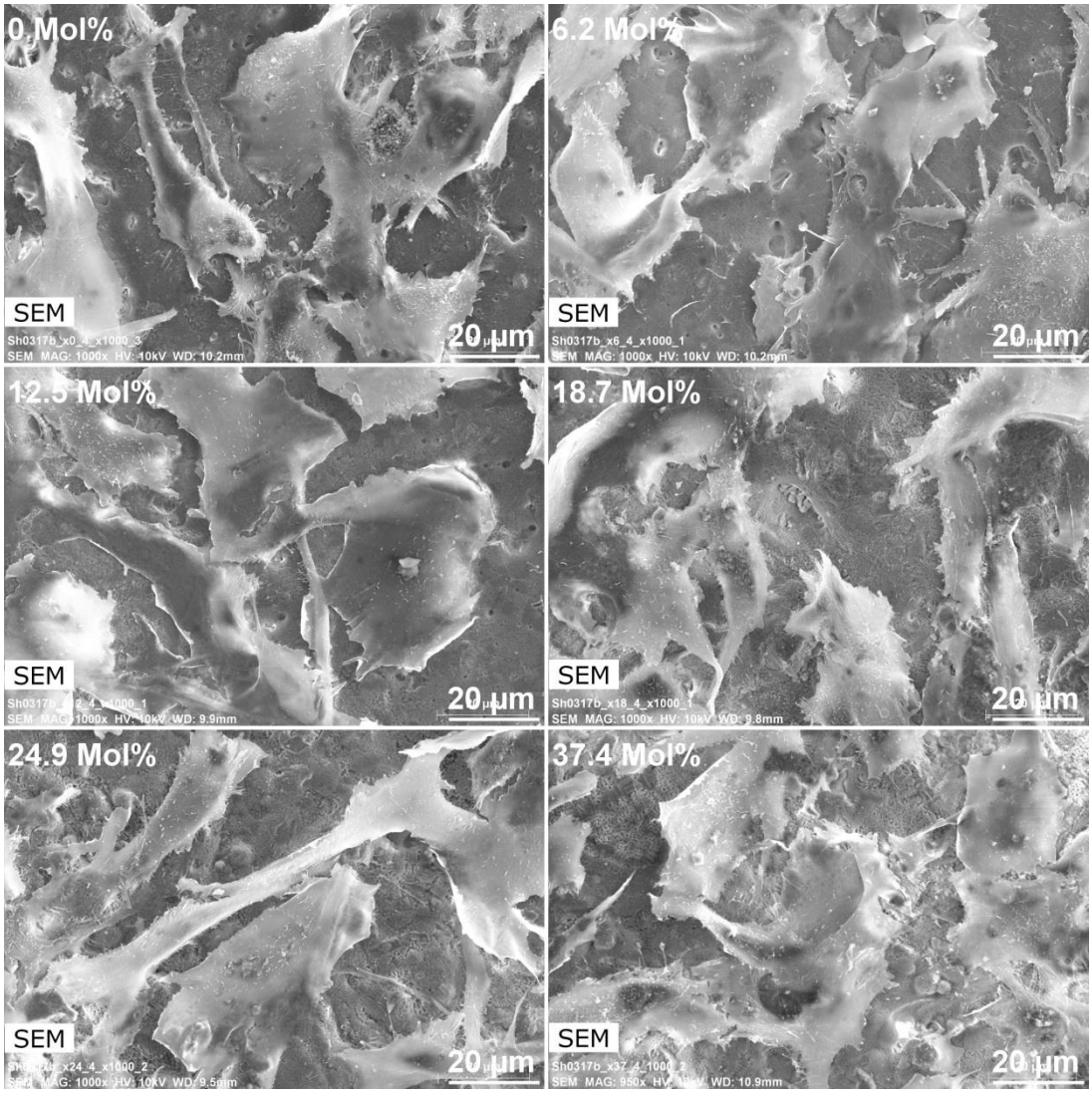


**Figure 35: Representative SEM of Y201 hTERT MSCs seeded on SrAWGC discs at 4x10$^4$ cells/cm$^2$ after 24 hours, with increasing strontium content in the discs (0, 6.2, 12.5, 18.7, 24.9 and 37.4 mol% Sr). Scale bar = 20µm.**

Representative EDS maps from three samples and two repeats for each composition are shown in Figure 36 and Figure 37, where red and blue showed the signal from carbon and silicon atoms, respectively. The increasing concentrations of cells are clearly visible against the SrAWGC disc surface as the carbon signal was seen to localise within the cells, excepting those areas where the cell is raised or lowered out of the plain of the image (where the x-rays detected quickly vanished to zero) due to the topography of the material.

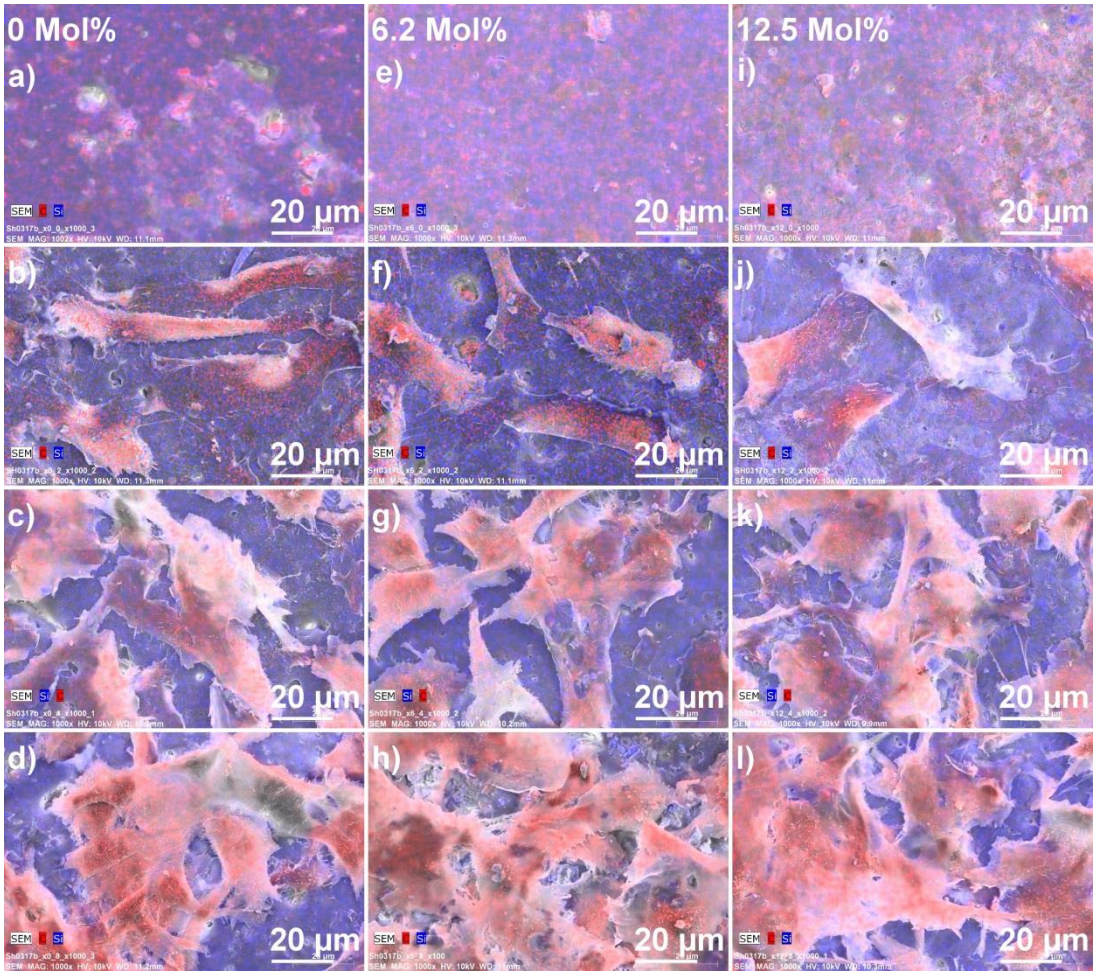


**Figure 36: Representative SEM and EDS of Y201 hTERT MSCs seeded at 0, 2, 4 and 8x10$^4$ cells/cm$^2$ on SrAWGC discs with 0 Mol% Sr (a,b,c,d), 6.2 Mol% Sr (e,f,g,h) and 12.5 Mol% Sr (I,j,k,l) content after 24 hours. The EDS displays carbon as red and silicon as blue.**

Again, the cells were observed to be spread out and extend processes into and across the surfaces all of the compositions and in all seeding densities. The strontium content was not seen to influence the seeding of the cells on the disc surface.

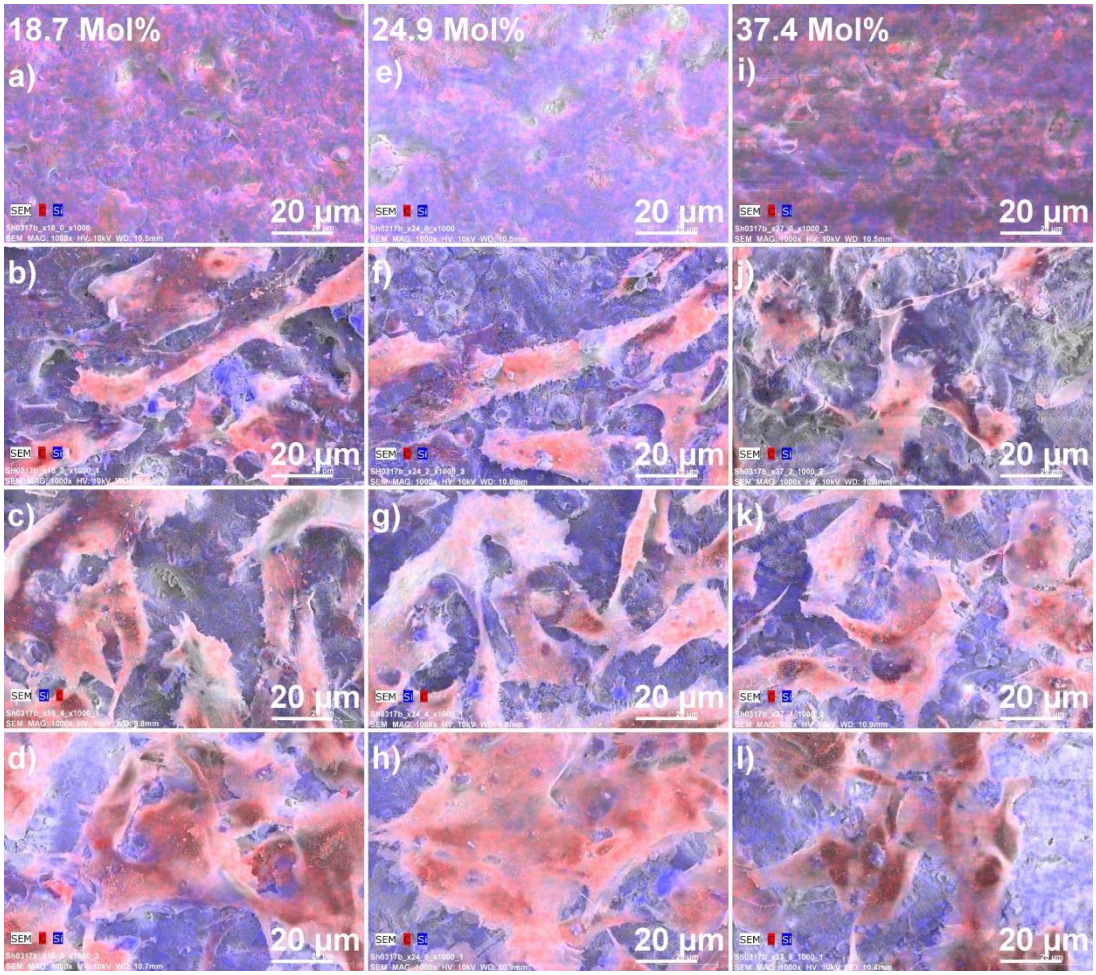


**Figure 37: Representative SEM and EDS of Y201 hTERT MSCs seeded at 0, 2, 4 and 8x10$^4$ cells/cm$^2$ on SrAWGC discs with 18.7 Mol% Sr (a,b,c,d), 24.9 Mol% Sr (e,f,g,h) and 37.4 Mol% Sr (I,j,k,l) content after 24 hours. The EDS displays carbon as red and silicon as blue.**

The samples where no cells were present show what seems to be a consistent carbon signal across the disc surface, however this was an artefact of the software. As the images were normalised to themselves relatively weak sources of carbon (such as fixatives on the disc surface) seem brighter in a sample without a strong source of carbon (the discs without cells).

Back scattered electron contrast mode on SEM was used to take images of the cells on the discs with the cells being easily distinguished from the surface as dark (low density) regions. Representative images from the same three samples from two repeats for each composition used in the earlier SEM and EDS analysis can be seen in Figure 38). The cells are observed to be clearly spread out on the surface of all of the compositions, with processes extending out to explore the surrounding material. The difference in surface morphology of the SrAWGC discs is also clear from back scattered electron images. This is because the technique exaggerates the differences in the surfaces, as areas of the surface which were out of plane also produce little signal (absence of material is effectively a very low density), and hence appear dark (which are seen as the dark cavities in (Figure 38).

As this technique gave a very clearly defined edge to the cell it made it possible to measure the cells morphology, and so determine whether or not the different compositions of SrAWGC with increasing strontium would alter the cell morphology. The morphology of the cells was quantified utilising ImageJ (229), where 10 cells for each sample were outlined with a polygon, then the software calculated the circularity and aspect ratio associated within this polygon (see Figure 39). The resulting circularities and aspect ratios can be seen in Figure 40, and differences were determined using ANOVA with no significant difference ($p < 0.05$) measured between the cells on the SrAWGC compositions with increasing Sr content.

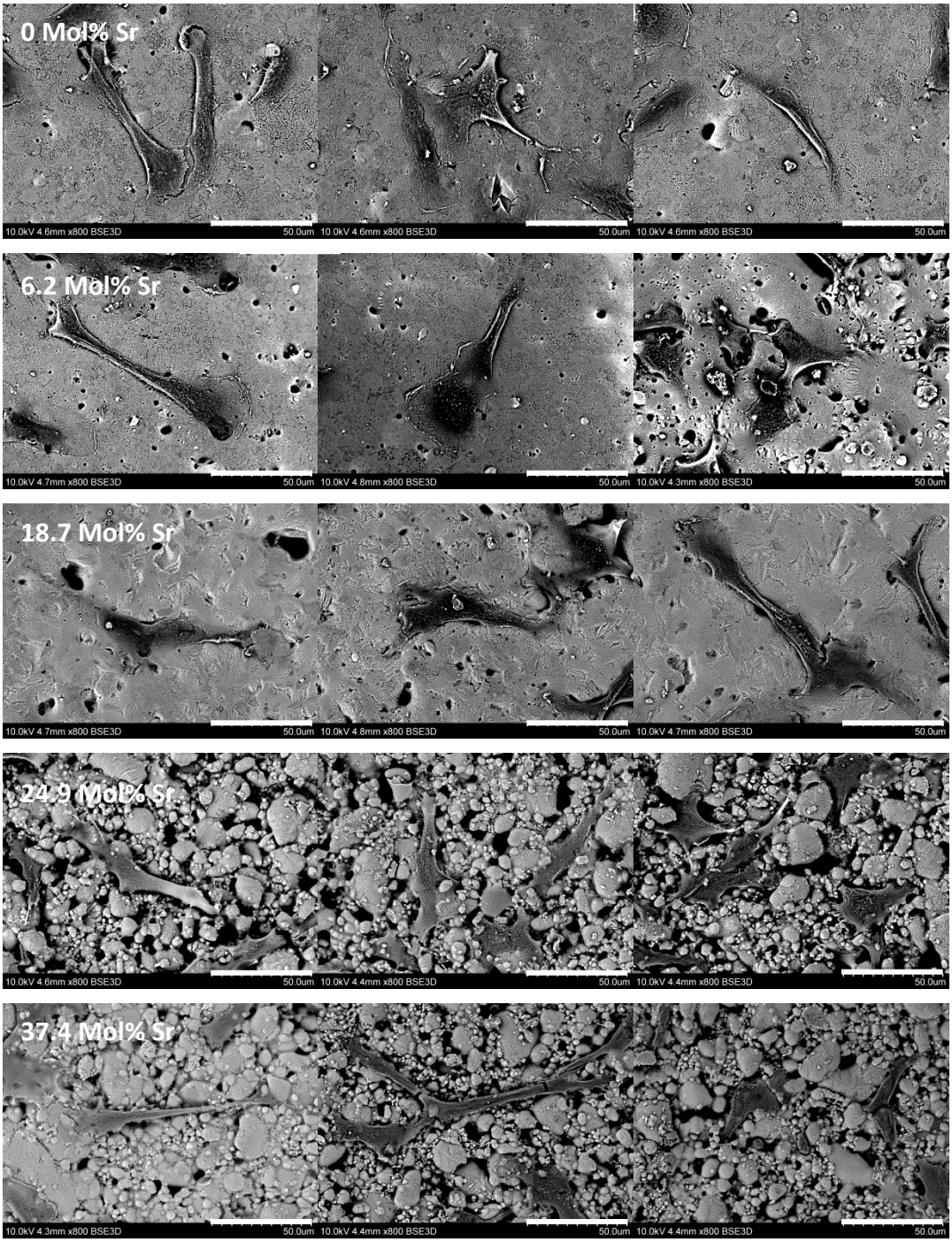


**Figure 38: Representative backscatter SEM images of human MSCs on the surface of six different compositions of SrAWGC discs (seeded at 2 x$10^4$ cells/$cm^2$). Scale bar indicates 50µm.**

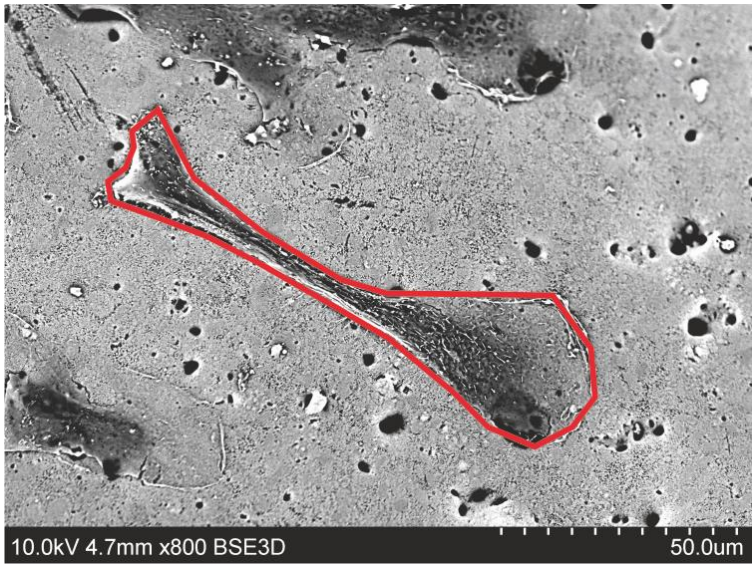


Figure 39**:** Representative backscatter SEM image of how the cell shape of Y201 hTERT MSCs on SrAWGC discs were defined within ImageJ.

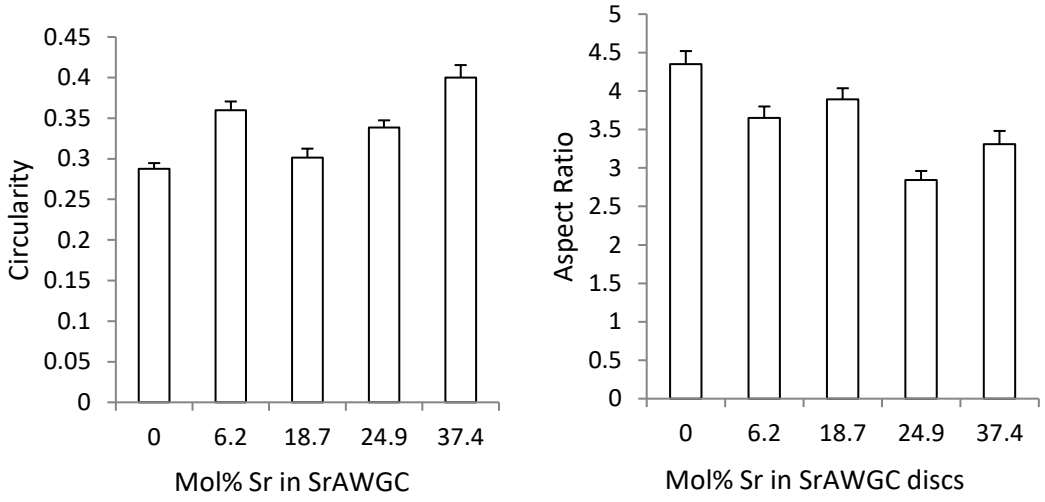


Figure 40**: The average circularit**y and aspect ratio of 10 MSCs grown on the surface of 5 different compositions of SrAWGC disc (the 12.5 mol% data is not displayed as the discs were not conductive enough). The values are means, with error bars representing the standard error. There were no significant differences between the conditions.

### 3.3.2 Ion content of glass and disc conditioned media determined using ICP-OES

As the ions released by the SrAWGC are considered to be a key part of the interaction between the material and the cells, it was important to determine how the addition of strontium to SrAWGC affected this. It is also important to determine the ions released by the SrAW glass, as the glass is theorised to

be the most bioactive component of the SrAWGC material. The ion release was measurements for the SrAW glass and SrAWGC discs was taken after 24 hours as this was a manageable amount of time over which to manufacture glass conditioned media for future experiments, and for the discs represented a mid-point between the discs being exposed to the media and the media being changed.

The results of the ICP-OES for glass conditioned media can be seen in Figure 41. For the glass conditioned media, strontium ion release was seen to rise with increasing strontium content, whilst calcium decreased. The other ions  did not change significantly between the conditions. There was a significant increase in silicon between the glass media and the control media, however the addition of strontium was did not affect this. There was also a small (non-significant) decrease in phosphorus content between the glass conditioned media and non-conditioned mineralisation media.

The  ion release from the SrAWGC discs  after 24 hours can be seen in Figure 42, however t. Release of strontium was seen to rise with strontium content of the disc, however only the 24.9 Mol% Sr had a significant increase compared 0 Mol% Sr . Silicon release also increased with increasing strontium content of the discs, as did calcium release, whilst phosphorus was seen to decrease at the highest strontium content. There was not observed be a change in magnesium between the control media and any of the SrAWGC compositions. The ion release from the discs was different than that measured for the glass conditioned media, but it is important to note that the materials are quite different. The glass powder conditioning the media had a very high surface area and was finely dispersed, whereas the glass-ceramic discs consisted of an amorphous phase (relatively similar to the glass powder) and two crystalline phases. The way in which these phases reacted to the culture media could have resulted in the differences.

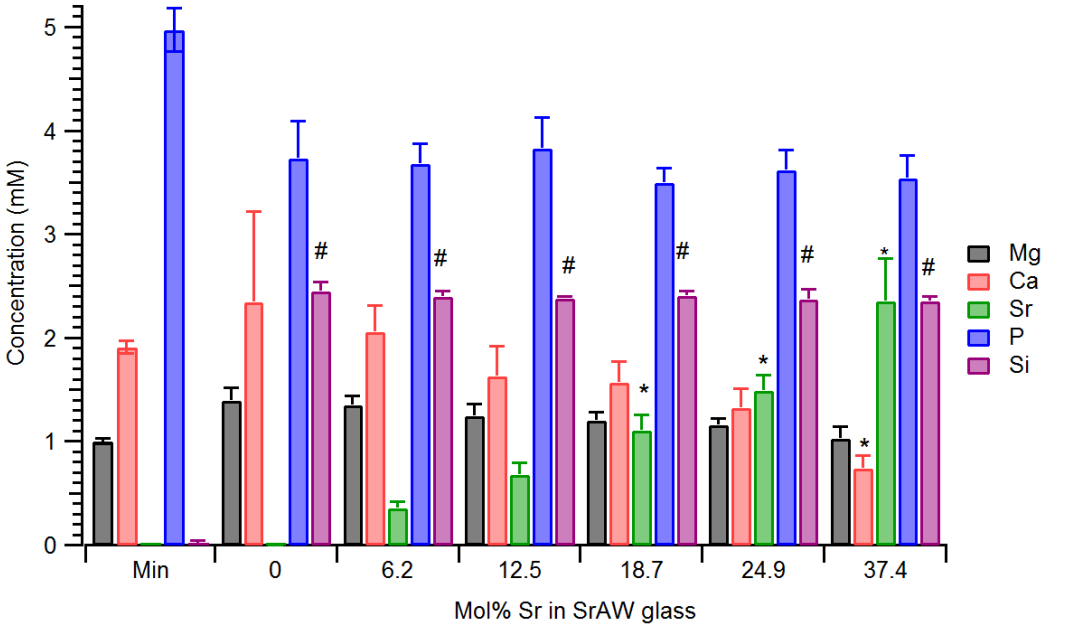


**Figure 41: Ions released from mineralisation (min) media mixed for 24 hours with SrAW glass powders with increasing strontium contents, measured using ICP-OES. The values are means of triplicate measurements, with error bars representing the standard error. * is significant difference (p<0.05) from 0 Mol% Sr composition, # is significant difference (p<0.05) from the mineralisation media alone.**

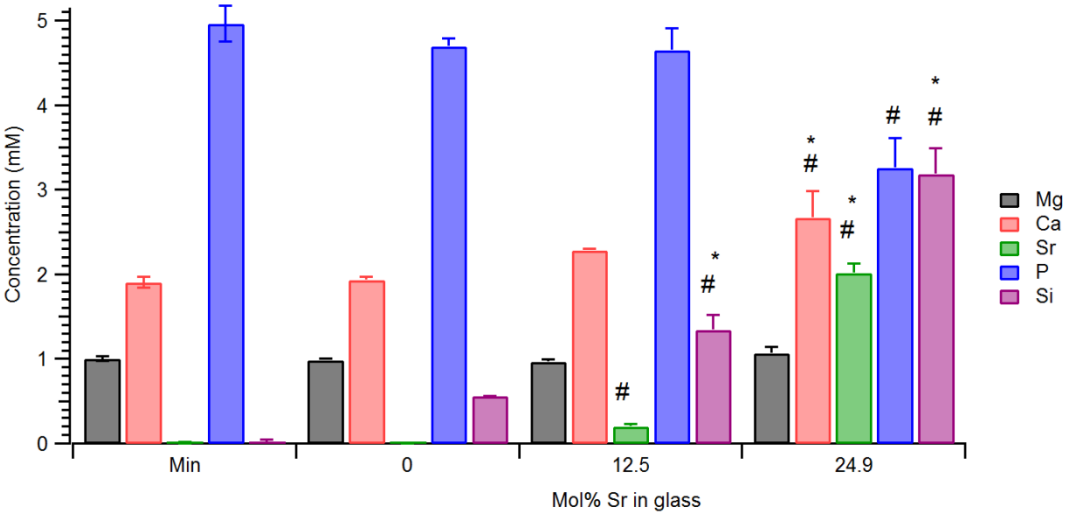


**Figure 42: Ions released from SrAWGC discs with increasing strontium content after exposure to mineralisation (min) media for 24 hours, measured using ICP-OES. The values are means of triplicate measurements, with error bars representing the standard error. * is significant difference (p<0.05) from 0 Mol% Sr composition, # is significant difference (p<0.05) from the mineralisation media (min) alone.**

### 3.3.3 The effects of Sr on Y201 MSC osteogenic response independent of SrAW glass

To understand how the MSCs respond to SrAWGC, it is important to establish the effects of strontium alone on both osteogenic differentiation potential and cell growth of the Y201 MSCs in the absence of potentially confounding influences (such as other elements released by the SrAWGC discs or into the conditioned medium, or material surface topography). This will indicate the baseline response we could expect from these cells, and will be a valuable reference when discussing the Y201 MSC response to SrAWGC.

The most appropriate media type to use in the osteogenic and proliferative experiments with strontium chloride ($SrCl_2$) was confirmed by measuring the ALP and DNA response of Y201 MSCs using basal, mineralisation and osteogenic media with 4mM $SrCl_2$. This is because the supplements, particularly dexamethasone (the main osteogenic component of osteogenic media), could potentially interfere with the mechanisms induced by Sr. However, basal media might not have the resources required by the cell (such as additional phosphorus and Ascorbic acid) to utilise Sr to alter differentiation or cell growth.

The results are presented in Figure 43, with the osteogenic media observed to produce increased ALP at day 9 when compared to basal medium, both with and without $SrCl_2$. The mineralisation media induced an effect between the basal and osteogenic media as it was observed to raise ALP compared to basal for no strontium and 4mM $SrCl_2$ at day 9. However, the addition of 4mM $SrCl_2$ resulted in a slightly lowered ALP compared to no strontium. Cell number was unchanged between the strontium and no strontium conditions, though it was seen to increase over time (Figure 44).

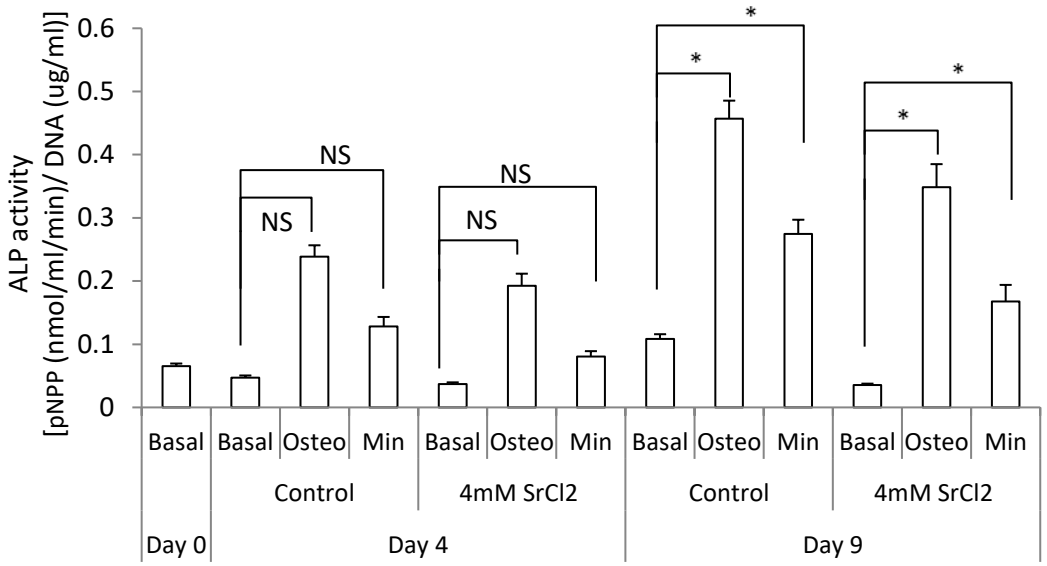


**Figure 43: ALP Per cell of Y201 MSCs after exposure to basal, osteogenic (osteo) and mineralisation (min) media with 4mM $SrCl_2$ content. The values are means of 6 repeats, with error bars representing standard error. Significant differences: * indicated a significant difference between the indicated conditions ($p<0.05$).**

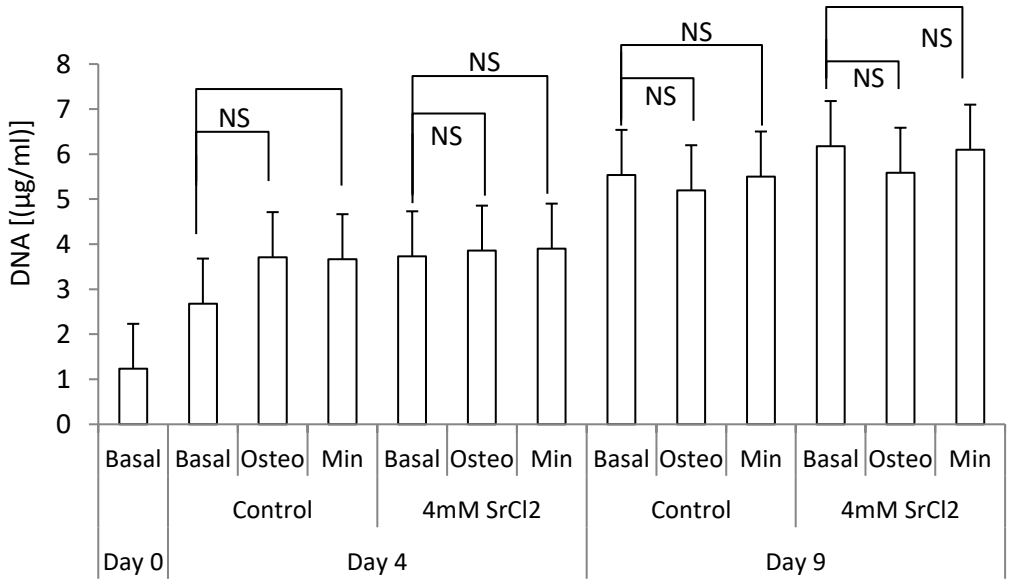


**Figure 44: Cell number (measured by DNA content) of Y201 MSCs after exposure to basal, osteogenic (osteo) and mineralisation (min) media with 4mM $SrCl_2$ content. The values are means of 6 repeats, with error bars representing SEM. There were no significant differences as shown ($p<0.05$).**

As mineralisation media was still capable of raising the ALP expression of the MSCs (at day 9), without Dexamethasone (a very strong osteogenic steroid), it was decided this was the superior media to screen the effectiveness of strontium (it minimised the stimuli and hence the variables the cells would be exposed to). Therefore, mineralisation media was taken forward and used to screen different concentrations of Sr (0, 0.125, 0.5, 1, 2, 4 and 8mM $SrCl_2$) for their effects on the osteogenic differentiation and proliferation of the Y201 MSCs. Over 9 days, osteogenic and mineralisation media were seen to induce a clear increase in ALP per cell for the Y201 cells when compared with basal media (Figure 45). The addition of $SrCl_2$ to the mineralisation media caused a dose-dependent effect, with the ALP per cell rising as increasing concentrations of $SrCl_2$ were added, peaking at 1mM $SrCl_2$, then falling as higher amounts were used. However, the addition of only 0.125 mM $SrCl_2$ lowered ALP significantly compared to mineralisation media.

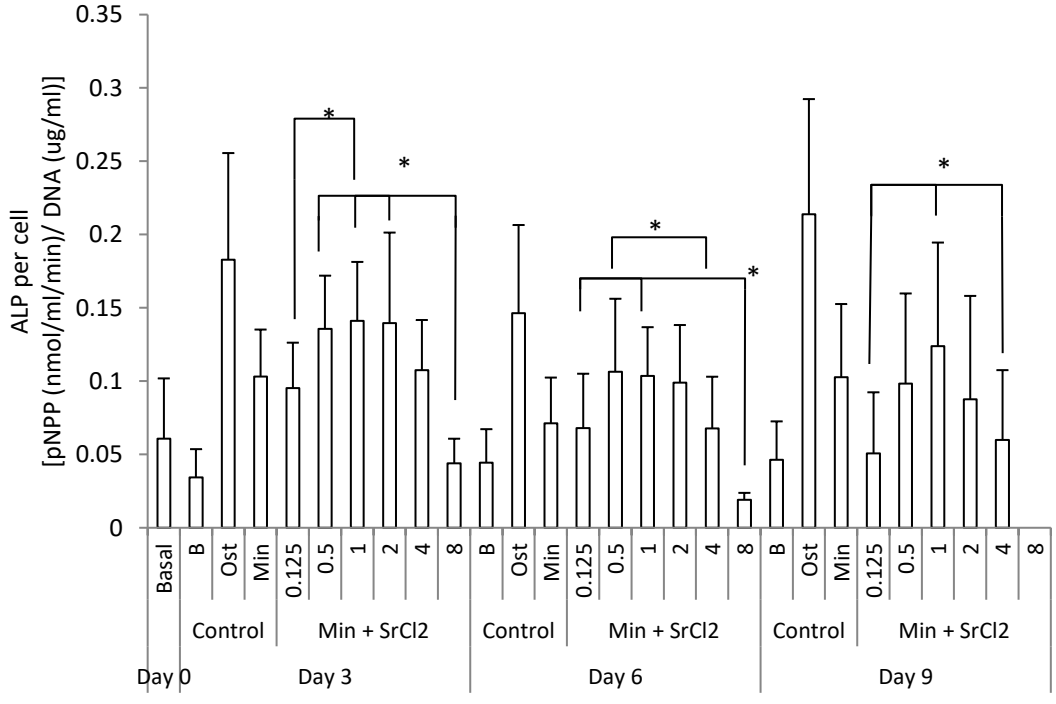


**Figure 45: ALP per cell of Y201 MSCs after exposure to mineralisation media with increasing $SrCl_2$ content for 3, 6 and 9 days. The values are means of 6 repeats, with error bars representing standard error. Significant differences: * indicated a significant difference between the indicated conditions ($p<0.05$).**

### 3.3.4 The effects of ion release from SrAW glass on Y201 MSC osteogenic differentiation and proliferation

As described previously, the ion release from the SrAWGC could be an important factor in any MSC response, hence SrAW glass conditioned media was used to model the ions released by the amorphous phase of the material, and the MSC response to the glass conditioned media was explored. As before, the experiments were performed with basal media (to determine whether strontium alone was sufficient to provoke a response in the cells), with osteogenic media (to determine whether the cells could differentiate with this well established stimulus and whether the strontium and other ions from the material would interfere with this) and with mineralisation media, which was osteogenic media without dexamethasone, to see if strontium could play the part of the osteoinducer.

Both the 0 and 12.5 mol% Sr glass conditioned osteogenic media were seen again to increase the ALP activity for the MSCs compared with the 0 and 12.5 mol% Sr glass conditioned basal media, respectively, at both days 4 and 9 (Figure 46). At day 4, the glass conditioned mineralisation media for the 0 and 12.5 mol% compositions also increased the ALP activity compared with the basal 0 and 12.5 mol% Sr conditioned media, respectively. However, at day 9, only the strontium containing 12.5 mol% Sr glass conditioned mineralisation media induced a significant increase in the ALP activity compared with the basal condition (12.5 mol% Sr glass conditioned basal media). For the glass conditioned media without Sr (0 Mol%) there was no significant difference at day 9 between the basal and mineralisation media conditions. This indicates that in the glass conditioned medium without strontium (0 mol% Sr), the osteogenic steroid dexamethasone (found in the osteogenic media) was required to induce an increase in ALP activity in the MSCs at day 9. However, for the glass conditioned media with strontium (12.5 mol% Sr) this was not the case, and at day 9 only the mineralisation media additives (β-glycerophosphate and L-ascorbic acid) were required to induce an increase in ALP activity.

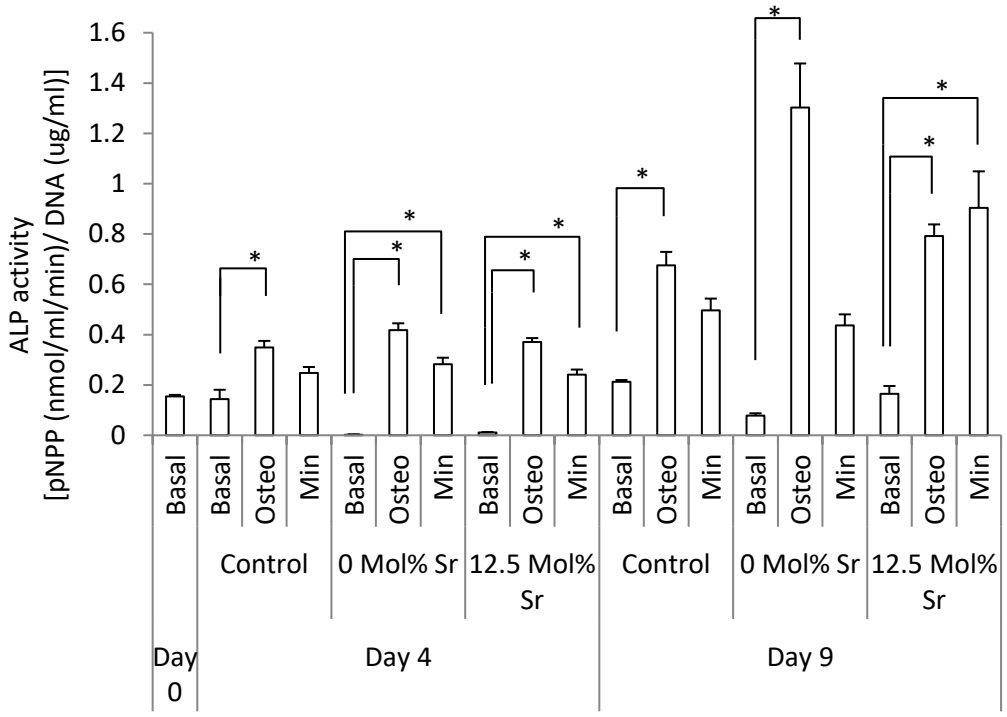


**Figure 46: ALP activity normalised to cell number of Y201 MSCs after exposure to basal, osteogenic and mineralisation media conditioned with glass powder containing 0 and 12.5 mol% Sr. The values are means of 6 repeats, with error bars representing standard error. Significant differences: * indicated a significant difference between the indicated conditions ($p<0.05$).**

Longer studies were performed on the glass conditioned basal media, using the six different compositions of SrAW with increasing strontium content. Again the osteogenic media control was observed to increase ALP activity (Figure 47). However, conditioning basal media with the SrAW glass resulted in no significant increase in ALP response, regardless of strontium content in the glass, again indicating that strontium in basal media is not sufficient to induce osteogenic differentiation. In contrast, there were significant increases in DNA for higher strontium compositions at day 7, followed by the remaining compositions at day 14 (Figure 48), which could signify that even in basal media, the Sr (and other ions) released by the glass into the conditioned media were able to increase cell growth.

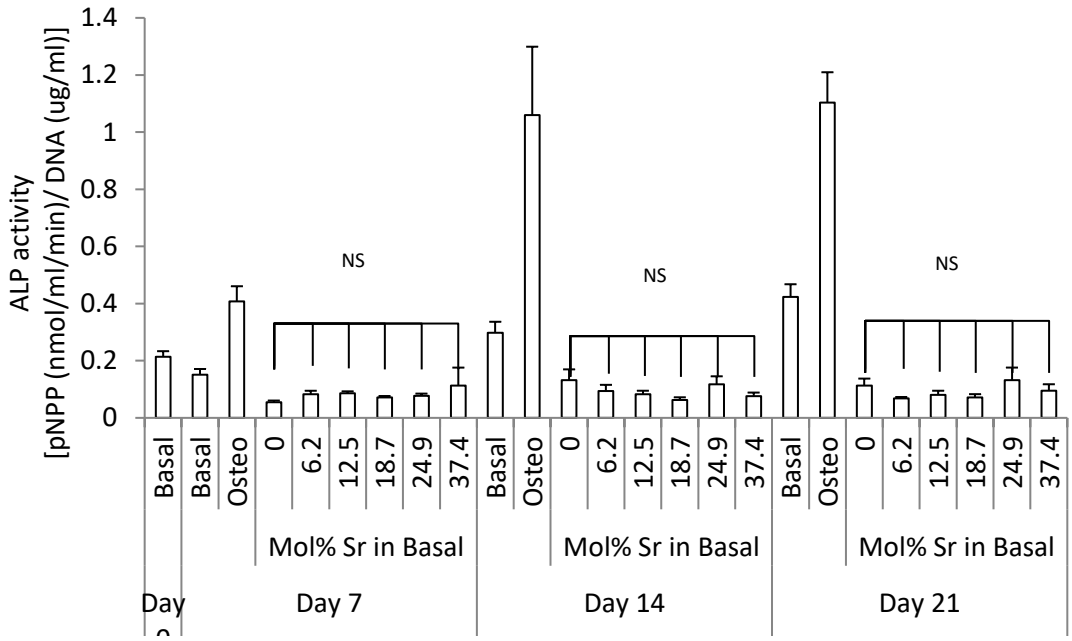


**Figure 47: ALP activity normalised to cell number of Y201 MSCs after exposure to basal medium conditioned with glass powder with 0, 6.2, 12.5, 18.7, 24.9 or 37.4 mol% Sr. The values are means of 6 repeats, with error bars representing standard error. There were no significant differences between the 0 mol% Sr and other Sr conditions (p<0.05).**

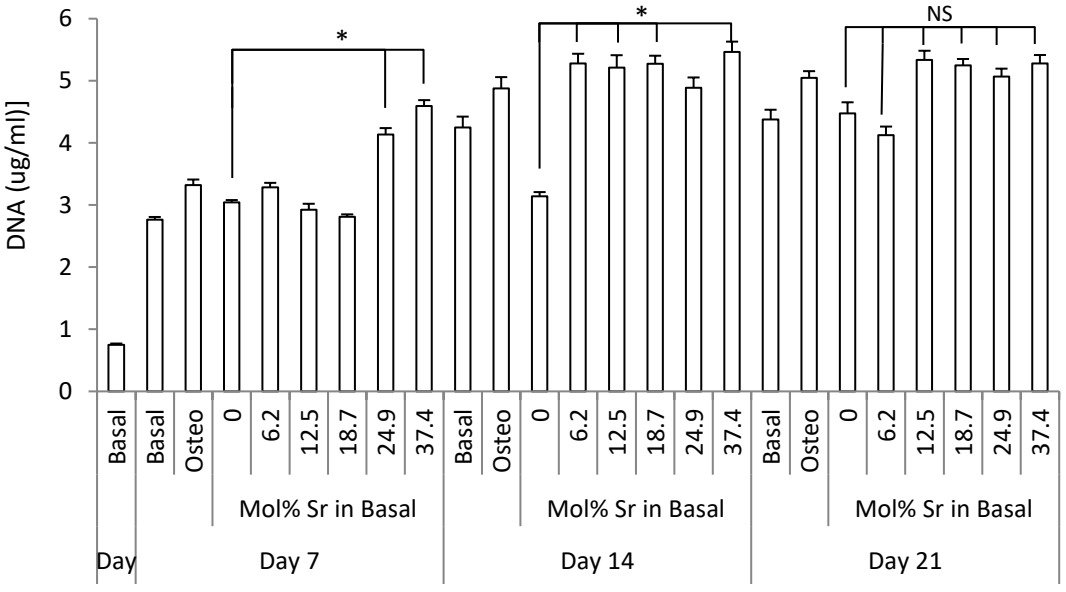


**Figure 48: Cell number (measured by DNA content) of Y201 MSCs after exposure to basal medium conditioned with glass powder with 0, 6.2, 12.5, 18.7, 24.9 or 37.4 mol% Sr. The values are means of 6 repeats, with error bars representing standard error. * indicates significant differences from 0 mol% Sr, NS indicates no significant differences from 0 mol% (p<0.05).**

Glass conditioned mineralisation media was used to determine whether the strontium (and other ions in the glass conditioned media) could fulfil the role of the dexamethasone found in the osteogenic media, with the results presented in Figure 49. Again, the control (osteogenic media) was observed to increase ALP activity in the Y201 MSCs however this was not observed with the glass conditioned mineralisation media, with the strontium containing conditions tending to lower ALP. The cell number, as measured by DNA, was observed to increase over time, and in particular increased in strontium-containing glass conditioned media when compared with 0 Mol% Sr glass conditioned media (Figure 50 and Figure 51). This was observed at both 8 days, and 21 days, with a dose dependent response, with greatest increase observed at 24 Mol% Sr. Hence, the main effects of strontium addition to the glass conditioned media, were that it tended to increase the cell number of Y201 MSCs in a dose dependent manner with the increasing strontium content of the material.

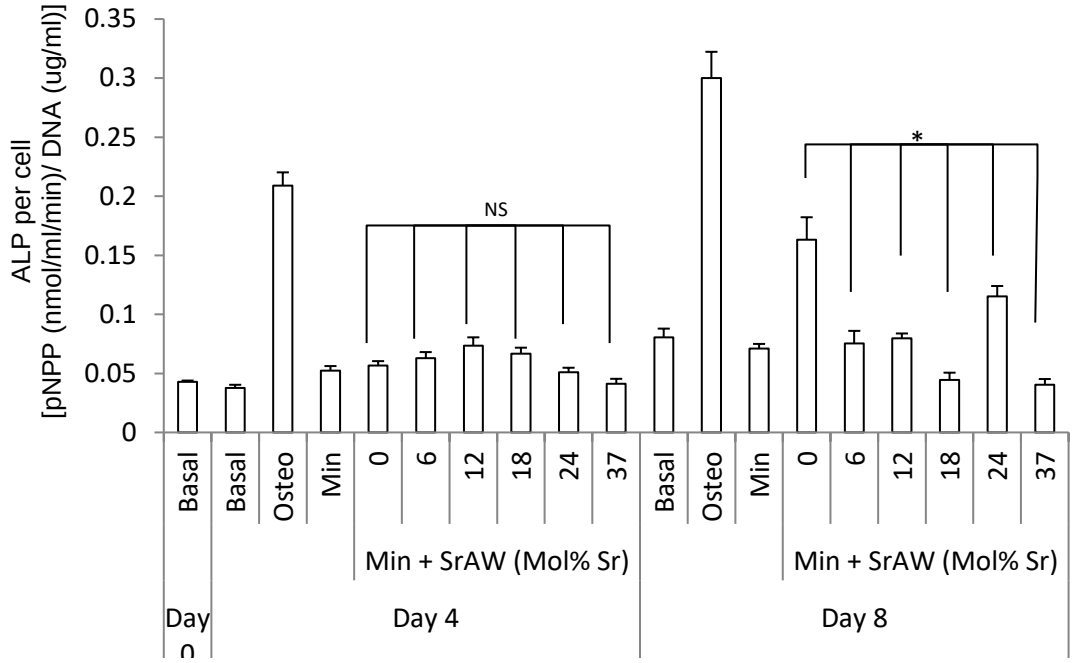


**Figure 49: ALP activity of Y201 MSCs after exposure to mineralisation media conditioned with glass powder with 0, 6.2, 12.5, 18.7, 24.9 or 37.4 mol% Sr for up to 8 days. The values are means of 6 repeats, with error bars representing standard error. * indicates significant differences, NS indicates no significant difference from 0 mol% Sr ($p<0.05$).**

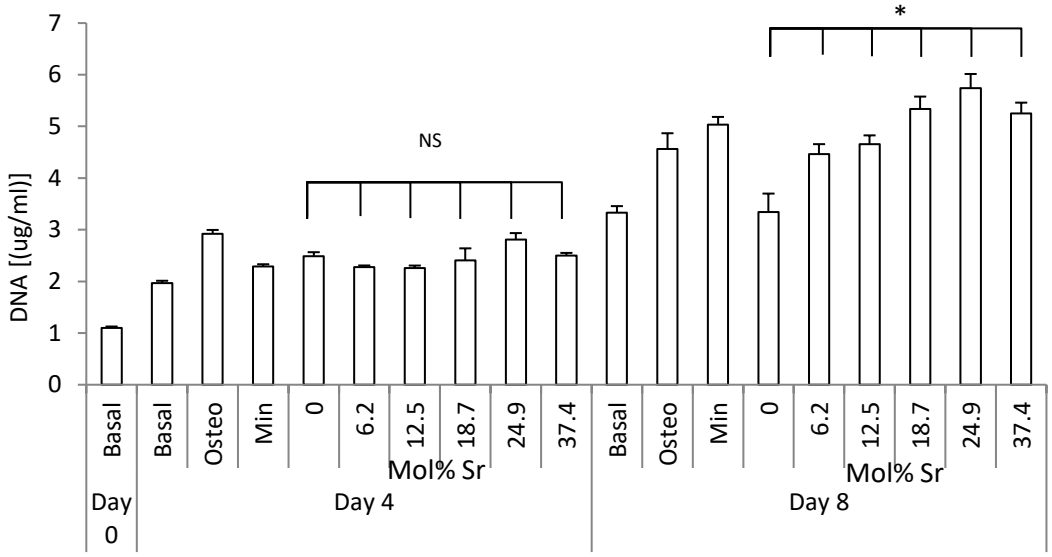


**Figure 50: Cell number (measured by DNA content) of Y201 MSCs after exposure to mineralisation media conditioned with glass powder with 0, 6.2, 12.5, 18.7, 24.9 or 37.4 mol% Sr for up to 8 days. The values are means of 6 repeats, with error bars representing standard error. * indicates significant differences, NS indicates no significant difference from 0 mol% Sr ($p<0.05$).**

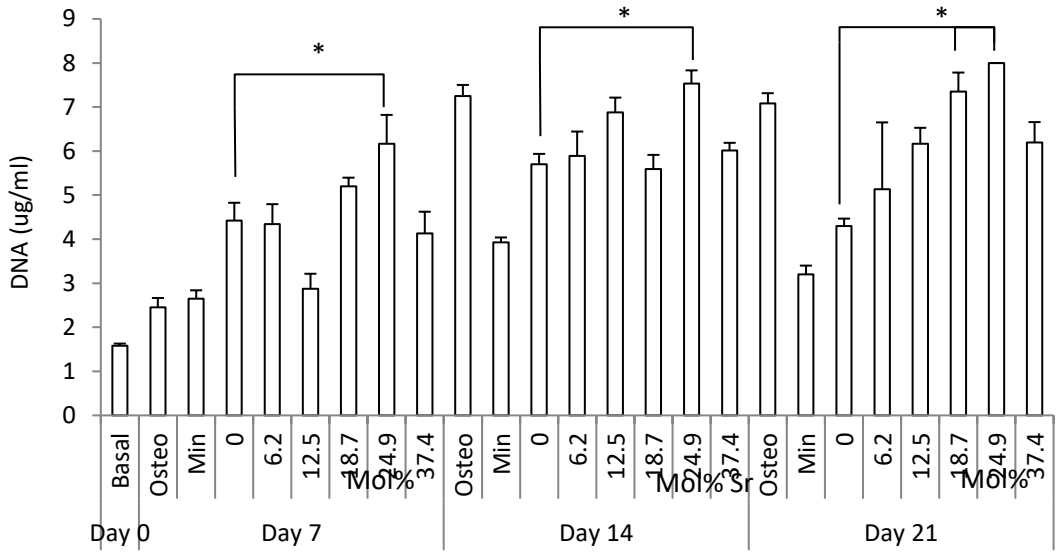


**Figure 51: Cell number (measured by DNA content) of Y201 MSCs after exposure to mineralisation media conditioned with glass powder with 0, 6.2, 12.5, 18.7, 24.9 or 37.4 mol% Sr for up to 21 days. The values are means of 6 repeats, with error bars representing standard error. * indicates significant differences from 0 mol% Sr ($p<0.05$).**

The cell number increase in response to strontium was confirmed using a WST-1 metabolism assay, in which tetrazolium salt being cleaved in the mitochondria during cell respiratory processes causes a colour change from pink to orange. For the glass conditioned media the 6.2, 12.5 and 24.9 Mol% Sr conditions significantly raised cell metabolic activity (potentially indicative of an increased number of cells) (Figure 52), which is supportive of results earlier in this section, which found DNA quantification was increased by SrAW compositions with more than 6 mol% Sr.

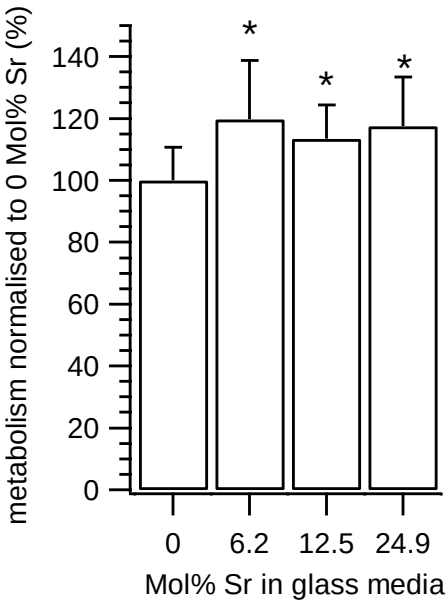


**Figure 52: WST-1 metabolic activity assay performed on Y201 MSCs exposed to glass conditioned media for 6 days. The three plots depict the different independent repeats of the experiment, performed with different passages of cells and different batches of conditioned media. Values are the means of 6 repeats, whilst the error bars display the standard deviation. * signifies $p<0.05$ compared to 0 Mol% Sr.**

EdU was used to measure the number of cells which had undergone proliferation. This attaches to nuclei during the S-phase is and is then measured using a fluorophore that attaches to EdU via a click-chemistry reaction. If the cells were initially synchronised, then cells which are proliferating faster will have more cells in the S-phase. The number of EdU positive nuclei (green, Alexa488) as a fraction of total nuclei (blue, Hoechst) was seen to not significantly change with strontium addition to the glass media (Figure 53), suggesting that the number of cells in S-phase and hence the rate of proliferation wasn't different with strontium addition to the glass conditioned media.

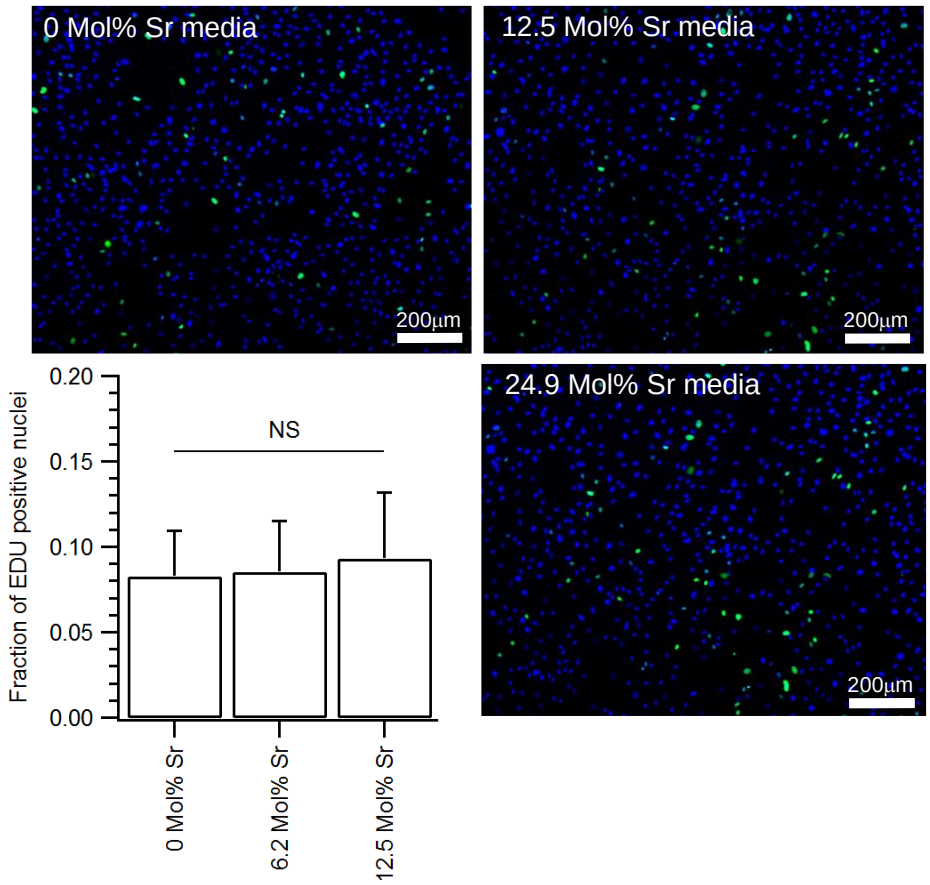


**Figure 53: Representative EdU-Hoechst stains (10x objective) performed on Y201 MSCs exposed to glass conditioned media for 48 hours. Green is EdU-Alexa488 representing cells which have started S-phase, blue is Hoechst, a nuclear stain. The plot depicts the quantification of EdU positive nuclei. Values are the means of 6 repeats, whilst the error bars display the standard error. NS indicates no significant difference between all of the conditions ($p<0.05$).**

### 3.3.5 The effects of SrAW Glass-ceramics on Y201 MSC osteogenic differentiation and proliferation

The previous sections have observed how strontium alone, and then the full range of ions released by the different compositions of SrAW affected the ALP production and cell number of the Y201 MSCs. However, to fully determine how the material will affect the MSCs it is important to grow them on its surface, as additional factors, such as surface topography, could influence the cells in ways which would be missed from simply exposing the cells to the ions released by the material.

Initially, as a pilot study the AWGC discs without strontium and 12.5 Mol% strontium SrAWGC discs were used to assess the effects of strontium addition to the material on Y201 MSC osteogenic differentiation (through ALP) and cell number. The 12.5 Mol% Sr composition was chosen as the representative strontium composition as it was a compromise between having enough strontium in the material that sufficient is released, whilst not having so much that the structure of the material is impaired (as shown by the altered surface properties in section 3.3.1). Initially, osteogenic media was used to determine whether the material was capable of supporting osteogenic differentiation which had been already initiated by the dexamethasone in the osteogenic media. For Y201 MSCs grown on SrAWGC discs in osteogenic media, the ALP activity (indicative of differentiation), was found to increase at a slower rate over the 14 days in the 12.5 mol% discs compared with the no-Sr discs (Figure 54). The cell number, as measured by DNA, was seen to rise slightly over time, though not significantly, and the addition of Sr to the discs did not have a clear effect (Figure 55).

The whole range of disc compositions with increasing Sr content were then explored, focussing on the cell number as measured by DNA content, as this had been particularly affected by the glass conditioned media. For Y201 MSCs grown on SrAWGC discs in osteogenic media, the cell number, as measured by DNA, was seen to rise over time, and in particular was seen to increase on strontium-containing AWGC discs when compared with 0 mol% Sr AWGC discs (Figure 56). This was observed at both 7 days, and 14 days, with a dose dependent response, yielding the greatest increase at 24.9 and 18.7 Mol% Sr at days 7 and 14 respectively (Figure 56).

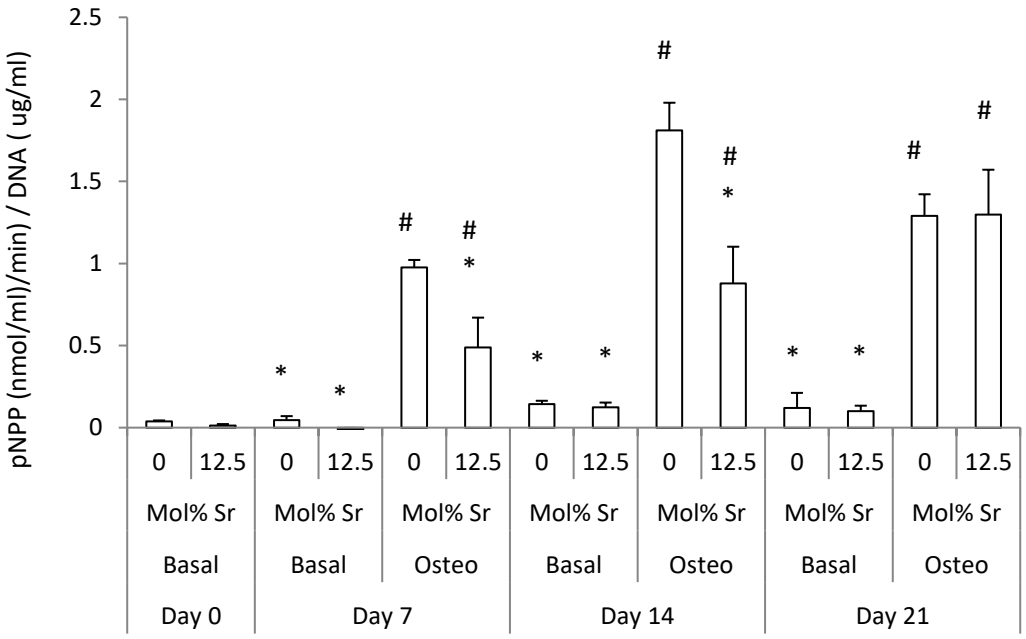


**Figure 54: ALP normalised to cell number (pNPP per DNA) of Y201 MSCs after growth in basal or osteogenic media on SrAWGC discs with or without strontium (0 and 12.5 mol% Sr) for up to 21 days. Values are means of three samples, with the error bars representing standard error. # indicates significant differences from basal 0 mol% Sr for that time point, * represents significant differences from the osteogenic 0 mol% Sr for that time point ($p<0.05$).**

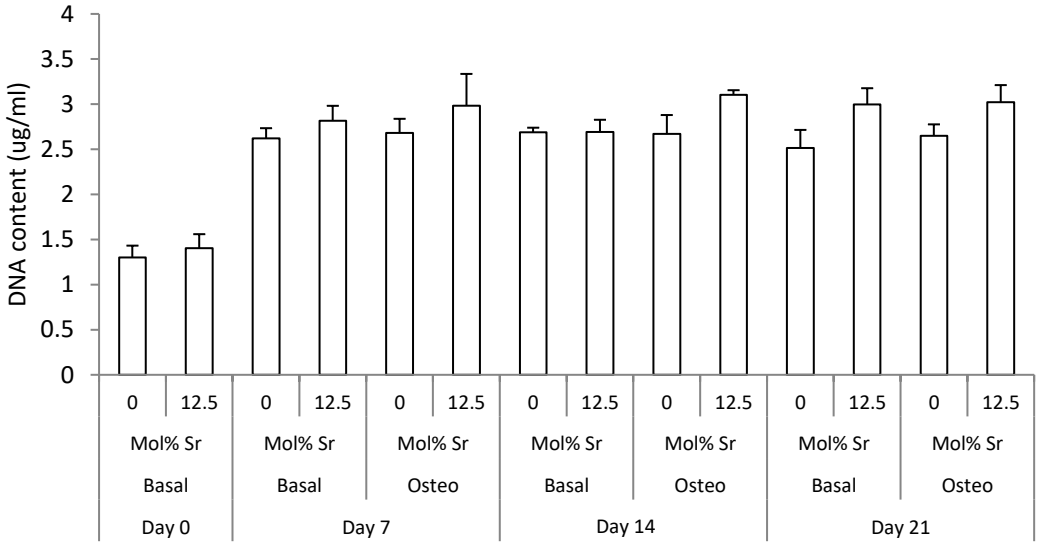


**Figure 55: Cell number (measured by DNA content) of Y201 MSCs after growth in basal and osteogenic media on SrAWGC discs with increasing strontium content (0, 12.5 mol% Sr) for up to 21 days. Values are means of three samples, with the error bars representing standard error. No significant differences were seen within the time points between the 0 and 12.5 Mol% Sr conditions ($p<0.05$).**

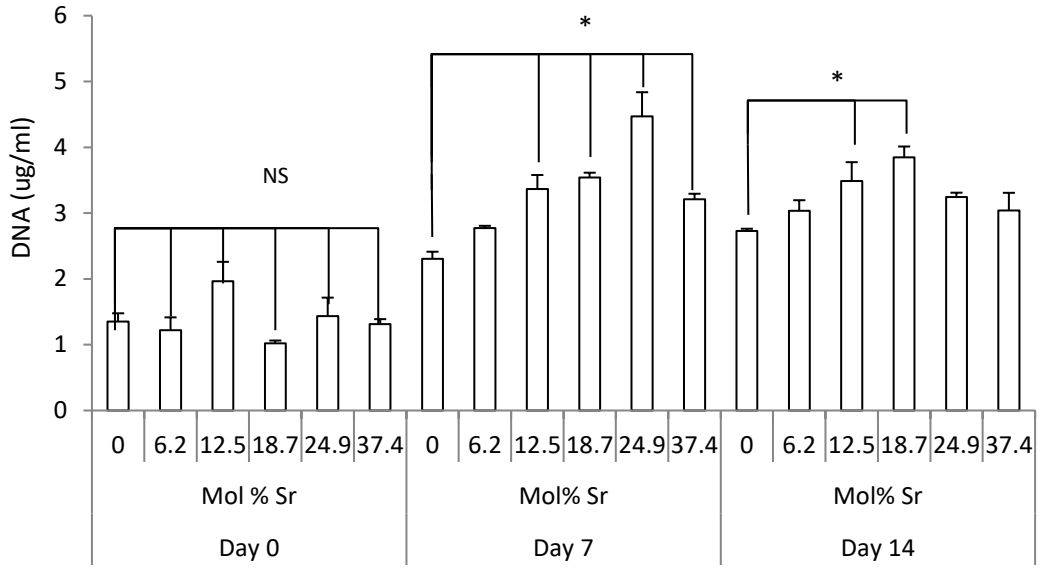


**Figure 56: Cell number (measured by DNA content) of Y201 MSCs after growth in osteogenic media on SrAWGC discs with increasing strontium content (0, 6.2, 12.5, 18.7, 24.9 or 37.4 mol% Sr) for up to 14 days. Values are means of three samples and error bars represent the standard error. * indicates significant differences, and NS indicates no significant differences between the 0 mol% Sr and other conditions ($p<0.05$).**

Next it was important to determine whether the discs alone could induce the changes in cell number with strontium content observed previously, or whether it was dependent on the dexamethasone in the osteogenic media. To determine this, the Y201 MSCs were grown on the different compositions of SrAWGC discs, but in mineralisation media, which has the same additives as osteogenic media, but without dexamethasone. For the Y201 MSCs grown on SrAWGC discs in mineralisation media the cell number was seen to lower over time (Figure 57). In addition, a dose dependent increase in DNA with Sr content in the discs was observed, with, 6.2 and 12.5 Mol% strontium resulting in a higher cell number compared to the 0 mol% Sr in at days 6 and 9 (6.2 Mol% Sr only) (Figure 57). The highest strontium contents resulted in slightly lowered DNA content. The main finding was that the addition of strontium to the discs improved cell growth when mineralisation media was used, however the response of the cells to the strontium content of the discs appeared to be different than compared when using osteogenic media.

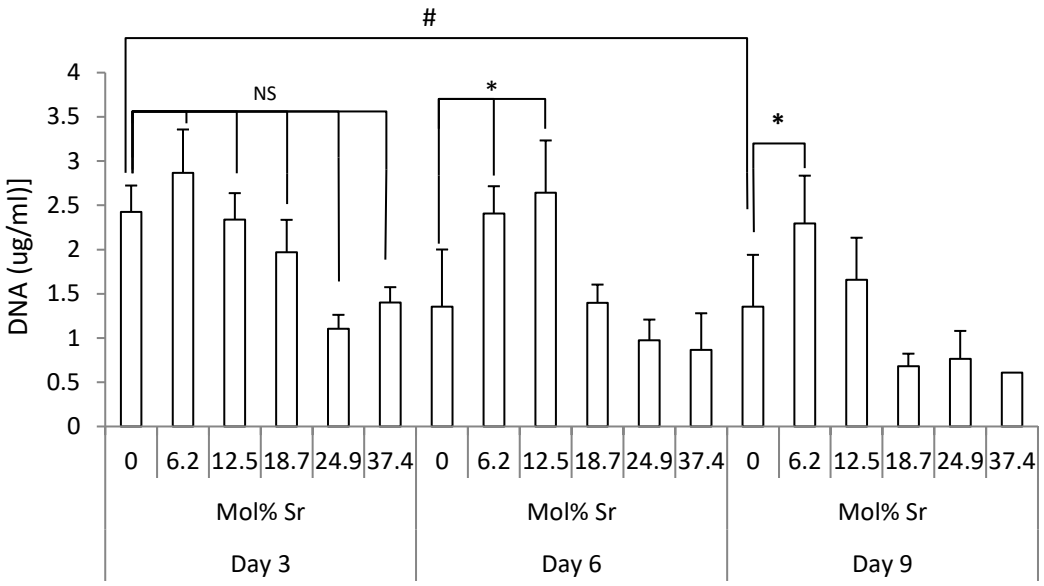


**Figure 57: Cell number (measured by DNA content) of Y201 hTERT MSCs after growth in mineralisation media on SrAWGC discs with increasing strontium content (0, 6.2, 12.5, 18.7, 24.9 or 37.4 mol% Sr) for up to 9 days. Values are means of three samples and error bars represent the standard error. * indicates a significant difference, and NS indicates no significant difference between 0 mol% Sr and the other conditions for that time point, whilst # indicates a significant difference between the shown conditions ($p<0.05$).**

The increased cell number experienced by the Y201 MSCs with strontium content of the SrAWGC discs was confirmed performing WST-1 metabolic activity assays Y201 MSCs grown on glass ceramic 12.5 mol% Sr discs showed significantly increased viability over the 0 mol% Sr discs (Figure 58). These results suggested an increase in cell metabolic activity, and therefore potentially cell number, at the correct Sr concentration in the SrAWGC.

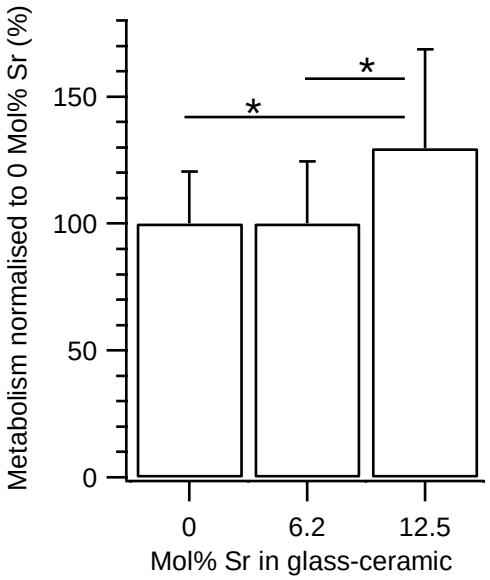


**Figure 58: WST-1 viability assay performed on Y201 hTERT grown on glass ceramic discs with increasing strontium content for 7 days beginning at 50% confluence. The values are means of 6 samples and the error bars display the standard error. * indicates a significant difference between the indicated conditions ($p<0.05$).**

EdU was used to measure the number of cells which had undergone proliferation, as EdU attaches to nuclei during the S-phase and (if the cells were initially synchronised) can then be later measured to indicate the number of cells which have reached this stage of the cell cycle, giving an indication of proliferation rate. The number of EdU positive nuclei (green, Alexa488) as a fraction of total nuclei (blue, Hoechst) was seen to not significantly change with strontium addition to the bioactive glass ceramic discs (Figure 59), suggesting that the addition of strontium the SrAWGC discs did not alter the proliferation rate of the Y201 MSCs.

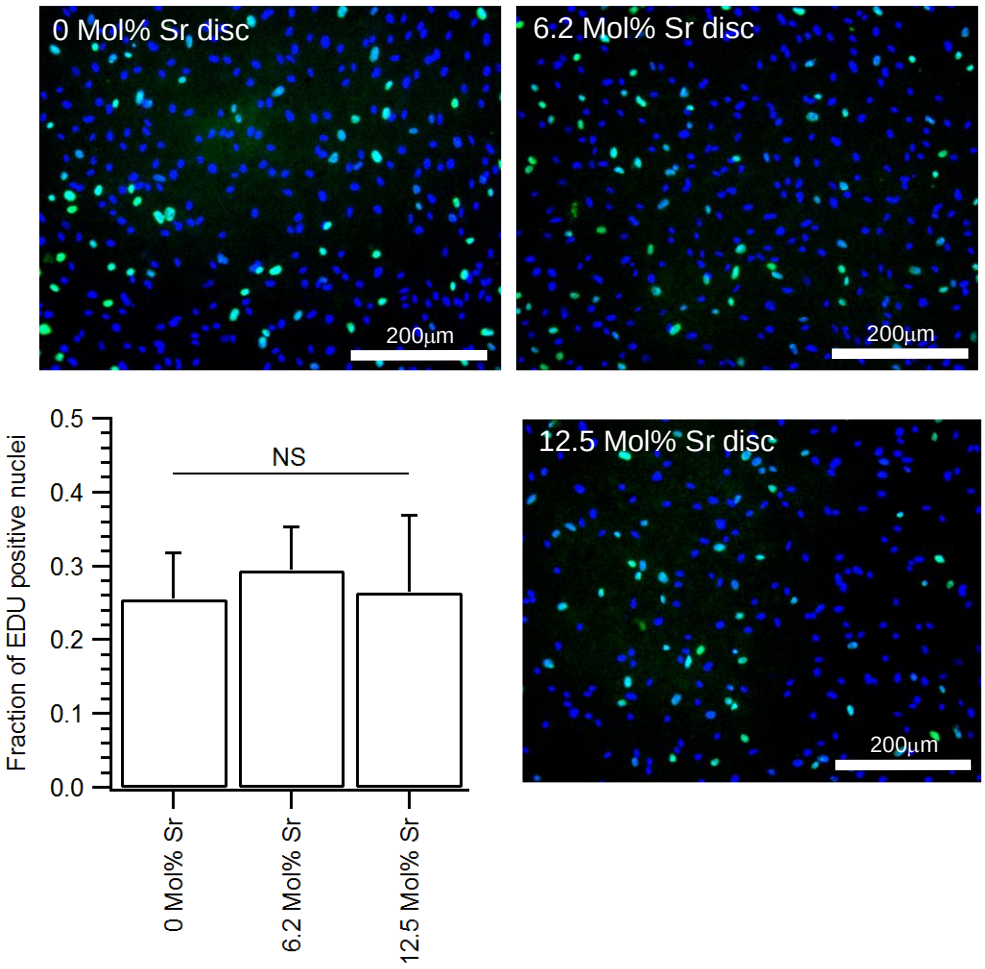


**Figure 59: Representative EdU-Hoechst stains (50x objective) performed on Y201 MSCs grown on glass ceramic discs with increasing strontium content for 48 hours. Green is EdU-Alexa488 representing cells which have started S-phase, blue is Hoechst, a nuclear stain. The plot depicts the quantification of the numbers of EdU positive nuclei and the values are means of 6 samples. The error bars display the standard error. NS indicates no significant difference between all of the conditions ($p<0.05$).**

### 3.3.6 The effects of SrAW glass on Y201 MSC colony forming

As a tissue engineering scaffold, the SrAWGC will have to support MSC colony growth when used as a therapy *in vivo*. To assess how the addition of strontium to the material alters this, a colony forming assay was performed on the Y201 MSCs, but with mineralisation media conditioned with the six different SrAW glass compositions. This experiment was intended to build on the results in section 3.3.4, where it was found that the strontium content of the glass conditioned mineralisation media improved cell growth.

The Y201 MSCs were observed to form colonies after 10 days, and these were quantified as seen in (Figure 60). The quantification of the colonies using ImageJ did not indicate any significant difference in the nature of the colonies with Sr content in the conditioned media, but demonstrated that the mineralisation media showed increased colony area and number when conditioned with any type of SrAW glass. The images of the colonies can be seen in Figure 61 and show a clear difference in the number of colonies between those growing in mineralisation media, and mineralisation media conditioned with the different compositions of SrAW glass (Figure 61).

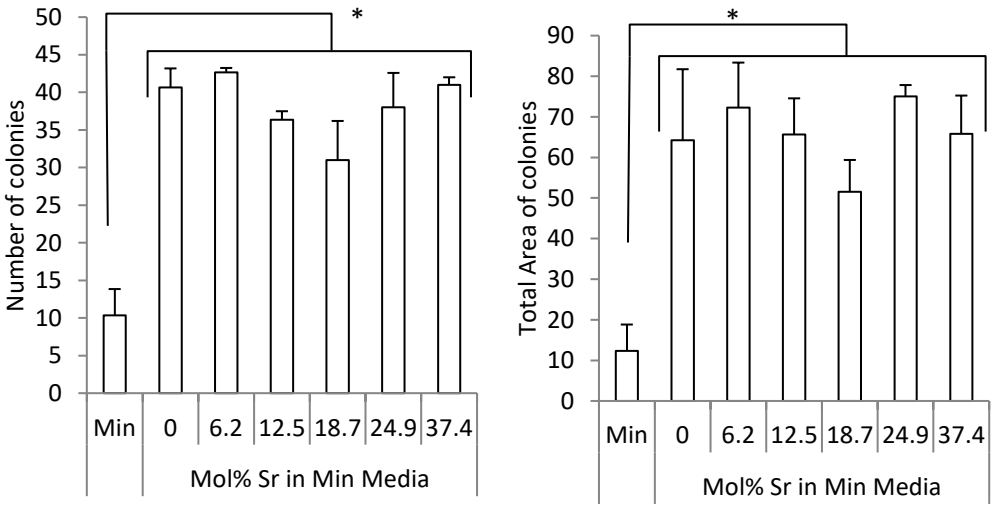


**Figure 60: The number of colonies and the average area of colonies as measured in ImageJ from a CFU-f assay of MSCs exposure for 10 days to control media, or 0, 6.2, 12.5, 18.7, 24.9 or 37.4 mol% SrAWGC conditioned media. The values are means of 3 and the error bars are the standard error. * indicates significant difference (P<0.05).**

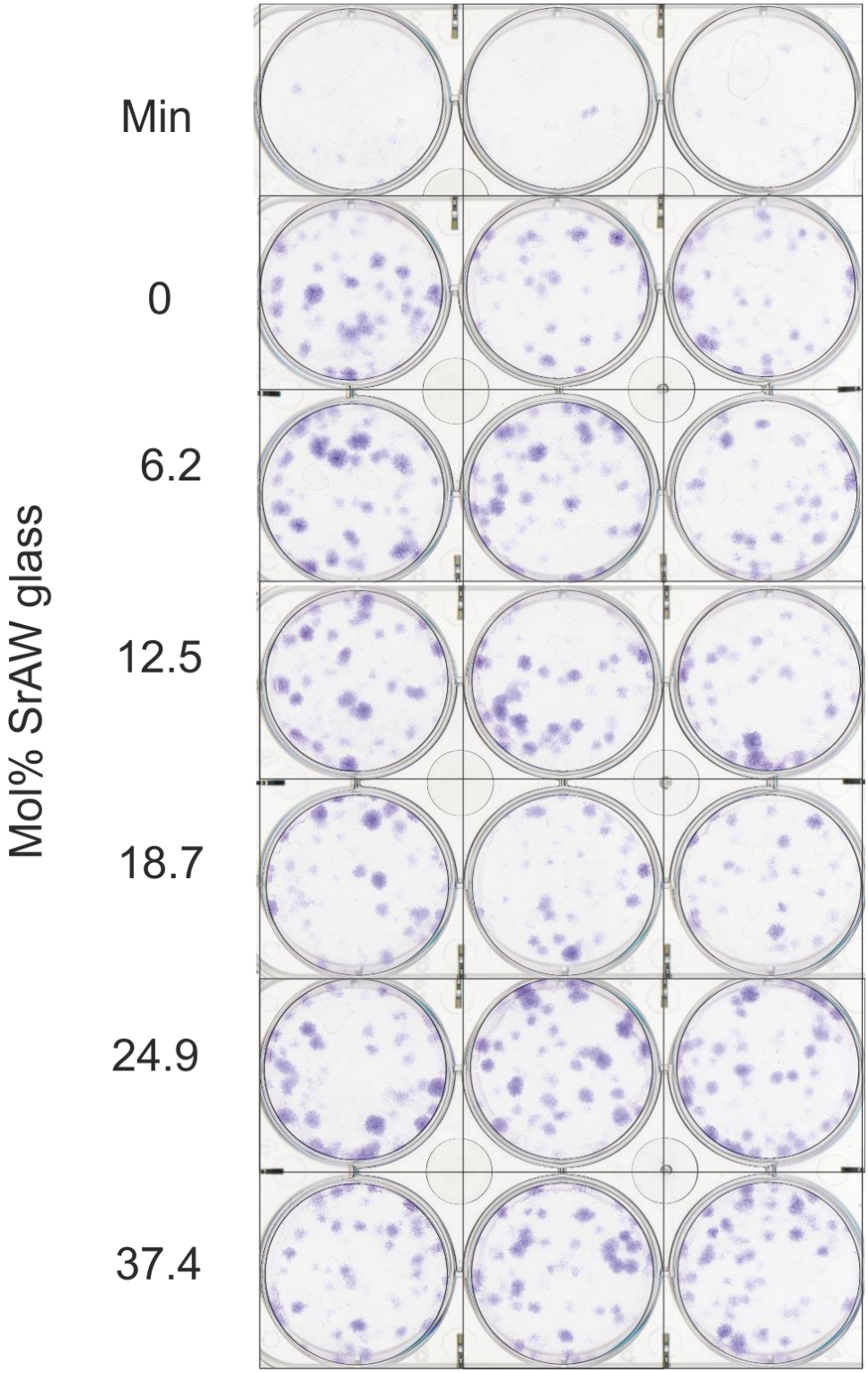


**Figure 61: Example Colony forming unit plates with the colonies seen as purple areas. This is from a CFU-f assay of MSCs exposure for 10 days to control media, or 0, 6.2, 12.5, 18.7, 24.9 or 37.4 mol% SrAWGC conditioned media. The wells are 34.8 mm in diameter.**

## 3.4 Discussion

The aim of the work in this chapter was to explore how the Y201 MSCs respond to SrAWGC and how the strontium content of SrAWGC would affect this response. The scaffolds used were described in Chapter 2 and they were shaped to fit into 96-well plates having undergone a heat treatment which transformed the SrAW glass into SrAWGC consisting of a glassy component and two crystalline components (apatite and wollastonite) for increased durability (121).

As SrAWGC is bioactive, before testing the cells, it was first important to establish how the material itself would respond to biological conditions (both the base SrAW glass and the SrAWGC discs), and whether the different compositions of the material (with increasing Sr content) would respond differently. Understanding how the material itself changes would provide context for any MSC response to the material, particularly if this response changed with the Sr content in the material. Next, it was important to determine whether the cells could attach to the material, their subsequent morphology on this surface and the quantity of cells needed to reach confluence. Additionally, it was important to determine whether the Sr content of the SrAWGC had any effect on the ability of cells to attach and their morphology. After this, a series of DNA and ALP experiments were performed to establish how the Y201 MSCs responded to the AWGC with and without strontium. Different media were used including different osteogenic and osteo-supportive supplements to establish to what extent the material could influence MSC function. Glass conditioned media and media doped with strontium chloride were also used to determine whether the ions released by the material (and strontium specifically) could mediate these effects, or whether any observed effects were primarily due to the cell's interaction with the material's surface itself.

### 3.4.1 Dissolution ions released by SrAW and SrAWGC

Initially, the bioactivity of the glass and the glass ceramic were determined by measuring the ions released by the SrAWGC compositions with increasing strontium contents after being exposed to mineralisation culture

media for 24 hours. Studying the SrAW glass alone can also be useful in understanding the bioactivity of the SrAWGC discs because the glassy part of a glass ceramic (SrAWGC) is the most bioactive and the ions released by the material are a critical part of its mechanism of action on human cells (72). For this reason, conditioned media is a valuable comparator and tool in determining the effectiveness and mode of action of bioactive glasses (and other biomaterials) and is well used in the literature (65,85,87,231). However, the glass conditioned media isn't necessarily a perfect model of the glassy phase of the glass-ceramic as previous work in the David Wood laboratory found that that the crystal phases (wollastonite and apatite) of the 18.7 and 24.9 Mol% Sr AWGC compositions depleted the amorphous phase of Mg and Si (102). This would result in the amorphous phase of SrAWGC having a different composition than the equivalent SrAW glass and therefore a potentially different ion release profile. The amount of glass used to condition the media was initially based on a previous study which had used Bioglass 45S4, a popular bioactive glass (87), however the concentration of glass used in this project was tailored to have strontium releases centred around 1mM (as AW glass dissolves at different rate than bioglass), and previous studies have found values between 2mM and 0.1mM to be optimum (124,129,230), whilst my own studies on $SrCl_2$ supported this. In addition, the amount of glass per millilitre was altered to correspond with the molecular weight of the different strontium compositions of the SrAW. This was important to ensure that there is a similar volume of materials in the media and hence a similar surface from which ions could be released. Although this was not considered in previous work (87), for this study it was an important consideration, as a large molar percentage of the material was being substituted with strontium (up to 37.4 mol%).

The glass conditioned media showed a steady increase in the release of Sr with glass Sr content (and a corresponding decrease in Ca), with the other elements remaining relatively unchanged. Furthermore, it is important to note the linear nature of the release, indicating the strontium addition did not alter the rate of degradation of the material, despite its larger atomic size. This compared well with the neutron diffraction results reported in Chapter 1, which indicated that the short range order of the glass powder was relatively

unchanged by the addition of strontium. Hence, from these data it is possible to infer that the SrAW glass releases strontium linearly with strontium content, and therefore the strontium release from the material could be adjusted in future studies by altering the strontium substitution into the SrAW glass.

When the SrAW glass conditioned media was compared with control media (that had also been exposed to the same mixing process but without glass), it was found that all of the glass compositions lowered the phosphorus content of the resulting conditioned media, regardless of Sr content. This has been observed in some other glass systems doped with Sr (87,222,232), potentially due to the initiation of hydroxyapatite formation. A loss of phosphorus in the media is important to consider as too little phosphate could inhibit the ability of the cells to osteogenically differentiate (it is needed for hydroxyapatite production and plays a role in osteogenic differentiation signalling (225)). However, it could potentially be a benefit as studies with pre-osteoblastic MC3T3-E1 cells have found too high phosphorus content (>10mM) can actually increase the expression of matrix gla protein (MGP), a powerful inhibitor of calcification (233). The ions released during the degradation of the SrAWGC discs were also measured and found to be released in different concentrations to the glass conditioned media. Although the Sr release increased with the Sr content of the material (much like the SrAW glass), so did the release of Si and Ca, which the higher strontium SrAWGC discs contained less of. Similar material degradation has been reported previously in other glass systems, where an increase in Si and Mg release was observed with increasing Sr content in a biphasic calcium phosphate ceramic (234). These would tend to indicate that material is breaking down faster, though the exact cause of this is uncertain. It was also observed that phases form with Sr substitution, disrupting the $Mg_2SiO_4$ crystal structure and hence increasing the degradation rate and weakening the material's mechanical properties (234). AWGC is a more complex material, as the base composition is already triphasic, with glassy, wollastonite and apatite phases (119), hence precisely how the addition of strontium alters the degradation of SrAWGC would require further study.

When comparing the ion release from the SrAW glass powder to that released from the SrAWGC discs it is important to recall that they are very different systems. The glass powder has a high surface area and is constantly in motion whilst being mixed, ensuring the whole of the material is exposed and releasing ions. In contrast, only the surfaces of the SrAWGC discs were exposed to the media. Previous work in the Wood laboratory found that the 0, 12.5 and 18.7 mol% strontium SrAWGC discs formed hydroxyapatite on their surfaces, which was theorised to be abrogating ion release from these materials (203). A hydroxyapatite layer obscuring the surface of the 0 and 12.5 Mol% strontium SrAWGC discs could therefore be a contributing factor to the differences seen between the ion release from the discs and the SrAW glass conditioned media, in this project.

It should also be noted that SrAWGC discs are not composed of only glass. The AWGC base material is composed of approximately 25% (w/w) glassy, 40% (w/w) wollastonite ($CaSiO_3$) and 35% (w/w) apatite ($Ca_5(PO_4)_3(F, OH)$) phases, and as calcium is replaced with strontium, this could incorporate into the glassy phases the wollastonite phase or the apatite phase, both partially and completely (119,235). Previous work on SrAWGC found that strontium was taken into the Fluoroapatite phase in the 6.2 and 12.5 Mol% SrAWGC compositions (102). This resulted in an expansion of the crystalline planes in the SrAWGC, increasing the ratio of the apatite to silicate phases (such as wollastonite (102)) found in the material. Although the apatite phase is generally not as reactive as the other two phases, studies have found that strontium apatite has shown increased solubility (235–237), hence if this phase became more prevalent in the SrAWGC with the addition of Sr, this could play a part in the increased degradation rate of the material. Previous work also found that the addition of Sr to SrAWGC caused two separate silicate phases to emerge (both being types of pseudo-wollastonite, $CaSiO_3$): one rich in magnesium with comparatively less Sr, and the other magnesium depleted but with comparatively more Sr (102). However, the degradation rate of wollastonite ($CaSiO_3$), which is highly bioactive, has been found to actually decrease when strontium was substituted for Ca (238), suggesting that this phase would not have degraded faster in the AWGC with strontium addition. Finally, there is the glassy phase to consider.

The neutron diffraction work in Chapter 2, and the ion release of the SrAW described in this chapter, both suggested the dissolution of the material is unaffected by the addition of strontium. This was done in a controlled condition with powders ground to a similar size and hence surface area. The glass-ceramic is more complex, as the presence of the other phases, and their willingness to degrade, alters the surface area of the material and could therefore appear to increase the solubility of the glass phase. In short, more study is required to fully determine the mechanism behind the Sr induced rise in degradation of the SrAWGC.

Before discussing how the material affected the cells, it is important to note that the ion release work presented in this project only studied the release after 24 hours. This was useful in providing an estimate of the way in which the material degrades, however the release rate can be dynamic and so study of the ion release at several time points can provide useful insights into how the material responds to culture media, and therefore how the cells respond to the material. This has been covered in previous work where the ion release of both the SrAWGC discs (as used in this project) and also foam replicated 3D porous SrAWGC scaffolds was in simulated body fluid (SBF) was measured at 1, 3, 7 and 14 days (203). It was found that only 24.9 and 37.4 Mol% Sr compositions showed a vast change in Ca, Sr, Si and Mg ion release over time, with the concentration of these ions steadily increasing over the time course (203)  However, this was not in a burst release. As in this project, the concentration of the P was seen to fall over time. Before interpreting this, it is also useful to summarize previous work on the formation of hydroxyapatite on the surface of the SrAWGC discs and 3D porous scaffolds in SBF. It was found that for the discs only the 0, 12.5 and 18.7 Mol% Sr compositions formed hydroxyapatite on their surface, and this layer could have been acting to slow down the dissolution of the material's surface. (203). This could explain the finding in this project, where the release rate of the SrAWGC discs increased with Sr content. Interestingly, the work by Pontiroli also highlighted how the form of the SrAWGC glass ceramic can alter how it breaks down. The 6.2 and 24.9 Mol% Sr discs did not form hydroxyapatite within 2 weeks, however it was found that for the

porous scaffolds all of the compositions except 37.4 Mol% Sr formed hydroxyapatite on the inner struts of the porous structure (203).

When considering the effects of the SrAWGC discs and the SrAW glass conditioned media on MSCs it is also important to note ion species released. Recent work found that two bioactive glasses with properties which promote osteogenic differentiation, Bioglass 45S5 and siloxane-doped vaterite (SiV), released different species of Si ions (239). The SiV was found to release $T^n$ Si ions (CSi(OSi)n(OH)3-n), whilst the Bioglass 45S5 release $Q^n$ Si ions, and these were seen to be taken up by the SaOS-2 cells in different concentrations and to induce differences in calcium staining and metabolic activity (239). Like Bioglass 45S5, SrAWGC is also a calcium silicate bioactive glass, and the NMR results in Chapter 2 found that the silicon took the form of $Q^n$ in the SrAW glass. Hence, it is possible that SrAWGC would also release $Q^n$ Si ion, however this would require further work to verify.

### 3.4.2 Cell seeding and morphology on SrAWGC discs

Next, SEM and complementary techniques were used to establish whether the cells could attach to the material and at what seeding density the cells reached confluence. The Y201 MSCs were seen to adhere to the surface and spread out well after 24 hours, with the flattened shape of the cells and the extended processes being indicative of good cell adhesion. By EDS, the presence of the cells was clear at the higher seeding densities due to the stark contrast between the silicon-rich surface and the carbon-rich cells, however on the discs without cells, interpreting the EDS could be misleading due to how the software treated contrast. The intensity of the EDS signal was normalised across the whole image, hence for the images with a strong source of carbon signal (such as ones that contained cells), there was a clear contrast between the material surface, and that of the cells. However, when there was no strong source of carbon, the weak residual carbon signal on the material surface (the fixative, or other residues from the preparation) was then the strongest signal and seemed comparatively bright, when in actuality it was very weak (the surface appears uniformly red). The cumulative spectra support this, showing that there was a very low carbon

signal on the discs without cells, which increased as more cells were seeded on the surface. The addition of more than 12.5 Mol% Sr caused noticeable changes to the surface of the SrAWGC, seen more clearly in the backscattered electron microscopy images, with the surface gaining more extreme peaks and troughs. This was not found to have any effect on the cell morphology, however the MSCs were only grown on the surface for 24 hours. Changes to the surface morphology of the material could be a valuable avenue for future work as it is well understood that changes in surface topology can have significant effects on cell behaviour over time (67,240). More specifically, it has been shown that simply changing the roughness of the surface of a bioactive glass can have significant effects on cell morphology and mineralised nodule formation (241).

### 3.4.3 Response of MSCs to Sr content of SrAWGC

The findings discussed so far indicate that the SrAW glass conditioned media and the SrAWGC glass ceramic discs are able to release strontium, but it is important to establish whether strontium alone is capable of inducing any effects on the MSCs, or whether the other elements (Si, Mg, P and Ca) also released by the materials are required. It was found that 4mM $SrCl_2$ doped mineralisation media and osteogenic media both increased ALP activity compared with 4mM $SrCl_2$ basal media. These findings suggested that strontium on its own, in basal media, was simply not sufficient to evoke a positive osteogenic response. This was potentially due to osteogenic differentiation requiring certain criteria to be met, such as the cells being confluent on a collagen ECM and there being sufficient phosphate present to produce ALP (225,242), which are accommodated by the L-Ascorbic acid and β-glycerophosphate found in the osteogenic and mineralisation medium, but lacking from the basal medium. However, it was also found that the addition of strontium to the osteogenic or mineralisation media actually reduced the ALP activity compared with osteogenic or mineralisation media without strontium. These data suggest that strontium potentially interferes with the action of osteogenic supplements (either just dexamethasone or also β-glycerophosphate and L-Ascorbic acid). Later work revealed that 4mM of $SrCl_2$ was potentially too high, as it was found that between only 0.5

and 1 mM $SrCl_2$ had the greatest stimulatory effect on ALP activity after 9 days. Nevertheless, no $SrCl_2$ concentrations were able to raise ALP significantly higher than mineralisation media on its own, again indicating that Sr could have some inhibitory effect. Although there is a body of evidence to support strontium being osteo-supportive, a recent study has found that Sr can actually interfere with osteogenic differentiation (243). Zhang *et al*. (2016) demonstrated that just 1mM Sr could greatly attenuate the osteoinductive effects of rhBMP-2 in human MSCs by forming a complex with the protein and inhibiting the BMP/Smad signalling pathway (243). Strontium is also known to interact with (and stimulate) the Wnt pathway via numerous potential routes, such as the Calcium Sensor Receptor (CaSR) or by inhibition of Wnt inhibitors(122,124), and this could also be blocking osteogenic differentiation of the MSCs (122,124,125,129). Although Wnt has been shown to encourage proliferation of human MSCs, the canonical Wnt pathway has been shown to inhibit their ability to mineralise the matrix (though their ability to synthesise matrix is undiminished)(244,245). As the SrAWGC releases more than just strontium, in addition to the $SrCl_2$ studies, the ion release of the material was modelled using glass conditioned media. The glass conditioned media's effects on the MSCs were found to partially resemble those of the $SrCl_2$ media experiments. It was found that basal media did nothing to the ALP of the cells, with or without any of the compositions of SrAW glass media. The osteogenic and mineralisation glass conditioned media alone were found to increase ALP activity. However, when conditioned with AW glass, the strontium conditions resulted in a lowered ALP activity compared with the non-strontium glass media conditions, agreeing with the $SrCl_2$ studies. These finding also suggest that strontium was responsible for the inhibition of ALP activity (compared with control media) in the Y201 MSCs. This is shown as the glass conditioned media itself without strontium (0 Mol% Sr) seems slightly beneficial to ALP activity in the Y201 MSCs (potentially due to Si and Mg naturally also being slightly osteoinductive (72)), and only with strontium addition did ALP activity decrease. This not only confirms the previous finding that the Sr alone is not sufficient to induce osteogenic differentiation in the MSCs used here, but also that the content of the other elements within the glass conditioned

medium (Si, Mg, P, Ca and F) are also not sufficient to induce osteogenic differentiation (as even without strontium, the glass conditioned mineralisation media was not able to match the ALP activity of osteogenic media). However, it must be considered that the reduced phosphorus content caused by the glass conditioned media could mask the potency of the other ions as even though Si ions have been shown to be slightly osteoinductive, principally through encouraging Collagen I formation, the collagen needs to phosphorylate before mineralisation can take place, which would be less likely in a phosphate deprived environment (72,243,246). Promoting cell growth is a requirement for a material to be an effective tissue engineering scaffold; hence the effect that Sr content of SrAWGC on the growth of the Y201 MSCs was explored. As explained previously, SrAW glass conditioned media studies were used to explore the effects of the increasing amount of Sr content in the dissolution ions of the material. After only 8 days of exposure to the different compositions of glass conditioned media (Figure 50) there was seen to be a clear dose-response between Sr and cell number. This was shown again at later time points, with the effect most pronounced at 21 days (Figure 51). As discussed previously, the SrAW glass released increasing concentrations of Sr with increasing Sr-content in the material. Hence, the strontium content of the SrAW glass conditioned media could be responsible for the increase in cell number. The other dissolution ions (such as Si and $Mg^{2+}$) could also have been responsible for the altered cell number, having been seen at later time points to raise the cell number above control mineralisation media (Figure 51). However, as the release of the other ions did not change significantly between the compositions, they probably did not contribute to the change in cell growth observed between the different compositions of SrAW glass conditioned media. The peak in the cell growth was observed with the 24.9 Mol% SrAW composition and further substitution of strontium resulted in the cell growth being less. This could have been because the 24.9 Mol% Sr composition was optimum, or alternatively could have been due to the large difference in strontium released between the 24.9 and 37.4 Mol% Sr glass conditioned media. Although the change in $Sr^{2+}$ ions released by the SrAW was linear with Sr content, after 24 hours the 37.4 and 24.9 Mol% glasses release

~2.5mM and ~1.5mM. This meant that the 37.4 Mol% Sr was then in excess of the optimum Sr levels found in previous studies, and could indicate that intermediate strontium substitutions should be explored, such as 30 Mol% SrAW (124,129,230).

Strictly, the experiments discussed previously measured only DNA content of the experimental wells. However the cell growth in response to the Sr content of SrAW glass conditioned media was confirmed using a metabolic (WST-1) assay. As the cell number was found to have increased with strontium content, this would have suggested an increase in proliferation with strontium at some stage in the experimental periods covered (between 0 and 21 days). However EdU assays found that that cell cycle turn over (and hence proliferation) did not increased with strontium addition to the mineralisation media during the 48 hour exposure period, straight after cell seeding. It is possible this was simply too early to see the effect, particularly as the earliest time point used in the other experiments was 6 days in the WST-1. Future work could repeat the proliferation assay, but instead expose the Y201 MSCs to the EdU after a period of one week (or longer), to more closely align with the findings of the other experiments. Interestingly, the CFU study suggested that some component of the glass conditioned media aids the formation of colonies. Exactly which elements, or combination of elements in the glass conditioned media had this effect are unclear. However, it seems the presence of strontium did not strongly affect the outcome, suggesting that Sr was not responsible. As mentioned previously, Si and Mg are known to have many positive effects on human cells, such as to encourage cell survival, adhesion and stability, all of which would have been beneficial in forming colonies (88,246–249).

The glass conditioned media studies are effective for studying the effects of what is released by the material on the cells, but this can only indicate so much about how a material will behave and how the cells will respond to it, because the surface of the material is complex, and can have significant effects on cell behaviour and function (67,68,240,250). Though the use of conditioned media to establish the bioactivity of biomaterials is well established (65,85,87,231), this study was also able to grow the cells directly on discs of the material. Much like the results from the conditioned media

work, it was found that the addition of strontium to the SrAWGC discs seemed to interfere with osteogenic differentiation of the Y201 MSCs, as it retarded the increase in ALP induced by osteogenic media. As in the SrAW glass conditioned media studies, increasing the strontium content of the SrAWGC discs resulted in greater DNA content in osteogenic, mineralisation and basal conditions. For Y201 MSCs the peak cell number increase with Sr for mineralisation media was seen for 12.5 Mol% at day 6, and 6.2 Mol% at day 9, with higher Sr contents then resulting in lesser increases. A further experiment using WST-1 found increased metabolism at day 7 for the 12.5 Mol% compositions, also suggesting an increased cell number. As with the glass conditioned media, the proliferation assay at 48 hours did not show any difference between the conditions, though again this could have been due to the timing of the measurement. Future work would involve letting the cells grow on the material surface for a number of days prior to exposure to the EdU. In the 0 Mol% SrAWGC conditions the cell number of the Y201 MSCs grown on the discs with mineralisation media was found to actually be decreasing over time, whereas the substitution of Sr abrogated this decrease. These two results taken together suggest the addition of strontium to the materials actually aided cell survival on these materials.

The 6.2 and 12.5 mol% SrAWGC discs were found to be the most favourable compositions as they promoted the most growth. However, these are not necessarily the optimum SrAWGC compositions for making a porous scaffold for bone tissue engineering. This is because the form of the material can greatly alter its properties and hence potentially alter how cells would respond. This has been indicated by other work on SrAWGC, where Pontiroli found that although SrAWGC discs with more than 12 mol% Sr did not form a hydroxyapatite surface, a porous SrAWGC scaffold formed hydroxyapatite on the inner struts for all compositions except 37.4 mol% Sr (203). Hence, further work will be needed to calibrate Sr content for the final format of the material. The glass conditioned media also showed a different optimum strontium content, with 24.9 Mol% Sr resulting in the highest cell number. However, it is important to recall that the glass conditioned media is not a direct analogue of the ions released by the SrAWGC discs. The ion release from the glass conditioned media is fixed, having been preconditioned, and

then the glass removed, whereas the ions release dynamically from the discs over time. For this reason, even though the ions released by the discs and the glass conditioned media were measured using ICP-OES in this work, that will not correspond with the ions the cells were exposed to, due to the regular media changes and dynamic release of the ions from the discs. Hence, an area of further study would be to explore how the cells responded to glass powder releasing ions over time, suspended above them in an insert, potentially more closely modelling the amorphous phase of the SrAWGC material. Additionally, the quantity of ions released from the glass powder into the media is proportional to the amount of glass used and the mixing time. Future work could calibrate the glass conditioned media production process so that it was more directly comparable to the SrAWGC itself. This could be done by changing the quantity of glass in the media to result in approximately the same Sr concentration.

There have been other studies on strontium (and other ions) added to bioactive glasses. However these have been used weaker glass compositions (such as Bioglass 45S5) and have frequently used osteogenic cell culture media (with the potent osteogenic steroid dexamethasone), pre-differentiated cells and non-human cells, potentially over representing strontium's potency (85,87,204,223). Furthermore, studies have found that strontium doped bioactive glasses can improve cell growth (55,85,257,258,87,204,251–256). These studies used non-human cells (such as rat and mouse MC3T3 cells)(55,204,252,253,256,258), whilst other studies used pre-differentiated cell types, typically osteoblasts, which are known to respond very readily to strontium and to quickly show signs of osteogenic activity (as they are already bone producing cells)(85,252,253,256). Furthermore, these studies used only simple metabolic dye conversion experiments (MTT etc.) to determine the effect strontium had. As discussed earlier, without further techniques it is difficult to interpret these results as they could mean that there are more cells, or that the cells are simply more viable. In particular, it is difficult to know if there was an increase in proliferation without some form of cell cycle analysis (as conducted in this project). Additionally, it is not certain whether the cells which have proliferated are MSCs which have remained undifferentiated, or

those which have begun to osteogenically differentiate and started to progress through the transit amplifying stage. Further work could explore this by measuring the gene expression of marker genes of osteogenic differentiation at time points after exposure to Sr, SrAW glass dissolution ions or SrAWGC. If the MSCs are proliferating whilst undifferentiated they will have high Twist and low ALP and Runx2 gene expression (30,259). Twist inhibits MSC differentiation by binding the Runx2 protein (259,260). If the MSCs have begun to differentiate they will show decreased Twist and increased Runx2, ALP and Osterix gene expression compared with undifferentiated MSCs (30,261,262). In particular, Osterix is associated with proliferation in differentiating MSCs (30,261,262).

Determining which aspect of SrAW and SrAWGC is responsible for the increased cell number is challenging, due to the number of different factors that the cells are exposed to. Given that the increased cell number was measured using the SrAWGC discs, as well as the SrAW conditioned media, it would suggest it was not solely some feature of the material's surface, but instead associated with ions being released from the material. This is important to note, as increasingly the literature is reporting that the surface of biomaterials has a much larger effect on cell growth and behaviour than previously thought (67,68,240,250).

Clearly, the interaction of human mesenchymal stem cells with bioactive glasses is complex. The difficulty arises because there are so many factors to consider, even when simply studying the interaction of the cells with AWGC on its own, as the material has a rich surface and here it has been shown to alter the composition of the cell culture media, particularly lowering the phosphate content, and releasing Si and Mg ions, all of which could have implications for stem cell development. This complexity is increased when Sr is added to the material to make SrAWGC, as the Sr can alter the material surface and ion release, and therefore it could alter the cell response to the baseline material in a number of ways. The material was found to increase cell number with Sr content, however as mentioned previously this could have been due to a number of factors. However, further work showed that the glass conditioned media from the strontium containing compositions of AW glass were able to induce this effect, suggesting that the ions released

by SrAWGC play a part in this change in cell number in human MSCs. Finally, although the glass conditioned media contained a number of different ions, $SrCl_2$ was found to also be able to raise cell number, and so together these results suggest the strontium being released from the material contributes to this effect. However, the ion release data for the both the glass conditioned media, and the discs themselves, show the addition of strontium to the material alters the release of other ions too. Hence, these could be inhibiting or aiding this effect, although further study centred around the MSC response to differing Si, Mg and P concentrations would be required to prove this unequivocally.

# Chapter 4 – Determining the mechanisms of the MSC response to SrAWGC

## 4.1 Introduction

The result discussed in the previous chapter it was found that both SrAWGC and SrAW glass conditioned medium have effects on human MSCs, perhaps most interestingly increasing cell number. This chapter will build on these findings by exploring more widely how SrAWGC affects the MSCs in an attempt to gain a better understanding of the mechanisms behind these responses, and to determine if it is due to the strontium content of the material, or other factors.

There is evidence that both strontium and bioactive glasses/ceramics are able to induce gene expression changes in osteoblasts and MSCs which result in higher proliferation, increased cell survival and differentiation into an osteogenic lineage (71,72,122,141). As bioactive glasses and ceramics have been typically created with the treatment of bone disease in mind, the studies exploring their interaction with human cells have often focussed specifically on genes (or proteins) which have some relation to tissue engineering bone, such those relating to extracellular matrix production (Col1) and osteogenesis, with early stage osteogenic differentiation markers such as BMP, Runx2, Col1, Osterix, Alkaline Phosphatase or later stage markers such as Osteocalcin and osteopontin (OPN) (55,83,204,232,255,263–267). The studies looking at the effects of strontium on MSCs have been similarly focused on any effects that Sr has which could aid tissue engineering or more broad medical outcomes, such as promoting cell growth, survival, osteogenesis and osteogenic differentiation. For example, multiple studies have used pre-osteoblastic MC3T3-E1 cells and found that bioactive glasses of various descriptions raises the expression of key osteogenic genes (or proteins they encode), such as Col1, ALP and BMP-2 (82,83,86,253,256,265,268). Other studies have used MSCs, but these have also tended to focus on bone tissue engineering outcomes, such as increased Runx2, Col1, ALP, Osteopontin, Osteocalcin and Osteonectin

gene expression (204,232,251,254,263,265,269). The ability of the material to induce osteogenic differentiation is not the only consideration when making a tissue engineering scaffold or construct. Indeed, many of these studies also examined proliferation, cell survival and viability, which again are important for a good healthy tissue engineered tissue to be formed from cells interacting with the scaffold. However, all of these factors are just a small facet of the function of the human MSC, and for some time there has been a lack of broader study into the effects of both Sr and bioactive glasses more generally on cell biology.

Bioglass 45S5, being the most popular and well-studied bioactive glass, is perhaps the exception. Recent reviews of studies on Bioglass 45S5 and simple binary and ternary sol-gel bioactive glass studies, have found that seven different families of genes in embryonic, osteoblast and primary MSCs were typically affected by the ions released by the glasses (78,80,133). Specifically, these were genes associated with cell cycle regulation, DNA synthesis and repair, apoptosis, growth factors cell surface antigens and receptors, and signal transduction molecules. A study by Autefage *et al*. (2015) used an RNA microarray to do a global gene analysis of how strontium substituted Bioglass 45S5 conditioned media affected human bone marrow MSCs, and found that not only were the usual osteogenic genes up-regulated, but that the largest change was in the previously un-associated area of sterol/steroid production resulting (87). However, it is important to note that Autefage *et al*. (2015) chose to use Bioglass 45S5 solely in its powder form, and this doesn’t necessarily provide information on how an actual scaffold with cells growing on its surface will affect the gene expression of those cells. Bioglass 45S5 can be made into scaffolds, however it has a tendency to crystallise above 1000°C, reducing its beneficial biological properties (59,101). Although modifications to the composition and heating regime have enable Bioglass 45S5 scaffolds, this was not included in their study. Hence, in this chapter it will be important to explore how the SrAWGC scaffold material itself affects the gene expression of the MSCs.

The aim of the work described in this chapter was to determine how SrAWGC affects human MSCs and the mechanisms behind the observed

increase in cell number. This will be necessary to further develop SrAWGC as a bone regeneration scaffold as it is important to determine whether any cellular effects derive from the material itself, and physical changes to the material as a result of strontium substitution, or from ions (including Sr) released from the material. To achieve this, high throughput gene expression techniques were used to study the effects of SrAWGC on MSCs, and whether the substitution of Sr into the material altered these effects. To further determine whether it is the ions released by the material, or the surface itself, both SrAWGC discs, and SrAW glass conditioned media were used (with the glass conditioned media simulating the ions released by the glassy phase of the SrAWGC). Initially RNA sequencing (RNAseq) was used to get a global view of how the MSC gene expression changed when exposed to SrAW glass media or SrAWGC glass ceramic discs, with and without strontium. Based on the findings of the RNAseq, more targeted arrays were used to provide complimentary data by confirming the change in expression of key genes using an alternative technique. Pathways of interest were then interrogated using appropriate inhibitors to determine the intracellular mechanisms by which any effects occurred. The findings of the high throughput gene expression techniques were further tested using an *in vivo* Rat study.

## 4.2 Materials and methods

### 4.2.1 Cell Culture

#### 4.2.1.1 Immortalised MSC line: Y201

Throughout this work an established, highly characterised immortalised MSC line was used, referred to as Y201 MSCs, (39). The Y201 MSCs have tri-lineage potential (osteogenic, chondrogenic and adipogenic), with the differentiation protocols established in the Genever Laboratory. The method by which the cells were immortalised is described elsewhere (39). However, in brief they were created from primary human MSCs extracted from the femoral head of routine hip replacement patients which were immortalised before passage 3 using a human Telomerase reverse transcriptase (hTERT)

lentiviral vector. hTERT allows lengthening of the telomeres and subsequent cell immortality. The cells were used in the experiments described in this work between passage 60 and passage 90.

#### 4.2.1.2 General cell culture technique

Y201 MSCs were used in all experiments unless otherwise indicated. All reagents were sterile. Cells were typically grown in T175 culture flasks at 37°C, with a 5% $CO_2$ atmosphere, between passages 60 and 90 and kept less than 80% confluent by regular passaging (assessed using a phase contrast microscope). Cells were cultured in basal media unless otherwise specified, consisting of Dulbecco's Modified Eagle's Medium (DMEM, Gibco, high glucose 4.5g/l with pyruvate and L-glutamine, ref no. 41966-029) with 10% (v/v) Foetal Bovine Serum (FBS, Sigma, F7524-500ML) and 1% (v/v) Penicillin-Streptomycin (Invitrogen, S15140-122). Cells were detached using 0.1% (v/v) trypsin ethylene-diamine-tetra-acetic-acid (trypsin-EDTA, Invitrogen, S25300-054) and counted using a haemocytometer.

### 4.2.2 Gene expression analysis of the effects of SrAWGC and SrAW conditioned media on MSCs using RNA sequencing

#### 4.2.2.1 RNA extraction

The gene expression of Y201 MSCs growing on SrAWGC discs and on culture plastic whilst exposed to SrAW glass conditioned medium, both of these with and without strontium (0 and 12.5 Mol% Sr compositions), were compared to determine how the ions released by the material and material surface altered MSC gene expression. These four conditions will be referred to as "Disc" and "Disc Sr", for MSCs grown on AWGC discs with and without Sr, and "Media" and "Media Sr" for MSCs exposed to glass conditioned media with and without strontium.

Discs were made as described previously in Chapter 2, but using a 24 well plate as a template. Once made, these were then autoclaved overnight. The autoclaved discs were washed in 1 x Phosphate Buffered Saline (PBS) before being placed in 24 well plates, with the curved face of the disc

downwards. Y201 MSCs were seeded in basal media into the wells at concentrations of $4.5x10^4$ cells/$cm^2$ for confluency. At the same time, $25cm^2$ culture flasks (T25 flasks) were seeded with Y201 MSCs ($112.5x10^4$ per flask to reach confluence) in basal media. These T25 flasks would be used for the glass conditioned media experiments.

The glass conditioned media was prepared as described in Chapter 3. Briefly, glass conditioned media was made by mixing 12mg/mL of 0 Mol% SrAW glass powder for the “Media” condition, or 12.86mg/mL of 12.5 Mol% SrAW glass powder for the “Media Sr” condition (both <45μm particle size) with high glucose DMEM for 24 hours at room temperature, before filtering to remove the glass powder (method adapted from (2015) (87)). The glass powder was autoclaved (121˚C for 20 minutes) in the mixing bottle prior to use.

After 24 hours (to allow the cells to attach) the cells on discs were exposed to mineralisation media for 24 hours. Mineralisation media was basal media (Chapter 3, Section 3.2.6) but supplemented with 50μg/ml L-ascorbic acid-2-phosphate and 5mM β-glycerophosphate. The glass conditioned media was also made into glass conditioned mineralisation media through the addition of these same supplements. The cells grown in the T25 flasks were then exposed to either 0 Mol% or 12 Mol% SrAW conditioned mineralisation media for 24 hours.

After 24 hours of exposure by the cells to either the SrAWGC discs, or the glass conditioned media, the media was removed, and the discs were transferred to new wells, prior to both the Y201 MSCs on discs and on culture plastic (in T25 flasks) undergoing RNA extraction. This used a NucleoSpin RNA kit (Machery-Nagel) and followed the manufacturer’s instructions. This contained proprietary buffers, namely lysis buffer RA1, wash buffer RAW2 and a further wash buffer RAW3. Briefly, each sample was first lysed in well using 350μl RA1 buffer (in the kit) with 3.5μl 1x β-mercaptoethanol. The cell lysis solution was pipetted up and down to fully lyse the cells and then passed through into a NucleoSpin filter (using a 1 minute 11,000 x g spin in a centrifuge at 4ºC) to reduce viscosity and to clear the lysate. 350μl of 70% (v/v) ethanol was added and mixed by pipetting to

adjust the RNA binding conditions, after which this was applied to the NucleoSpin RNA Column (using a 30 seconds 11,000 x g spin in a centrifuge at 4ºC). The silica membrane on the column was then desalted (to make the following rDNase step more effective), using 250µl of the Membrane Desalting Buffer (provided in the kit) and a 1 minute 11,000 x g spin at 4ºC. The DNA on the column was then digested for 15 minutes using 95µl of rDNase reaction mixture (10ul reconstituted rDNase with 90µl Reaction Buffer for rDNase, both in the kit). The membrane was then washed, using 200µl RAW buffer (provided, spun for 30 seconds at 10,000 x g at 4ºC), then using 600µl RA3 Buffer (provided, spun for 30 seconds at 10,000 x g at 4ºC) and finally using 250µl of RA3 buffer again before spinning at 11,000 x g at 4ºC for 2 minutes to dry the membrane. The RNA was then eluted from the membrane using 40ul of RNase-free $H_2O$ passed twice through the membrane. The experiment was performed once, with triplicate samples for each condition.

The RNA samples were then sent to the University of York Technology Facility for preparation prior to sequencing. The RNA yields for each condition (Disc, Disc Sr, Media and Media Sr) were then counted using a Nanodrop Spectrophotometer with 1.2ul sample volume and the quality checked by running an Agilent Bioanalyser RNA nano chip. The mRNA sequencing library was prepared with 1 µg of good quality total RNA using the NEBNext RNA Ultra Library preparation kit for Illumina in conjunction with the NEBNext Poly(A) mRNA Magnetic Isolation Module (New England BioLabs Inc.), and NEBNext single 6bp indexing primers, in accordance with the manufacturer's instructions. The sample libraries were pooled at equimolar ratios and the pool was sent for 2 x 150 base paired end sequencing on a HiSeq 3000 at the University of Leeds Next Generation Sequencing Facility. The data received was a series of 125 base start and end read fragments and this was processed by the University of York Technology facility to produce differentially expressed gene FPKM values using the following process. In brief, these sequence reads were trimmed to remove any adapter sequences using Cutadapt version 1.8.3 (270). The trimmed reads were then aligned to version GRCh38 of the human genome using HISAT2 (271) and the transcriptomes assembled and gene expression

quantified using the Tuxedo pipeline (version 2.2.1)(272), where the Transcriptome was assembled using Cufflinks, merged using Cuffmerge, and then quantified and normalised by the lengths of the genes into fragments per kilobase per million mapped reads (FPKM) in Cuffnorm (272).

### 4.2.3 T-test and ANOVA analysis

The analysis of the gene expression values followed the pipeline described in Figure 62. The gene expression values for the four conditions (Disc, Disc Sr, Media and Media Sr) were mathematically compared to determine if there were changes in gene expression between the conditions. They were transformed (Log(FPKM+0.1)), and then these were used to form fold changes between conditions by subtracting the Log(FPKM+0.1) values from each other. Python was then used to perform t-tests on the fold change values and false detection rate (FDR) tests, between the conditions.

To determine which functional groupings of genes any differentially expressed genes between the four conditions belonged to, Geneset Enrichment was performed. This compared the genes against established “genesets” resulting in a list of genesets with which the differentially expressed genes related to and confidence values for that relationship. Geneset Enrichment was performed on the differentially expressed genes (both up and down regulated) utilising the oposSOM RNAseq R-package. This specifically enriched the genes on the Hallmark genesets from the Broad Institute (a curated aggregate of other genesets providing a relatively redundancy free map of gene to function) and using the Geneset Z (GSZ) scoring mechanism (273–276). Typical gene expression analysis (Ordered Gene List (OGL) analysis) orders the genes by difference in expression level and then performs analysis on the tail ends, either large increases or decreases, with arbitrary thresholds in expression. GSZ analysis considers both the magnitude of expression of the gene, and its membership of functional groups (genesets) to provide a score for how a whole geneset is represented between the conditions being analysed.

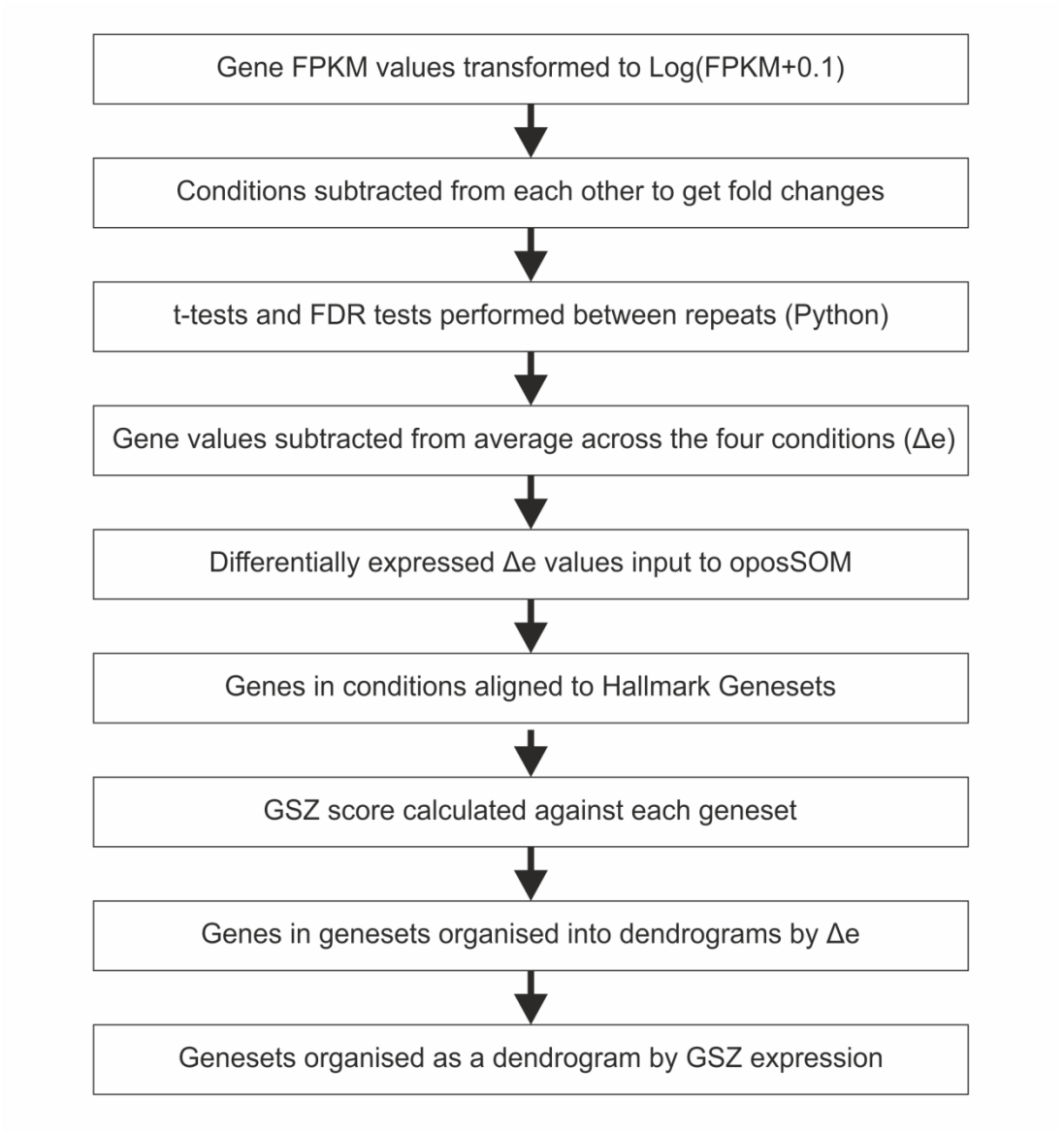


**Figure 62: The analysis pipeline of the gene expression data starting with normalised FPKM values.**

This provides a more stable assessment of how the gene expression has changed between conditions because it is based on the average change across many genes in meaningful biological processes and systems, rather than the potentially changeable measurements of individual genes (275). In oposSOM, a GSZ score of 1.5 is thresholded as significantly increased in enrichment, whilst -1.5 is significantly less enriched. OposSOM also produced heat-maps of the geneset enrichments, and the gene expression within a single geneset, and dendrograms arranging the genesets, genes

and conditions by order of similarity and overall strength of gene-expression/geneset enrichment.

### 4.2.4 Type 1 Interferon PCR array to determine effects of SrAWGC and SrAW glass on MSC cytokine gene expression

A PCR array was used to confirm the findings of the RNAseq using a different technique. The Y201 MSCs were seeded on the SrAWGC discs (corresponding with the RNAseq Disc and Disc Sr conditions) and also (separately) exposed to SrAW glass conditioned mineralisation media (0 and 12.5 Mol% Sr, corresponding to the RNAseq Media and Media Sr conditions) as for the RNAseq (24 hours) (see section 4.2.2.1). The RNA was extracted using the same process as described previously (see section 4.2.2.1). The cDNA was prepared from the RNA samples using the Qiagen $RT^2$ First Strand Kit. Manufacturer's instructions were followed. In brief they were, for each sample 2 µl of Buffer GE (genomic elimination buffer) was mixed with 0.5 µg of RNA sample and RNase-free $H_2O$ to make a 10 µl solution. This was then incubated for 5 minutes at 42ºC to destroy any genomic DNA, then placed on ice for 1 minute. Next the reverse transcription mix was made. This was 5 µl of Buffer BC3 (reverse transcription buffer), 1 µl of Control P2, 2 µl of RE3 Reverse Transcriptase Mix and 3 µl of RNase-free $H_2O$. For each sample, 10 µl of this mix was added to 10 µl of each sample mix, and mixed gently. These were then incubated for 15 minutes at 42°C, and the reaction stopped with a 5 minute 95°C incubation. 91 µl of RNase-free $H_2O$ was added to each sample and they were mixed, then prepared cDNA was frozen for later use.

The cDNA samples were later applied to the Human Type I Interferon Response PCR Array (PAHS-016ZC Qiagen) utilising the manufacturer's instructions. The PCR master mix for each sample was prepared by combining 102 µl of cDNA made previously with 1350 µl of $RT^2$ SYBR Green ROX (Qiagen) and 1248 µl RNase-free $H_2O$. This was mixed and transferred to a freshly opened RNase-free reservoir and a multichannel pipette was then used to apply 25 µl of this solution onto each well of the array (see

Table 21). Once cDNA addition was complete, the optical film was used to seal the plate and it was move to an ABI StepOnePlus PCR machine where a series of non-fast cycles were performed. These consisted of one 10-minute stage at 95ºC, followed by forty stages consisting each of a 15 seconds at 95ºC and a further 1 minute at 60ºC. After this a melt curve was performed. The experiment was performed three times independently.

The cycle threshold ($C_T$) for each gene was determined by the PCR machine. The data was saved and part analysed on the ThermoFisher cloud with the normalisation and figures produced by a bespoke Excel spreadsheet which came with the kit. The four conditions were cross compared using a $\Delta\Delta C_T$ approach (277). This meant there were comparisons between SrAW glass conditioned media with 0 Mol% Sr (control) and 12.5 Mol% Sr (experimental), between the SrAWGC discs with 0 Mol% Sr (control) and 12.5 Mol% Sr (experimental), between the 0 Mol% strontium SrAW glass conditioned media (control) and SrAWGC discs (experimental) and between the 12.5 Mol% strontium SrAW glass conditioned media (control) and SrAWGC discs (experimental). There was also comparison across strontium and non-strontium conditions, with the 0 Mol% strontium SrAW glass media and disc conditions averaged (control) and compared against the 12.5 Mol% strontium SrAW glass media and disc conditions (experimental). Finally, the different forms of the material were compared with the averaged values for the SrAW glass media 0 and 12.5 Mol% Sr conditions (control) compared against the average of the SrAWGC 0 and 12.5 Mol% Sr conditions (experimental).

The housekeeping gene $C_T$ values were averaged together to make “housekeeping experimental” (HE) and “housekeeping control” (HC) values and these were then subtracted from the gene tested experimental (TE) and gene tested control (TC) values. This formed a $\Delta C_T$ value for each gene in the experimental ($\Delta C_{TE}$) and control ($\Delta C_{TC}$) conditions. These were then subtracted to form $\Delta\Delta C_T$ values for each gene and each comparison (i.e. between 0 and 12.5 Mol% Sr glass conditioned media). The $\Delta\Delta C_T$ values were then transformed into fold-change values ($2^{-\Delta\Delta C_T}$). Student’s T-test was used to determine the significance of the differences with significance set as $p < 0.05$.

| | | | | | | | | | | | |
|---|---|---|---|---|---|---|---|---|---|---|---|
| ADAR | BAG3 | BST2 | CASP1 | CAV1 | CCL2 | CCL5 | CD70 | CD80 | CD86 | CDKN1B | CIITA |
| CRP | CXCL10 | DDX58 | EIF2AK2 | GBP1 | HLA-A | HLA-B | HLA-E | HLA-G | IFI16 | IFI27 | IFI30 |
| IFI6 | IFIH1 | IFIT1 | IFIT2 | IFIT3 | IFITM1 | IFITM2 | IFITM3 | IFNA1 | IFNA2 | IFNA4 | IFNAR1 |
| IFNAR2 | IFNB1 | IFNE | IFNW1 | IL10 | 1L15 | IL6 | IRF1 | IRF2 | IRF3 | IRF5 | IRF7 |
| IRF9 | ISG15 | ISG20 | JAK1 | JAK2 | MAL | MET | MNDA | MX1 | MX2 | MYD88 | NMI |
| NOS2 | OAS1 | OAS2 | PML | PRKCZ | PSME2 | SH2D1A | SHB | SOCS1 | STAT1 | STAT2 | STAT3 |
| TAP1 | TICAM1 | TIMP1 | TLR3 | TLR7 | TLR8 | TLR9 | TMEM173 | TNFSF10 | TRAF3 | TYK2 | VEGFA |
| ACTB | B2M | GAPDH | HPRT1 | RPLP0 | HGDC | RTC | RTC | RTC | PPC | PPC | PPC |

**Table 21: Primers on Type 1 Interferon Response PCR array used to confirm the results from the RNAseq by using a more focussed selection of genes associated with inflammation. The shaded cells are the housekeeping genes.**

### 4.2.5 Use of inhibitors to study the mechanism behind MSC response to SrAW glass

Inhibitor studies were performed to further study the mechanisms by which the SrAW glass conditioned media (with 0 and 12.5 Mol% Sr) acted on Y201 MSCs. Ras signalling has been implicated in the response of MSCs to strontium in previous work (128), and was also found to be one of the gene sets associated with the strontium SrAW glass in this project. Therefore the cell number (measured by total DNA) was measured in response to the glass conditioned media with inhibitors for K-Ras signalling, Salirasib. Salirasib (also known as FTS) is a small molecule inhibitor which prevents K-Ras localising to the cell membrane (278), preventing interaction with Sos and further signalling(279). Salirasib is not specific to K-Ras and does also inhibit N-Ras and H-Ras, however it is well established as a K-Ras inhibitor and is used clinically for the purposes of cancer treatment (279–281).

The RNA sequencing results indicated the SrAW glass and glass-ceramic interacted with inflammatory genesets and cytokines specifically, hence inhibitors for inflammatory signalling mediators were used. JAK could

potentially act as a bridge between inflammatory cytokines, STAT signalling (282), Ras/MAPK signalling and the PI3K pathway (associated with Sr (124))(283), hence it was targeted: Ruxolitinib was chosen as it is a highly specific dose-dependent inhibitor of JAK1 and JAK2/STAT signalling, and has been seen to affect MSC growth (284). Src signalling also occurs in response to cytokine signalling (285–287), and it's inhibition has been seen to affect MSC differentiation (288). Hence, Src was explored as another potential mechanism behind Sr induced and cytokine mediated increase in cell number. Dasatinib was used as the Src inhibitor as it is an established Src inhibitor with protocols defined for use with human MSCs (288). These are all small molecule inhibitors.

Y201 hTERT MSCs were seeded in 96 well plates at $4.5x10^4$ cell/$cm^2$ and after 24 hours exposed to SrAW (0 Mol% Sr and 12.5 Mol% Sr) glass conditioned mineralisation media with different concentrations of the following inhibitors: Salirasib (0, 1, 5µM, for K-Ras), Dasatinib (0, 0.001, 0.005, 0.01µM, for Src), and Ruxolitinib (0, 0.05, 0.25, 0.5µM, for JAK2). The specific inhibitors used were Salirasib (>98% purity, Sigma Aldrich), Dasatinib (>98% purity, Cambridge Bioscience/TOKU-E) and Ruxolitinib (>98% purity, CAYM11609-1 VWR/Cayman). Media was changed every 3 to 4 days and after 9 days exposure the experiment was ended. At the time point, the media was aspirated from the well and washed twice in 0.2M Carbonate Buffer (2:1 volume to volume ratio of 0.2M $Na_2CO_3$ to 0.2M $NaHCO_3$, pH 10.2) after which, 0.1% (v/v) Triton X was added to lyse the cells (150µl in a 96 well plate), and then the well plate was frozen. The well plates were freeze thawed three times, after which 50µl from each experimental well was moved to a fresh well in a black 96-well plate, along with DNA standards (in triplicate) made from a 10µg/ml stock of salmon sperm (Invitrogen). To begin the measurement 50µl of PicoGreen (Invitrogen, P7581) diluted 1:50 in TE Buffer (10mM Tris,1mM EDTA at pH 7.5) was added to the experimental and standard well. This was agitated to mix, then after 10 minutes under foil at the fluorescence emission was measured using 485nm excitation whilst monitoring emission at 538nm on a BMG Labtech POLARstar OPTIMA plate reader.

### 4.2.6 *In vivo* study to determine the extent of the inflammatory effects on MSCs by SrAWGC and SrAW glass

A short term *in vivo* study was done to determine whether the MSCs which had been exposed to the SrAWGC discs or the SrAW glass conditioned media (0 and 12.5 Mol% Sr, corresponding with the Disc, Disc Sr, Media and Media Sr conditions in the RNAseq), would worsen, or sustain any inflammatory response, based on the results of the gene expression analysis. As inflammatory response typically declines within 1 week, the experiment had two time points at 1 and 3 days, with the aim to measure the period of peak inflammation. Y201 MSCs were seeded in 6-well plates (34mm diameter) at confluency (450,000 cells per 6-well) on both culture plastic, and on 6-well sized (34mm diameter) SrAWGC discs (0 and 12.5 Mol%). The discs were made as described in Chapter 2 and were autoclaved and washed in sterile PBS prior to use. Glass conditioned media was made as described in Chapter 3. Briefly, glass conditioned media was made by mixing 12mg/mL of 0 Mol% SrAW glass powder, or 12.86mg/mL of 12.5 Mol% SrAW glass powder (both <45µm particle size) with high glucose DMEM for 24 hours at room temperature, before filtering to remove the glass powder (method adapted from (87)). The glass powder was autoclaved (121$^{o}$C for 20 minutes) in the mixing bottle prior to use.

After 24 hours (to allow the cells to attach) the cells on discs were exposed to mineralisation media (4ml per 6-well) for 24 hours. Mineralisation media was basal media (as described in Chapter 3 Section 3.2.2) but supplemented with 50µg/ml L-ascorbic acid-2-phosphate and 5mM β-glycerophosphate. The glass conditioned media was also made into glass conditioned mineralisation media through the addition of the same supplements. The cells grown in the wells without SrAWGC discs were then exposed to either 0 Mol% (Media condition) or 12 Mol% SrAW (Media Sr condition) conditioned mineralisation media (4ml per 6-well) for 24 hours. There was a control set of cells where the media was replaced with fresh basal media.

After 24 hours exposure the SrAWGC discs with cells on were moved to new wells and washed with PBS (with no Ca or Mg). The cells exposed to the

glass conditioned media had their media aspirated and were washed with PBS. Then all cells (on either discs or culture plastic exposed to glass conditioned media) were detached from their substrate using 1ml of Trypsin/EDTA for 10 minutes, followed by gentle pipetting to loosen. The trypsin was deactivated using basal media and the cells for each condition were then counted and resuspended at concentration.

Collagen gels were prepared using a 3mg/ml collagen in 0.02M acetic acid previously harvested from rat tails. This was mixed with 10xPBS and neutralised with NaOH 1M to begin polymerisation from fluid into a gel, however it was kept on ice to temporarily halt the process. An appropriate volume of cell solution was then mixed with the collagen gel to result in 1 million cells per 100µl of collagen gel. Each of the conditions (control cells, Disc, Disc Sr, Media and Media Sr) were then drawn into syringes and kept on ice for implantation into the rats.

The hydrogels were then implanted subcutaneously into fourteen Sprague Dawley (SD) male rats (200-250 g), with each rat being identified by ear and tail markings. The Rats were placed in a trifluorane chamber and anaesthetised for approximately 2-3 minutes (level 5 trifluorane and 2.5% (v/v) oxygen). After losing consciousness, the rats were transferred onto a heated mat and anaesthesia was maintained (level 2.5 trifluorane and 2.5% (v/v) oxygen) via a nose cone. The backs of the animals were shaved and sterilised with 70% (v/v) ethanol, and four full thickness skin incisions were made at both sides of upper (one for each side) and lower (one for each side) back regions. To create pockets, the subcutaneous tissues were then bluntly dissected using artery forceps and four hydrogels (100µL each) were injected within these pockets (away from the incision). The wounds were then closed using 5-0 ethilion sutures. The hydrogels were intended to polymerise at room temperature, hence would fully gel *in situ*. After the wound was closed, the wound site was cleaned with sterile injection water and a Vetergesic injection (0.03 mg/mL) was administered to each rat. The trifluorane was then switched off and the rats were transferred to a heated chamber until they were fully recovered.

After 24 hours, the rats for the first time point were checked for any obvious signs of discomfort or infection at the wound site, and then sacrificed using schedule 1 where they were transferred into a carbon dioxide chamber for 6 minutes followed by cervical dislocation. The collagen gels were then extracted from the subcutaneous pockets and placed into 10% (v/v) neutral buffered formalin. This was repeated at day three.

The fixed tissue samples for each condition were moved to tissue processing cassettes and processed into paraffin wax in a Leica APS2000 tissue processing machine (Leica Microsystems, UK) using an overnight programme, seen in Table 22.

The samples were then wax embedded on a Leica EG1150C embedding station in CellWax plus wax (Cellpath Ltd, UK). Tissue was sectioned on a Leica RM 2235 microtome at 4µm and placed on a glass microslide (Solmedia Ltd, Shrewsbury, UK) and then dried on a hot plate for 2 hours at 70°C. The slides were dewaxed through two 5 minute xylene steps (VWR International Ltd, UK) and two 5 minute absolute ethanol steps (Sigma, Poole, Dorset, UK) and then rehydrated in running tap water before staining with Mayer's Haematoxylin for 3 minutes. This was followed by rinsing in running tap water followed by differentiation with 0.3% (v/v) acid alcohol (70% (v/v) ethanol in ultrapure water with 0.3% (v/v) concentrated hydrochloric acid), further rinsing in running tap water and then rinsing in Scott's tap water (ultrapure water with 2g/ml sodium hydrogen carbonate and 20g/ml of magnesium sulphate). After further rinsing in tap water, the slides were stained in Eosin for 30 seconds, after which they were rinsed in tap water and then dehydrated in two changes of absolute ethanol and two changes of xylene before mounting on a cover-slip in DPX (Solmedia). The slides were dried then later imaged using a Leica DM IRB inverted microscope.

| Reagent % (v/v) | Time | Temperature |
|---|---|---|
| 70% ethanol | 30 min | 37°C |
| 80% ethanol | 30 min | 37°C |
| 90% ethanol | 30 min | 37°C |
| 95% ethanol | 30 min | 37°C |
| 100% ethanol | 1:00h | 37°C |
| 100% ethanol | 1:00h | 37°C |
| 100% ethanol | 1:30h | 37°C |
| xylene | 1:00h | 37°C |
| xylene | 1:30h | 37°C |
| xylene | 1:30h | 37°C |
| wax | 1:00h | 65°C |
| wax | 1:00h | 65°C |
| wax | 1:00h | 65°C |

**Table 22: The tissue processing programme used for the 10% (v/v) FBS fixed collagen gels extracted from the rat sub-cutaneous pockets.**

## 4.3 Results

### 4.3.1 Global gene expression analysis of the effects of the SrAWGC discs SrAW glass conditioned media on MSCs using RNA sequencing

RNAseq was performed on cells grown on SrAWGC discs and exposed to SrAW glass conditioned media, with 0 and 12.5 Mol% Sr, to determine any broad-spectrum gene expression changes in the cells in response to the strontium content of the material, but also whether the surface of the material (as opposed to the ions released) were an important factor. The conditions will be referred to as Disc and Disc Sr for the MSCs grown on 0 and 12.5 Mol% SrAWGC discs, respectively, and these two collectively as the “disc conditions”. Media and Media Sr will be used to refer to the MSCs exposed to SrAW glass conditioned media with 0 and 12.5 Mol% Sr, respectively, with these collectively referred to as the “media conditions”.

#### 4.3.1.1 RNAseq data processing

mRNA was successfully extracted for all samples, RNA sequencing performed and the data processed. The data was run through the data analysis pipeline described in Section 4.2.2.1 returning a list of gene FPKM values for the different conditions. There were instances where two (or more) genes were associated with a particular entry. This occurs when two mRNAs are essentially assembled from the same region of a chromosome, but reading in different directions, or starting at different points. If the whole RNA transcript is preserved, clearly they result in different proteins and are distinguishable. However, due to way in which the RNA-sequencing fragments the RNA and then reassembles it later, it can result in some entries being assigned to multiple genes. This is where the fragments assigned did not clearly identify one gene over another. For example, one entry is: AC007246.3 and MAP4K3. A search on GenBank shows that these are quite different (289). One is part of the MAPK pathway, the other is a gene that encodes for THUMPD2. But they belong to the same region of a chromosome, and actually overlap, which is where the confusion arises. As it was difficult to decompose such entries into the contributions from the genes which composed it, these entries were removed from the analysis.

#### 4.3.1.2 Genes aligned from the RNAseq

The number of genes identified through the RNAseq analysis for each of the four conditions, Disc, Disc Sr, Media and Media Sr were compared to find which genes were present in both conditions and these are displayed in a Venn diagram in Figure 63.

The media conditions were seen to have more genes identified in the RNAseq than the disc conditions (Figure 63). There was also a very high level of overlap between the two conditioned media conditions, with only 14 strontium glass media genes not appearing in the control glass media.

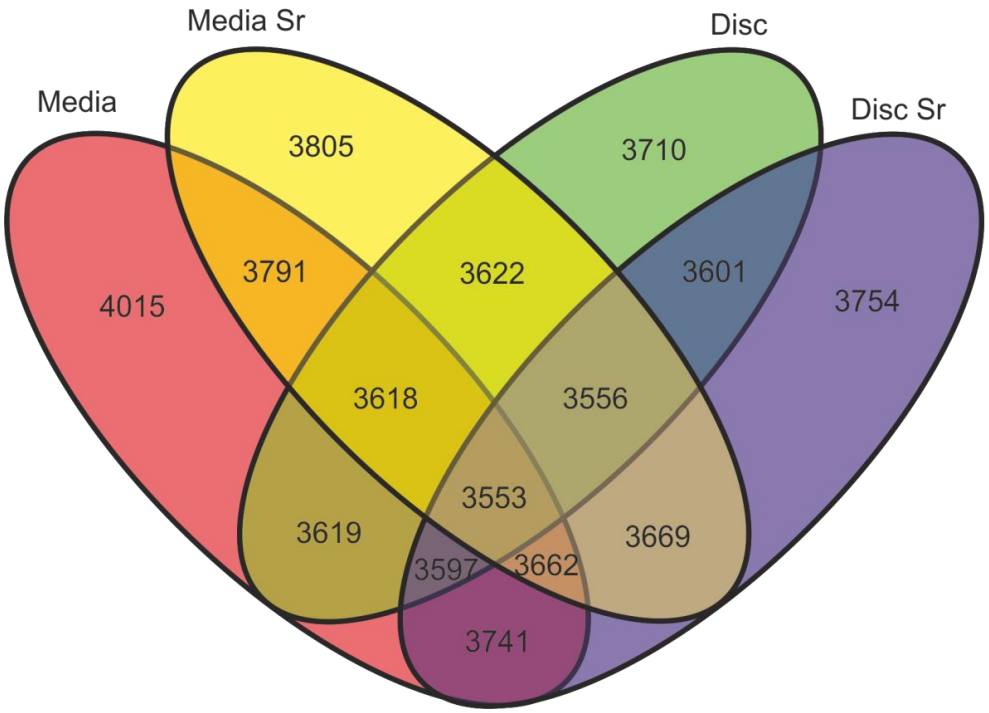


**Figure 63: Venn diagram of genes identified from RNAseq using mRNA extracted from MSCs grown on SrAWGC discs and exposed to SrAW glass conditioned media with 0 and 12.5 Mol% Sr, referred to as the Disc, Disc Sr, Media and Media Sr conditions. Genes with a mean FPKM of greater than 1 were included.**

The number of genes shared between all four conditions was high, with the 3553 genes found in all conditions representing ~95% of the genes in the control glass-ceramic disc condition (the one with the lowest number of genes).

#### 4.3.1.3 Differentially expressed genes between MSCs grown on SrAWGC discs or exposed to SrAW glass media with and without strontium.

The differentially expressed genes between the MSCs grown on the SrAWGC discs or exposed to the SrAW glass media (with and without strontium) were determined using t-tests to establish whether the addition of Sr to the material, and the surface of the material itself, altered MSC gene expression. Volcano plots were made of the log fold changes between the conditions in the RNAseq. First the differences in expression between the disc and media conditions were assessed. The largest and most significant changes occurring between the media and disc conditions (both without

strontium) are shown in Figure 64a (the orange and yellow dots indicate changes which are above the threshold of 1 fold change and significant, with yellow indicating they pass further Bonferonni corrections). The Disc condition was seen to upregulate the expression of CXCL10, CXCL11, MMP1, COL5A3 amongst other genes, whilst FOS, PTX3 and CXCL2 were down regulated. The differentially expressed genes between the Media Sr and Disc Sr conditions are shown in Figure 64b, where it is seen that CXCL11, IFIT2, COL5A3 and CCL8, amongst others, were upregulated, whilst numerous genes were also down regulated, with FOS, CXCL2 showing the largest changes. The prominently expressed cytokines CXCL10 and CXCL11 are associated with inflammatory response (290). Hence, the disc conditions were seen to elicit a change in gene expression in the MSC compared with the media conditions (both with and without Sr).

The differences in gene expression between the conditions with and without strontium were also examined. The largest and most significant changes between the Media and Media Sr conditions can be seen in Figure 65a, along with the changes between the Disc and Disc Sr conditions in Figure 65b. The differential expression was small and of low significance with the addition of Sr, particularly when compared with that found when comparing between the Media and Disc (and Media Sr and Disc Sr) conditions. Hence, the addition of strontium the discs or glass conditioned media was not observed to have a great effect on the gene expression of the MSCs.

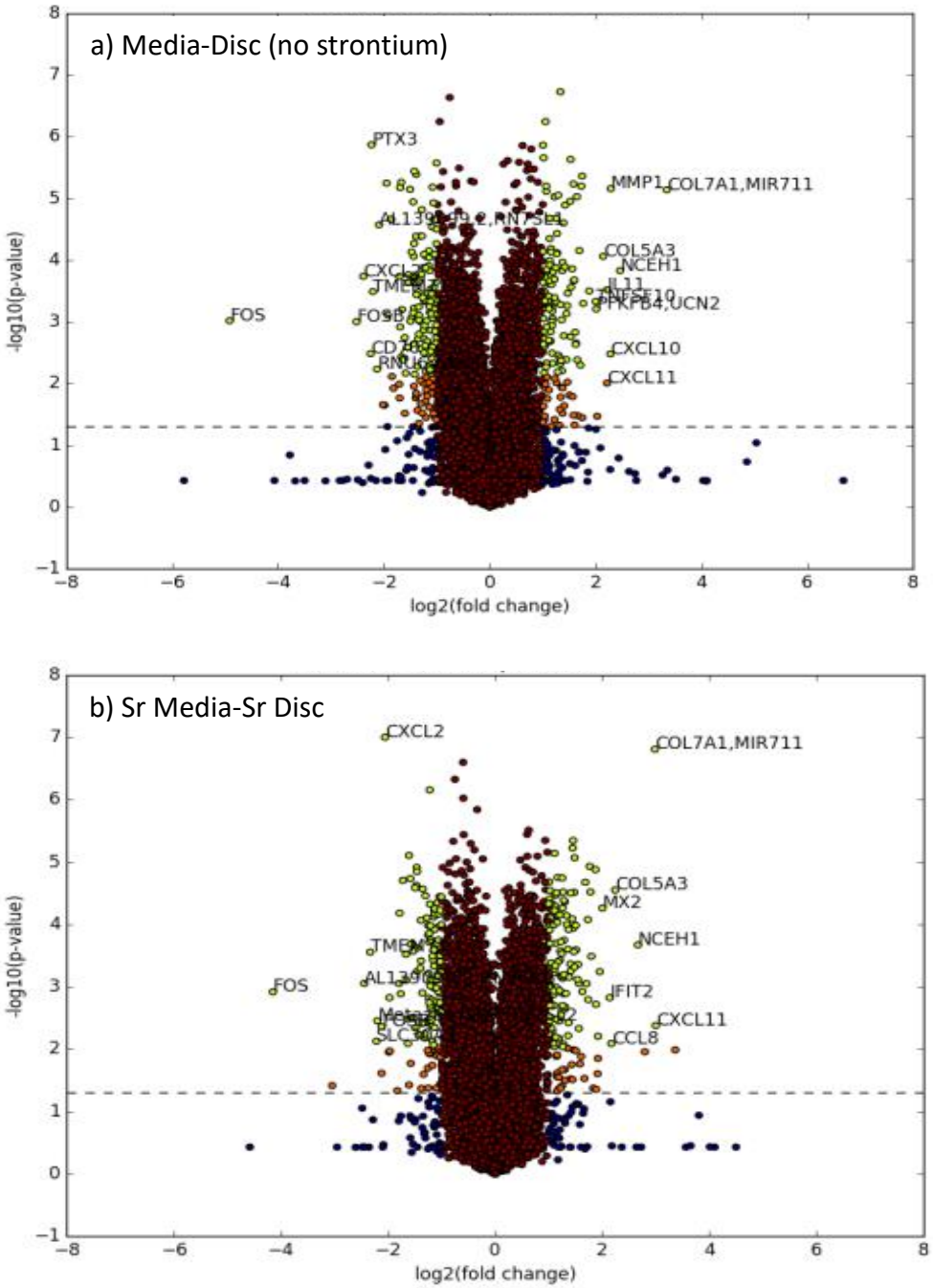


**Figure 64: Volcano plots of the t-test comparisons between the a) Media and Disc RNAseq conditions, b) Sr Media and Sr Disc RNAseq conditions. They show the p-value of any significant different against the fold change (log scale). The red dots indicate genes with a small and insignificant change (<1 fold change, p > 0.05). The blue dots are large changes which are insignificant. The orange dots are large changes which are also significant. The yellow dots are large changes, which are also significant and pass the Bonferroni correction.**

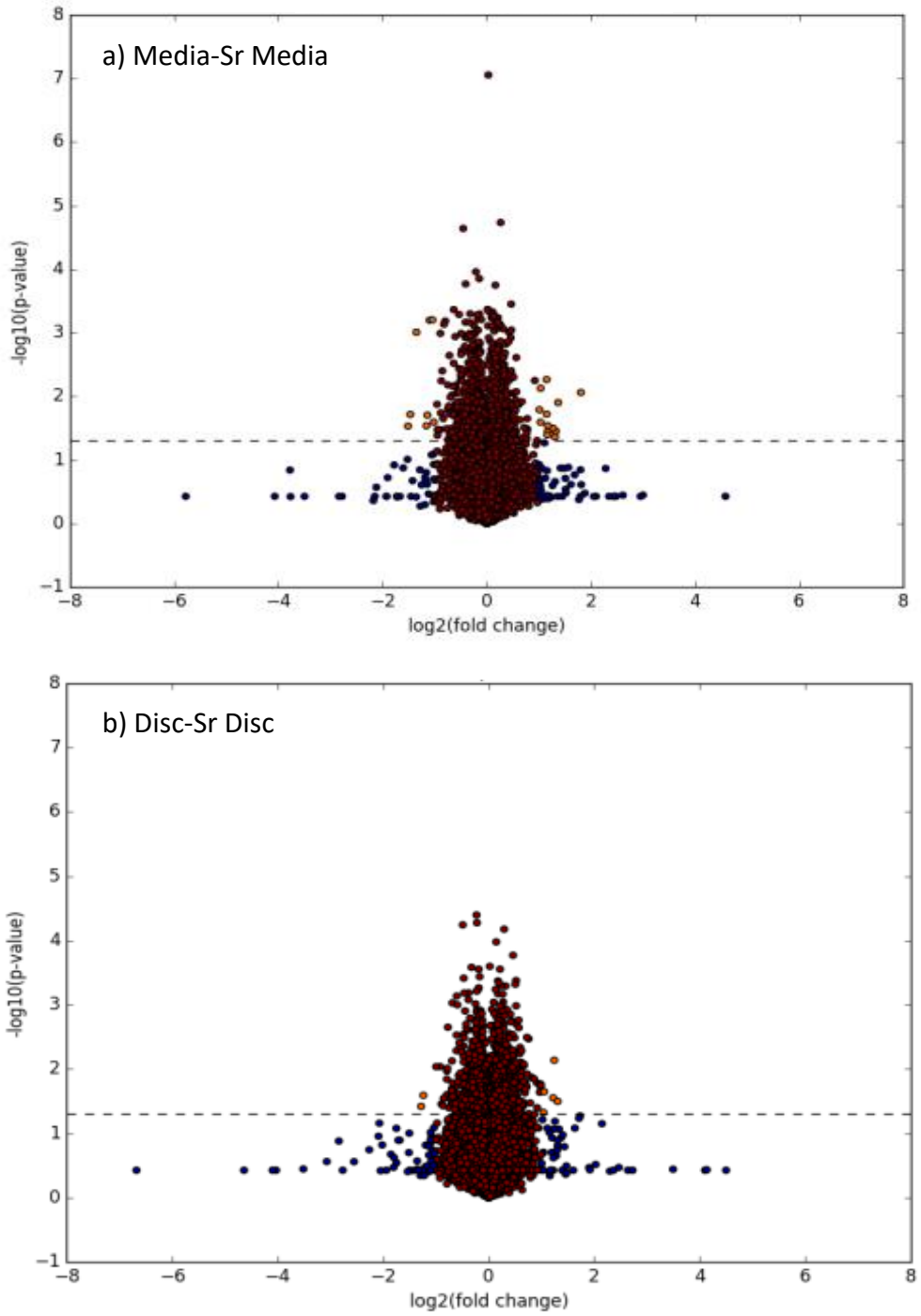


**Figure 65: Volcano plots of the t-test comparisons between a) Media and Media Sr RNAseq conditions, b) Disc and Disc Sr RNAseq conditions. They show the p-value of any significant different against the fold change (log scale). The red dots indicate genes with a small and insignificant change (<1 fold change, p > 0.05). The blue dots are large changes which are insignificant. The orange dots are large changes which are also significant. The yellow dots are large changes, which are also significant and pass the Bonferroni correction.**

The statistical analysis just described compared only one condition against another, however it is also beneficial to compare the sets of conditions against each other, as this can indicate whether the discs (or media) themselves, or the presence or lack of strontium has an effect on MSC gene expression. The differentially expressed genes between the cells grown on discs and those exposed to media, and those grown without and those grown with Sr were then calculated (using ANOVA). Volcano plots of the log fold changes between the all of the strontium and non-strontium conditions, and between all of the disc and media conditions can be seen in Figure 66. There are many genes which were significantly up and down regulated between the MSCs grown in the two disc and the two media conditions (see Figure 66a), indicating the discs themselves regardless of strontium content) have a significant effect on MSC gene expression. As with the individual comparisons of the Disc and Media, and Disc Sr and Media Sr conditions, MMP1, CXCL10, CXCL11, COL5A1 were amongst the genes upregulated, whilst FOS, CXCL2 and TMEM71 were down regulated. The cytokines CXCL10 and CXCL11 are closely associated with inflammatory response (290). Gene expression between the two conditions with strontium (Media Sr and Disc Sr) and the two without strontium (Media and Disc) was also compared (Figure 66b), showing that there were no significant changes in gene expression, and the general fold change and significance of the change was observed to be far lower than that observed for the all Disc and all Media comparison.

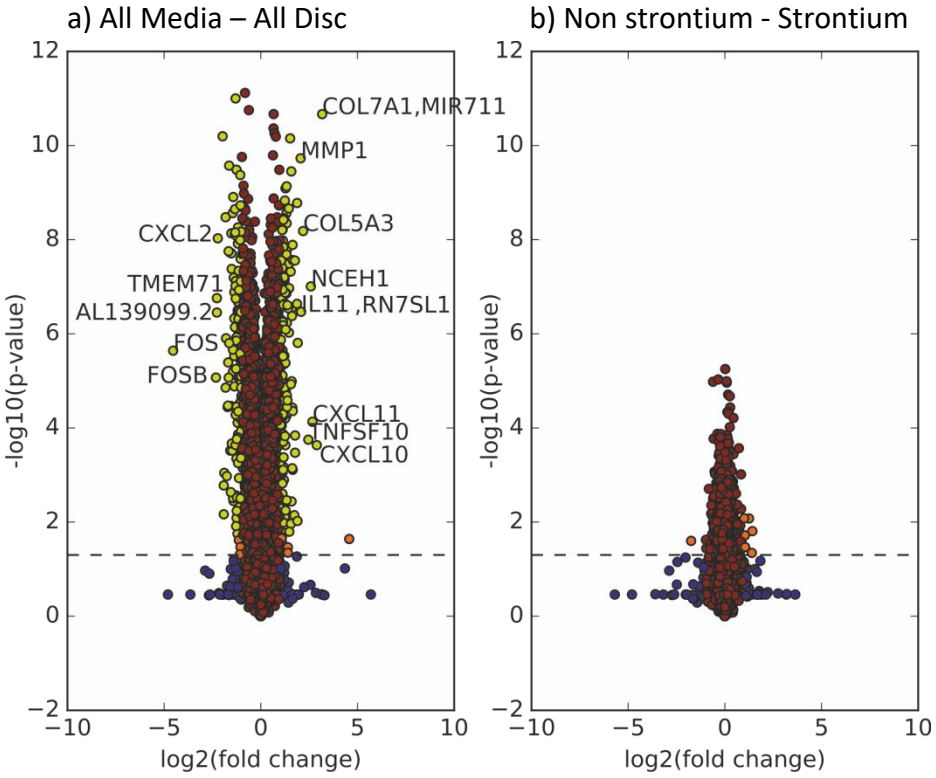


**Figure 66: Volcano plots of the different ANOVA comparisons between the RNAseq conditions, a) All media (Media and Media Sr) compared against all disc (Disc and Disc Sr), b) All non-strontium (Media and Disc) conditions against all strontium conditions (Media Sr and Disc Sr). They show the p-value of any significant different against the fold change (both logarithmed). The blue dots are large changes which are insignificant. The orange dots are large changes which are also significant. The yellow dots are large changes, which are also significant and pass the Bonferroni correction.**

,

### 4.3.2 Gene-set Enrichment

The gene expression data for all of the conditions were enriched against the Hallmark genesets to produce GSZ scores, and then sorted as a dendrogram to produce a heat-map of the enrichment of the these genesets, which can be seen in Figure 67. The most enriched and strongly contrasting genesets are found at the bottom of the figure, and these relate to inflammatory signalling (interferon alpha and gamma response) and epithelial to mesenchymal transition (EMT), which were found to be more enriched in the Disc and Disc Sr conditions, and less enriched in the Media and Media Sr conditions. Other inflammatory genesets also showed altered enrichment in the disc conditions, with TNFα being less enriched between Disc and Media, but others such as “inflammatory response”, “allograft rejection” and “TGF beta signalling” showing increased enrichment between Disc and Media conditions. However, the addition of strontium was seen to increase the enrichment of these genesets for Disc Sr, but lower it for Media Sr, indicating the addition of strontium to the discs and glass conditioned media had differential effects upon the gene expression of the MSCs (Figure 67). Complement, also associated with inflammation was found to be enriched with the addition of strontium, in both Media Sr and Disc Sr, compared with the non-strontium conditions.

There were also seen to be differences in the enrichment of several genesets associated with proliferation and survival, with DNA Repair, MYC targets, and K-Ras Signalling showing increased enrichment, and P53 (which is pro-apoptotic) and MTORC signalling showing decreased enrichment, in the Disc condition, compared with the Media condition. The addition of strontium was seen to increase enrichment of DNA Repair and MYC Targets in Media Sr and lower enrichment in Disc Sr, again suggesting the addition of strontium has differential effects depending on whether it is to the discs or the glass conditioned media (Figure 67).

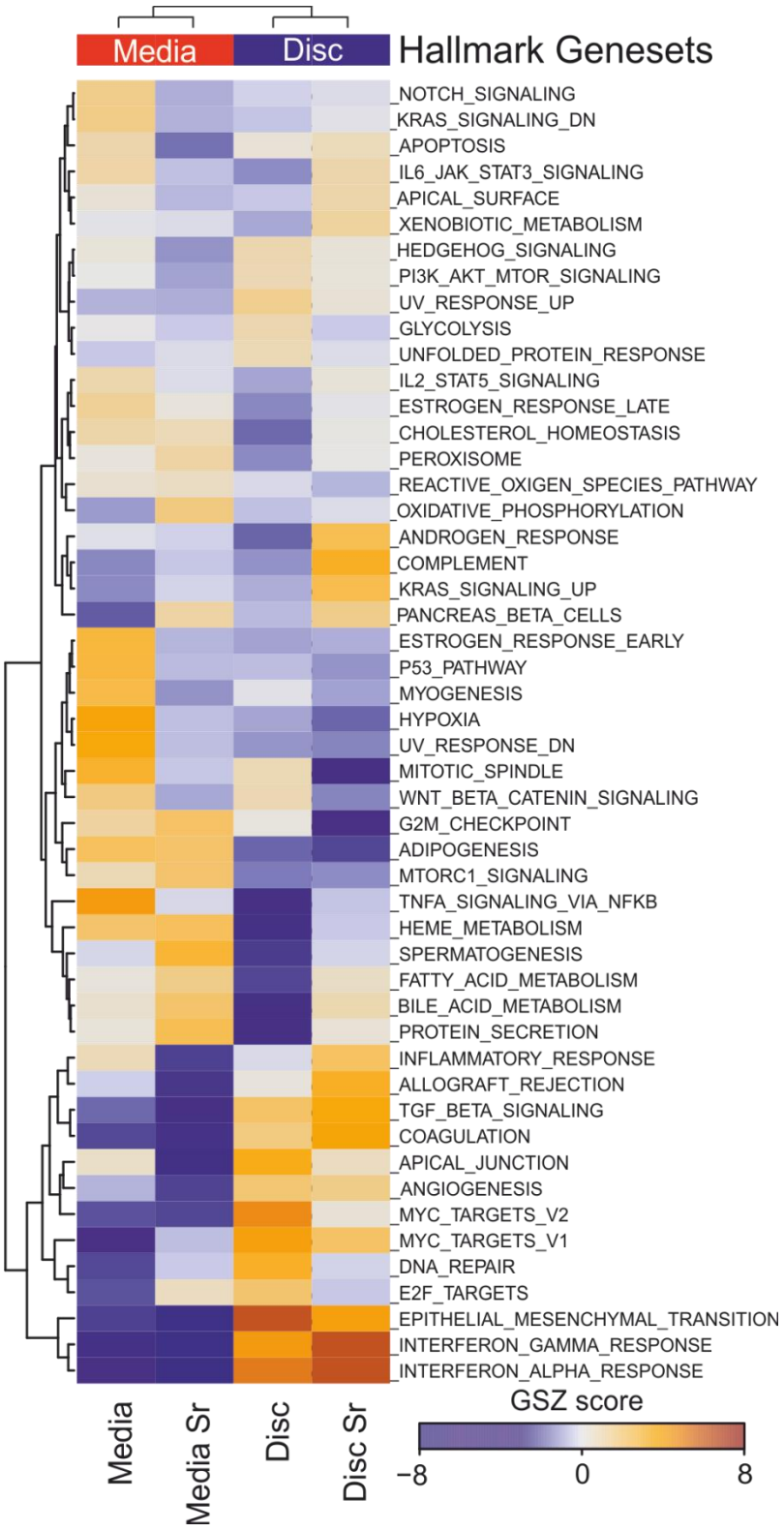


**Figure 67: The hallmark geneset enrichment across all genes from Y201 MSCs exposed to glass media with and without strontium (AW and SrAW respectivelt) and grown on glass ceramic discs with and without strontium (AWGC and SrAWGC). The GSZ scores indicate the enrichment of each geneset. The genesets and conditions have also been sorted using dendrograms by similarity.**

The inflammatory genesets in Figure 67 were then examined more closely, and the way in which the genes composing the genesets changed between the conditions was determined. The Interferon (IFN) Alpha and Gamma response genesets showed a clear upregulation in genes associated with these processes between the disc and media conditions, with CXCL10, CXCL11 and TNFSF10 being the most increased (Figure 68). The TGF Beta signalling showed a similar pattern with a strong difference in enrichment between the disc and media conditions, with the SERPINE1 gene being the most upregulated in the Disc condition and CDH1 in Disc Sr. The difference in gene expression between the strontium and non-strontium conditions was much smaller than that observed between the disc and media conditions for these three genesets. Although a large number of genes showed a slight increase between the Disc and Disc Sr condition. The CXCL10, CXCL11 and TNFSF10 genes showed a much greater difference between these two conditions in the IFN genesets, and the SERPINE1 and CDH1 genes for the TGF Beta signalling and were mostly likely the primary contributors to the higher GSZ score for the Disc Sr condition compared to the Disc condition (Figure 68). The enrichment of the IFN and TGF Beta genesets was observed to lower between the Media and Media Sr genesets, with ITGB7 (IFN gamma) and THBS1 (TGF Beta) genes d the most, thus adding strontium to the glass conditioned media lowered inflammatory gene expression.

Hence, the discs themselves were seen to raise the expression of a number of genes associated with IFN response and also Allograft rejection, whilst the addition of strontium to the discs further raised the expression of CXCL10, CXCL11, and TNFS10, in particular, strengthening the inflammatory response. However, the addition of strontium to the glass conditioned media was seen to have the opposite effect, lowering the over-all enrichment of the IFN and TGF Beta genesets.

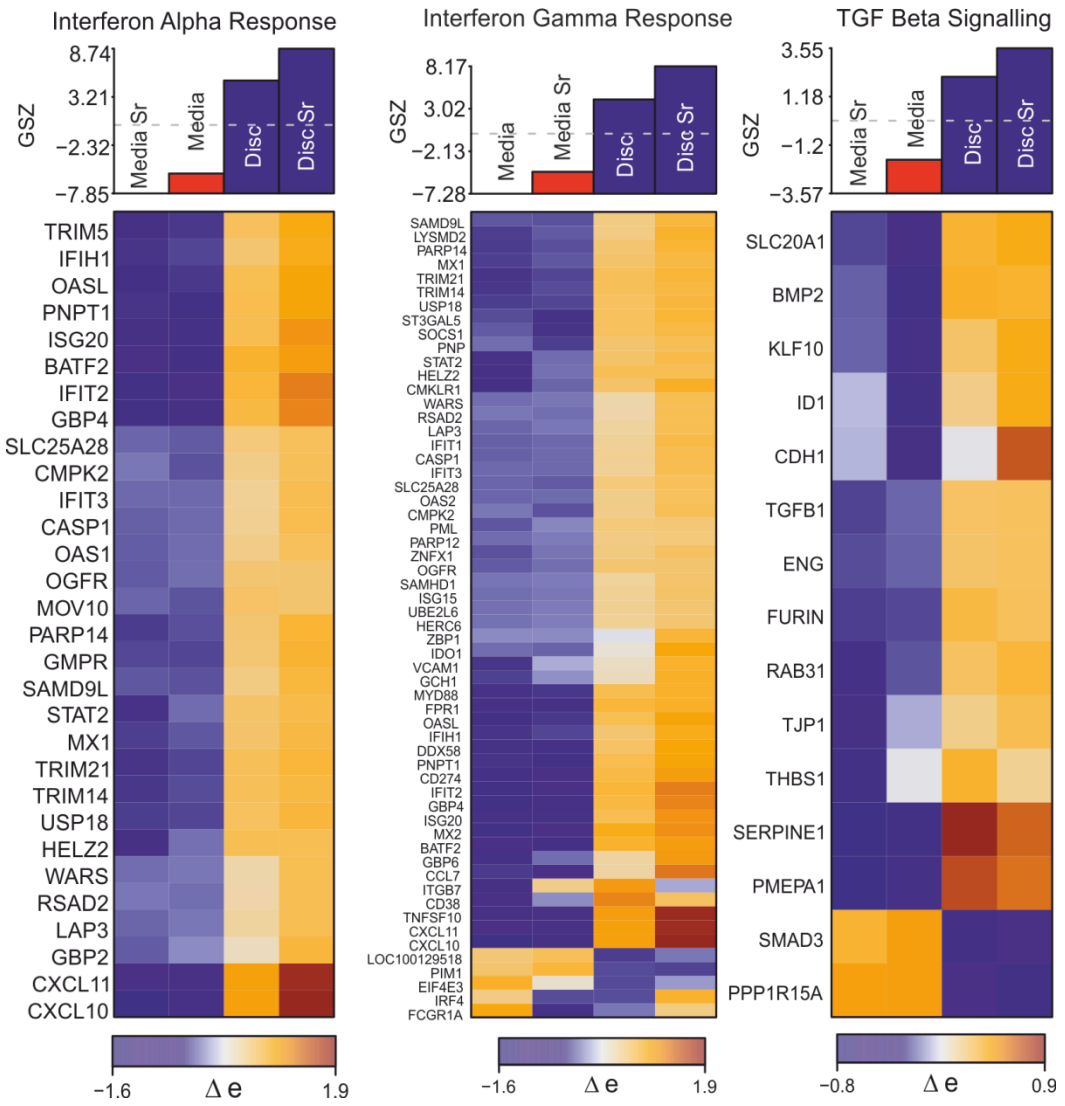


**Figure 68: The GSZ scores, component genes and relative expression of the Interferon Alpha and Gamma response and TGF Beta signalling genesets identified within spots in the Hallmark Geneset enrichment. The GSZ scores indicate how enriched that geneset is for each condition in the RNAseq. Media and Media Sr being non-strontium and strontium glass powder media, whilst Disc and Disc Sr are non-strontium and strontium AWGC discs.**

Figure 69 shows the GSZ scores of more inflammatory genesets found to have been enriched on the conditions. The inflammatory response geneset covered genes associated more broadly with inflammation in response to stimulus and showed low enrichment, along with allograft rejection, another inflammatory geneset, in the Disc and Media conditions (Figure 69). However, the addition of strontium to the discs resulted in increased enrichment for the Disc Sr condition, whilst the Media Sr condition showed decreased enrichment compared with the Media condition (Figure 69). The genes composing the “Inflammatory Response” geneset were observed to be both up and down regulated between the disc and media conditions, however as observed for the IFN genesets CXCL10, CXCL11, CCL7 and TNFSF10 all showed greatly increased expression in the disc conditions compared with the media conditions, and further raised expression in the Disc Sr condition compared with the Disc condition (Figure 69). The genes composing the Allograft response geneset were both up and down regulated between the disc and media conditions, however the much higher expression of the F2 and IL4 genes resulted in the Media and Disc conditions having raised GSZ scores compared with the Media Sr condition, and the raised CCL7 gene expression further increased the GSZ of the Disc Sr condition compared with the Disc condition (Figure 69).

Unlike the other inflammatory genesets, the TNF alpha signalling geneset showed a similar level of enrichment in the Disc Sr and Media Sr conditions, with the Media condition raising the enrichment, and the Disc condition lowering it, acting in the opposite manner to the other inflammatory genesets (Figure 69). Despite CXCL10 and CXCL11 showing high expression in the disc conditions, the strong rise in expression of FOS, along with FOSB and CXCL2 in the Media and Media Sr conditions, most likely contributed to their high GSZ score for TNF alpha signalling (Figure 69).

Hence, as with the IFN response genesets, the addition of strontium was seen to have differential effects, resulting in an increase in inflammatory genes in the discs (between Disc and Disc Sr), whilst it lowered the expression of inflammatory genes in the media (between Media and Media Sr) (Figure 69).

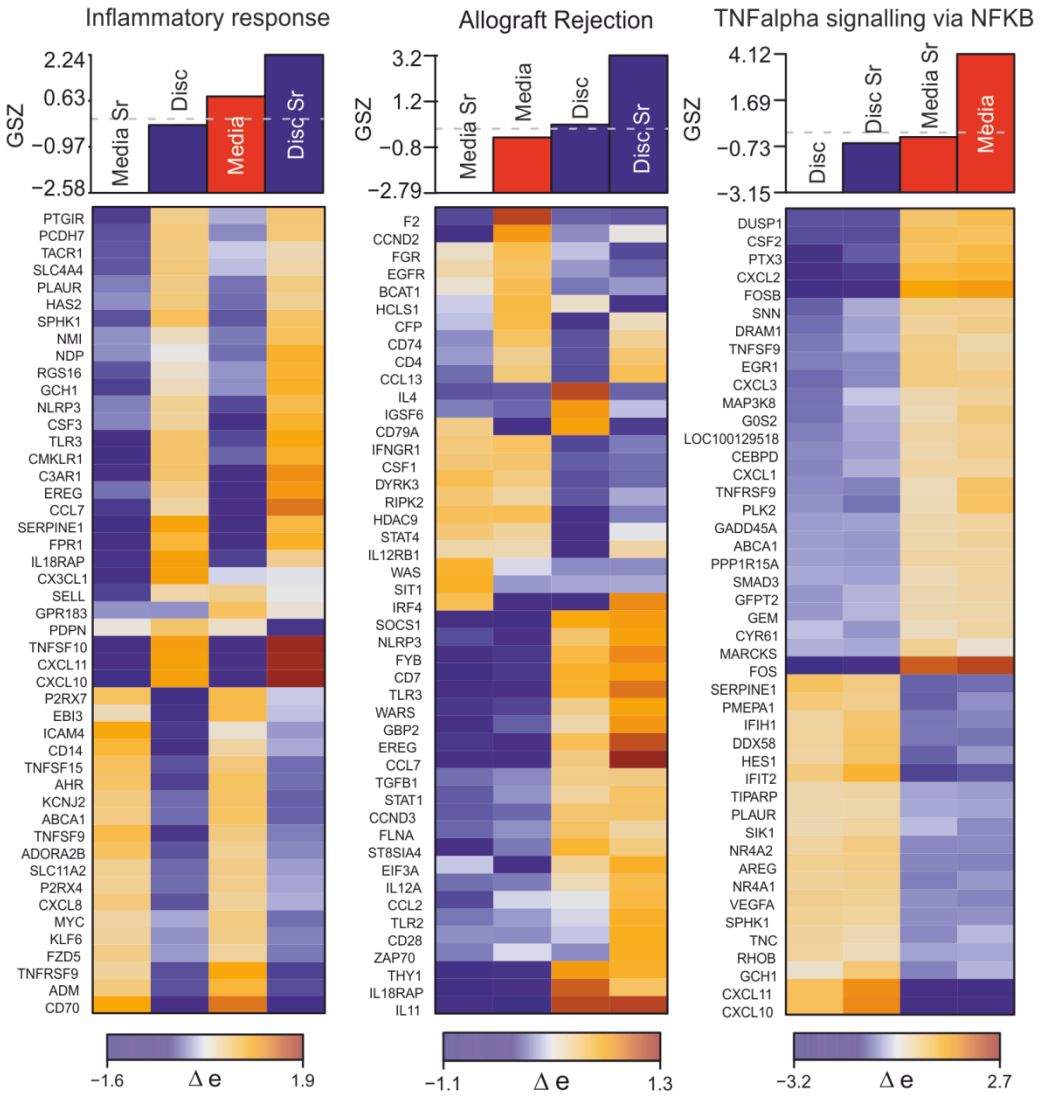


**Figure 69: The GSZ scores, component genes and relative expression of the TNFα signalling via NFkB, the inflammatory response and Allograft rejection genesets identified in the Hallmark Geneset enrichment. The GSZ scores indicate how enriched that geneset is for each condition in the RNAseq. Media and Media Sr being non-strontium and strontium glass powder media, whilst Disc and Disc Sr are non-strontium and strontium AWGC discs.**

In addition to inflammatory genesets, multiple proliferative/survival genesets showed changes between the conditions. The Epithelial to Mesenchymal Transition (EMT) geneset showed increased enrichment for the Disc and Disc Sr conditions, when compared with the Media and Media Sr conditions (Figure 70). However, the addition of Sr was seen to lower the enrichment of EMT in both the disc and media conditions. The expression of the genes in the EMT geneset were generally increased for the Disc and Disc Sr, with COL5A3 and MMP1 being particularly upregulated compared with Media and Media Sr. COL5A3 was more highly expressed in the Disc Sr condition and further lowered in the Media Sr condition (Figure 70). Generally, the differences in EMT gene expression induced by the addition of strontium were much less than between the disc and media conditions. Together, this indicates that the SrAWGC discs raised the expression of genes associated with EMT in the MSCs, with the substitution of strontium into the material acting to inhibit this effect.

The P53 pathway (potentially associated with cell apoptosis) was seen to have increased enrichment only in the Media condition, most likely associated with the high FOS gene expression for Media, compared with Media Sr and disc conditions (Figure 70). The apoptosis geneset showed a similar response, with the Media condition showing increased enrichment over the Media Sr condition. However, unlike for the P53 pathway geneset, the enrichment of Disc and Disc Sr was at a similar level to the Media condition (Figure 70). The high enrichment of the Media condition occurred, despite the low TNFSF10 gene expression, potentially due to a slightly higher expression of a number of genes, with F2 being amongst the most changed between the Media and Media Sr conditions (Figure 70).

Together these results indicated that the addition of Sr to the media lowered expression of these potentially apoptotic pathways, but that Sr had no effect on the expression of these apoptotic genesets for the disc conditions.

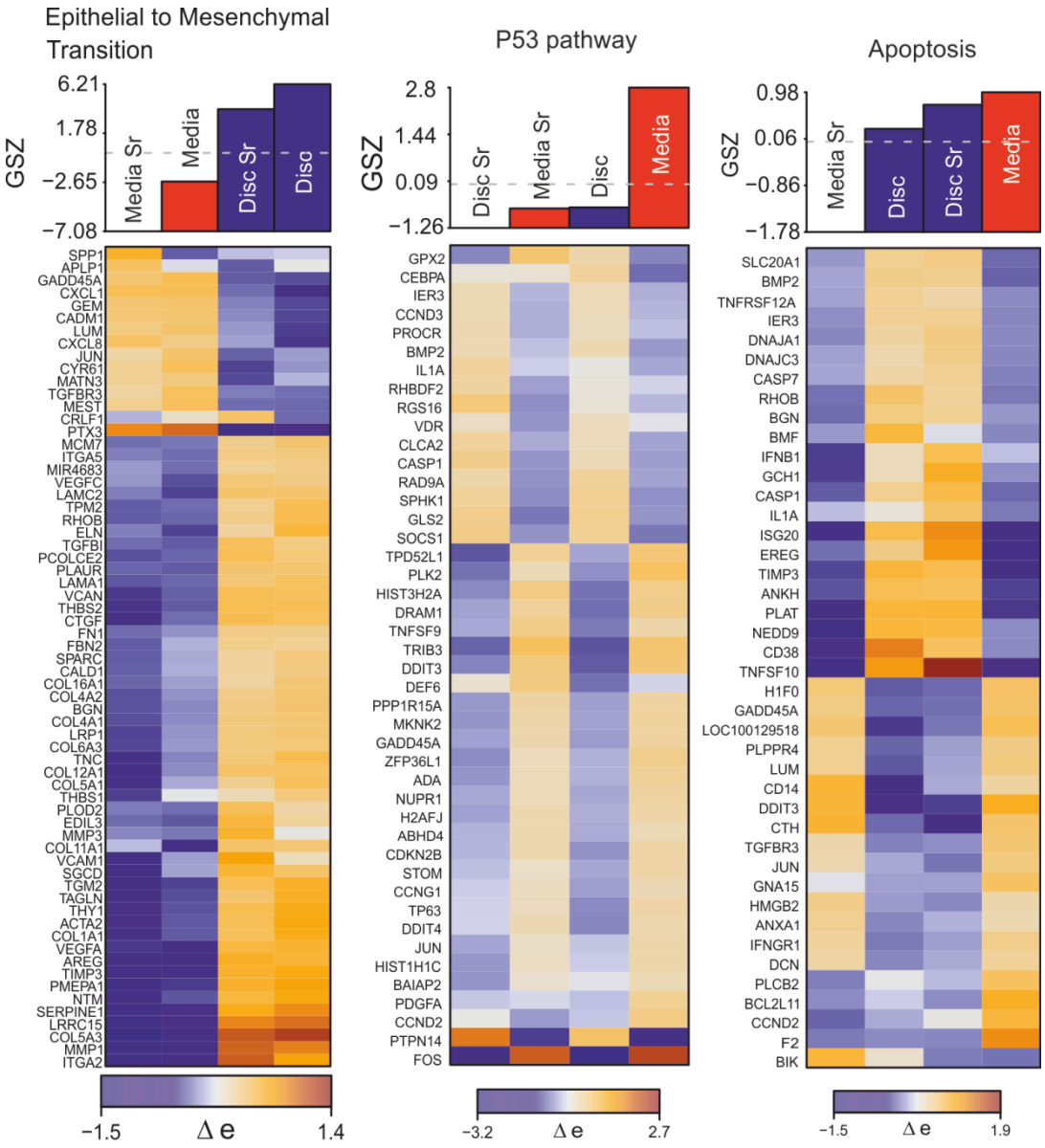


**Figure 70: The GSZ scores, component genes and relative expression of the epithelial to mesenchymal transition, P53 pathway and apoptosis genesets identified within spots in the Hallmark Geneset enrichment. The GSZ scores indicate how enriched that geneset is for each condition in the RNAseq. Media and Media Sr being non-strontium and strontium glass powder media, whilst Disc and Disc Sr are non-strontium and strontium AWGC discs.**

In addition to EMT, P53 and apoptosis genesets, more proliferative and survival genesets were found to differ in enrichment levels between the conditions and these are displayed in Figure 71. Two of these concerned K-Ras signalling, which is associated with MAPK signalling and proliferation. “K-Ras Signalling Down” contained genes downregulated by K-Ras signalling, and only the Media condition showed a high GSZ score (Figure 71). This indicated that the other conditions had reduced expression of these K-Ras genes over-all compared to the media condition, meaning increased K-Ras signalling in the strontium and Disc conditions, compared with the Media condition. “K-Ras Signalling Up” contained genes which were upregulated by K-Ras signalling and increased with strontium addition, as the strontium conditions (Media Sr and Disc Sr) had a higher GSZ score than the Media and Disc conditions (Figure 71). However, the increase was much larger for the Disc Sr condition, associated with the high CXCL10 expression in Disc Sr. These results indicate that the discs themselves and strontium were associated with K-Ras signalling, and the combination of the two resulted in further K-Ras gene expression.

In addition to K-Ras signalling, MTORC1 signalling (an element of Akt signalling and hence potentially proliferative) was identified in the Hallmark geneset expression analysis as changing between the conditions. When the genes composing the geneset were analysed it was found to be strongly reduced in the Disc and Disc Sr conditions with TRIB3, PLK1 and DDIT3 genes being those with the largest difference (Figure 71). The addition of strontium was found to increase the GSZ score of MTORC1 signalling for Media Sr.

Together, these results suggest that Sr addition to the material was seen to promote the expression of proliferative and survival genesets.

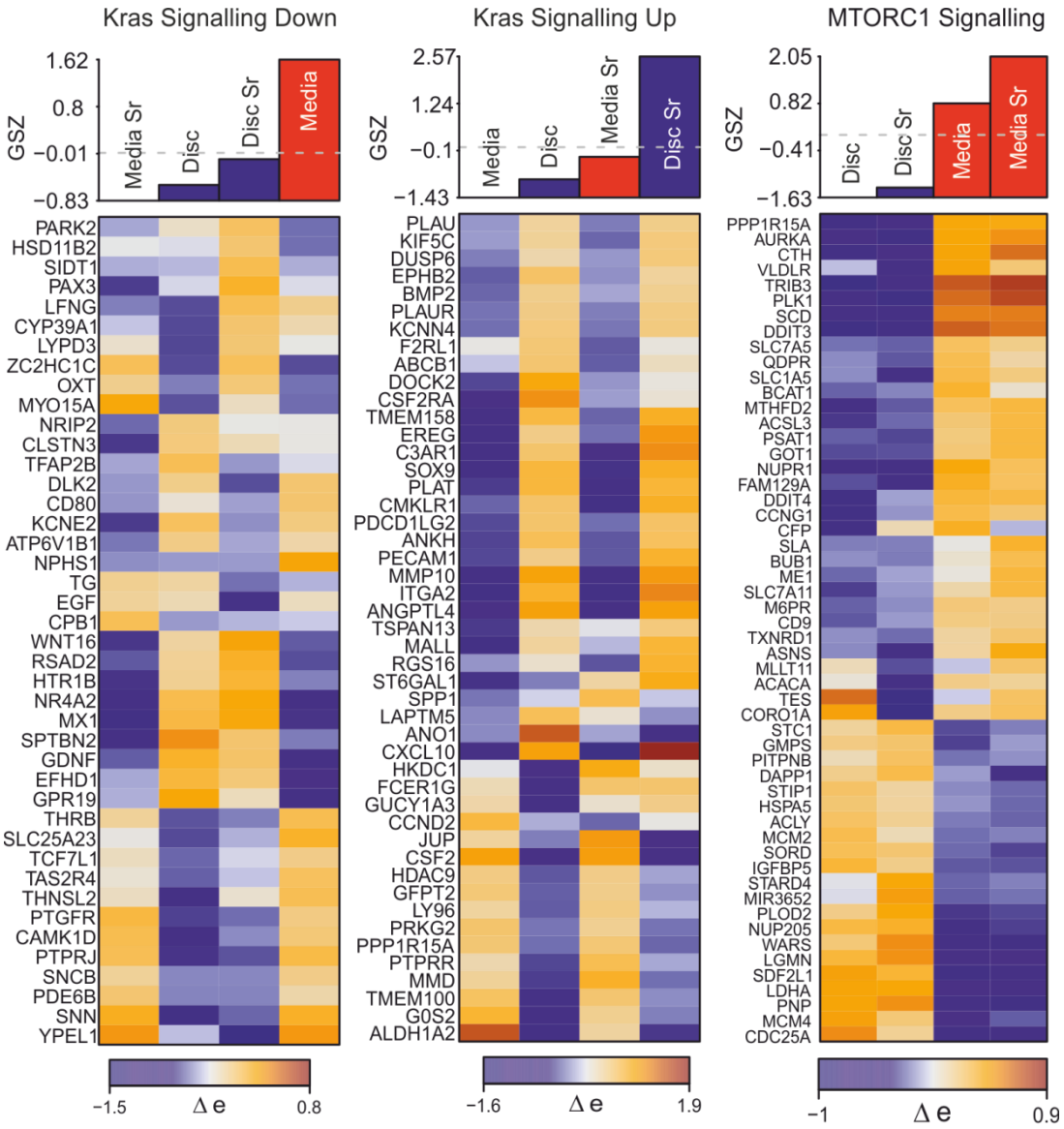


**Figure 71: The GSZ scores, component genes and relative expression of the K-Ras Signalling and MTORC1 signalling genesets identified within spots in the Hallmark Geneset enrichment. The GSZ scores indicate how enriched that geneset is for each condition in the RNAseq. Media and Media Sr being non-strontium and strontium glass powder media, whilst Disc and Disc Sr are non-strontium and strontium AWGC discs.**

Hence, the RNA sequencing found that the largest change in gene expression was associated with the difference between the glass conditioned media (Media and Media Sr conditions) and the glass-ceramic discs (Disc and Disc Sr conditions), where the discs were found to raise the expression of a number of genes associated with inflammatory response, IFN response and TGFβ signalling. The addition of strontium to the discs was seen to further enhance these inflammatory responses. A number of proliferative/survival genesets also showed altered gene expression for the disc conditions compared with the media conditions, such as K-Ras signalling and MTORC1 (both associated with MAPK signalling), in addition to P53 and Epithelial to Mesenchymal Transition..

### 4.3.3 Type 1 Interferon PCR array to determine effects of SrAWGC and SrAW glass on MSC cytokine gene expression

A PCR array was used to independently validate the findings of the RNAseq by measuring how a panel of inflammatory genes responded to the Media, Media Sr, Disc and Disc Sr conditions, and so to determine whether the discs themselves and, or, the strontium content of the discs or the glass conditioned media could alter the expression of genes associated with inflammation.

The PCR array found that there were a number of genes differing in expression between the glass conditioned media and disc conditions without strontium (Media and Disc conditions, Figure 72). Most of the genes composing the array were found to be upregulated in the Disc condition, compared with the Media condition, with the CXCL10 and TNFSF10 showing the greatest increase, independently confirming the findings of the RNA sequencing. Although the majority were upregulated, the CD70 gene was down regulated in the Disc condition. This again suggests that the discs themselves, without strontium, raise the expression of inflammatory genes compared with the ions released by the material.

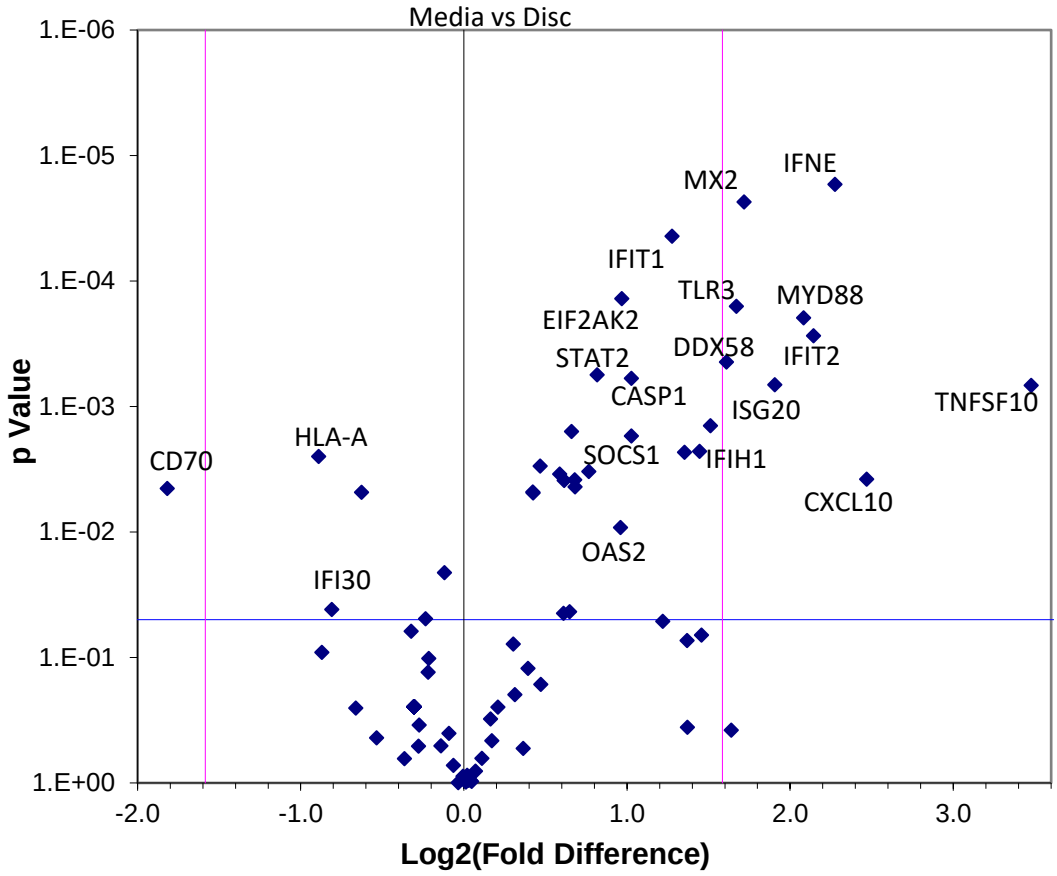


**Figure 72: A volcano plot of the t-test comparison between the PCR array conditions without Sr (Media against Disc). They show the p-value of any significant different against the fold change (both as $log_2$ values). The lines indicate the fold difference threshold.**

When strontium was added to the media and discs, the PCR array showed the MSCs responded in largely the same manner to the Disc and Media without Sr, with the majority of the Type 1 interferon genes being upregulated when comparing between the Media Sr and Disc Sr genesets (Figure 73). The Disc Sr condition upregulated those inflammatory genes more when compared with Media Sr, than the Disc condition did when compared with the Media condition (again, TNFSF10 and CXCL10 were the most affected) suggesting the addition of strontium exacerbated whatever feature or process was responsible. There were more genes generally down regulated between the Disc Sr and Media Sr conditions, when compared with the Disc and Media conditions, though the fold change and significance were not as high, in particular for CD70.

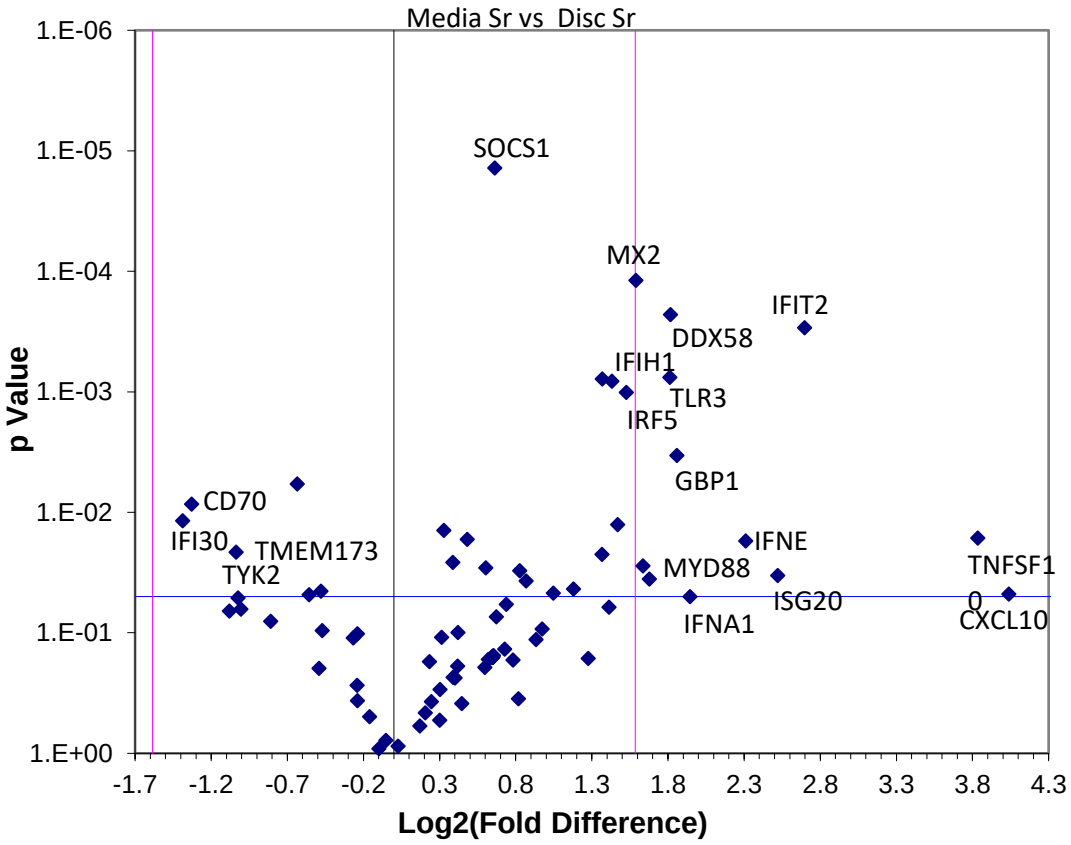


**Figure 73: A volcano plot of the t-test comparison between the PCR array conditions with Sr (Media Sr against Disc Sr). They show the p-value of any significant different against the fold change (both as $log_2$ values). The lines indicate the fold difference threshold.**

Again, these data independently confirm the findings of the RNA sequencing, which found that for the inflammatory genesets (such as IFN signalling, TGFβ and inflammatory response) the addition of strontium to the discs and media further increased and decreased inflammatory geneset enrichment, respectively.

The previous two figures have compared only the non-strontium (Disc and Media) and the strontium (Disc Sr and Media Sr) condition groups, however Figure 74 shows the change in gene expression across all of the disc and media conditions, regardless of strontium content. Once again, this shows that the majority of the genes in the Type 1 Interferon array were upregulated by the disc conditions in comparison with the media conditions, across the conditions with and without strontium content, and clearly agrees

with the previous analyses of the Disc-Media, and Disc Sr-Media Sr comparisons. Some genes were down regulated in the disc conditions compared with media (with CD70 being the most changed). Again, and independently verifying the RNA sequencing result, it was found that the TNFS10 and CXCL10 genes were the most upregulated by the disc conditions. As this analysis was aggregated over more results (both the strontium and non-strontium conditions), this improved the significance of the gene expression changes in comparison to the disc-media strontium and non-strontium comparisons presented earlier.

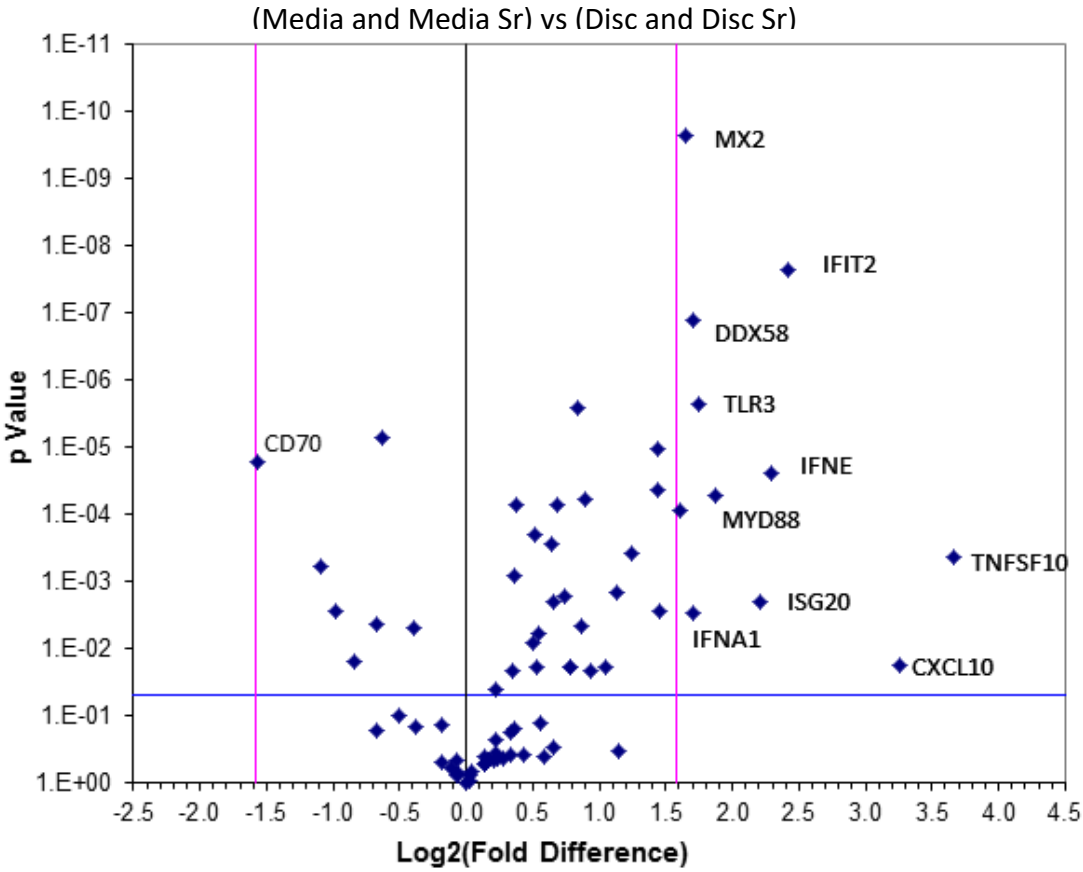


**Figure 74: A volcano plot of the t-test comparison between the PCR array between the disc (Disc and Disc Sr) and media (Media and Media Sr) conditions, across strontium content. They show the p-value of any significant different against the fold change (both as $log_2$ values). The lines indicate the fold difference threshold.**

The difference in gene expression between the strontium and non-strontium conditions was also analysed, to determine what effect adding strontium to the material would have on MSC gene expression, and to confirm the findings of the RNA sequencing. The Disc Sr condition was seen to induce a relatively large, but an insignificant increase in some of the inflammatory genes, with CXCL10 again being amongst the most highly changed (Figure 75). However, the addition of strontium to the discs was also seen to produce a significant but relatively small decrease in the expression of a number of genes, with TYK2 being the most decreased. Hence, in addition to the discs themselves altering the expression of inflammatory genes in the MSCs, the addition of strontium to the discs has a small effect on these genes, partially confirming some of the RNA sequencing findings.

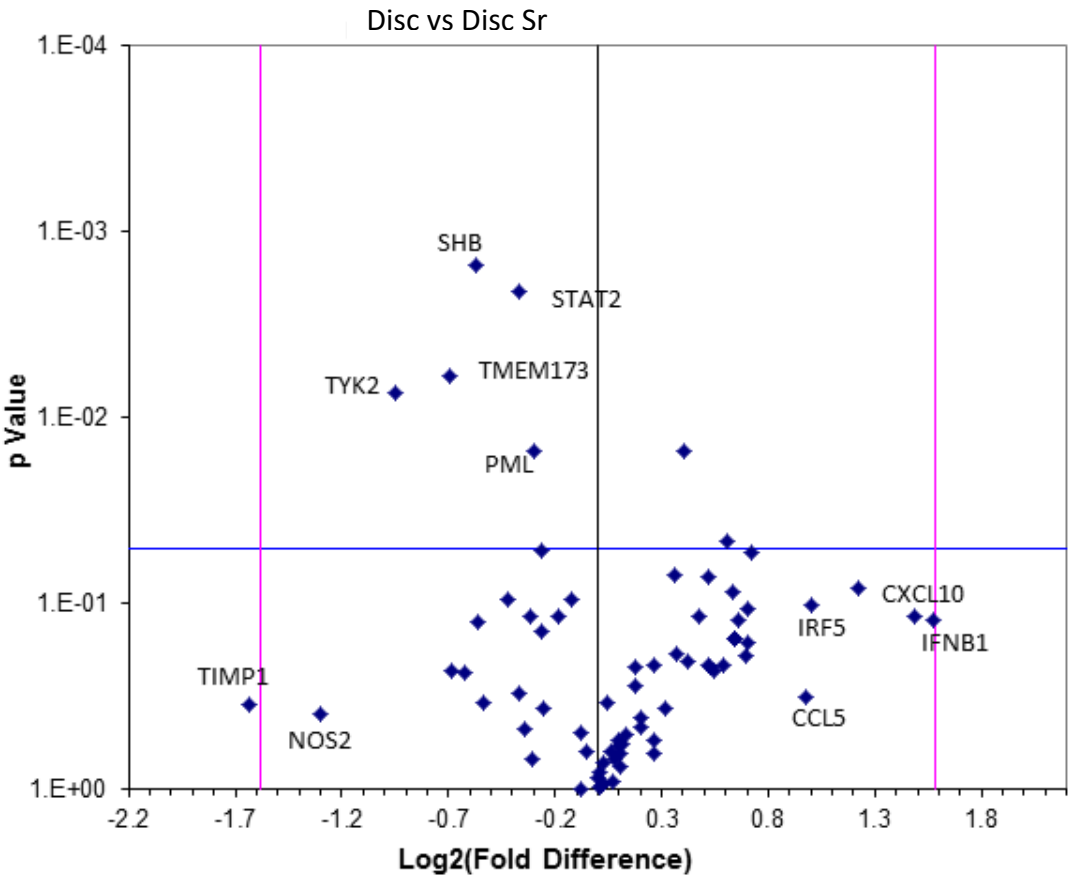


**Figure 75: A volcano plot of the t-test comparison between the PCR array disc conditions (Disc Sr and Disc). They show the p-value of any significant different against the fold change (both as $log_2$ values). The lines indicate the fold difference threshold.**

When the difference in gene expression between the media conditions with and without strontium (Media and Media Sr) was analysed, it was found that there were few significant changes, with TICAM1 showing a 0.5 fold increase, whilst TAP1 showed a 0.4 fold decrease (Figure 76). The size and significance of the gene expression changes between the Media and Media Sr conditions was lower than observed for the Disc and Disc Sr conditions, and considerably lower when comparing between the Media and Disc conditions. This indicates that the influence of Sr addition to the ions released from the AWGC glass was relatively small in comparison to that of the disc itself. This again, independently confirms the RNA sequencing findings where it was found that the differences between the Media and Media Sr conditions were not as pronounced as between the media and disc, or Disc and Disc Sr conditions.

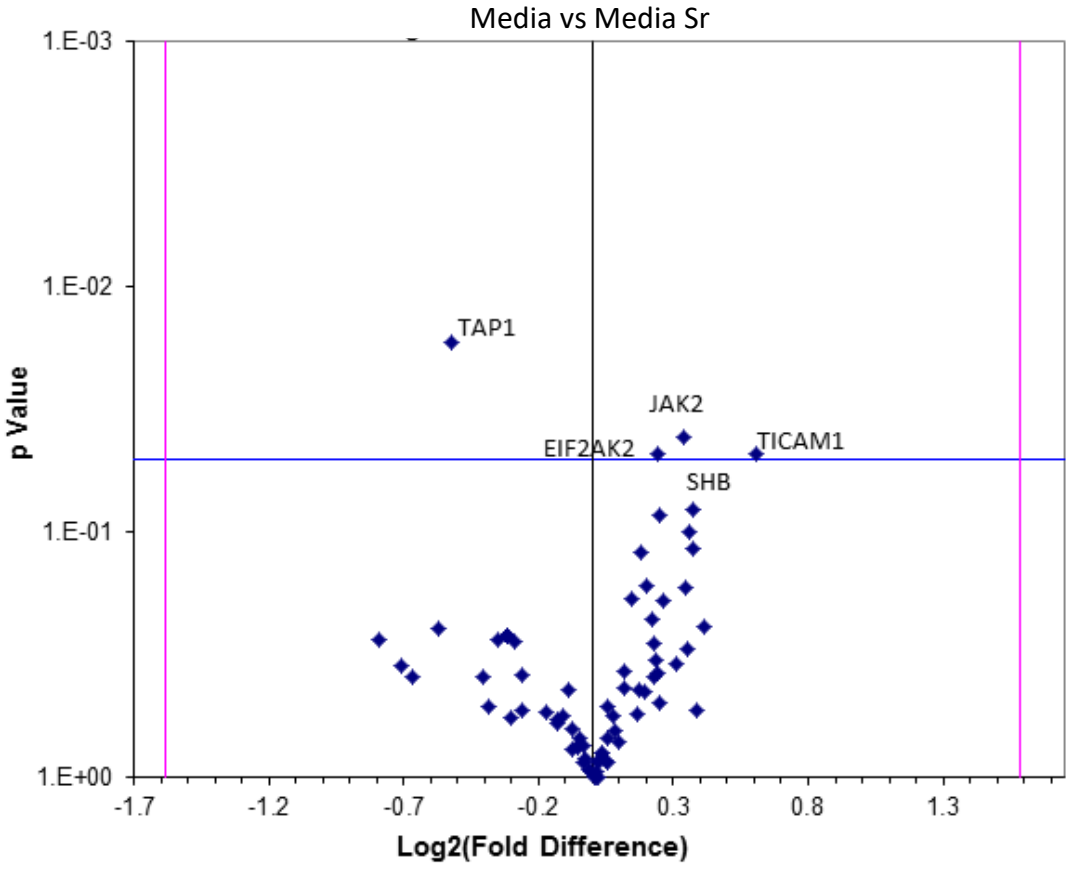


**Figure 76: A volcano plot of the t-test comparison between the PCR array glass media conditions (Media Sr and Media). They show the p-value of any significant different against the fold change (both as $log_2$ values). The lines indicate the fold difference threshold.**

Finally, as with the disc-media comparison, the gene expression change between all of the strontium conditions (Disc Sr and Media Sr) and all of the non-strontium conditions (Disc and Media) was calculated, to determine what gene expression changes induced by the addition of strontium were common between the discs and media. The strontium induced Type 1 interferon gene expression changes across both disc and media conditions can be seen in (Figure 77). As with the gene expression changes induced by the addition of strontium to the discs, and glass conditioned media, it shows that although the tendency was for the genes to be upregulated, the changes were both of low significance and of low fold changed.

The Type 1 interferon PCR array was used to independently validate the RNA sequencing finding that the MSCs showed increased inflammatory gene expression on the discs (both the Disc and Disc Sr condition), when compared with the cells being exposed to the glass conditioned media (the Media and Media Sr condition). The PCR array confirmed this, and confirmed that CXCL10 and TNFS10 were associated with this response. The PCR also confirmed that the addition of strontium to the SrAW glass conditioned media, and hence potentially to the ion release products of the SrAWGC material itself, had little effect on the inflammatory genes in this PCR array. Finally, it was also confirmed that the addition of strontium to the discs, did appear to enhance the inflammatory gene expression induced by the discs themselves.

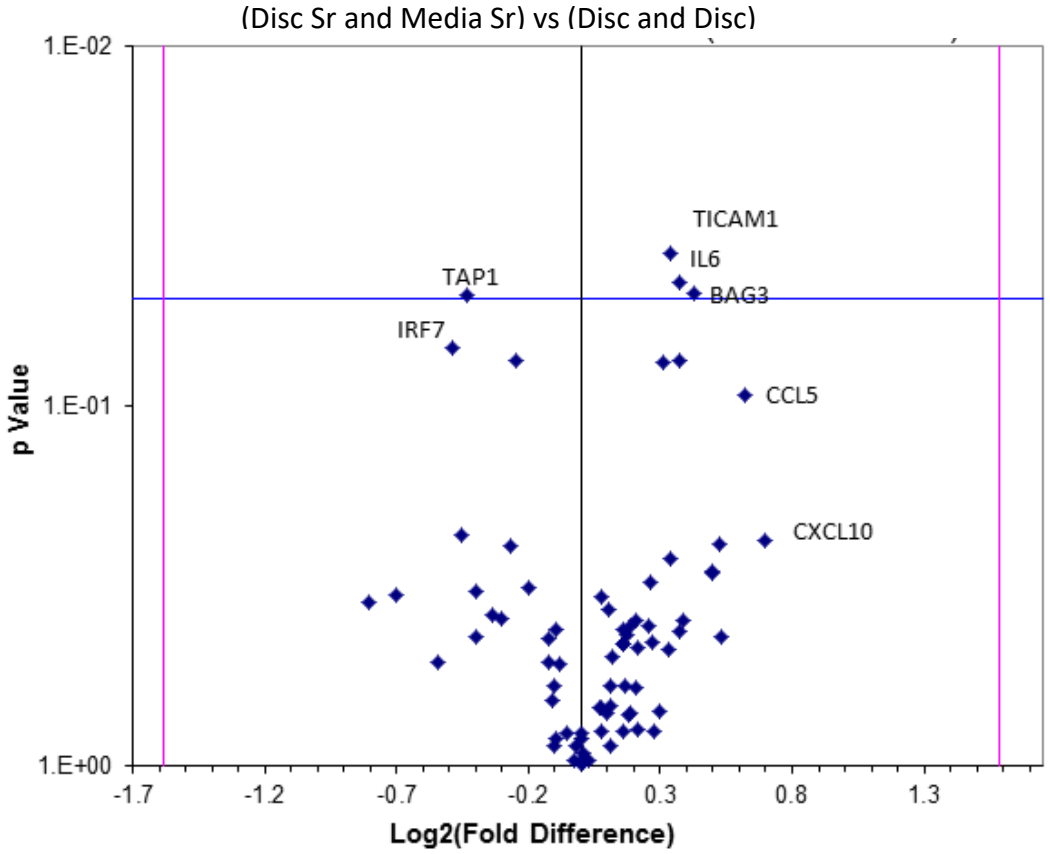


**Figure 77: A volcano plot of the t-test comparison between the PCR array aggregates of the strontium and non-strontium conditions (Media and Disc against Media Sr and Disc Sr). They show the p-value of any significant different against the fold change (both as $log_2$ values). The lines indicate the fold difference threshold.**

### 4.3.4 Determining the mechanism behind MSC response to SrAW glass

Previously discussed results indicated that SrAWGC increased cell number, and that the discs and the addition of strontium to the discs increased the expression of a number of inflammatory genes. Inhibitors was used to explore the role of intracellular signalling pathways in the increased cell number response and whether this was associated with the inflammatory cytokine gene expression.

The role of PI3K/Akt signalling in the cell number response to the SrAW glass was explored as there is evidence to suggest this is a mechanism by which Sr affects MSCs (124). As PI3K/Akt signalling can act via different

paths, multiple inhibitors were used to explore these different mechanisms. To explore potential Src (which can be activated downstream of cytokine receptors (286,287)) mediated strontium response, the cells were exposed to the Src inhibitor Dasatinib in addition to the SrAW glass conditioned media with 0 and 12.5 Mol% Sr (corresponding with the Media and Media Sr conditions in the RNAseq). The addition of Dasatinib to glass conditioned mineralisation media did not abrogate the cell number increase induced by strontium (Figure 78). PI3K/Akt signalling could also have been associated with JAK (which can be activated downstream from cytokine receptors), and so the JAK inhibitor Ruxolitinib was used to determine its effect on the strontium response. The MSCs were exposed to the SrAW glass conditioned media with 0 and 12.5 Mol% Sr (Media and Media Sr in the RNAseq) with increasing concentrations of Ruxolitinib. The addition of Ruxolitinib was seen to increase the strontium induced DNA increase for glass conditioned mineralisation media, with the 0 Mol% condition showing no decrease.

These results suggest that if the PI3K/Akt signalling pathway plays a role in the strontium response of the MSCs, then it does not act via the cytokine associated Src and JAK mediated pathways (Figure 79).

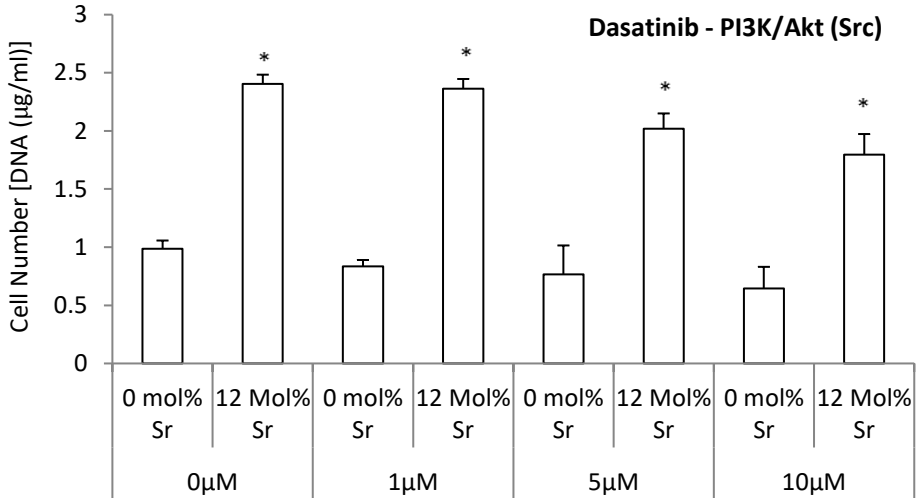


**Figure 78: The cell number (measured using DNA) of Y201 hTERT MSCs after 9 days of exposure to 0 and 12.5 Mol% Sr glass conditioned mineralisation media with 0, 1 and 5 and 10µM Dasatinib (Src inhibitor). Values are means with error bars signifying the standard deviation, of six measurements. * indicates significant difference between the 0 and 12.5 Mol% conditions for that concentration of inhibitor (p-value <0.05).**

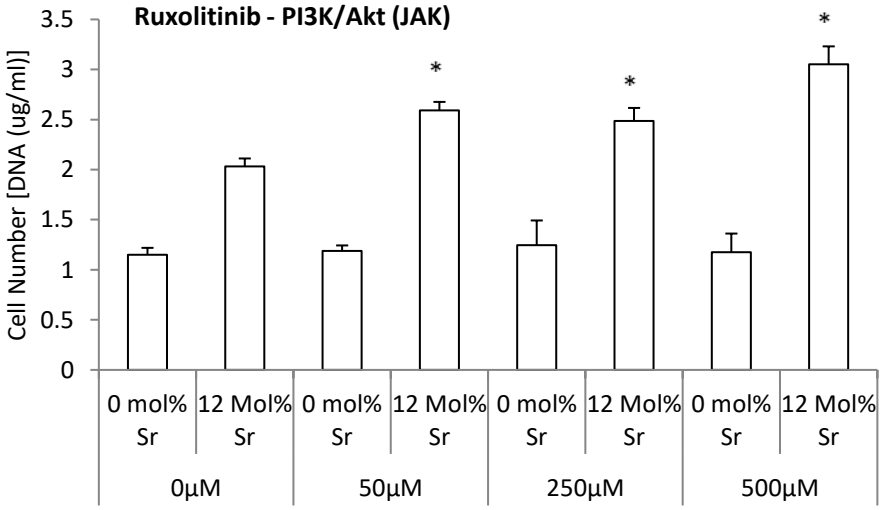


**Figure 79: The cell number (measured using DNA) of Y201 hTERT MSCs after 9 days of exposure to 0 and 12.5 Mol% Sr glass conditioned mineralisation media with 0, 50 and 250 and 500nM Ruxolitinib (JAK inhibitor). Values are means with error bars signifying the standard deviation, of six measurements. * indicates significant difference between the 0 and 12.5 Mol% conditions for that concentration of inhibitor (p-value < 0.05).**

The RNAseq data indicated that K-Ras was upregulated in response to the glass conditioned media and strontium conditions more generally. To explore any potential role of K-Ras mediated signalling on the cell number response to the SrAW glass, the cells were exposed to the Ras inhibitor Salirasib in addition to the SrAW glass conditioned media with 0 and 12.5 Mol% Sr (corresponding with the Media and Media Sr conditions in the RNAseq). The inhibitor Salirasib was seen to block the strontium-induced increase in cell number seen for cells grown with glass conditioned mineralisation media (Figure 80). As the Salirasib concentration in the glass conditioned mineralisation media is increased from 0 to 50μM, the DNA concentration of the strontium condition was decreased, and eventually reached a level below that of the control (non-strontium) condition. This indicates that Ras signalling (of which K-Ras is one mediator) plays a role in the cell number increase induced by the strontium containing AW glass dissolution products.

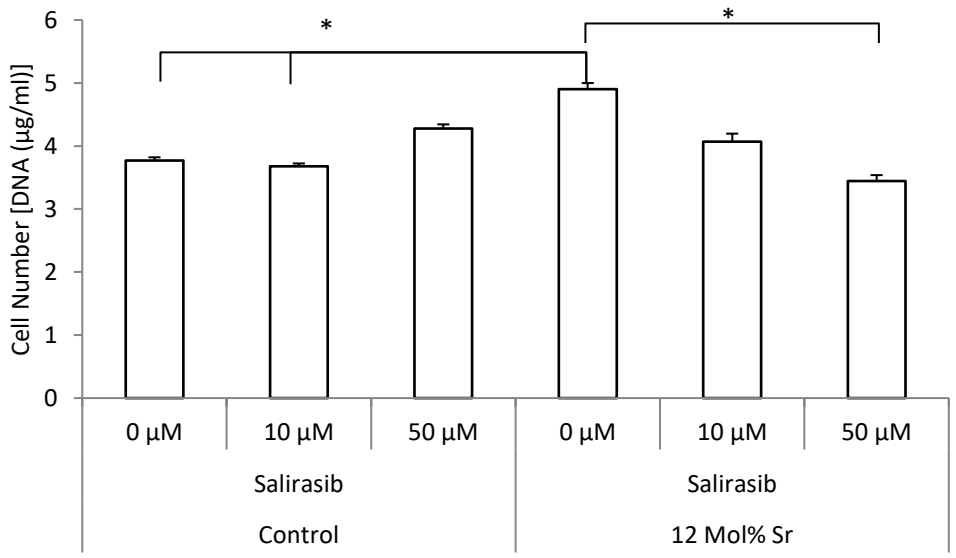


**Figure 80: The cell number (measured using DNA concentration) of Y201 hTERT MSCs after 9 days of exposure to 0 and 12.5 Mol% Sr glass conditioned mineralisation media with 0, 10 and 50μM Salirasib (K-Ras inhibitor). Values are means with error bars signifying the standard deviation, N=3. * indicates significant difference between the values a shown (p-value < 0.05).**

### 4.3.5 *In vivo* study to determine the extent of the inflammatory transformation of MSCs by SrAWGC and SrAW glass

#### 4.3.5.1 Implantation and extraction

Following from the gene expression work, and the finding that the discs (Disc and Disc Sr conditions compared with Media and Media Sr conditions) raised inflammatory gene expression in the MSCs, a rat model was used to determine whether this pro-inflammatory gene expression could have a functional influence on inflammatory function *in vivo*.

The Y201 hTERT MSCs were successfully conditioned in four different conditions (Disc, Disc Sr, Media, and Media Sr), extracted, mixed into collagen gels and these were all successfully injected into subcutaneous pockets whereupon they gelled *in situ*. All rats survived the study with no obvious signs of distress or discomfort. All wound sites remained closed, with none of them appearing infected or disturbed (Figure 81). At one day and three days, rats were sacrificed for each of the conditions, and the four gels and surrounding tissue were successfully extracted.

**Figure 81: One of the subject rats after termination. The implant sites are representative of the other subjects in the study. The experiment involved subcutaneous implantation of collagen gels containing MSCs conditioned by SrAW glass media and SrAWGC discs with and without Sr.**

The subcutaneous pockets for one day and three days can be seen in Figure 82 and Figure 83 (only two of the Disc condition images at one day are shown), respectively. The wound sites were noticeably more inflamed at one day compare to 3 days, after which the visible inflammation was reduced in every single condition, becoming more localised around the gel, in comparison to the more widespread inflammation observed a one day. The level of visible inflammation varied substantially between implantation sites (all four implantation sites for one condition, at one time point, were in a single animal).

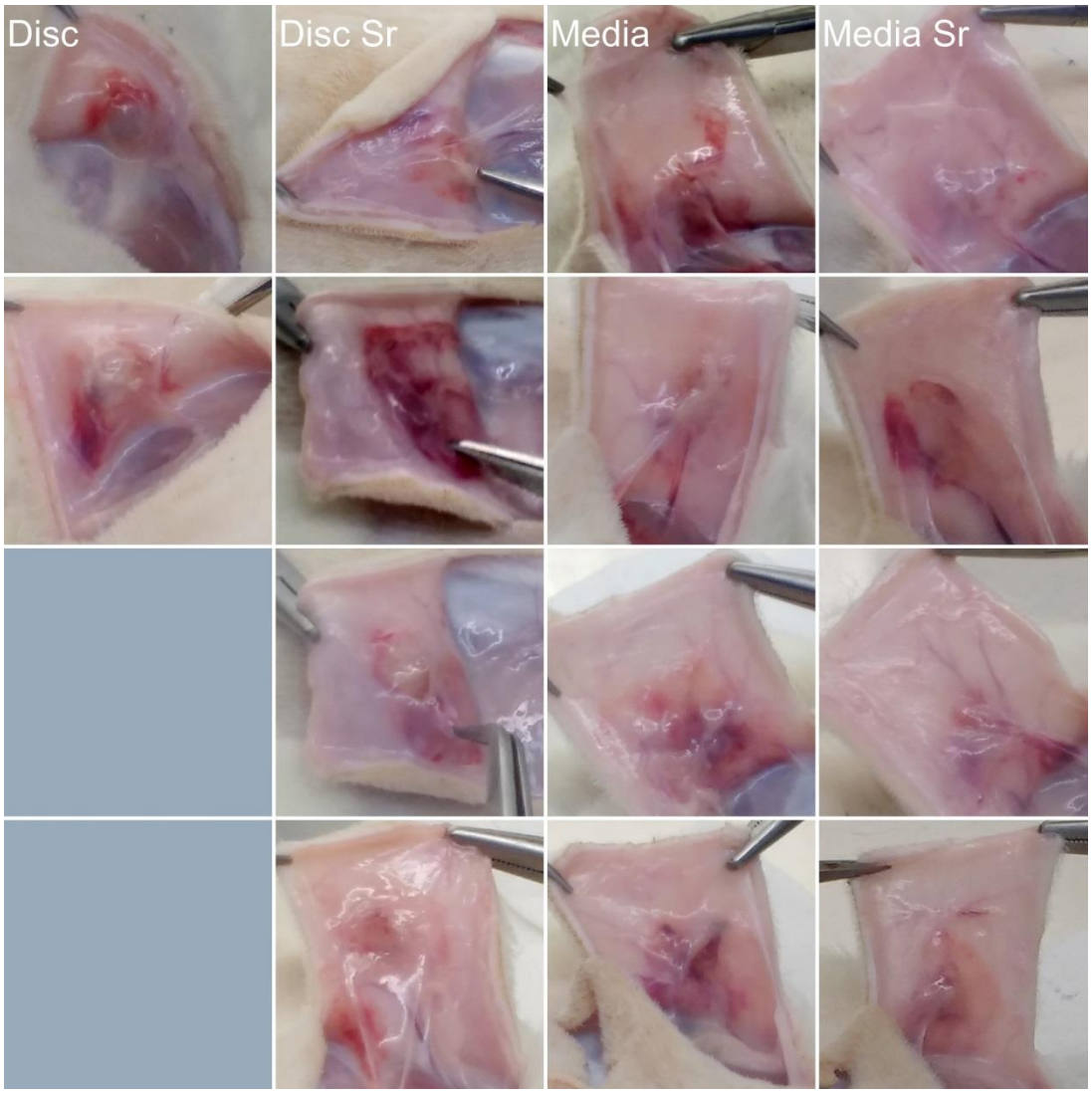


**Figure 82: Photographs after one day of the subcutaneous extraction site of the MSCs in collagen gels for each rat, which had been conditioned on glass ceramic discs (Disc and Disc Sr) or with glass conditioned media (Media and Media), both with either 0 or 12.5 Mol% Sr).**

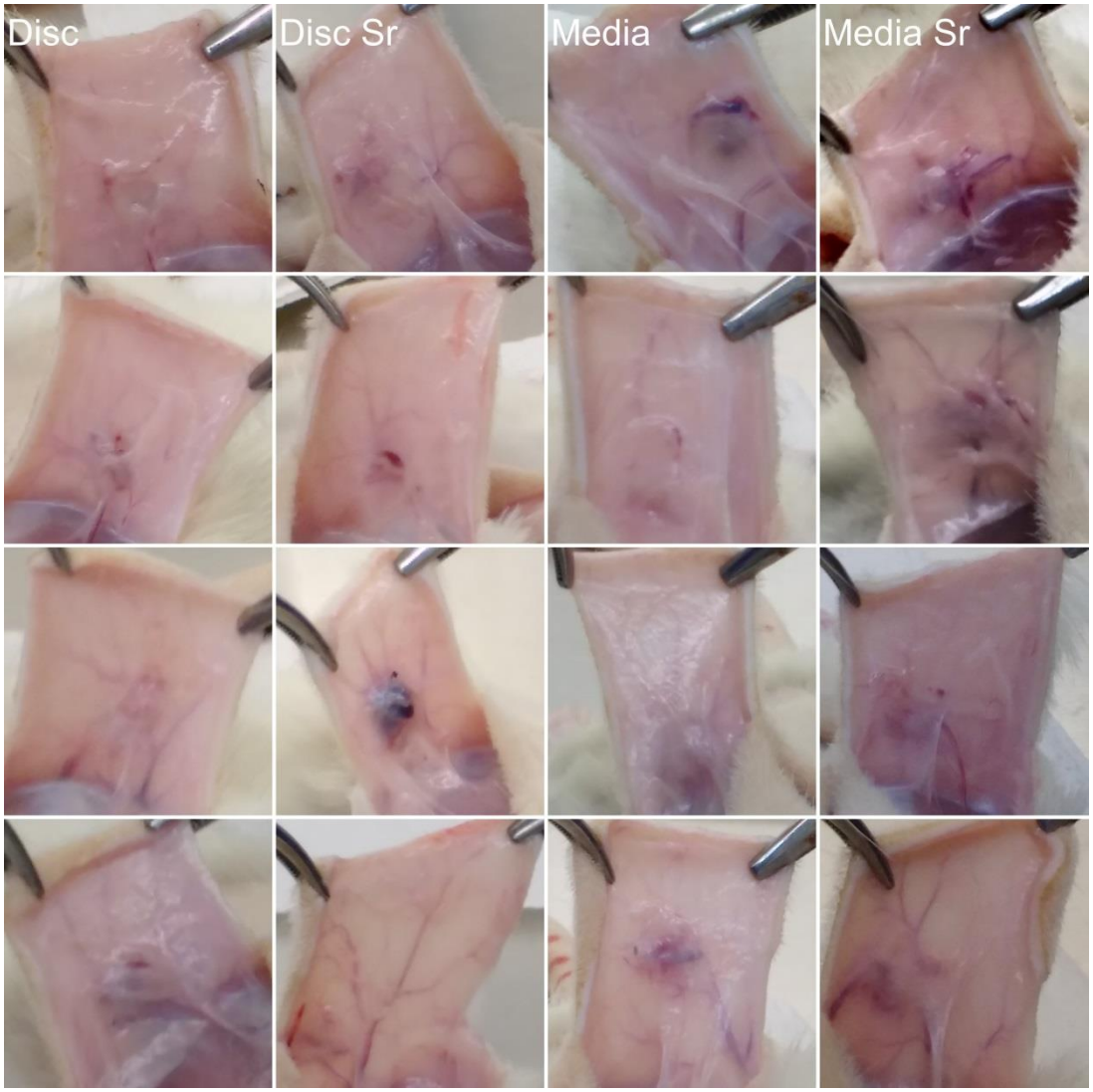


**Figure 83: Photographs after 3 days of the subcutaneous extraction site of the MSCs in collagen gels for each rat, which had been conditioned on glass ceramic discs (Disc and Disc Sr) or with glass conditioned media (Media and Media), both with either 0 or 12.5 Mol% Sr).**

#### 4.3.5.2 Haematoxylin and eosin staining of rat subcutaneous tissue samples

The collagen gels were extracted, fixed and embedded in wax and then sectioned and Haematoxylin & Eosin (H&E) stained. Not all of the collagen gels could be found within the implant site. The collagen gels were clearly visible in the stains of the “gel-only” control (Gel), and the “MSC and gel” (Gel + MSC) control (where the cells had not been conditioned with either glass conditioned media or growth on discs) (Figure 84). The gels appeared distinct against the surroundings, with a gap separating them from the surrounding tissue. At 24 hours after implantation numerous cell types were observed, with the gels tending to be populated primarily with relatively small nuclei (with examples indicated by blue arrows in Figure 84). As the collagen gels were implanted loaded with MSCs, these nuclei were assigned as the MSCs. The periphery of the gels, the surrounding tissues and the space of the subcutaneous pocket were seen to contain a large number of cells with larger, rounder and more strongly stained nuclei than those in the gel (examples shown by green arrows in Figure 84). The surgery and gel implantation would provoke a wound response resulting in immune cells moving to the site, hence these cells were assigned to peripheral blood mononuclear cells, potentially lymphocytes. By 3 days, the number of the darker nuclei cells was seen to clearly decrease, indicating a reduction in the initial immune response to the control gels. Red blood cells were also occasionally seen in some samples, more commonly in those at one day. The Gel control condition (not seeded with MSCs) was seen to remain largely without cells at one and three days, with the exception of a few cells having infiltrated around the periphery.

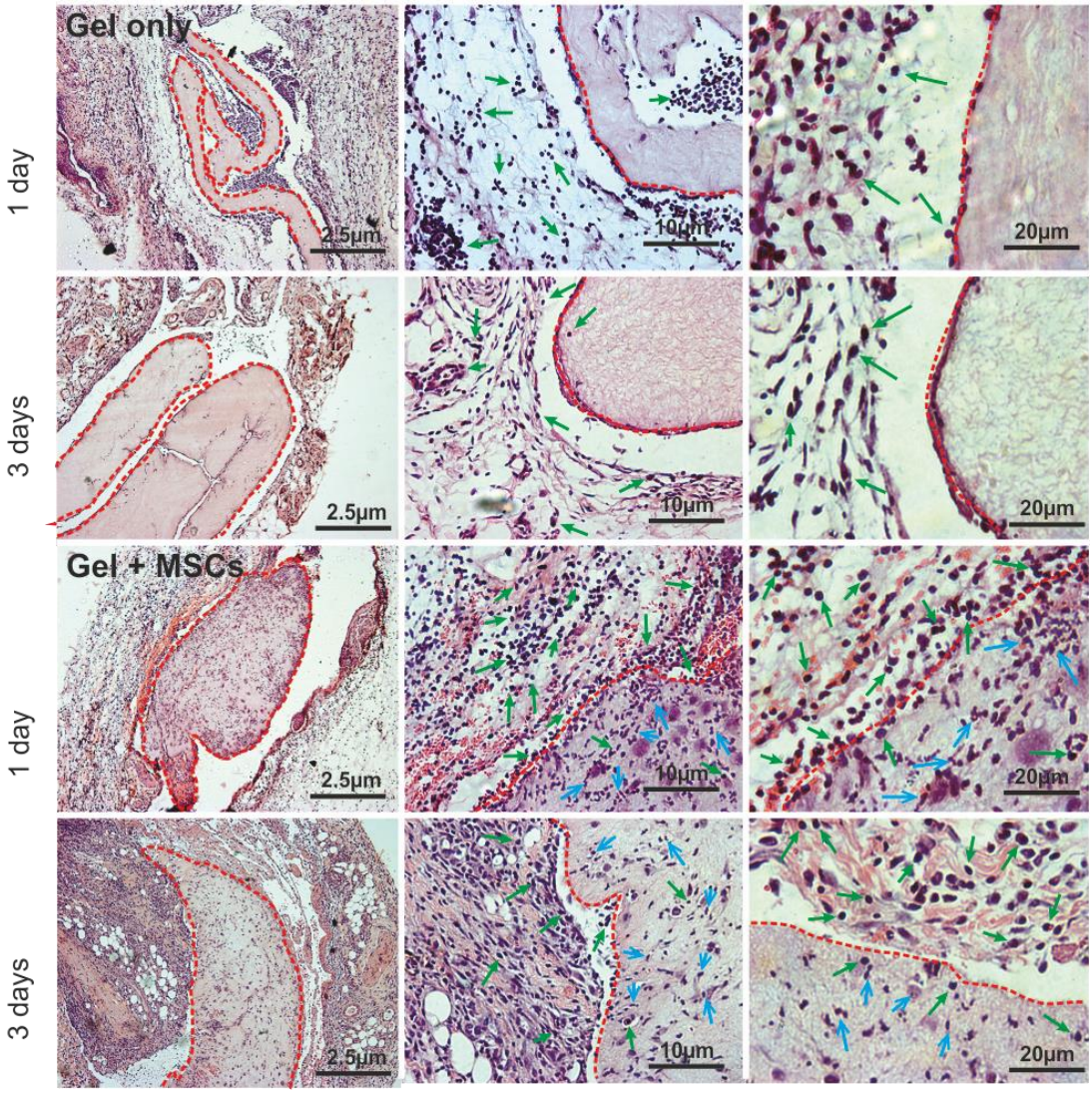


**Figure 84: H&E stains of collagen gels (at increasing magnifications from left to right) removed from rats after subcutaneous implantation for one and three days. The gels had either no cells (Gel only) or MSC grown in basal media (Gel plus MSCs). The edge of the gel is indicated by a red-dashed line. The green arrows indicate example mononuclear immune cells. The blue arrows indicate example MSCs.**

The main purpose of the experiment was to determine whether or not inflammatory response *in vivo* could be worsened by the MSCs induced to have raised inflammatory gene expression by the SrAWGC. Representative stains of the rat tissue where the MSCs had been conditioned by 0 (Disc) and 12 (Disc Sr) Mol% strontium SrAWGC discs for one and three days hours are presented inn Figure 85. At one day the gel can be seen clearly, and as with the controls, there were different cell types observed, however within the gels there was an abundance of cells with relatively small nuclei (MSCs, examples indicated by blue arrows in Figure 85), whilst cells with larger darker and rounder nuclei were in the periphery of the gels, in the surrounding tissues and in the space between the gels and the tissue (identified with green arrows in Figure 85). These were identified as peripheral blood mononuclear cells, and potentially lymphocytes, and therefore represented an immune response to the gel and the MSCs, which had been conditioned by the SrAWGC discs. At 72 hours the gel is still clearly visible, and the MSC Disc and MSC Disc Sr conditions tended to show fewer of the larger darker nuclei, particularly those associating very close to the gel edge (Figure 85). This would suggest that the immune response decreased over time. Additionally, there was no clear difference between the Sr condition (MSC Disc Sr) and those without strontium (MSC Disc), with a similar distribution of the peripheral blood mononuclear immune cells in both conditions at both time points.

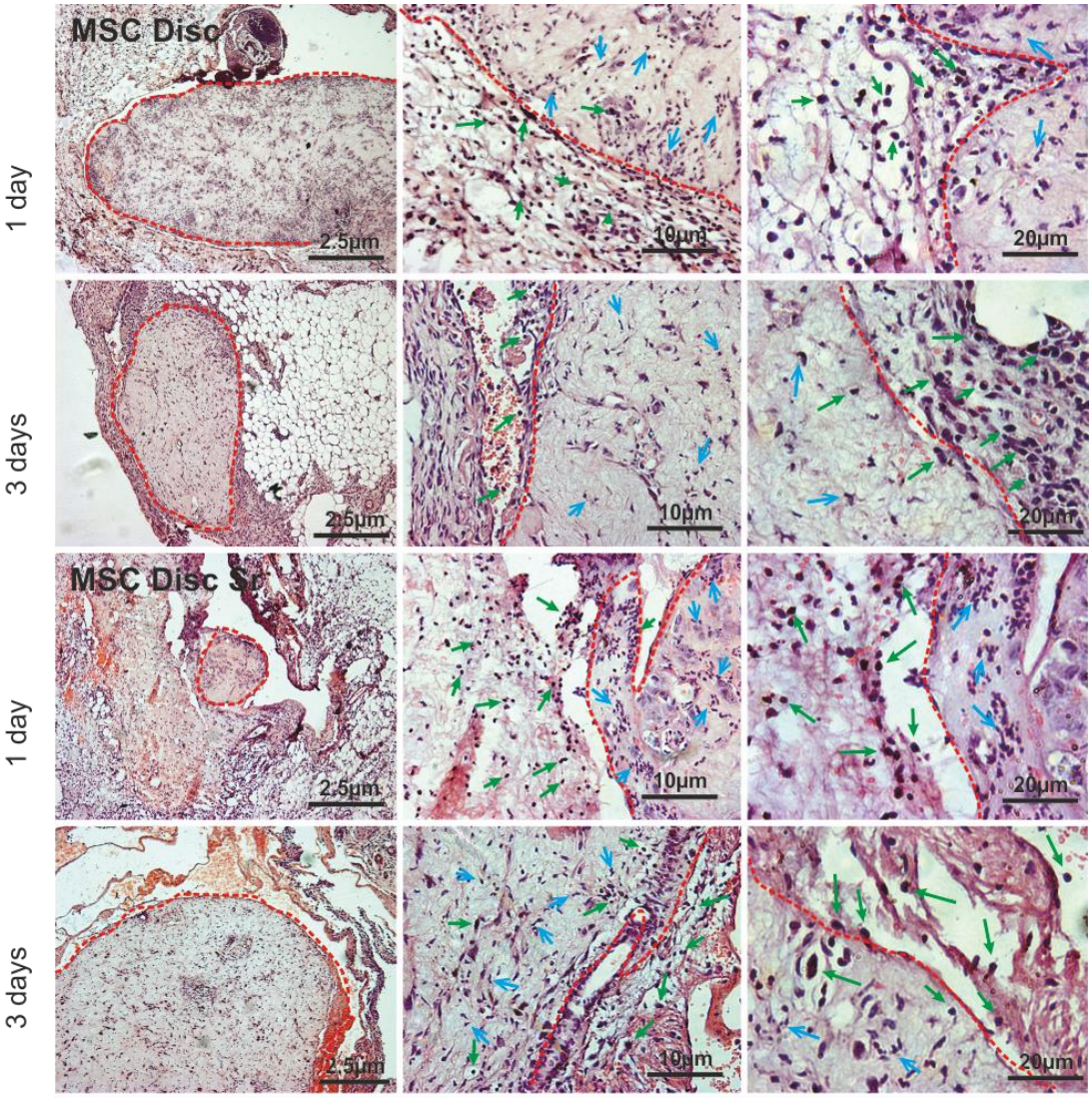


**Figure 85: H&E stains (at increasing magnifications from left to right) after one day and three day of collagen gels with Y201 hTERT MSCs which had been pre-conditioned through growth on glass-ceramic discs with either 0 (Disc) or 12.5 Mol% Sr (Disc Sr), shown as MSC Disc and MSC Disc Sr above. The edge of the gel is indicated by a red-dashed line. The green arrows indicate example mononuclear immune cells. The blue arrows indicate example MSCs.**

In addition to testing how the SrAWGC conditioned MSCs might affect inflammation, the SrAW glass conditioned media was also used to condition MSCs to determine whether the ions released by the material could also have an inflammatory effect, separate from the material surface itself. Representative stains of the subcutaneous rat tissue and collagen gels with MSCs conditioned by 0 and 12.5 Mol% SrAW glass conditioned media, (Media and Media Sr, respectively), are presented in Figure 86. After one day, the gels are clearly visible compared with the surrounding tissue, and throughout the region a number of cell types are observed. In the gels there were a large number of cells with relatively small nuclei, potentially the MSCs, whilst in the tissue surrounding the gels, in the space of the subcutaneous pocket and around the periphery of the gels were a large number of cells with larger, darker and more round nuclei (Figure 86). As in the control gels and those for the Disc and Disc Sr conditions, these cells were identified as peripheral blood mononuclear cells, potentially lymphocytes, and represent the immune response to the subcutaneous gel implantation. After three days, the gel is still clearly identifiable and, as had been seen in the control and disc conditions, the number of cells with the darker nuclei had visually decreased, particularly those in close proximity to the gel surface (Figure 86). This indicates that the gel and the MSCs in the gel conditioned by the glass conditioned media (with and without Sr, Media and Media Sr) did not invoke a prolonged immune response. When the Media and Media Sr conditions were compared, it was found that there was not a clear visual difference in the number of immune cells, and therefore in the *in vivo* inflammatory response.

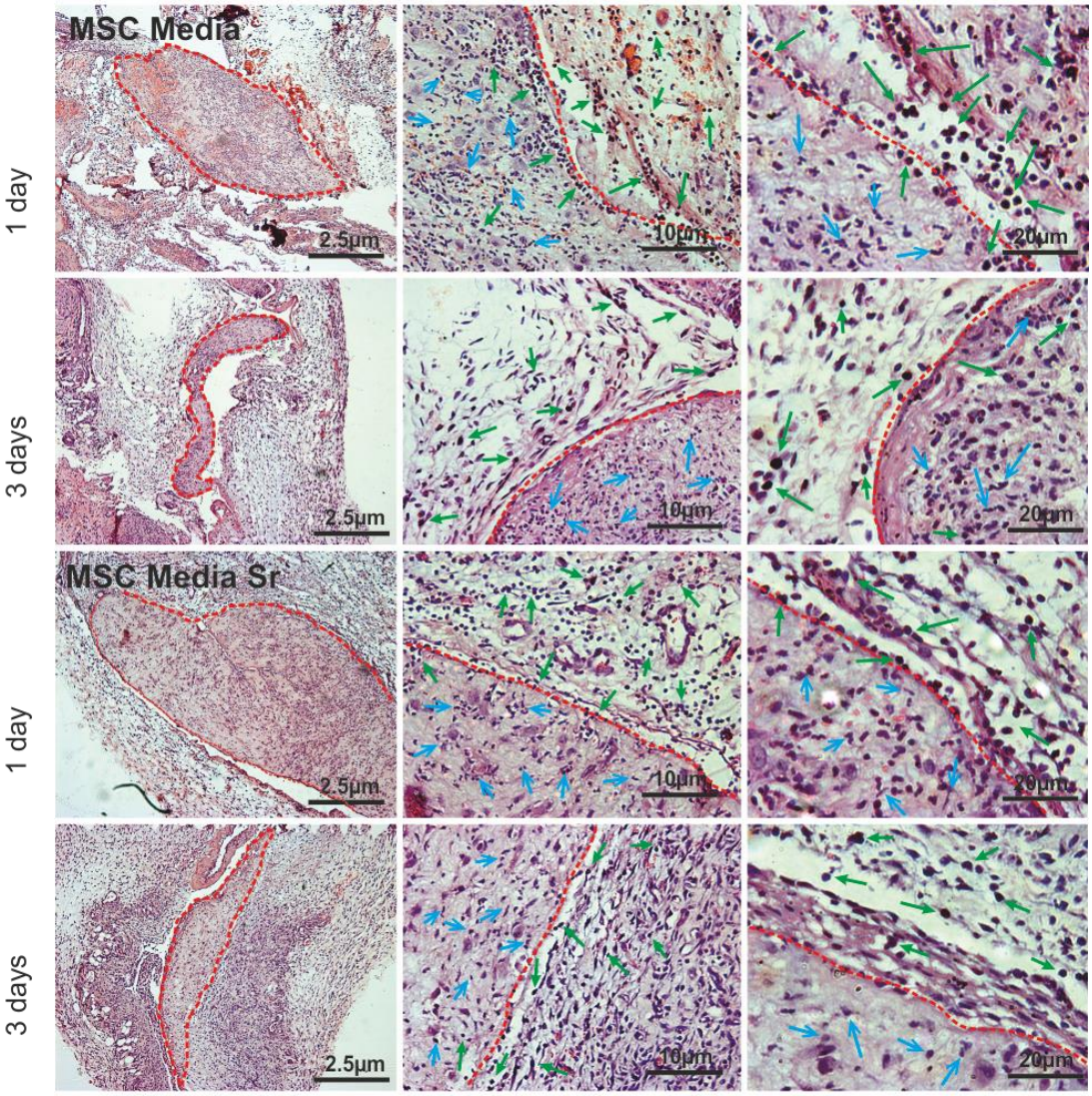


**Figure 86: H&E stains (at increasing magnifications from left to right) after one and three days of collagen gels with Y201 hTERT MSCs which had been pre-conditioned through exposure to glass conditioned mineralisation media with either 0 (Media) or 12.5 Mol% Sr (Media Sr), shown as MSC Media and MSC Media Sr above. The edge of the gel is indicated by a red-dashed line. The green arrows indicate example mononuclear immune cells. The blue arrows indicate example MSCs.**

## 4.4 Discussion

The previous chapter found that one of the main effects of adding Sr to AW and AWGC was to increase cell numbers on the material surface. In a clinical setting, increasing the survivability of the cells on a scaffold would be very desirable, however there remain many unanswered questions as to how strontium, and glass and glass-ceramic biomaterials more generally, induce their effects on human cells, and MSCs in particular. Therefore, the work described in this chapter explored how AWGC, and more specifically the addition of strontium to this material (the Disc and Disc Sr conditions), and media conditioned with AW and SrAW (the Media and Media Sr conditions) affect MSCs by global transcriptome analysis using RNAseq. RNA sequencing reads every RNA fragment extracted from the sample, potentially allowing the change in every gene in the sample to be measured though the processing of these can be somewhat more complicated, compared to simpler gene array data (291).

### 4.4.1 SrAWGC promotes the expression of inflammatory genesets compared with SrAW glass dissolution products

The four different RNAseq conditions (Disc, Disc Sr, Media and Media) were compared statistically, to produce volcano plots and determine how individual genes varied in expression. To determine the functional meaning of these gene expression changes, they were enriched on Hallmark genesets, producing a GSZ score indicating how strongly that geneset was represented, and therefore how a particular functional grouping of genes was affected by the Disc, Disc Sr, Media and Media Sr conditions. The volcano plots of the RNAseq data showed how although the addition of strontium had some effects, these were dwarfed by the difference between the discs and the media. This can also be seen clearly in the hallmark geneset enrichments (Figure 67) where not only does the gene expression between the disc conditions seem more similar (compared to the media conditions) but also the dendrogram was able to sort them without guidance into groups based on disc and media conditions. The strong difference in MSC gene expression between the glass-ceramic discs and those exposed

to the glass conditioned media was also later confirmed with the PCR array. Many studies on bioactive glasses which have measured the effects on gene expression have used glass power, or glass conditioned media (the ions released by the material)(65,85,87,231), hence this is an important finding. Exactly what feature of the material induces the gene expression changes remains to be determined, however the surface of tissue engineering materials can have significant effects on the behaviour and gene expression of human cells (67,68,98,292), with Ohgushi *et al*. finding that the MSCs grown on the AWGC surface show more osteogenic differentiation, and that altering the surface roughness could also further increase this effect (293). There were many genes upregulated between the MSCs grown in the Disc and Disc Sr conditions, on the material surface, and MSCs grown in the Media and Media Sr conditions, exposed to the ion released by the material. However, amongst the most changed were MMP1, COL7A1, CXCL10 and CXCL11, suggesting an inflammatory response to the material. This is an important finding as for the SrAWGC to be an effective bone regeneration scaffold it must not promote a response in the MSCs which could be detrimental to the healing process. Interestingly, another study found that human Osteoclasts showed a significant increase in the expression of CXCL10 and CXCL12 when grown on a calcium phosphate coated surface rather than culture plastic (294). Although the AWGC material is quite different to calcium phosphate, there are similarities; hence this could indicate that bioactive ceramics may work to induce inflammatory cytokine production from both lineages of bone cell. The mechanism behind the inflammatory response of the MSCs to the SrAWGC is unknown, however other studies have found that roughened titanium surfaces can induce cytokine (TGFβ) production (295–297). This is important because the surface of AWGC is not flat unless polished, hence it has a different topography (and perhaps higher surface area) than culture plastic, which could be a factor in the inflammatory response. Additionally, it was observed (Chapter 2, Section 2.3.6) that as strontium was added to the SrAWGC discs, the disc surface grew more rough, and so the roughness of the material could potentially be associated with inflammatory gene expression in the MSCs. Determining the mechanism behind Sr-induced roughening of

the SrAWGC discs would require further study, however previous work in the Wood and Genever laboratories on mesoporous AWGC scaffolds provided an indication of these mechanisms (102,203). The mesoporous AWGC was produced in a different way with a much greater crystal size than the AWGC discs presented in this thesis. However, it was found that Sr substitution into the material caused the surface to turn from being mostly flat interlocked crystals to having large regions of spherulites, roughening the surface, due to the material responding differently during the heating process (102). There are other ways in which altered surface topography could alter the cell response. Prior work discussed how increasing the roughness of the hydroxyapatite surfaces could increase the adsorption of certain proteins from the media (*e.g*. fibronectin), which could then explain the improved cell response to the SrAWGC surface (298). Another study built on this work by exploring how the combined effects of many surface features, such as surface charge, roughness, adsorption, porosity, solubility and crystallinity can have effects on cell function, altering cell attachment and TGF-β1 expression (299). To attach meaning to the lists of the differentially expressed genes, the functional groupings most associated with them were determined using gene set enrichment analysis, and Hallmark genesets (273,274). Inflammatory genesets featured prominently in the most enriched Hallmark genesets, differing in enrichment between the disc and glass conditioned media groups, further establishing that the gene expression changes induced by the material itself are potentially inflammatory.

The main effect of the disc conditions (Disc and Disc Sr) was that they increased the expression of a number of genesets associated with inflammatory/stress response, raising “Interferon Gamma Response” (IFNγ), “Interferon Alpha Response” (IFNα) and TGFβ. Some of the key genes responsible for this were CXCL10, CXCL11, various IFIT genes and TNFSF10, all of them associated with immune responses. MSCs constitutively produce a number of cytokines and growth factors such as TGFβ (300,301). However, bone marrow MSCs do not normally produce CXCL10 and CXCL11, though stimuli, such as from TNFα, can promote their production (302). This suggests that the MSCs are being prompted to produce these cytokines by some feature of the SrAWGC discs, and further

implies this process is exacerbated when strontium is added to the glass ceramic, as their gene expression was even higher in the Disc Sr condition. The more general “inflammatory response” geneset also displayed increased expression for the Disc Sr condition compared with the Disc condition, but interestingly addition of strontium to the glass conditioned media was observed to lower its expression, acting in an opposite manner. This same response was also observed for the “TNFα signalling via NFκB” geneset, where the Disc Sr showed increased expression, whilst the expression of Media Sr was lowered (compared to the non-strontium conditions Disc and Media), though for this geneset the baseline expression was actually lower for the discs than for the glass conditioned media. This suggests that although the Sr itself may be anti-inflammatory, its addition to the material causes the SrAWGC to interact with the cells in such a way that it enhances the inflammatory response. This is supported by studies on monocytes and joint tissue in rats, where it was found that Sr Hydroxyapatite powder and strontium ranelate, respectively, were able to lower TNFα expression and reduce inflammation (303,304).

Exactly what caused the increased expression of these inflammatory cytokine pathways is not clear, however studies have found cells ingesting bioactive glass particulate can show increased inflammatory cytokine production, with fibroblasts having been shown to both experience increased gene expression and secrete more TGFβ, IL-6 and TNFα after phagocytosis of HA particles (305,306). The SrAWGC showed increased dissolution with increased strontium content (see Chapter 3 section 3.2.5), and clearly had a more granular surface (see Chapter 2 section 2.3.6), potentially indicating that addition of strontium to the material could cause faster breakdown of the surface and potentially release more particulates to which the cells could then respond. Furthermore, association of MSCs with macrophage soluble factors are observed to encourage MSC production of cytokines such as CXCL10, IL-6 and CCL5, though whether these same factors can be prompted by other sources of cell stress is not known (307).

Amongst the most strongly up regulated gene sets for both of the disc conditions was Epithelial to Mesenchymal Transition (EMT); however, the addition of strontium to both the discs and the glass media dampened the

expression of the EMT genes, such as COL5A3. This pathway is thoroughly studied in the literature, though often in the context of MSCs or other cells releasing TGFβ which prompts the EMT in cancer cells, whereby they transform from being more epithelial (with clear polarity) to becoming more motile and with some cell types more stem-cell-like (308–312). Furthermore, control of EMT genes in MSCs has been associated with cytokines such as TGFβ in cardiac tissue engineering, where this process is important for encouraging development of the correct tissues (313). The MSCs growing on the SrAWGC and AWGC discs (Disc Sr and Disc conditions) showed increased TGFβ signalling and EMT gene expression compared to the MSCs exposed to the glass conditioned media potentially indicating TGFβ and the EMT response were associated. However, the addition of strontium to the AWGC discs raises further questions, as it was observed to both slightly lower the EMT expression, whilst increasing TGFβ expression (contrary to what is seen above). This goes against a TGFβ driven EMT response, perhaps suggesting some other process was responsible.

### 4.4.2 Sr substitution into SrAWGC and SrAW promotes expression of survival and proliferative genes

The disc conditions were also observed to alter the expression of genesets associated with proliferation/survival such as by increasing expression of genes associated with “c-MYC Targets” and TGFβ signalling, whilst also lowering mTORC1 signalling. c-MYC is a transcription factor which is associated with raised proliferation and both cell survival and potentially increasing susceptibility to apoptosis (314–317). However, c-MYC also has a complex association with apoptosis, as deregulation of c-MYC has been found to make cells more susceptible to apoptotic stimuli and could induce apoptosis dependent on p53 expression (318,319), with the absence of p53 allowing c-MYC to act in a more proliferative manner (318,319). For the Disc and Disc Sr conditions, the targets of c-MYC showed increased expression alongside a decrease in p53 expression, compared with the Media and Media Sr conditions, suggesting c-MYC could be acting in a more proliferative/survival capacity. The Media Sr condition also increased c-MYC and lowered p53 expression, compared with the Media condition (without

strontium), perhaps also explaining the observed increase in cell number with Sr content found for the glass conditioned media. More recent studies have found that c-MYC overexpression in MSCs (in one study associated with a p53 knockout) can assist in osteogenic differentiation via other osteogenic factors (315,320), a potentially useful property for bone tissue engineering. Two further studies of MSCs found that c-MYC expression was associated with immortalisation of their MSCs, and hence with survival and proliferative gene expression, along with raised expression of DNA repair mechanisms (316,317). This could also explain the increase in expression of the DNA-repair gene sets found between the non-strontium Disc condition and Media condition and also when Sr was added to the glass conditioned media (Media Sr). Hench (2009) noted DNA-repair as one of the seven families of genes most altered by the ions released by Bioglass 45S5 (80), hence it is possible that the AW glass conditioned media also induced upregulation of DNA-repair genes themselves (compared to the baseline gene expression of the MSCs, although this would require further study), and that the AWGC discs further upregulate these genes. The Disc Sr condition showed decreased DNA-repair geneset expression when compared with the Disc condition, which coincides with higher expression of the inflammatory genes, though no mechanisms for this connection are known. This requires further investigation, particularly as a previous study found DNA repair signalling increased interferon signalling in HeLa cells (321).

The disc conditions were seen to increase expression of TGFβ, compared with the media conditions however, the addition of strontium to the discs was seen to further increase the TGFβ expression, whilst addition of Sr to the glass conditioned media slightly lowered TGFβ expression. TGFβ is known to have a wide range of effects on cells, such as encouraging proliferation, migration, differentiation and even apoptosis (322). As mentioned previously, the increased TGFβ expression could be a result of the increased dissolution rate (and hence perhaps glass particulate debris released) of the 12.5 Mol% SrAWGC discs (Disc Sr condition), or perhaps related to the altered surface topography (295–297,305,306). In agreement with the Disc Sr condition, but contrary to the Media Sr condition, Strontium ranelate has been seen to

increase the expression of TGFβ in rat chondrocytes (323) and human osteoblast-like cells (co-cultured with osteoclasts) (324). This difference in response could have been caused by the other ions in the SrAW glass conditioned media, or could have been associated with the fall in phosphorus in the media induced by the glass; however, this would require further study. MSCs normally produce TGFβ (300,301), and it is chemoattractant to MSCs, suggesting that increased expression by the SrAWGC discs could be useful in a tissue engineering context as it could encourage cell migration in and through the scaffold (29,322). Additionally, while short term TGFβ exposure has been reported to aid early stage osteoblast differentiation (325,326), it also inhibits further differentiation trough repressing the transcriptional activity of Runx2 (327), a key osteogenic transcription factor (30,327). Thus, further work could involve determining whether the disc induced rise in TGFβ expression was time limited, to ensure its usefulness to the bone tissue engineering process.

The MSCs grown on discs also displayed a lower mTORC1 geneset expression, whilst the addition of Sr to the glass media resulted in slightly increased mTORC1 expression. mTORC1 is an element of the Akt pathway, which is associated with MSC differentiation and proliferation (328), and importantly is also a pathway through which strontium has been shown to act (122,124,127), hence this could be evidence of MSCs sensing and responding to the Sr in the glass conditioned media. However, the reasoning behind the lowered mTORC1 geneset expression in the discs is currently unknown and would need further study.

The strontium content of the disc and glass media were also seen to potentially affect MAPK/ERK signalling as shown by the increase in K-Ras Signalling Up, and the fall of K-Ras Signalling Down, for the 12.5 Mol% Sr disc and glass conditioned media conditions (Disc Sr and Media Sr), respectively. This result suggests the addition of strontium to the material activates the K-Ras signalling pathway. Another member of the Ras family of proteins (H-Ras) has been established as a component of strontium signalling (128), where it was shown that the increased ALP activity, osteocalcin (OCN) expression and Alizarin red stain staining could be abrogated with the addition of H-Ras siRNA. Hence, given the similarities in

function between the H-Ras and K-Ras proteins this would suggest the strontium released from the material has some effect on Ras signalling in the cells, apart from any effect of debris or other ions released (329). This is further supported by the Ras inhibitor work carried out in this thesis, where Salirasib was seen to block the Sr-induced increase in cell number, sequentially decreasing this to control level as Salirasib concentration increased. These findings strongly implicate K-Ras signalling as a mediator of the proliferative response of MSCs to Sr, and more specifically to the strontium doped SrAWGC material. It should be noted that Salirasib (also known as FTS) is not specific to K-Ras and does also inhibit N-Ras and H-Ras (by blocking association of the Ras proteins with the cell membrane) though Salirasib is being used clinically as a K-Ras inhibitor for the purposes of cancer treatment (279–281).

### 4.4.3 The role of K-Ras and cytokine signalling in the SrAW MSC growth response

In the previous chapter, it was presented that strontium addition to the SrAW glass and SrAWGC glass ceramic discs increased cell number, potentially also meaning improved cell survival, and as the addition of SrAWGC to the AWGC also increased the expression of genes associated with inflammatory response, thus it was decided to explore (utilising inhibitors) whether inflammatory cytokines were involved in the Sr-induced cell number/survival response induced. Strontium is known to interact with the MAPK/ERK and PI3K related pathways (126,128,330), which can be affected by inflammatory cytokines via Src and JAK (inhibited by Dasatinib and Ruxolitinib, respectively) (286,287). However, Src and JAK inhibition did not affect the Sr induced rise in cell number, suggesting that cytokine receptor mediated pathways were not involved in the cell number increases.

Given the previous findings that the  glass ceramic (both with and without Sr) increased the expression of various inflammatory genes, a pilot study was performed to determine whether these disc conditioned MSCs could then promote an inflammatory response *in vivo*. AWGC itself is known to be well accepted by the body having been used since the 1980s in studies on

rabbits (120,331), mice (118), and clinical to repair long bone defects in humans (332). In previous work they showed the presence of giant cell formation at 24 weeks along the surfaces of the material, in response to glass granules released from the surface of the material (333). However, in separate work they showed very little macro-inflammatory response at 4 and 8 weeks with a somewhat less porous material, perhaps indicating that the form of the material is integral to the inflammatory response (118).

### 4.4.4 The extent of the inflammatory effects on MSCs by SrAWGC and SrAW glass *in vivo*

Although too severe an inflammatory response could be detrimental to the healing process and potentially cause rejection of the material (334), a controlled short term inflammatory stimulus has been found to promote improved healing by encouraging cell recruitment to the engineered tissue, improved tissue healing, vascularisation and subsequently resulting in a better engineered tissue compared to conditions with no inflammatory response (334–338). A sub-cutaneous model was used as a pilot study to explore whether the MSCs which had been conditioned by the AWGC discs into a more inflammatory phenotype could have potential effects *in vivo*. The MSCs were grown in a manner identical to that used for the RNA sequencing, with the Media, Media Sr, Disc and Disc Sr conditions. The MSCs were then embedded into a collagen gel and implanted into the rats for a time course. Collagen is well utilised and known to induce a low immune response (339–341).

The control conditions determined the baseline response of the rat tissues to a collagen gel-MSC construct. The gels were observed to be the faint pink structures (342), and at 24 hours had little infiltration by other cells, with the MSCs appearing to be the cell type with relatively small nuclei. However, for all of the conditions the periphery of the gels tended to show the presence of larger darker nuclei, most likely immune cells such as lymphocytes. In this pilot study, the most obvious change was the decrease in the presence of these darker cells with larger nuclei at the three day point, suggesting that in all of the conditions there was no prolonged inflammatory response. This is

supported by the rats maintaining good health and the subcutaneous implantation sites tending to show much lessened inflammation for all conditions. Further to this, the addition of strontium to either the discs or the glass conditioned media was not seen to result in an obvious difference between the immune response, or its subsequent reduction. This suggests that whatever gene expression changes were induced by the Sr conditions on the MSCs they were not sufficient to worsen or prolong the inflammatory response.

The MSC-collagen gel control appeared to show more immune cell infiltration compared to any of the glass-ceramic disc, or glass conditioned media conditions, however there was not a clear difference between the glass ceramic discs and glass conditioned media conditions. This either suggests that the MSCs were not affected by the discs in a way that could worsen inflammation, that gene expression changes were not large enough to have any effect, or that the experiment was conducted in a way that masked this effect. Either way, as this was a pilot study, further investigation would be necessary to establish fully how the SrAWGC and SrAW glass conditioned media (representing the ions released by the material) affect human MSCs, and what effects these have *in vivo*.

It is important to reiterate, that this study did not determine the immunogenicity of the AWGC material. Prior work has found that the base composition of AWGC without Sr integrates well in mice and induce no inflammation at four weeks (118). Instead, this study has explored whether the MSCs grown on the glass ceramic discs became more immunogenic. In this study there was observed to be a short-term immune response from the rat which was over within three days. This is largely confirmed by the literature, as numerous studies have been performed with sub-cutaneous implant of collagen gels with MSCs in rats and mice and at time points ranging from 3 days to 6 weeks tended to find the presence of immune cells around the construct, but observed little inflammation around the collagen hydrogels (confirming what was observed in this study in the photographs at day 3) (343–347).

In summary, this work has determined that addition of strontium to the SrAWGC material promotes the expression of a number of genesets associated with proliferation and survival, such as through lowering the expression of apoptotic and P53 associated genes and activating K-Ras associated genes, which through the use of a Ras inhibitor has been shown to be a requirement for the Sr induced increase in cell number shown in Chapter 3. However, the most significant finding was that the AWGC material itself increased the expression of genes associated with a number of inflammatory genesets, such as Interferons Gamma and TNFα, with CXCL10, CXCL11 and TNFSF10 being the most changed genes in these genesets. Interestingly, the addition of strontium further increased the expression of these genesets, but this was not found in the strontium glass conditioned media conditions. This suggests that the inflammatory response of the MSCs could instead be due to some property of the material itself which changed with strontium content (rather than the strontium itself), such as the faster dissolution of the SrAWGC itself or its altered surface with strontium content. A pilot *in vivo* study found that the MSCs conditioned by the material to have an increased inflammatory gene expression probably did not provoke a prolonged inflammation response, indicating that the material could be a valuable tissue engineering scaffold as a controlled inflammatory response can improve vascularisation (334–338).

# Chapter 5 – General discussion

## 5.1 Rational of the project

Treating large bone defects, which are incapable of self-repair, is a growing clinical challenge. These non-union defects can result from trauma, infection and cancer treatment and their incidence increases for patients who smoke, suffer from osteoporosis or have diabetes (2,3). Additionally, the population of the UK is aging which will increase the incidence of non-union fracture (51). However, the current gold standard treatments are autografts, which are expensive and require complex and painful surgery leading to morbidity in the donor site (3,6). Additionally older patients, with lower quality bone, may not have sufficient bone suitable for the procedure (6). Tissue engineering could act as a solution to the increasing need for improved bone regeneration strategies. However to tissue engineer fully functional bone tissue requires the correct combination of a scaffold to support the wound site and the framework on which the new tissue is formed. Cells are required to populate the scaffold, form the functional tissue and finally to provide the correct environment for cell differentiation into a functional tissue. The patient's own resident stem cells represent a potential source of cells for bone tissue engineering, whilst bioactive glasses and glass-ceramics (in particular apatite wollastonite glass ceramic, AWGC) are promising bone tissue engineering scaffolds due to their bioactivity (ability to form hydroxyapatite *in vivo*), strength (useful for load bearing bone repair) and ability to support cell attachment, growth and proliferation (9,102,104,118,119,121). However, although some bioactive glasses can intrinsically induce osteogenic differentiation in MSCs, they are osteoinductive (348), they do not have the high bending strength and fracture toughness of AWGC (119,121). AWGC has already been used successfully in 60,000 patients as a bone substitute, such as in artificial vertebrae and iliac crests (10). However, AWGC can still be improved as a scaffold by altering it so that the cells growing on its surface are encouraged to osteogenically differentiate, resulting in bone growth and repair. The ions

released by the bioactive glasses/ceramics have been found to be a key to influencing cell function (79,80,87,246,348), hence the addition of Sr to various materials has been explored as a method of inducing osteogenic MSC differentiation within a tissue engineering scaffold. This is because Sr is an established osteoporosis drug known to raise bone density by inducing osteoblast formation and activation (via numerous signalling pathways, amongst them CaSR-Akt signalling and MAPK signalling) whilst also inhibiting osteoclast formation (122,124,135,349). Previous work in the Wood/Genever laboratories showed that Sr could be successfully incorporated into mesoporous AWGC scaffolds without compromising the mechanical properties of the material and the addition of Sr appeared to have had beneficial effects on MSC osteogenic differentiation and proliferation (102). However, the exact mechanisms behind how SrAWGC (and numerous other Sr substituted scaffolds) affect cells have not been fully elaborated. This is important to determine because the addition of strontium has been seen to alter various properties of bioactive glasses/ceramics. Previous studies have found that Sr addition can alter physical properties such as the surface topography and the mechanical properties (102,257,350). Strontium is also known to alter more dynamic features of these materials, such as the dissolution rate, the ions released by the material (not only Sr) and its ability to  form hydroxyapatite (102,208,350). Additionally, substitution of strontium has also been found to change the glass and crystallisation temperatures, potentially altering the crystals formed during any heat treatment(102,207).

The aim of this thesis was to determine how increasing substitution of strontium for calcium in AWGC affects MSCs, and to determine the mechanisms behind this response. This would allow the material to be improved as a tissue engineering scaffold for large load bearing bone defect repair.

## 5.2 The effect of Sr on AW glass short and medium range order

Initially, the effects of strontium substitution on the material itself were determined to better understand how its addition to the material could alter the cell response. The medium range order was found to change with the addition of Sr, resulting in a lowered percentage of $Q^3$ Si tetrahedra, and subsequently lowering the NC. A fall in NC indicates the silicon network is less interconnected, and so could suggest an increased dissolution rate and potentially increased bioactivity. This has been shown in previous work on other bioactive glass compositions where (for a fixed phosphorus content) lowering the NC was seen to shorten the time to first HA formation (112). Interestingly, another group did not find a large change in the percentage of $Q^3$ Si tetrahedra (and hence NC) when they fully substituted the Ca for Sr in Bioglass 45S5 (150). However, their 50% substitution (corresponding with 24.9 Mol% in this thesis) did show a drop from 17 to 11% $Q^3$ Si (150), which should also result in a drop in NC. This suggests that the strontium itself may not have been responsible for the fall in NC, and potentially the raised bioactivity of the material. Strontium was also found to raise the density of the SrAW glass, whilst lowering the oxygen density, due to both the higher mass of strontium, and its larger size. This has been associated with faster dissolution in other studies (204,211), and could also have expanded the glass network, lowering the bond strength in the orthophosphate (85,150,181).

However, despite the medium range order showing some changes with Sr content and changes in the density, the short range order did not change with Sr content. Alongside this, the phosphorus component of the glass was always found to be orthophosphate, regardless of Sr content. This is important as phosphate plays a key role in bioactive glass bioactivity (112), and therefore the phosphate phase being similar between the compositions supports that there might not be large differences in the way the material breaks down. Additionally, the different glass compositions released ions at a similar rate. When considered together these data would suggest that the strontium content of the glass did not alter its structure in a way that would

significantly change how it broke down. Other glass compositions have both agreed and disagreed with these findings. The A glass studied elsewhere also found the Sr content largely didn't alter the breakdown of the material (86). However, the dissolution ions (particularly Si and P) of higher Si content glasses were altered by glass Sr content (55,232), whilst a composition similar to Bioglass 45S5 actually showed reduced release of Si with Sr substitution (84). These studies also found that strontium altered the way in which the ions were released at different time points (55,84,86,232). This would be an important area of future study on the SrAW glass as an altered dissolution profile could affect HA formation on the surface of the material (112), potentially changing its bioactivity with Sr content.

## 5.3 The effect of Sr on the ion release of SrAW and SrAWGC discs

In contrast with the SrAW glass studies, increasing the Sr content in the SrAWGC discs raised their Sr, Si and Ca ion release, suggesting the material as a whole was breaking down faster with Sr substitution. Determining the cause behind this is challenging as there are many components of the glass-ceramic which could change with the addition of strontium. The surface topography of the SrAWGC could have contributed to the increased dissolution as this was seen to change with Sr content, and a rougher surface, with a greater surface area, should release more ions. The ions released by the SrAW glass did not change with Sr content; hence this would suggest the same for the glassy phase of the SrAWGC. However, it is important to note that the SrAW glass is not a perfect model of SrAWGC, as the formation of the crystal phases can deplete the residual glass phase of ions (102). It is also possible that the substitution of Sr could have changed the dissolution of the material by altering the apatite and wollastonite phases of the glass ceramic. Previously, we found that for mesoporous AWGC 3D scaffolds the addition of Sr both increased the amount of apatite formed (the least soluble phase) whilst also lowering the amount of wollastonite formed (the more soluble phase) (102). The apatite phase is generally the least reactive phase in AWGC, however, studies have found that strontium apatite

has shown increased solubility (235–237). Therefore, the rise in dissolution rate of the SrAWGC with Sr content could have been associated with a more soluble Sr-apatite phase. However, studies have also found that the degradation rate of wollastonite ($CaSiO_3$) falls with Sr substitution for Ca (238). This could indicate that the effect Sr has on the degradation rate of the material will depend on the heating regime applied, and hence the crystal phases which were formed.

## 5.4 The effect of SrAW and SrAWGC on growth of MSC

The substitution of Sr into the material was seen to have a number of effects on human MSCs. The SrAWGC discs with Sr, the glass conditioned media with Sr, and Sr itself in the form of $SrCl_2$, were all seen to decrease the osteogenic differentiation of the MSCs studied. This could have been due to some property of the discs, such as the surface area or ion release rate, which changed with strontium content and thus negatively affected the differentiation of the MSCs. Another consideration is that the discs and the glass conditioned media both reduced the phosphorus content in the media, and this could have masked the osteoinductive properties of the material. The material released Si ions, which are slightly osteoinductive. However, Si ions act principally by encouraging Collagen I formation, which requires phosphorylation to mineralise, and which would be less likely in a phosphate deprived environment (72,243,246). However, the glass conditioned media and $SrCl_2$ studies indicated that the Sr released by the material could also potentially slow down the osteogenic differentiation of the MSCs. This is supported by recent work that has found that Sr can interfere with osteogenic differentiation, as well as induce it (243). Strontium is known to interact with (and stimulate) the Wnt pathway via numerous potential routes, such as the Calcium Sensor Receptor (CaSR) or by inhibition of Wnt inhibitors(122,124), and this could also block osteogenic differentiation of the MSCs (122,124,125,129).

Another, more thoroughly studied effect of strontium substitution into the SrAWGC discs and the glass conditioned media, was that it raised Y201 MSC cell number. Other studies on strontium bioactive glasses have found

that it could be beneficial to cell function, but typically these studies used only metabolic dye conversion experiments and thus could not establish whether there was truly increased cell proliferation (85,252,253,256). However, in this project DNA and metabolic activity were used to determine that Sr substitution into the SrAWGC discs and glass conditioned media could increase cell number. This indicated that strontium substitution into the material increased cell growth for both the discs and in the glass conditioned media, suggesting it could be associated with the ions released from the material (see Figure 87). In particular, the released strontium itself was likely a factor in the increased cell growth, as other studies have found that strontium ranelate raised osteoblast cell number and reduced apoptosis (123,351). Additionally, the RNAseq experiments found that Sr in the disc and glass conditioned media induced K-Ras associated gene expression, and that the Ras family inhibitor Salirasib could abrogate the Sr induced rise in cell number for the glass conditioned media.

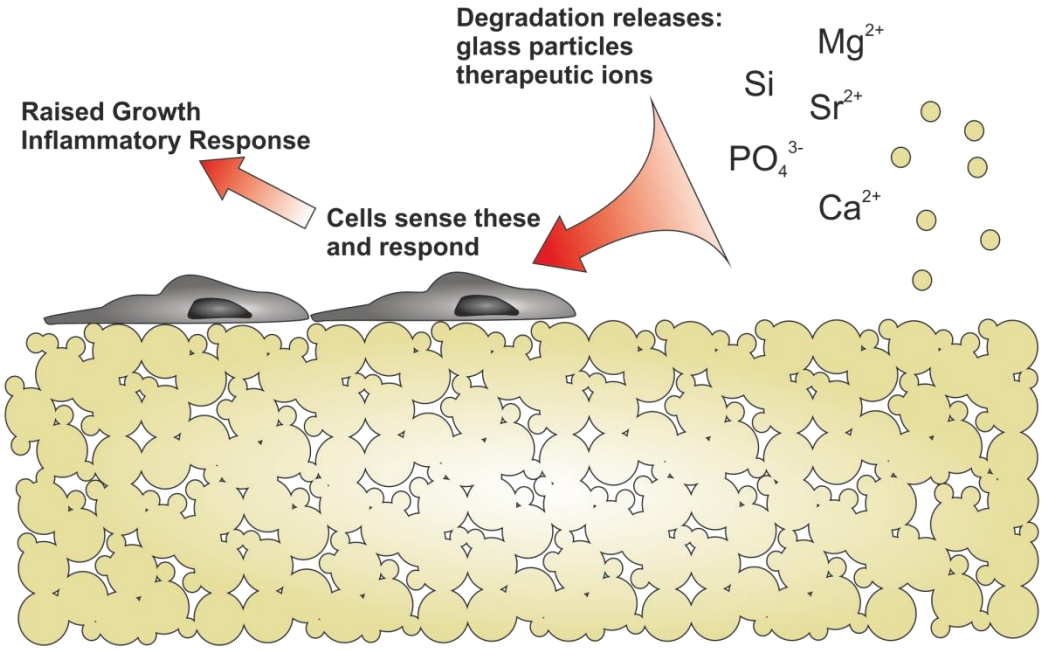


**Figure 87: Illustration of the propose method of interaction between the MSCs and the SrAWGC. The material breaks down releasing glass particles and ions. The cells respond to these, with increased growth, but also an inflammatory response to the glass particles. Strontium increases the rate of material breakdown.**

This indicates that K-Ras could be associated with the increase in cell number found for the MSCs grown with the Sr containing material compositions. Studies have associated Ras family proteins with strontium signalling previously (126–128), further suggesting that the Sr released from the SrAW and SrAWGC actively influences the cell response, rather than the Sr substitution into the material acting through altering the surface topography. Sr will not have been affecting the cells in isolation, and could have been working together with the other ions released by the material. For example, Si and Mg are known to have many positive effects on osteoblasts (88,246,247,249) and MSCs (248), such as to encourage cell survival. However, there was a different response seen between the discs and glass conditioned media, with the higher Sr content discs (>12.5 Mol%) being detrimental to cell number. This could have been associated with the differing release rate of ions between the discs and glass conditioned media, or with the surface topography of the SrAWGC discs. Other studies have found osteogenic cells to be sensitive to material surfaces, as it was previously found that some heat treatments of the CaP sputter coating (altering the surface) could drastically lower cell proliferation (352). Another study found that simply changing the roughness of a bioactive glass surface had significant effects on cell morphology and mineralised nodule formation (241).

The glass conditioned media was relatively consistent and well defined, whilst the cells grown on the discs would have been exposed to a more dynamic environment. This is because as the cells were growing during the experiment, the disc would have been undergoing ion exchange with the media. Future work could determine more about the ion release profile of the discs, and perhaps determine whether there were events which could have been detrimental to the cells, such as an initial burst release of ions. This could have been the case for the higher strontium content discs as they showed increased ion release, and could explain the decreased cell number. For example, although Si is beneficial to cell growth, there is a critical threshold (>4 mM for osteosarcoma cells) above which it lowered cell number after just 1 day (249), hence controlled release of these ions is essential.

## 5.5 SrAWGC induces inflammatory gene expression in MSCs

The strongest finding of the RNAseq results was that the SrAWGC discs themselves raised the expression of cytokine induced inflammatory/stress response genesets such as “inflammatory response”, “Interferon Gamma Response” (IFNγ), “Interferon Alpha Response” (IFNα), and TGFβ in MSCs. Addition of strontium to the discs further enriched the inflammatory genesets, however, this was potentially not due to the strontium itself, as the Sr glass conditioned media instead lowered inflammatory gene expression. Instead, it could have been due to the increased dissolution of the Sr discs, potentially releasing debris (see Figure 87). It has been shown that macrophages and stromal cell types can show increased inflammatory cytokine production in response to glass particulate (305,306,353). Alternatively, it could have been associated with the rougher surface of the Sr discs (compared with culture plastic), particularly as previous studies have found that roughened titanium surfaces can induce cytokine (TGFβ) production in osteoblasts (295–297). Determining the mechanism behind this response would require further study, and could involve testing different aspects of the discs (such as surface roughness, or glass particulate) in isolation, to determine their effects on cell inflammatory gene expression.

As a bone tissue engineering scaffold it is important that the SrAWGC did not promote too severe an inflammatory response, as this could cause the failure of the therapy (334). The pilot rat *in vivo* study found that MSCs, induced by the SrAWGC to have increased inflammatory gene expression did not appear to prolong the normal sub-cutaneous implantation inflammatory response, as it was observed to decrease by day 3. This is beneficial, because controlled short term inflammatory stimuli can actually promote improved healing by encouraging cell recruitment to the engineered tissue, improved tissue healing, vascularisation and subsequently resulting in a better engineered tissue than one which induced next to no inflammatory response (334–338). The pilot study in this project has tested only whether the MSCs transformed by the SrAWGC could have a functional influence on inflammatory function. Given the results in this project indicate

that the SrAWGC actually raises the expression of inflammatory genes in MSCs, it would be important to determine what effects it could have on the other cells present at a wound site, such as immune cells.

This project has determined how Sr can alter the AWGC material, and what affects this can have on the MSCs. These findings will be useful in further developing SrAWGC into a 3D porous structure which would more closely resemble the architecture of bone. This could potentially be made by foam replication (103), 3D printing through selective laser sintering (104) or other methods (71). However, 3D structures add a great deal of complexity, not only in the fabrication and final form of the material, but also in the way the cells would respond. The addition of strontium to the AW glass affected how the material sintered, the resulting much larger surface area found in a porous 3D scaffold, could magnify any differences in the ion release rates, degradation, and consequently mechanical properties in the final scaffold. Furthermore, cells respond to 3D environments differently, as compared to 2D environments, and depending on the size of the pores could experience local differences in ion, waste and nutrient concentrations within the scaffold, thus future studies on these materials may have to be conducted with more dynamic culture conditions. This would involve using a spinner flask, or some form of microfluidics chamber to ensure media flowed over the scaffold-cell construct.

# Chapter 6 – Conclusions and Future Work

This work focused on exploring the effects of strontium substitution into apatite wollastonite glass-ceramic on MSCs, which together are a promising bone regeneration therapy. First the effect of the addition of strontium on the short and medium range order of the apatite wollastonite glass (associated with material degradation) was determined. The interactions between human Y201 mesenchymal stem cells and apatite wollastonite glass-ceramic with 0, 6.2, 12.5, 18.7, 24.9 and 37.4 Mol% Sr (and its dissolution products modelled using glass conditioned media) were explored using a range of media and osteogenic differentiation and growth/proliferation assays, alongside a global gene expression analysis using RNA sequencing gene expression analysis and an *in vivo* model. The key findings were:

- The substitution of Sr into the apatite wollastonite glass did not result in a change in short range order of the material, as the nearest neighbour atomic separations were found to be unchanged in distance (r), coordination (N) and disorder (σ). The Ca-O and Sr-O separations were found to exist in two populations.
- The substitution of Sr into the apatite wollastonite glass altered the medium range order of the material, gradually moving the orthophosphate to lower bond energy and decreasing its disorder. Additionally the percentage of $Q^3$ silica tetrahedrons (except at 24.9 Mol% Sr) and the oxygen density also decreased, whilst the density increased.
- All compositions of strontium apatite wollastonite glass could be successfully formed into apatite wollastonite glass-ceramic discs. The surface of the material was seen to change with increasing strontium content, becoming more granular and rough.
- The strontium apatite wollastonite glass and strontium apatite wollastonite glass-ceramic discs released ions after 24 hours in culture media. For the glass powder, the Sr and Ca were released in proportion to the Sr and Ca content of the glass. The Si and Mg release was not seen to change with Sr content in the glass. The

strontium apatite wollastonite glass-ceramic discs were also seen to release ions, with Sr release increasing with Sr content, alongside Si, Mg and Ca release, indicating the whole of the material broke down more quickly with strontium substitution. All glass and disc conditioned media showed reduced phosphorus content compared with control media.

- The Y201 MSCs attached to all of the compositions of the Sr apatite wollastonite glass-ceramic discs and the discs induced an increase in Y201 MSC number at 9 days with strontium substitution (reaching a peak at 6.2 Mol% Sr), though proliferation was not seen to change, suggesting improved cell survival. Strontium substitution into the discs was also seen to retard cell osteogenic differentiation.
- The ions released by the material (modelled using glass conditioned media) were seen to raise Y201 MSC number and retard osteogenic differentiation with Sr substitution (peaking at 12.5 Mol% Sr). Additionally, Y201 MSC number was found to rise in response to Sr alone (peaking at 1mM).
- The global gene expression analysis of Y201 MSCs showed that at 24 hours of exposure the discs raised the expression of genes associated with inflammation (primarily Interferon Gamma and Alpha response) and proliferation/survival (K-Ras signalling and lowering P53). The addition of strontium to the material was seen to exacerbate the expression of many of these gene groupings. Strontium addition (12.5 Mol%) induced a relatively small change in gene expression
- *In vivo* analysis showed that MSCs exposed to the glass-ceramic and implanted subcutaneously in collagen gels in rats did not induce a prolonged inflammatory response. The strontium content and exposure of the cells to the glass ceramic discs or glass conditioned media had no observable effect on the result.

Therefore, this material represents a promising bone tissue engineering scaffold because a small level of strontium substitution can support mesenchymal stem cell growth and survival and potentially induce a brief inflammatory stimulus which could be beneficial to wound healing.

This study focused not only on the effects adding strontium had on the SrAWGC, but also specifically what the strontium in the material was doing to the cells. However, this was just one facet of the material and there remain many avenues which could be explored. The glass and glass-ceramic were seen to release Ca, Mg, Si and to remove P in addition to releasing Sr. Future work could expose MSCs to different concentrations of these elements, to determine what effects these other components of the material were having on the cells. This is important as its well known that therapeutic ions released by bioactive glasses can have a number of beneficial effects, with Si and Mg having been associated with differentiation and proliferation (72).

It was found that one of the effects of strontium addition to the SrAWGC was to alter the surface topography of the material, and this could have also altered MSC behaviour and gene expression. Hence, a significant area of future work would be to characterise this change in surface roughness precisely as a function of strontium content in the material. This could be using a surface profilometre (either with stylus or using light) or through Atomic Force Microscopy (which would offer a much higher spatial resolution measurement of surface roughness). The impact of the surface roughness on cell behaviour could also be explored by polishing the surface of the different strontium compositions flat, to provide a consistent surface. Cells could then be grown on the polished discs and compared with those grown on unpolished discs. These polished discs could also be used to explore the mechanism behind the differing ion release rate between the different compositions, as it could have been related to differing surface areas between the different strontium compositions.

The SrAWGC was tested using immortalised Y201 human MSCs as a reproducible model cell line. It would be valuable to do further studies with primary MSCs taken from donors to confirm the findings of MSC growth and changes in gene expression. Additionally, other cell types could be used, such as immune cells to explore the consequences of the raised cytokine production of the MSCs when exposed to the SrAWGC.

Perhaps the most important area of future work is the progression of this material into a 3D tissue engineering scaffold, and subsequent confirmation of the findings here. There are a vast number of ways in which the material could be formed into a 3D scaffold, of which three have already been used on the base composition of AWGC, namely selective laser sintering (or other forms of 3D printing)(118), loose powder moulding (102) and foam-slurry method (103). Redesigning the material into a 3D scaffold would, however, be a substantial piece of work as many aspects of the scaffold could be altered to refine it. These include particle size of the glass used in its creation, the type of mould or foam (different materials could be used), the quantity of strontium used (which could depend on how readily it is released) and the heating regime that must be employed to produce the correct final material. In particular, given the observed differences in the strontium AWGC discs from those without strontium, it would useful to determine whether different heating regimes for the strontium conditions could alter the final surface of the material and perhaps make them more similar.

As the ultimate aim is to use this material in the clinic as a bone regeneration aid, further *in vitro* and *in vivo* testing will be required on any subsequent 3D scaffolds. The *in vitro* tests performed on the 3D scaffolds would be necessary to confirm that the 3D iteration of the material encouraged the cells to respond in a similar (and positive) manner as was observed for the 2D discs. *In vivo* studies would be necessary to gauge both the response of the material to the more complex environment of living tissue, but also to better model how cells could grow and respond to the material when they were immersed in a more representative biological fluid. This could be performed in a number of ways, with sub-cutaneous implantation being a relatively simple surgery which could be used to easily explore the material-cell interaction and surrounding tissue response, whilst a bone defect study could be used to study the long term ability of the cell-scaffold construct to actually repair bone *in situ*. This could then progress eventually from animal to human trials, to further refine the material into an effective bone regeneration therapy.

# Appendix A

Neutron diffraction GEM detector bank data combination.

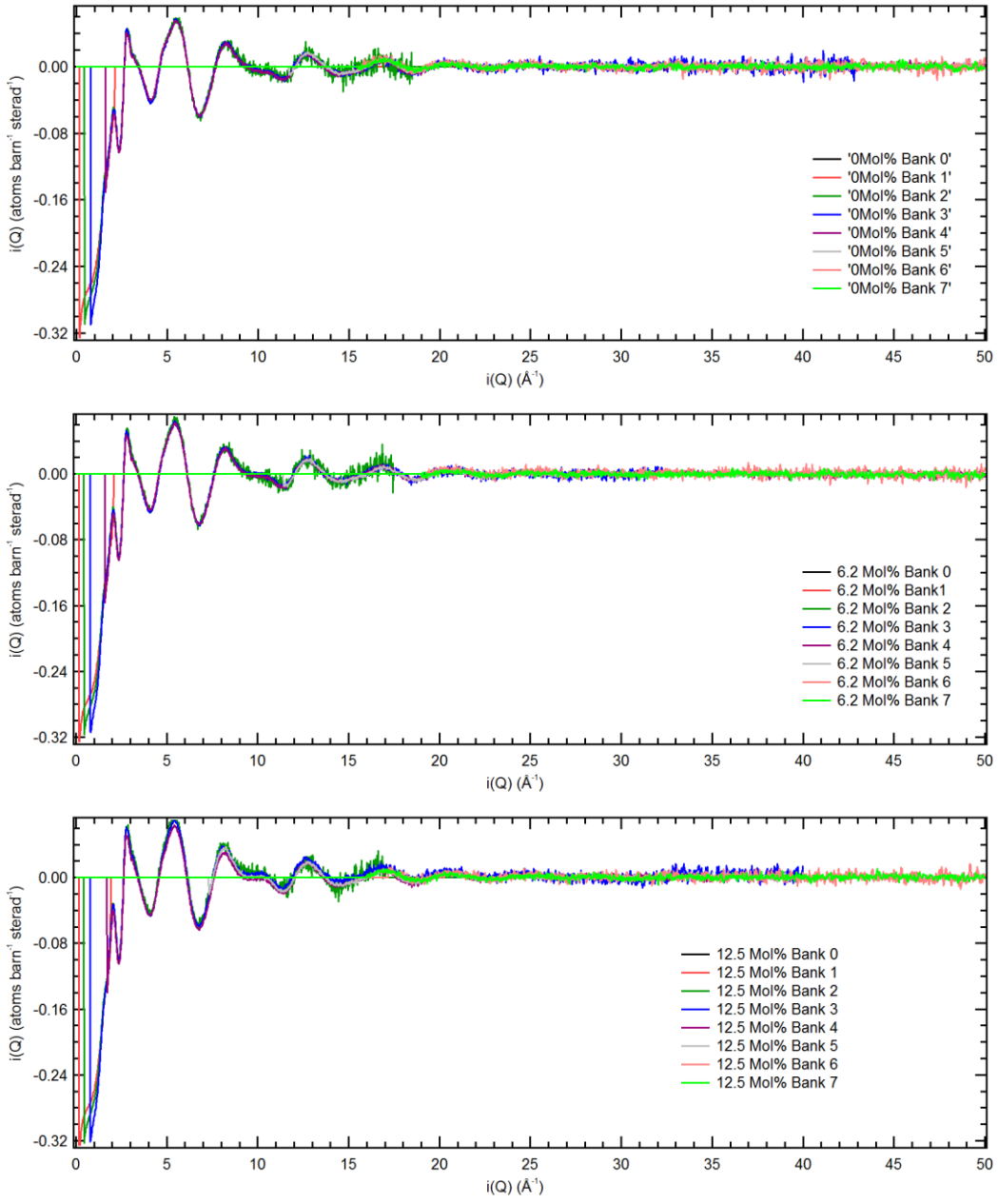


**Figure 88: The reciprocal space neutron diffraction signal (the DCS, i(Q)) for the individual GEM detector banks for the 0, 6.2 and 12.5 Mol% Sr glass compositions.**

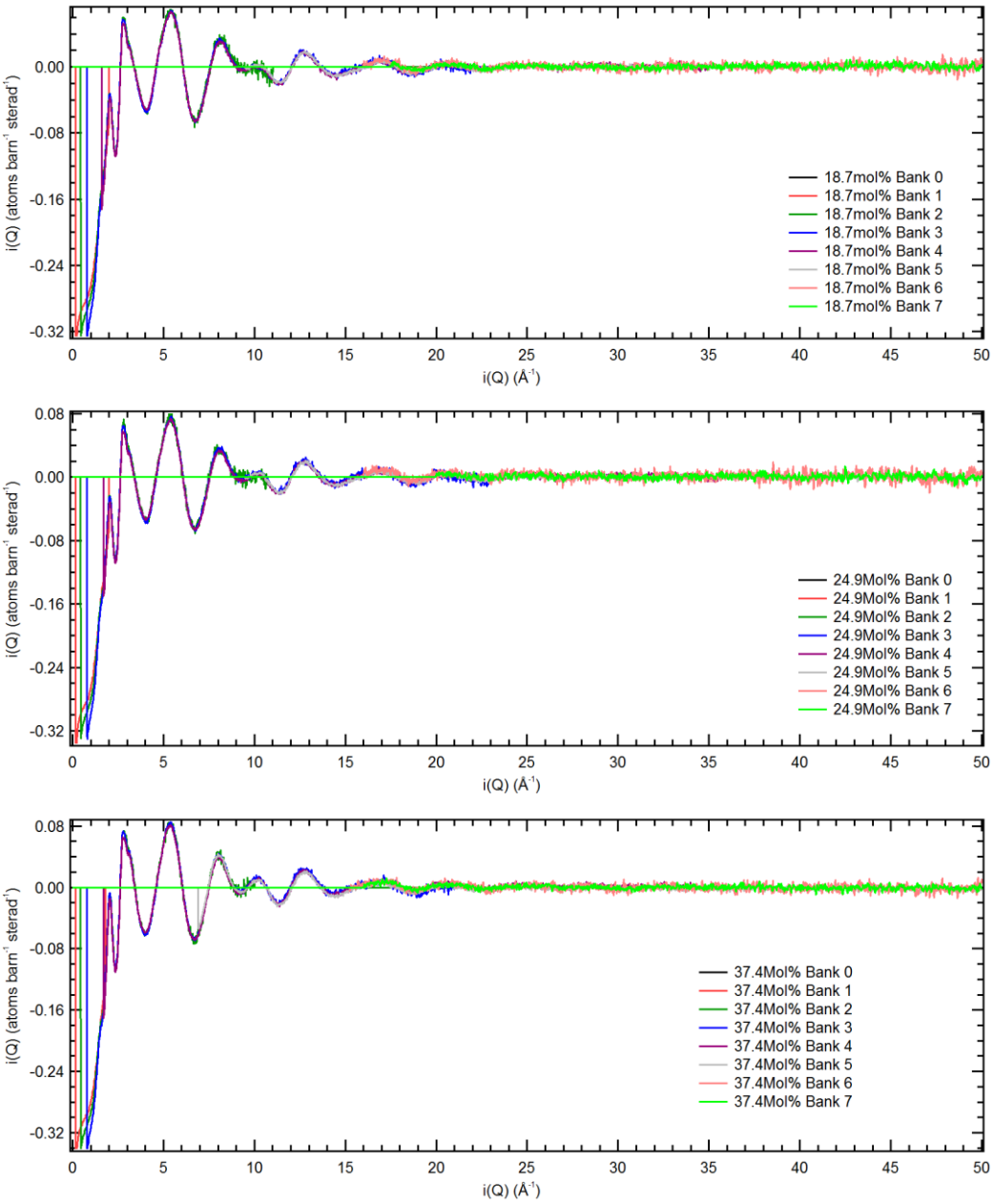


**Figure 89: The reciprocal space neutron diffraction signal (the DCS, i(Q)) for the individual GEM detector banks for the 18.7, 24.9 and 37.4 Mol% Sr glass compositions.**

# Appendix B

Convergence tests on the Raman spectra taken of the SrAW glass. The change in the percent standard error in the Peak 860 again Peak 950 ratio was used to determine whether sufficient measurements were taken.

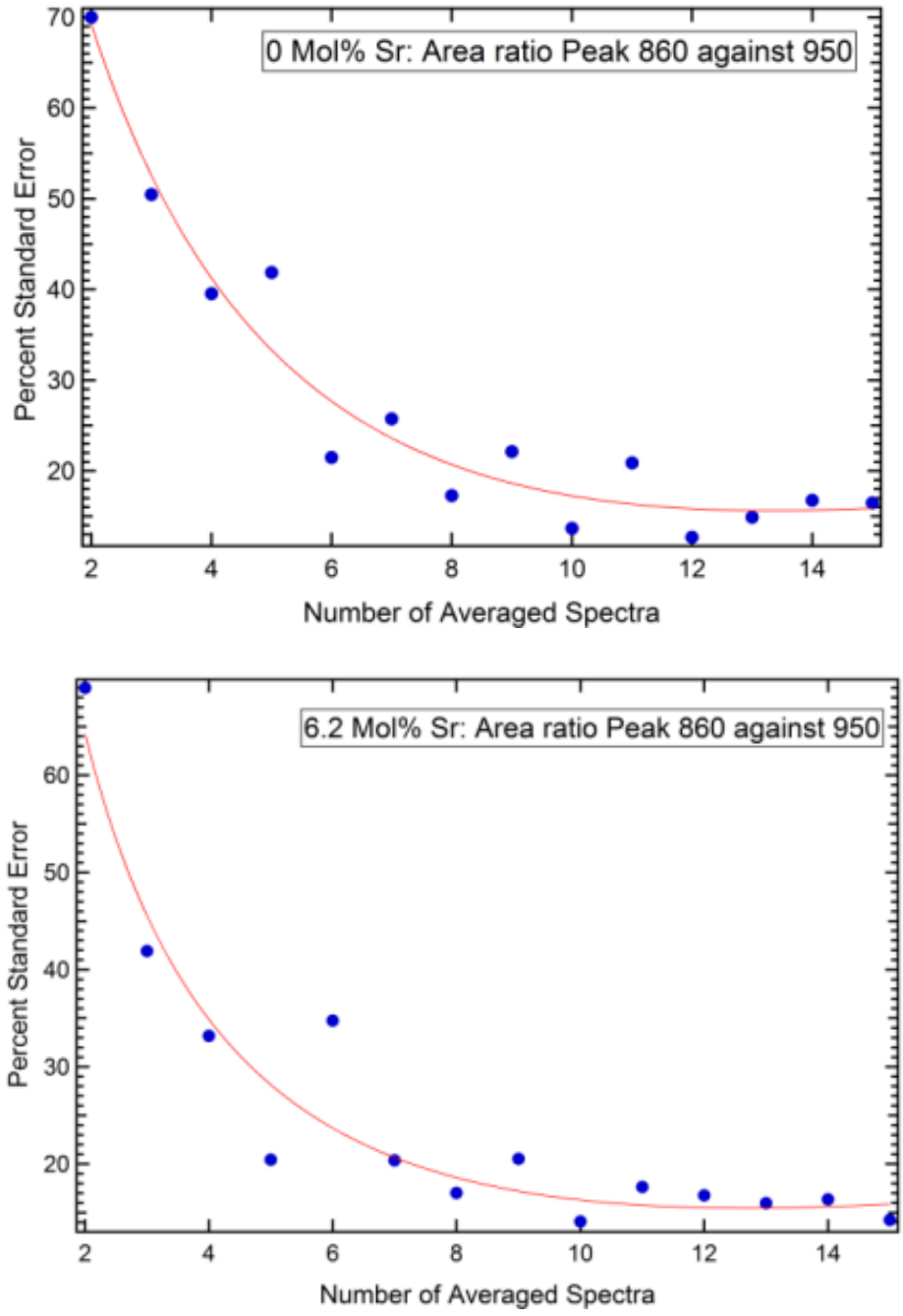


**Figure 90: Convergence tests of Peak 1 / Peak 2 area ratios averages of up to 15 Raman spectra taken of the 0 and 6.2 compositions of SrAW glass.**

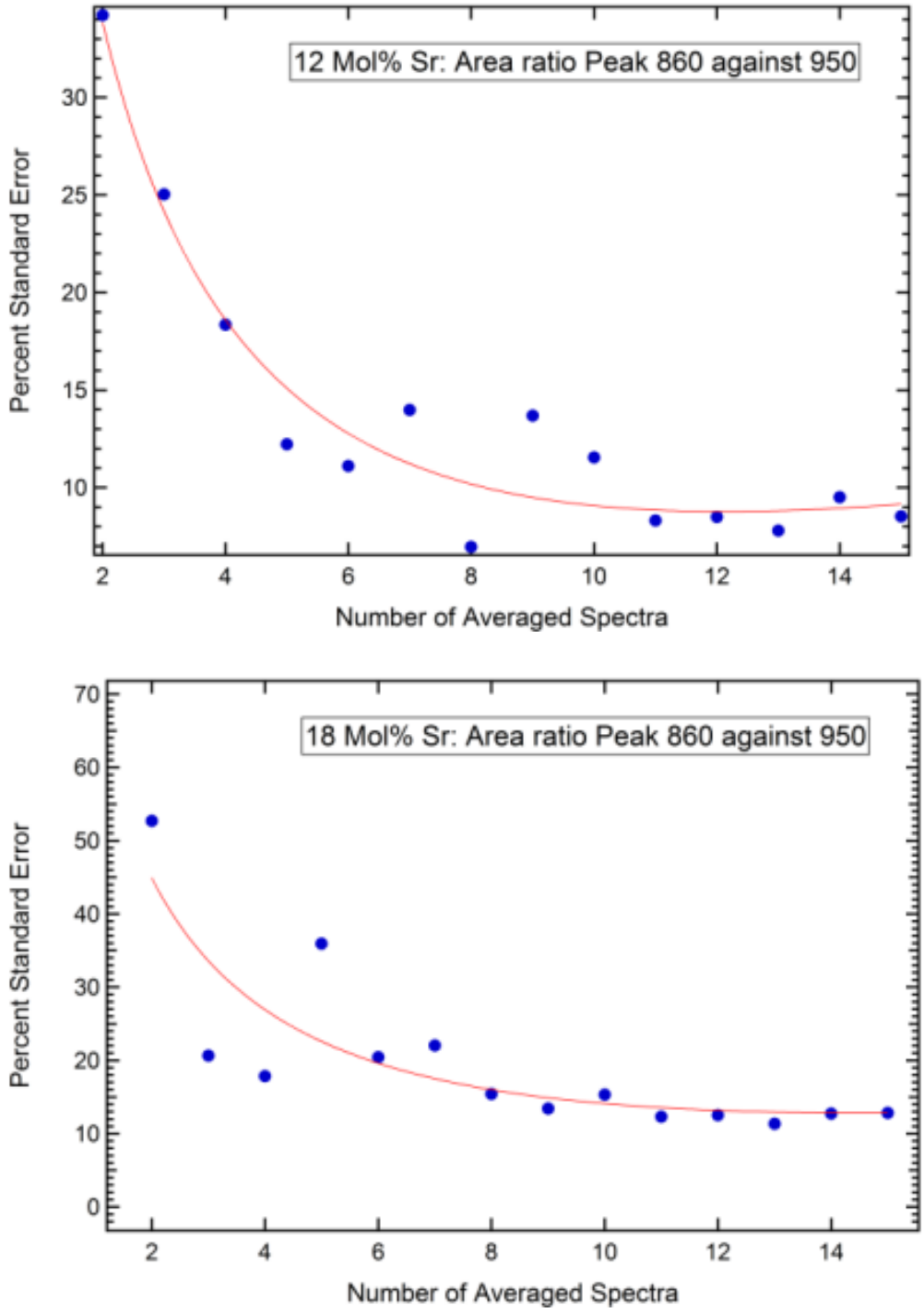


**Figure 91: Convergence tests of Peak 1 / Peak 2 area ratios averages of up to 15 Raman spectra taken of the 12.5 and 18.7 Mol% compositions of SrAW glass.**

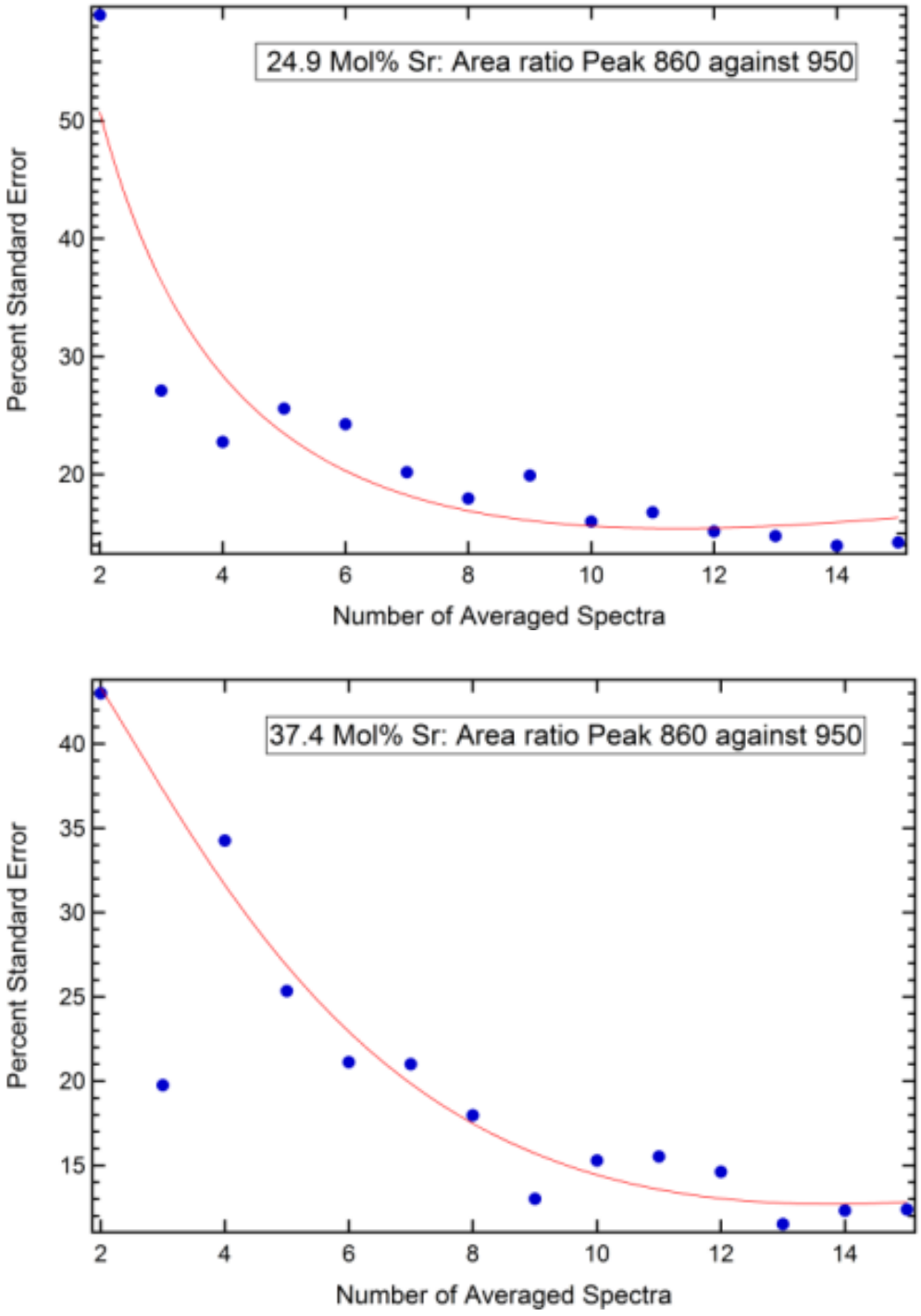


**Figure 92: Convergence tests of Peak 1 / Peak 2 area ratios averages of up to 15 Raman spectra taken of the 24.9 and 37.4 Mol% compositions of SrAW glass.**

# Abbreviations

| | |
|---|---|
| ALP | Alkaline phosphatase |
| AW | Apaptite wollastonite |
| AWGC | Apatite wollastonite glass-ceramic |
| BMP | Bone morphogenic protein |
| BMU | basic multicellular unit |
| BO | Bridging oxygen |
| c-MYC | c-Myelocytomatosis |
| DCS | Differential Cross Section |
| DMEM | Dulbecco’s Modified Eagles Medium |
| EDTA | Ethylene-diamine-tetra-acetic-acid |
| EMT | Epithelial–mesenchymal transition |
| ERK | Extracellular signal regulated kinase |
| FBS | Foetal Bovine Serum |
| FGF | Fibroblast Growth Factor |
| FWHM | Full width half maximum |
| HA | Hydroxyapatite |
| hTERT | human Telomerase reverse transcriptase |
| HWB | High Wavenumber Band |
| i(Q) | coherent neutron diffraction scattering intensity |
| lFNα | Interferon alpha |
| lFNβ | Interferon gamma |
| IL6 | Interleukin 6 |
| MAPK | Mitogen activated protein kinase |

| | |
|---|---|
| MAS-NMR | Magic Angle Spinning Nuclear Magnetic Resonance |
| Mol% | Mole percent |
| NBO | Non bridging oxygen |
| NC | Network Connectivity |
| NFATc | Calcineurin/Nuclear Factor of Activated T cell |
| NFκB | Nuclear Factor κB |
| $N_x$ | Coordination number |
| $O_B$ | Bridging oxygen |
| OCN | Osteocalcin |
| $O_{NB}$ | Non bridging oxygen |
| OPG | Osteoprotegerin |
| OPN | Osteopontin |
| OSX | Osterix |
| PBMC | Peripheral blood mononuclear cells |
| PBS | Phosphate Buffered Saline |
| PCL | Polycaprolactone |
| PEG | Poly(ethylene glycol) |
| pNPP | p-Nitrophenyl Phosphate |
| PVA | Polyvinyl alcohol |
| RANKL | Receptor activator of nuclear factor kappa-B ligand |
| SEM | Scanning electron microscope |
| SrAW | Strontium apatite wollastonite |
| SrAWGC | Strontium apatite wollastonite glass-ceramic |
| T(r) | Total neutron diffraction correlation function |
| TGFβ | Transforming Growth Factor Beta |

| | |
|---|---|
| TNFα | Tumour Necrosis Factor Alpha |
| $\sigma_x$ | disorder parameter |

## References

1. Miranda MA, Moon M. Treatment strategy for nonunions and malunions. Surg Treat Orthop Trauma. 2007;
2. Nandra R, Grover L, Porter K. Fracture non-union epidemiology and treatment. Trauma. 2016.
3. Schlundt C, Bucher CH, Tsitsilonis S, Schell H, Duda GN, Schmidt-Bleek K. Clinical and Research Approaches to Treat Non-union Fracture. Current Osteoporosis Reports. 2018.
4. Van Staa TP, Dennison EM, Leufkens HGM, Cooper C. Epidemiology of fractures in England and Wales. Bone. 2001;29(6):517–22.
5. Harvey N, Dennison E, Cooper C. Osteoporosis: Impact on health and economics. Nat Rev Rheumatol. Nature Publishing Group; 2010;6(2):99–105.
6. Henkel J, Woodruff MA, Epari DR, Steck R, Glatt V, Dickinson IC, et al. Bone Regeneration Based on Tissue Engineering Conceptions — A 21st Century Perspective. Bone Res. Sichuan University; 2013;1(3):216–48.
7. Hinsenkamp M, Muylle L, Eastlund T, Fehily D, Noël L, Strong DM. Adverse reactions and events related to musculoskeletal allografts: Reviewed by the World Health Organisation Project NOTIFY. Int Orthop. 2012;36(3):633–41.
8. Moore WR, Graves SE, Bain GI. Synthetic bone graft substitutes. ANZ Journal of Surgery. 2001.
9. Kokubo T. Bioactive glass ceramics: properties and applications. Biomaterials. 1991;12(2):155–63.
10. Kokubo T, Yamaguchi S. Novel Bioactive Materials Derived by Bioglass: Glass-Ceramic A-W and Surface-Modified Ti Metal. Int J Appl Glas Sci. 2016;
11. Pilmane M, Salma-Ancane K, Loca D, Locs J, Berzina-Cimdina L.

Strontium and strontium ranelate: Historical review of some of their functions. Mater Sci Eng C. 2017;

12. Aaseth J, Boivin G, Andersen O. Osteoporosis and trace elements - An overview. J Trace Elem Med Biol. Elsevier GmbH.; 2012;26(2–3):149–52.

13. Bar-Shavit Z. The osteoclast: A multinucleated, hematopoietic-origin, bone-resorbing osteoimmune cell. J Cell Biochem. 2007;102(5):1130–9.

14. Cowen SC. Bone Mechanics Handbook. 2nd ed. London: CRC Press; 2001.

15. Crockett JC, Rogers MJ, Coxon FP, Hocking LJ, Helfrich MH. Bone remodelling at a glance. J Cell Sci. 2011 Apr 1;124(7):991–8.

16. Clarke B. Normal bone anatomy and physiology. Clin J Am Soc Nephrol. 2008 Nov 1;3 Suppl 3(17):S131-9.

17. Baroli B. From natural bone grafts to tissue engineering therapeutics: Brainstorming on pharmaceutical formulative requirements and challenges. J Pharm Sci. 2009 Apr;98(4):1317–75.

18. Servier Medical Art. Bone Structure [Internet]. 2018. Available from: https://smart.servier.com/

19. Alford AI, Kozloff KM, Hankenson KD. Extracellular matrix networks in bone remodeling. Int J Biochem Cell Biol. 2015 May;

20. Fantner GE, Adams J, Turner P, Thurner PJ, Fisher LW, Hansma PK. Nanoscale ion mediated networks in bone: Osteopontin can repeatedly dissipate large amounts of energy. Nano Lett. 2007;7(8):2491–8.

21. Poundarik AA, Diab T, Sroga GE, Ural A, Boskey AL, Gundberg CM, et al. Dilatational band formation in bone. Proc Natl Acad Sci. 2012;109(47):19178–83.

22. Parfitt AM. Targeted and nontargeted bone remodeling: Relationship to basic multicellular unit origination and progression. Bone. 2002;30(1):5–7.

23. Jilka RL, Noble B, Weinstein RS. Osteocyte apoptosis. Bone. 2013 Jun;54(2):264–71.

24. Raggatt LJ, Partridge NC. Cellular and Molecular Mechanisms of Bone Remodeling. J Biol Chem. 2010 Aug 13;285(33):25103–8.

25. Hadjidakis DJ, Androulakis II. Bone remodeling. Ann N Y Acad Sci. 2006;1092:385–96.

26. Florencio-Silva R, Sasso GR da S, Sasso-Cerri E, Simões MJ, Cerri PS. Biology of Bone Tissue: Structure, Function, and Factors That Influence Bone Cells. Biomed Res Int. 2015;2015:1–17.

27. Simonet W., Lacey D., Dunstan C., Kelley M, Chang M-S, Lüthy R, et al. Osteoprotegerin: A Novel Secreted Protein Involved in the Regulation of Bone Density. Cell. 1997;89(2):309–19.

28. Tang Y, Wu X, Lei W, Pang L, Wan C, Shi Z, et al. TGF-B1-induced migration of bone mesenchymal stem cells couples bone resorption with formation. Nat Med. 2009;15(7):757–65.

29. Crane JL, Cao X. Bone marrow mesenchymal stem cells andTGF-ß signaling in bone remodeling. J Clin Invest. 2014;124(2):466–72.

30. Frith J, Genever P. Transcriptional Control of Mesenchymal Stem Cell Differentiation. Transfus Med Hemotherapy. 2008;35(3):216–27.

31. Franz-Odendaal TA, Hall BK, Witten PE. Buried alive: How osteoblasts become osteocytes. Developmental Dynamics. 2006.

32. Schaffler MB, Cheung W-Y, Majeska R, Kennedy O. Osteocytes: Master Orchestrators of Bone. Calcif Tissue Int. 2014 Jan 17;94(1):5–24.

33. O'Brien CA, Nakashima T, Takayanagi H. Osteocyte control of osteoclastogenesis. Bone. 2013 Jun;54(2):258–63.

34. Li X, Zhang Y, Kang H, Liu W, Liu P, Zhang J, et al. Sclerostin binds to LRP5/6 and antagonizes canonical Wnt signaling. J Biol Chem. 2005;280(20):19883–7.

35. Mann V, Huber C, Kogianni G, Jones D, Noble B. The influence of mechanical stimulation on osteocyte apoptosis and bone viability in

human trabecular bone. J Musculoskelet Neuronal Interact. 2006;6(4):408–17.

36. Heino TJ, Hentunen TA, Kalervo Vnnen H. Osteocytes inhibit osteoclastic bone resorption through transforming growth factor-??: Enhancement by estrogen. J Cell Biochem. 2002;85(1):185–97.

37. Nombela-Arrieta C, Ritz J, Silberstein LE. The elusive nature and function of mesenchymal stem cells. Nat Rev Mol Cell Biol. 2011 Feb 1;12(2):126–31.

38. da Silva Meirelles L. Mesenchymal stem cells reside in virtually all post-natal organs and tissues. J Cell Sci. 2006;119(11):2204–13.

39. James S, Fox J, Afsari F, Lee J, Clough S, Knight C, et al. Multiparameter Analysis of Human Bone Marrow Stromal Cells Identifies Distinct Immunomodulatory and Differentiation-Competent Subtypes. Stem cell reports. Elsevier Inc.; 2015;4(6):1004–15.

40. Ḃuhring HJ, Battula VL, Treml S, Schewe B, Kanz L, Vogel W. Novel markers for the prospective isolation of human MSC. Annals of the New York Academy of Sciences. 2007. p. 262–71.

41. Wu M, Chen G, Li YP. TGF-β and BMP signaling in osteoblast, skeletal development, and bone formation, homeostasis and disease. Bone Res. 2016;4(March).

42. Gao F, Chiu SM, Motan DAL, Zhang Z, Chen L, Ji H-L, et al. Mesenchymal stem cells and immunomodulation: current status and future prospects. Cell Death Dis. 2016;7(1):e2062.

43. McKibbin B. The biology of fracture healing in long bones. J Bone Joint Surg Br. 1978;

44. Harten RD, Lee FY, Zimmerman MC, Hurowitz E, Arakal R, Behrens FF. Regional and temporal changes in the acoustic properties of fracture callus in secondary bone healing. J Orthop Res. 1997 Jul;15(4):570–6.

45. Marsell R, Einhorn TA. The biology of fracture healing. Injury. 2011 Jun;42(6):551–5.

46. Mountziaris PM, Dennis Lehman E, Mountziaris I, Sing DC, Kurtis Kasper F, Mikos AG. Effect of temporally patterned TNF-α delivery on in vitro osteogenic differentiation of mesenchymal stem cells cultured on biodegradable polymer scaffolds. J Biomater Sci Polym Ed. 2013;24(15):1794–813.

47. Pricola KL, Kuhn NZ, Haleem-Smith H, Song Y, Tuan RS. Interleukin-6 maintains bone marrow-derived mesenchymal stem cell stemness by an ERK1/2-dependent mechanism. J Cell Biochem. 2009 Oct 15;108(3):577–88.

48. Yang X, Ricciardi BF, Hernandez-Soria A, Shi Y, Pleshko Camacho N, Bostrom MPG. Callus mineralization and maturation are delayed during fracture healing in interleukin-6 knockout mice. Bone. 2007;41(6):928–36.

49. Keating JF. The management of fractures with bone loss. J Bone Jt Surg - Br Vol. 2005;87–B(2):142–50.

50. Ayoub MA, El-Rosasy MA. Hybrid grafting of post-traumatic bone defects using β-tricalcium phosphate and demineralized bone matrix. Eur J Orthop Surg Traumatol. 2014;24(5):663–70.

51. Szulc P, Seeman E. Thinking inside and outside the envelopes of bone : DDDedicated to PDD. Osteoporos Int. 2009;20(8):1281–8.

52. Raisz LG. Pathogenesis of osteoporosis: concepts, conflicts, and prospects. J Clin Invest. 2005 Dec 1;115(12):3318–25.

53. Gómez-Barrena E, Rosset P, Lozano D, Stanovici J, Ermthaller C, Gerbhard F. Bone fracture healing: Cell therapy in delayed unions and nonunions. Bone. The Authors; 2015;70:93–101.

54. Shrivats AR, McDermott MC, Hollinger JO. Bone tissue engineering: State of the union. Drug Discov Today. 2014;19(6):781–6.

55. Isaac J, Nohra J, Lao J, Jallot E, Nedelec J-MM, Berdal A, et al. Effects of strontium-doped bioactive glass on the differentiation of cultured osteogenic cells. Eur Cell Mater. 2011 Jan;21:130–43.

56. Langer R, Vacanti JP. Tissue engineering. Science. 1993;260:920–6.

57. Mahfouz W, Elsalmy S, Corcos J, Fayed AS. Fundamentals of bladder tissue engineering. African J Urol. Pan African Urological Surgeons' Association.; 2013;19(2):51–7.

58. Gaalen S van, Kruyt M, Meijer G, Mistry A, Mikos A, Beucken J van den, et al. Chapter 19 – Tissue engineering of bone. Tissue Engineering. Elsevier; 2008. p. 559–610.

59. Fu Q, Saiz E, Rahaman MN, Tomsia AP. Bioactive glass scaffolds for bone tissue engineering: state of the art and future perspectives. Mater Sci Eng C. Elsevier B.V.; 2011 Oct 10;31(7):1245–56.

60. Billström GH, Blom AW, Larsson S, Beswick AD. Application of scaffolds for bone regeneration strategies: current trends and future directions. Injury. Elsevier Ltd; 2013 Jan;44 Suppl 1:S28-33.

61. Hench LL. Third-Generation Biomedical Materials. Science (80- ). 2002 Feb 8;295(5557):1014–7.

62. García-Gareta E, Coathup MJ, Blunn GW. Osteoinduction of bone grafting materials for bone repair and regeneration. Bone. 2015 Jul 8;81:112–21.

63. Burg KJ., Porter S, Kellam JF. Biomaterial developments for bone tissue engineering. Biomaterials. 2000 Dec;21(23):2347–59.

64. Albrektsson T, Johansson C. Osteoinduction, osteoconduction and osseointegration. Eur Spine J. 2001 Oct;10 Suppl 2(S):S96-101.

65. Jell G, Notingher I, Tsigkou O, Notingher P, Polak JM, Hench LL, et al. Bioactive glass-induced osteoblast differentiation: a noninvasive spectroscopic study. J Biomed Mater Res A. 2008 Jul;86(1):31–40.

66. Yuan H, De Bruijn JD, Zhang X, Van Blitterswijk CA, De Groot K. Bone induction by porous glass ceramic made from Bioglass® (45S5). J Biomed Mater Res. 2001;58(3):270–6.

67. Dalby MJ, Gadegaard N, Tare R, Andar A, Riehle MO, Herzyk P, et al. The control of human mesenchymal cell differentiation using nanoscale symmetry and disorder. Nat Mater. 2007 Dec 23;6(12):997–1003.

68. Lei B, Chen X, Wang Y, Zhao N, Du C, Fang L. Surface nanoscale patterning of bioactive glass to support cellular growth and differentiation. J Biomed Mater Res - Part A. 2010;94(4):1091–9.

69. de Peppo GM, Agheli H, Karlsson C, Ekström K, Brisby H, Lennerås M, et al. Osteogenic response of human mesenchymal stem cells to well defined nanoscale topography in vitro. Int J Nanomedicine. 2014;accepted f:2499–515.

70. Jeong K-H, Park D, Lee Y-C. Polymer-based hydrogel scaffolds for skin tissue engineering applications: a mini-review. J Polym Res. Journal of Polymer Research; 2017;24(7):112.

71. Jones JR. Review of bioactive glass: from Hench to hybrids. Acta Biomater. Acta Materialia Inc.; 2013 Sep;9(1):4457–86.

72. Hoppe A, Güldal NS, Boccaccini AR. A review of the biological response to ionic dissolution products from bioactive glasses and glass-ceramics. Biomaterials. 2011;32(11):2757–74.

73. Roura S, Farré J, Soler-Botija C, Llach A, Hove-Madsen L, Cairó JJ, et al. Effect of aging on the pluripotential capacity of human CD105+ mesenchymal stem cells. Eur J Heart Fail. 2006;8(6):555–63.

74. Pennock R, Bray E, Pryor P, James S, McKeegan P, Sturmey R, et al. Human cell dedifferentiation in mesenchymal condensates through controlled autophagy. Sci Rep. 2015 Aug 20;5:13113.

75. Sittichokechaiwut A. Dynamic mechanical stimulation for bone tissue engineering. University of Sheffield; 2009.

76. Park SH, Park SA, Kang YG, Shin JW, Park YS, Gu SR, et al. PCL/β-TCP Composite Scaffolds Exhibit Positive Osteogenic Differentiation with Mechanical Stimulation. Tissue Eng Regen Med. Korean Tissue Engineering and Regenerative Medicine Society; 2017;14(4):349–58.

77. Mouriño V, Cattalini JP, Boccaccini AR. Metallic ions as therapeutic agents in tissue engineering scaffolds: an overview of their biological applications and strategies for new developments. J R Soc Interface. 2012;9(68):401–19.

78. Xynos ID, Edgar AJ, Buttery LDKK, Hench LL, Polak JM. Gene-expression profiling of human osteoblasts following treatment with the ionic products of Bioglass® 45S5 dissolution. J Biomed Mater Res. 2001 May;55(2):151–7.

79. Xynos ID, Edgar a J, Buttery LD, Hench LL, Polak JM. Ionic products of bioactive glass dissolution increase proliferation of human osteoblasts and induce insulin-like growth factor II mRNA expression and protein synthesis. Biochem Biophys Res Commun. 2000;276(2):461–5.

80. Hench LL. Genetic design of bioactive glass. J Eur Ceram Soc. 2009 Apr;29(7):1257–65.

81. Kapoor S, Goel A, Tilocca A, Dhuna V, Bhatia G, Dhuna K, et al. Role of glass structure in defining the chemical dissolution behavior, bioactivity and antioxidant properties of zinc and strontium co-doped alkali-free phosphosilicate glasses. Acta Biomater. Acta Materialia Inc.; 2014 Jul;10(7):3264–78.

82. Pina S, Vieira S, Rego P, Torres P, da Cruz e Silva O, da Cruz e Silva E, et al. Biological responses of brushite-forming Zn- and ZnSr-substituted beta-tricalcium phosphate bone cements. Eur Cells Mater. 2010;20:162–77.

83. Hu D, Li K, Xie Y, Pan H, Zhao J, Huang L, et al. Different response of osteoblastic cells to Mg2+, Zn2+ and Sr2+ doped calcium silicate coatings. J Mater Sci Mater Med. 2016 Mar 19;27(3):56.

84. Gentleman E, Fredholm YC, Jell G, Lotfibakhshaiesh N, O'Donnell MD, Hill RG, et al. The effects of strontium-substituted bioactive glasses on osteoblasts and osteoclasts in vitro. Biomaterials. Elsevier Ltd; 2010;31(14):3949–56.

85. O'Donnell MD, Candarlioglu PL, Miller C a., Gentleman E, Stevens MM. Materials characterisation and cytotoxic assessment of strontium-substituted bioactive glasses for bone regeneration. J Mater Chem. 2010;20(40):8934.

86. Liu J, Rawlinson SCFF, Hill RG, Fortune F. Strontium-substituted

bioactive glasses in vitro osteogenic and antibacterial effects. Dent Mater. The Academy of Dental Materials; 2016 Jan;32(3):412–22.

87. Autefage H, Gentleman E, Littmann E, Hedegaard MAB, Von Erlach T, O'Donnell M, et al. Sparse feature selection methods identify unexpected global cellular response to strontium-containing materials. Proc Natl Acad Sci. 2015 Apr 7;112(14):4280–5.

88. Zreiqat H, Howlett CR, Zannettino A, Evans P, Schulze-Tanzil G, Knabe C, et al. Mechanisms of magnesium-stimulated adhesion of osteoblastic cells to commonly used orthopaedic implants. J Biomed Mater Res. 2002 Nov;62(2):175–84.

89. Zhang J, Ma X, Lin D, Shi H, Yuan Y, Tang W, et al. Magnesium modification of a calcium phosphate cement alters bone marrow stromal cell behavior via an integrin-mediated mechanism. Biomaterials. Elsevier Ltd; 2015 Jun;53:251–64.

90. Wu C, Zhou Y, Xu M, Han P, Chen L, Chang J, et al. Copper-containing mesoporous bioactive glass scaffolds with multifunctional properties of angiogenesis capacity, osteostimulation and antibacterial activity. Biomaterials. 2013 Jan;34(2):422–33.

91. Zhao S, Wang H, Zhang Y, Huang W, Rahaman MN, Liu Z, et al. Copper-doped borosilicate bioactive glass scaffolds with improved angiogenic and osteogenic capacity for repairing osseous defects. Acta Biomater. 2014 Dec;

92. Duminis T, Shahid S, Hill RG. Apatite Glass-Ceramics: A Review. Front Mater. 2017;3(January):1–15.

93. Kokubo T. Bioactive Glass Ceramics. In: Kokubo T, editor. Bioceramics and their clinical applications. Elsevier; 2008. p. 284–301.

94. Kaur G, Pandey OP, Singh K, Homa D, Scott B, Pickrell G. A review of bioactive glasses: Their structure, properties, fabrication and apatite formation. J Biomed Mater Res Part A. 2014 Jan 6;102(1):254–74.

95. Boskey AL. Natural and Synthetic Hydroxyapatites. Third Edit. Biomaterials Science: An Introduction to Materials: Third Edition. Elsevier; 2013. 151-161 p.

96. El-Rashidy AA, Roether JA, Harhaus L, Kneser U, Boccaccini AR. Regenerating bone with bioactive glass scaffolds: A review of in vivo studies in bone defect models. Acta Biomater. Acta Materialia Inc.; 2017;62:1–28.

97. Wagoner Johnson AJ, Herschler BA. A review of the mechanical behavior of CaP and CaP/polymer composites for applications in bone replacement and repair. Acta Biomater. 2011;7(1):16–30.

98. Jell G, Stevens MM. Gene activation by bioactive glasses. J Mater Sci Mater Med. 2006;17(11):997–1002.

99. Boccardi E, Ciraldo FE, Boccaccini AR. Bioactive glass-ceramic scaffolds: Processing and properties. MRS Bull. 2017;42(3):226–32.

100. Turunen T, Peltola J, Yli-Urpo A, Happonen RP. Bioactive glass granules as a bone adjunctive material in maxillary sinus floor augmentation. Clin Oral Implants Res. 2004;

101. Chen QZ, Thompson ID, Boccaccini AR. 45S5 Bioglass-derived glass-ceramic scaffolds for bone tissue engineering. Biomaterials. 2006 Apr;27(11):2414–25.

102. Vickers WOM. The Effect of Strontium Substitution on Apatite-Wollastonite Glass- Ceramics. 2013;(August).

103. Serna CA. Development of a synthetic trabecular bone graft utilizing a two phase glass-ceramic. University of Leeds; 2016.

104. Dyson JA, Genever PG, Dalgarno KW, Wood DJ. Development of custom-built bone scaffolds using mesenchymal stem cells and apatite-wollastonite glass-ceramics. Tissue Eng. 2007 Dec;13(12):2891–901.

105. Shelby JE. Structures of glasses. In: Shelby JE, editor. Introduction to Glass Science and Technology. 2nd ed. Cambridge: Royal Society of Chemistry; 2005. p. 72–110.

106. Zachariasen WH. THE ATOMIC ARRANGEMENT IN GLASS. J Am Chem Soc. 1932 Oct;54(10):3841–51.

107. Rawlings RD. Bioactive glasses and glass-ceramics. Clin Mater. 1993

Jan;14(2):155–79.

108. Shelby JE. Principles of glass formation. In: Shelby JE, editor. Introduction to Glass Science and Technology. 2nd ed. Cambridge: Royal Society of Chemistry; 2005. p. 7–25.

109. Hench LL. The story of Bioglass®. J Mater Sci Mater Med. 2006 Nov 22;17(11):967–78.

110. Jones JR. Bioactive Glass. In: Kokubo T, editor. Bioceramics and their Clinical Applications. 1st ed. Cambridge: Woodhead Publishing; 2008.

111. Crovace MC, Souza MT, Chinaglia CR, Peitl O, Zanotto ED. Biosilicate® — A multipurpose, highly bioactive glass-ceramic. In vitro , in vivo and clinical trials. J Non Cryst Solids. 2016 Jan;432:90–110.

112. Hill RG, Brauer DS. Predicting the bioactivity of glasses using the network connectivity or split network models. J Non Cryst Solids. 2011 Dec;357(24):3884–7.

113. Edén M. The split network analysis for exploring composition-structure correlations in multi-component glasses: I. Rationalizing bioactivity-composition trends of bioglasses. J Non Cryst Solids. Elsevier B.V.; 2011;357(6):1595–602.

114. Hill R. An alternative view of the degradation of bioglass. J Mater Sci Lett. 1996;15:1122–5.

115. O'Donnell MD, Watts SJ, Hill RG, Law R V. The effect of phosphate content on the bioactivity of soda-lime-phosphosilicate glasses. Journal of Materials Science: Materials in Medicine. 2009.

116. Kokubo T, Ito S, Sakka S, Yamamuro T. Formation of a high-strength bioactive glass-ceramic in the system MgO-CaO-SiO2-P2O5. J Mater Sci. 1986;21:536–40.

117. Champion E. Sintering of calcium phosphate bioceramics. Acta Biomater. Acta Materialia Inc.; 2013;9(4):5855–75.

118. Lee JA, Knight CA, Kun X, Yang XB, Wood DJ, Dalgarno KW, et al. In vivo biocompatibility of custom-fabricated apatite-wollastonite-mesenchymal stromal cell constructs. J Biomed Mater Res Part A.

2015 Oct;103(10):3188–200.

119. Kokubo T, Ito S, Shigematsu M, Sakka S, Yamamuro T. Mechanical properties of a new type of apatite-containing glass-ceramic for prosthetic application. J Mater Sci. 1985;20:2001–4.

120. Nakamura T, Yamamuro T, Higashi S, Kokubo T, Itoo S. A new glass-ceramic for bone replacement: Evaluation of its bonding to bone tissue. J Biomed Mater Res. 1985 Jul;19(6):685–98.

121. Kokubo T, Ito S, Shigematsu M, Sanka S, Yamamuro T. Fatigue and life-time of bioactive glass-ceramic A-W containing apatite and wollastonite. J Mater Sci. 1987;22:4067–70.

122. Saidak Z, Marie PJ. Strontium signaling: Molecular mechanisms and therapeutic implications in osteoporosis. Pharmacol Ther. Elsevier Inc.; 2012 Nov;136(2):216–26.

123. Fromigué O, Haÿ E, Barbara A, Petrel C, Traiffort E, Ruat M, et al. Calcium sensing receptor-dependent and receptor-independent activation of osteoblast replication and survival by strontium ranelate. J Cell Mol Med. Blackwell Publishing Ltd; 2009;13(8b):2189–99.

124. Rybchyn MS, Slater M, Conigrave AD, Mason RS. An Akt-dependent Increase in Canonical Wnt Signaling and a Decrease in Sclerostin Protein Levels Are Involved in Strontium Ranelate-induced Osteogenic Effects in Human Osteoblasts. J Biol Chem . 2011 Jul 8;286(27):23771–9.

125. Fromigué O, Haÿ E, Barbara A, Marie PJ. Essential role of nuclear factor of activated T cells (NFAT)-mediated Wnt signaling in osteoblast differentiation induced by strontium ranelate. J Biol Chem. 2010 Aug 13;285(33):25251–8.

126. Caverzasio J. Strontium ranelate promotes osteoblastic cell replication through at least two different mechanisms. Bone. 2008 Jun;42(6):1131–6.

127. Caverzasio J, Thouverey C. Activation of FGF receptors is a new mechanism by which strontium ranelate induces osteoblastic cell growth. Cell Physiol Biochem. 2011 Jan;27(3–4):243–50.

128. Peng S, Zhou G, Luk KDK, Cheung KMC, Li Z, Lam WM, et al. Strontium Promotes Osteogenic Differentiation of Mesenchymal Stem Cells Through the Ras/MAPK Signaling Pathway. Cell Physiol Biochem. 2009 Jan;23(1–3):165–74.

129. Yang F, Yang D, Tu J, Zheng Q, Cai L, Wang L. Strontium enhances osteogenic differentiation of mesenchymal stem cells and in vivo bone formation by activating Wnt/catenin signaling. Stem Cells. 2011 Jun;29(6):981–91.

130. Kim W, Kim M, Jho E. Wnt/β-catenin signalling: from plasma membrane to nucleus. Biochem J. 2013 Feb 15;450(1):9–21.

131. Caverzasio J, Manen D. Essential Role of Wnt3a-Mediated Activation of Mitogen-Activated Protein Kinase p38 for the Stimulation of Alkaline Phosphatase Activity and Matrix Mineralization in C3H10T1/2 Mesenchymal Cells. Endocrinology. 2007 Nov;148(11):5323–30.

132. Bikkavilli RK, Feigin ME, Malbon CC. p38 mitogen-activated protein kinase regulates canonical Wnt- -catenin signaling by inactivation of GSK3. J Cell Sci. 2008 Nov 1;121(21):3598–607.

133. Christodoulou I, Buttery LDKK, Tai G, Hench LL, Polak JM. Characterization of human fetal osteoblasts by microarray analysis following stimulation with 58S bioactive gel-glass ionic dissolution products. J Biomed Mater Res Part B Appl Biomater. 2006 May;77B(2):431–46.

134. Caudrillier A, Hurtel-Lemaire A-S, Wattel A, Cournarie F, Godin C, Petit L, et al. Strontium Ranelate Decreases Receptor Activator of Nuclear Factor- B Ligand-Induced Osteoclastic Differentiation In Vitro: Involvement of the Calcium-Sensing Receptor. Mol Pharmacol. 2010;78(4):569–76.

135. Bonnelye E, Chabadel A, Saltel F, Jurdic P. Dual effect of strontium ranelate: Stimulation of osteoblast differentiation and inhibition of osteoclast formation and resorption in vitro. Bone. 2008;42:129–38.

136. Peng S, Liu XS, Huang S, Li Z, Pan H, Zhen W, et al. The cross-talk between osteoclasts and osteoblasts in response to strontium

treatment: Involvement of osteoprotegerin. Bone. Elsevier Inc.; 2011;49(6):1290–8.

137. Hurtel-Lemaire AS, Mentaverri R, Caudrillier A, Cournarie F, Wattel A, Kamel S, et al. The calcium-sensing receptor is involved in Strontium ranelate-induced osteoclast apoptosis new insights into the associated signaling pathways. J Biol Chem. 2009;284:575–84.

138. Atkins GJ, Welldon KJ, Halbout P, Findlay DM. Strontium ranelate treatment of human primary osteoblasts promotes an osteocyte-like phenotype while eliciting an osteoprotegerin response. Osteoporos Int. 2009 Apr 2;20(4):653–64.

139. Baino F. Bioactive glasses – When glass science and technology meet regenerative. Ceram Int. Elsevier Ltd and Techna Group S.r.l.; 2018;(April):0–1.

140. Hench LL, Jones JR. Bioactive Glasses: Frontiers and Challenges. Front Bioeng Biotechnol. 2015;3(November):1–12.

141. Gerhardt L-C, Boccaccini AR. Bioactive Glass and Glass-Ceramic Scaffolds for Bone Tissue Engineering. Materials (Basel). 2010 Jul 6;3(7):3867–910.

142. Brauer DS. Bioactive Glasses-Structure and Properties. Angew Chemie Int Ed. 2015 Mar 27;54(14):4160–81.

143. Henstock JR, Canham LT, Anderson SI. Silicon: the evolution of its use in biomaterials. Acta Biomater. Acta Materialia Inc.; 2014 Sep;

144. Owens FJ, Poole CP. The Physics of Bulk Solids. The Physics and Chemistry of Nanosolids. 2008. p. 2.

145. Hench LL. Bioceramics. Stress Int J Biol Stress. 1998;28:1705–28.

146. Magallanes-Perdomo M, Luklinska ZBB, De Aza AHH, Carrodeguas RGG, De Aza S, Pena P. Bone-like forming ability of apatite–wollastonite glass ceramic. J Eur Ceram Soc. 2011 Aug;31(9):1549–61.

147. Yamanuro T. Clinical Application of Bioactive Glass-Ceramics. In: Kokubo T, editor. Bioceramics and their clinical applications. Elsevier;

2008. p. 583–605.

148. Squires GL. Introduction to the Theory of Thermal Neutron Scattering. Cambridge University Press; 1978.

149. Lovesey SW. Theory of neutron scattering from condensed matter. Clarendon Press, Oxford; 1984.

150. Martin R a., Twyman HL, Rees GJ, Barney ER, Moss RM, Smith JM, et al. An examination of the calcium and strontium site distribution in bioactive glasses through isomorphic neutron diffraction, X-ray diffraction, EXAFS and multinuclear solid state NMR. J Mater Chem. 2012;22(41):22212–23.

151. Polenova T, Gupta R, Goldbourt A. Magic Angle Spinning NMR Spectroscopy: A Versatile Technique for Structural and Dynamic Analysis of Solid-Phase Systems. Anal Chem. 2015 Jun 2;87(11):5458–69.

152. Lowe IJ. Free Induction Decays of Rotating Solids. Phys Rev Lett. 1959 Apr 1;2(7):285–7.

153. Vij DR. Handbook of applied solid state spectroscopy. Springer Verlag; 2006.

154. Ashbrook SE. Recent advances in solid-state NMR spectroscopy of quadrupolar nuclei. Phys Chem Chem Phys. 2009;11(32):6892.

155. Fujikura K, Karpukhina N, Kasuga T, Brauer DS, Hill RG, Law R V. Influence of strontium substitution on structure and crystallisation of Bioglass® 45S5. J Mater Chem. 2012;22(15):7395.

156. Vogel W. Classic Theories of glass Structure. In: Vogel W, editor. Glass Chemistry. Berlin, Heidelberg: Springer Berlin Heidelberg; 1994. p. 46.

157. Martin R a, Yue S, Hanna J V, Lee PD, Newport RJ, Smith ME, et al. Characterizing the hierarchical structures of bioactive sol-gel silicate glass and hybrid scaffolds for bone regeneration. Philos Trans A Math Phys Eng Sci. 2012 Mar 28;370(1963):1422–43.

158. Hench LL, Wilson J. Introduction. An Introduction to Bioceramics.

World Scientific Publishing; 1993. p. 17.

159. Martin R a, Moss RM, Lakhkar NJ, Knowles JC, Cuello GJ, Smith ME, et al. Structural characterization of titanium-doped Bioglass using isotopic substitution neutron diffraction. Phys Chem Chem Phys. 2012 Dec 5;14(45):15807–15.

160. Martin RA, Twyman HL, Rees GJ, Smith JM, Barney ER, Smith ME, et al. A structural investigation of the alkali metal site distribution within bioactive glass using neutron diffraction and multinuclear solid state NMR. Phys Chem Chem Phys. 2012;14(35):12105.

161. Larkin P. Basic Principles. Infrared and Raman Spectroscopy. 2011. p. 7–25.

162. Aguiar H, Serra J, González P, León B. Structural study of sol–gel silicate glasses by IR and Raman spectroscopies. J Non Cryst Solids. 2009 Apr;355(8):475–80.

163. Malz F, Aguiar H, Solla EL, Serra J, González P, León B, et al. Combined Structural Investigations of Bioactive Silicate Glasses. Key Eng Mater. 2008;361–363:257–60.

164. Tulyaganov D, Abdukayumov K, Ruzimuradov O, Hojamberdiev M, Ionescu E, Riedel R. Effect of alumina incorporation on the surface mineralization and degradation of a bioactive glass (CaO-MgO-SiO2-Na2O-P2O5-CaF2)-glycerol paste. Materials (Basel). 2017;10(11).

165. Goel A, Tulyaganov DU, Agathopoulos S, Ribeiro MJ, Basu RN, Ferreira JMF. Diopside-Ca-Tschermak clinopyroxene based glass-ceramics processed via sintering and crystallization of glass powder compacts. J Eur Ceram Soc. 2007;27(5):2325–31.

166. Tamari S, López-Hernández RI. Optimum design of the comparative gas pycnometer for determining the volume of solid particles. Geotech Test J. 2006;29(1):64–9.

167. Hannon AC. Results on disordered materials from the GEneral Materials diffractometer, GEM, at ISIS. Nucl Instruments Methods Phys Res Sect A Accel Spectrometers, Detect Assoc Equip. 2005 Oct;551(1):88–107.

168. Hannon AC. Xsect [Internet]. 1990 [cited 2018 Apr 3]. Available from: http://alexhannon.co.uk/software.htm

169. Moreton-Smith CM, Johnston SD, Akeroyd FA. Open GENIE - a generic multi-platform program for the analysis of neutron scattering data. J Neutron Res. 1996 Dec 1;4(1):41–7.

170. Hannon AC. GEM Software [Internet]. 2014. Available from: https://www.isis.stfc.ac.uk/Pages/Gem-software.aspx

171. Pickup D, Moss R, Newport R. NXFit : a program for simultaneously fitting X-ray and neutron diffraction pair-distribution functions to provide optimized structural parameters. J Appl Crystallogr. 2014 Sep 1;47(5):1790–6.

172. Kohara S. Glass Formation at the Limit of Insufficient Network Formers. Science (80- ). 2004 Mar 12;303(5664):1649–52.

173. Martin R a, Salmon PS, Fischer HE, Cuello GJ. Structure of dysprosium and holmium phosphate glasses by the method of isomorphic substitution in neutron diffraction. J Phys Condens Matter. 2003 Dec 17;15(49):8235–52.

174. Martin R, Salmon P, Benmore C, Fischer H, Cuello G. Structure of lanthanum and cerium phosphate glasses by the method of isomorphic substitution in neutron diffraction. Phys Rev B - Condens Matter Mater Phys. 2003;68(5).

175. Wasse JC, Salmon PS. Structure of molten lanthanum and cerium tri-halides by the method of isomorphic substitution in neutron diffraction. J Phys Condens Matter. 1999;11(6):1381.

176. Smith JM, Martin R a., Cuello GJ, Newport RJ. Structural characterisation of hypoxia-mimicking bioactive glasses. J Mater Chem B. 2013;1(9):1296.

177. Candeloro P, Grande E, Raimondo R, Di Mascolo D, Gentile F, Coluccio ML, et al. Raman database of amino acids solutions: a critical study of Extended Multiplicative Signal Correction. Analyst. 2013;138(24):7331.

178. Balamurugan A, Balossier G, Kannan S, Michel J, Rebelo AHS, Ferreira JMF. Development and in vitro characterization of sol-gel derived CaO-P2O5-SiO2-ZnO bioglass. Acta Biomater. 2007 Mar;3(2):255–62.

179. Agathopoulos S, Tulyaganov DU, Ventura JMG, Kannan S, Saranti a., Karakassides M a., et al. Structural analysis and devitrification of glasses based on the CaO–MgO–SiO2 system with B2O3, Na2O, CaF2 and P2O5 additives. J Non Cryst Solids. 2006 Apr;352(4):322–8.

180. Mysen B, Ryerson FJ, Virgo V. The structural role of phosphorus in silicate melts. Am Mineral. 1981;66:106–17.

181. O'Donnell MD, Fredholm Y, de Rouffignac A, Hill RG. Structural analysis of a series of strontium-substituted apatites. Acta Biomater. 2008 Sep;4(5):1455–64.

182. McMillan P, Piriou B, Navrotsky A. A Raman spectroscopic study of glasses along the joins silica-calcium aluminate, silica-sodium aluminate, and silica-potassium aluminate. Geochim Cosmochim Acta. 1982 Nov;46(11):2021–37.

183. YADAV AK, Singh P. A Review on Structure of Glasses by Raman Spectroscopy. RSC Adv. 2015;

184. Echlin P. Handbook of Sample Preparation for Scanning Electron Microscopy and X-Ray Microanalysis. Springer US; 2011.

185. Aguiar H, Solla EL, Serra J, González P, León B, Almeida N, et al. Orthophosphate nanostructures in SiO2-P2O5-CaO-Na2O-MgO bioactive glasses. J Non Cryst Solids. 2008;354(34):4075–80.

186. Watts SJ, Hill RG, O'Donnell MD, Law RV. Influence of magnesia on the structure and properties of bioactive glasses. J Non Cryst Solids. 2010 Mar;356(9–10):517–24.

187. Oliveira J., Correia R., Fernandes M., Rocha J. Influence of the CaO/MgO ratio on the structure of phase-separated glasses: a solid state 29Si and 31P MAS NMR study. J Non Cryst Solids. 2000 Mar;265(3):221–9.

188. Yang W-H, Kirkpatrick RJ, Turner G. 31P and 29Si Magic-Angle Sample-Spinning NMR Investigation of the Structural Environment of Phosphorus in Alkaline-Earth Silicate Glasses. J Am Ceram Soc. 1986 Oct;69(10):C-222-C-223.

189. Elgayar I, Aliev AE, Boccaccini AR, Hill RG. Structural analysis of bioactive glasses. J Non Cryst Solids. 2005 Jan;351(2):173–83.

190. Dietrich E, Oudadesse H, Floch M Le, Bureau B, Gloriant T. In vitro chemical reactivity of doped bioactive glasses: An original approach by solid-state NMR spectroscopy. Adv Eng Mater. 2009;11(8):98–105.

191. Dupree R, Holland D, Mortuza MG, Collins JA, Lockyer MWG. Magic angle spinning NMR of alkali phospho-alumino-silicate glasses. J Non Cryst Solids. 1989 Oct;112(1–3):111–9.

192. Lockyer MWG, Holland D, Dupree R. NMR investigation of the structure of some bioactive and related glasses. J Non Cryst Solids. 1995 Aug;188(3):207–19.

193. Newport RJ, Skipper LJ, FitzGerald V, Pickup DM, Smith ME, Jones JR. In vitro changes in the structure of a bioactive calcia-silica sol-gel glass explored using isotopic substitution in neutron diffraction. J Non Cryst Solids. 2007 Jun;353(18–21):1854–9.

194. FitzGerald V, Pickup DM, Greenspan D, Sarkar G, Fitzgerald JJ, Wetherall KM, et al. A Neutron and X-Ray Diffraction Study of Bioglass® with Reverse Monte Carlo Modelling. Adv Funct Mater. 2007 Dec 17;17(18):3746–53.

195. Wilding M, Guthrie M, Kohara S, Bull CL, Akola J, Tucker MG. Corrigendum: The structure of MgO–SiO 2 glasses at elevated pressure. J Phys Condens Matter. 2012 Aug 22;24(33):339501.

196. Walter G, Vogel J, Hoppe U, Hartmann P. The structure of CaO-Na2O-MgO-P2O5 invert glass. J Non Cryst Solids. 2001 Dec;296(3):212–23.

197. Martin RA, Salmon PS, Fischer HE, Cuello GJ. Structure of rare-earth phosphate glasses by neutron diffraction. J Non Cryst Solids. 2004;345–346:208–12.

198. Aguiar H, Solla EL, Serra J, González P, León B, Malz F, et al. Raman and NMR study of bioactive Na2O–MgO–CaO–P2O5–SiO2 glasses. J Non Cryst Solids. 2008 Nov;354(45–46):5004–8.

199. Pryce RS, Hench LL. Tailoring of bioactive glasses for the release of nitric oxide as an osteogenic stimulus. J Mater Chem. 2004;14(14):2303.

200. Saranti A, Koutselas I, Karakassides MA. Bioactive glasses in the system CaO–B2O3–P2O5: Preparation, structural study and in vitro evaluation. J Non Cryst Solids. 2006 May;352(5):390–8.

201. Mysen B, Virgo D, Kushiro I. The structural role of aluminum in silicate melts; a Raman spectroscopic study at 1 atmosphere. Am Mineral. 1981;66:678–701.

202. McMillan P. RAMAN SPECTROSCOPIC STUDY OF GLASSES IN THE SYSTEM CaO-MgO-SiO//2. Am Mineral. 1984;69(6–8):645–59.

203. Pontiroli L. Characterisation of Strontium-Containing Apatite-Wollastonite Porous Scaffolds. University of Leeds; 2018.

204. Santocildes-Romero ME, Crawford A, Hatton P V., Goodchild RL, Reaney IM, Miller CA. The osteogenic response of mesenchymal stromal cells to strontium-substituted bioactive glasses. J Tissue Eng Regen Med. 2015;4(7):n/a-n/a.

205. Dessou NS, Theodorou GS, Kantiranis N, Papadopoulou L, Zorba T, Patsiaoura D, et al. Influence of strontium for calcium substitution on the glass–ceramic network and biomimetic behavior in the ternary system SiO2–CaO–MgO. J Mater Sci. Springer US; 2017;

206. Hill R., Stamboulis A, Law R., Clifford A, Towler M., Crowley C. The influence of strontium substitution in fluorapatite glasses and glass-ceramics. J Non Cryst Solids. 2004 May;336(3):223–9.

207. Fredholm YC, Karpukhina N, Law R V., Hill RG. Strontium containing bioactive glasses: Glass structure and physical properties. J Non Cryst Solids. Elsevier B.V.; 2010;356(44–49):2546–51.

208. Fredholm YC, Karpukhina N, Brauer DS, Jones JR, Law R V, Hill RG.

Influence of strontium for calcium substitution in bioactive glasses on degradation, ion release and apatite formation. J R Soc Interface. 2011 May 7;9(70):rsif20110387.

209. Xiang Y, Du J. Effect of Strontium Substitution on the Structure of 45S5 Bioglasses. Chem Mater. 2011 Jun 14;23(11):2703–17.

210. Du J, Xiang Y. Effect of strontium substitution on the structure, ionic diffusion and dynamic properties of 45S5 Bioactive glasses. J Non Cryst Solids. Elsevier B.V.; 2012;358(8):1059–71.

211. O'Donnell MD, Hill RG. Influence of strontium and the importance of glass chemistry and structure when designing bioactive glasses for bone regeneration. Acta Biomater. Acta Materialia Inc.; 2010 Jul;6(7):2382–5.

212. Tilocca A. Current challenges in atomistic simulations of glasses for biomedical applications. Phys Chem Chem Phys. 2014;16(9):3874.

213. Tilocca A. Structure and dynamics of bioactive phosphosilicate glasses and melts from ab initio molecular dynamics simulations. Phys Rev B - Condens Matter Mater Phys. 2007 Dec;76(22):224202.

214. Karlsson C, Zanghellini E, Swenson J, Roling B, Bowron DT, Börjesson L. Structure of mixed alkali/alkaline-earth silicate glasses from neutron diffraction and vibrational spectroscopy. Phys Rev B - Condens Matter Mater Phys. 2005;72(6):1–12.

215. Skipper LJ, Sowrey FE, Pickup DM, Drake KO, Smith ME, Saravanapavan P, et al. The structure of a bioactive calcia–silica sol–gel glass. J Mater Chem. 2005;15(24):2369.

216. Marsh RE, Herbstein FH. Some additional changes in space groups of published crystal structures. Acta Crystallogr Sect B Struct Sci. 1983 Apr 1;39(2):280–7.

217. Kahlenberg V. Preparation and crystal structure of Na2SrSi2O6—a cyclosilicate with perovskite-type features. J Alloys Compd. 2004;366(1):132–5.

218. Al-Hasni BM, Mountjoy G. A molecular dynamics study of the atomic

structure ofx(MgO)100 - X(SiO2). J Non Cryst Solids. Elsevier B.V.; 2014;400:33–44.

219. Patel U, Moss RM, Hossain KMZ, Kennedy AR, Barney ER, Ahmed I, et al. Structural and physico-chemical analysis of calcium/strontium substituted, near-invert phosphate based glasses for biomedical applications. Acta Biomater. Acta Materialia Inc.; 2017;60:109–27.

220. González P, Serra J, Liste S, Chiussi S, León B, Pérez-Amor M. Raman spectroscopic study of bioactive silica based glasses. J Non Cryst Solids. 2003 Jun;320(1–3):92–9.

221. Chatzistavrou X, Zorba T, Chrissafis K, Kaimakamis G, Kontonasaki E, Koidis P, et al. Influence of particle size on the crystallization process and the bioactive behavior of a bioactive glass system. J Therm Anal Calorim. 2006;85(2):253–9.

222. Zhang W, Shen Y, Pan H, Lin K, Liu X, Darvell BW, et al. Effects of strontium in modified biomaterials. Acta Biomater. 2011 Feb;7(2):800–8.

223. Gorustovich AA, Steimetz T, Cabrini RL, Porto LÃ$^3$pez JM. Osteoconductivity of strontium-doped bioactive glass particles: A histomorphometric study in rats. J Biomed Mater Res Part A. 2010 Jan;92A(1):232–7.

224. Yuasa M, Yamada T, Taniyama T, Masaoka T, Xuetao W, Yoshii T, et al. Dexamethasone Enhances Osteogenic Differentiation of Bone Marrow- and Muscle-Derived Stromal Cells and Augments Ectopic Bone Formation Induced by Bone Morphogenetic Protein-2. PLoS One. 2015;10(2):e0116462.

225. Langenbach F, Handschel J. Effects of dexamethasone, ascorbic acid and β-glycerophosphate on the osteogenic differentiation of stem cells in vitro. Stem Cell Res Ther. 2013;4(5):117.

226. Dominici M, Le Blanc K, Mueller I, Slaper-Cortenbach I, Marini F, Krause D, et al. Minimal criteria for defining multipotent mesenchymal stromal cells. The International Society for Cellular Therapy position statement. Cytotherapy. 2006 Jan;8(4):315–7.

227. Saleh F, Carstairs A, Etheridge SL, Genever P. Real-Time Analysis of Endogenous Wnt Signalling in 3D Mesenchymal Stromal Cells. Stem Cells Int. 2016;2016.

228. Duan P, Toumpaniari R, Partridge S, Birch MA, Genever PG, Bull SJ, et al. How cell culture conditions affect the microstructure and nanomechanical properties of extracellular matrix formed by immortalized human mesenchymal stem cells: An experimental and modelling study. Mater Sci Eng C. Elsevier; 2018;89(September 2017):149–59.

229. Schneider CA, Rasband WS, Eliceiri KW. NIH Image to ImageJ: 25 years of image analysis. Nat Methods. 2012;

230. Peng S, Liu XS, Wang T, Li Z, Zhou G, Luk KDK, et al. In vivo anabolic effect of strontium on trabecular bone was associated with increased osteoblastogenesis of bone marrow stromal cells. J Orthop Res. 2010 Sep;28(9):1208–14.

231. Azevedo MM, Tsigkou O, Nair R, Jones JR, Jell G, Stevens MM. Hypoxia Inducible Factor-Stabilizing Bioactive Glasses for Directing Mesenchymal Stem Cell Behavior. Tissue Eng Part A. 2014 Oct 2;00(00):1–8.

232. Wu X, Meng G, Wang S, Wu F, Huang W, Gu Z. Zn and Sr incorporated 64S bioglasses: Material characterization, in-vitro bioactivity and mesenchymal stem cell responses. Mater Sci Eng C Mater Biol Appl. 2015 Jul 1;52:242–50.

233. Julien M, Khoshniat S, Lacreusette A, Gatius M, Bozec A, Wagner EF, et al. Phosphate-Dependent Regulation of MGP in Osteoblasts: Role of ERK1/2 and Fra-1. J Bone Miner Res. 2009 Nov;24(11):1856–68.

234. Roohani-Esfahani S-I, Wong KY, Lu Z, Juan Chen Y, Li JJ, Gronthos S, et al. Fabrication of a novel triphasic and bioactive ceramic and evaluation of its in vitro and in vivo cytocompatibility and osteogenesis. J Mater Chem B. The Royal Society of Chemistry; 2014;2(13):1866–78.

235. Pan HB, Li ZY, Lam WM, Wong JC, Darvell BW, Luk KDK, et al.

Solubility of strontium-substituted apatite by solid titration. Acta Biomater. Elsevier; 2009 Jun 1;5(5):1678–85.

236. Christoffersen J, Christoffersen MR, Kolthoff N, Bärenholdt O. Effects of strontium ions on growth and dissolution of hydroxyapatite and on bone mineral detection. Bone. Elsevier; 1997 Jan 1;20(1):47–54.

237. Sugiyama S, Moriga T, Goda M, Hayashi H, Moffat JB. Effects of fine structure changes of strontium hydroxyapatites on ion-exchange properties with divalent cations. J Chem Soc Faraday Trans. 1996;92(21):4305.

238. Wu C, Ramaswamy Y, Kwik D, Zreiqat H. The effect of strontium incorporation into CaSiO3 ceramics on their physical and biological properties. Biomaterials. 2007;28(21):3171–81.

239. Obata A, Iwanaga N, Terada A, Jell G, Kasuga T. Osteoblast-like cell responses to silicate ions released from 45S5-type bioactive glass and siloxane-doped vaterite. J Mater Sci. Springer US; 2017;52(15):8942–56.

240. Wan Y, Wang Y, Liu Z, Qu X, Han B, Bei J, et al. Adhesion and proliferation of OCT-1 osteoblast-like cells on micro- and nano-scale topography structured poly(l-lactide). Biomaterials. 2005 Jul;26(21):4453–9.

241. Gough JE, Notingher I, Hench LL. Osteoblast attachment and mineralized nodule formation on rough and smooth 45S5 bioactive glass monoliths. J Biomed Mater Res A. 2004;68(4):640–50.

242. Song SJ, Jeon O, Yang HS, Han DK, Kim B-S. Effects of culture conditions on osteogenic differentiation in human mesenchymal stem cells. J Microbiol Biotechnol. 2007 Jul;17(7):1113–9.

243. Zhang W, Tian Y, He H, Chen R, Ma Y, Guo H, et al. Strontium attenuates rhBMP-2-induced osteogenic differentiation via formation of Sr-rhBMP-2 complex and suppression of Smad-dependent signaling pathway. Acta Biomater. 2016 Mar;33:290–300.

244. De Boer J, Siddappa R, Gaspar C, Van Apeldoorn A, Fodde R, Van Blitterswijk C. Wnt signaling inhibits osteogenic differentiation of

human mesenchymal stem cells. Bone. 2004;34(5):818–26.

245. Boland GM, Perkins G, Hall DJ, Tuan RS. Wnt 3a promotes proliferation and suppresses osteogenic differentiation of adult human mesenchymal stem cells. J Cell Biochem. 2004;93(6):1210–30.

246. Valerio P, Pereira MM, Goes AM, Leite MF. The effect of ionic products from bioactive glass dissolution on osteoblast proliferation and collagen production. Biomaterials. 2004;25(15):2941–8.

247. Yamasaki Y, Yoshida Y, Okazaki M, Shimazu A, Uchida T, Kubo T, et al. Synthesis of functionally graded MgCO3 apatite accelerating osteoblast adhesion. J Biomed Mater Res. 2002 Oct;62(1):99–105.

248. Zhang M, Wu C, Lin K, Fan W, Chen L, Xiao Y, et al. Biological responses of human bone marrow mesenchymal stem cells to Sr-M-Si (M = Zn, Mg) silicate bioceramics. J Biomed Mater Res Part A. 2012;100A(11):2979–90.

249. Shie MY, Ding SJ, Chang HC. The role of silicon in osteoblast-like cell proliferation and apoptosis. Acta Biomater. Acta Materialia Inc.; 2011;7(6):2604–14.

250. Engler AJ, Sen S, Sweeney HL, Discher DE. Matrix Elasticity Directs Stem Cell Lineage Specification. Cell. 2006;126(4):677–89.

251. Strobel L a., Hild N, Mohn D, Stark WJ, Hoppe A, Gbureck U, et al. Novel strontium-doped bioactive glass nanoparticles enhance proliferation and osteogenic differentiation of human bone marrow stromal cells. J Nanoparticle Res. 2013 Jul 20;15(7):1780.

252. Moghanian A, Firoozi S, Tahriri M. Characterization, in vitro bioactivity and biological studies of sol-gel synthesized SrO substituted 58S bioactive glass. Ceram Int. Elsevier; 2017 Dec 1;43(17):14880–90.

253. Bellucci D, Sola A, Cacciotti I, Bartoli C, Gazzarri M, Bianco A, et al. Mg- and/or Sr-doped tricalcium phosphate/bioactive glass composites: Synthesis, microstructure and biological responsiveness. Mater Sci Eng C. 2014 Sep;42:312–24.

254. Raucci MG, Giugliano D, Alvarez-Perez M a., Ambrosio L. Effects on

growth and osteogenic differentiation of mesenchymal stem cells by the strontium-added sol–gel hydroxyapatite gel materials. J Mater Sci Mater Med. 2015;26(2):90.

255. Wu C, Zhou Y, Lin C, Chang J, Xiao Y. Strontium-containing mesoporous bioactive glass scaffolds with improved osteogenic/cementogenic differentiation of periodontal ligament cells for periodontal tissue engineering. Acta Biomater. Acta Materialia Inc.; 2012 Oct;8(10):3805–15.

256. Zhao S, Zhang J, Zhu M, Zhang Y, Liu Z, Tao C, et al. Three-dimensional printed strontium-containing mesoporous bioactive glass scaffolds for repairing rat critical-sized calvarial defects. Acta Biomater. 2015 Jan 15;12:270–80.

257. Weng L, Boda SK, Teusink MJ, Shuler FD, Li X, Xie J. Binary Doping of Strontium and Copper Enhancing Osteogenesis and Angiogenesis of Bioactive Glass Nanofibers while Suppressing Osteoclast Activity. ACS Appl Mater Interfaces. 2017;9(29):24484–96.

258. Naruphontjirakul P, Porter AE, Jones JR. In vitro osteogenesis by intracellular uptake of strontium containing bioactive glass nanoparticles. Acta Biomater. Elsevier; 2017 Nov 10;

259. Bialek P, Kern B, Yang X, Schrock M, Sosic D, Hong N, et al. A Twist Code Determines the Onset of Osteoblast Differentiation. Dev Cell. 2004 Mar;6(3):423–35.

260. Yousfi M, Lasmoles F, Marie PJ. TWIST inactivation reduces CBFA1/RUNX2 expression and DNA binding to the osteocalcin promoter in osteoblasts. Biochem Biophys Res Commun. 2002 Sep;297(3):641–4.

261. Tu Q, Valverde P, Chen J. Osterix enhances proliferation and osteogenic potential of bone marrow stromal cells. Biochem Biophys Res Commun. 2006;341:1257–65.

262. Kim YJ, Kim HN, Park EK, Lee BH, Ryoo HM, Kim SY, et al. The bone-related Zn finger transcription factor Osterix promotes proliferation of mesenchymal cells. Gene. 2006;366:145–51.

263. Zhang X, Zeng D, Li N, Wen J, Jiang X, Liu C, et al. Functionalized mesoporous bioactive glass scaffolds for enhanced bone tissue regeneration. Sci Rep. 2016 Jan 14;6:19361.

264. Rath SN, Nooeaid P, Arkudas A, Beier JP, Strobel LA, Brandl A, et al. Adipose- and bone marrow-derived mesenchymal stem cells display different osteogenic differentiation patterns in 3D bioactive glass-based scaffolds. J Tissue Eng Regen Med. 2016 Oct;10(10):E497–509.

265. Montesi M, Panseri S, Dapporto M, Tampieri A, Sprio S. Sr-substituted bone cements direct mesenchymal stem cells, osteoblasts and osteoclasts fate. PLoS One. 2017;12(2):1–13.

266. Houreh AB, Labbaf S, Ting H-K, Ejeian F, Jones JR, Esfahani M-HN. Influence of calcium and phosphorus release from bioactive glasses on viability and differentiation of dental pulp stem cells. J Mater Sci. Springer US; 2017 Aug 1;52(15):8928–41.

267. Yun H-S, Park J-W, Kim S-H, Kim Y-J, Jang J-H. Effect of the pore structure of bioactive glass balls on biocompatibility in vitro and in vivo. Acta Biomater. 2011 Jun;7(6):2651–60.

268. Zhou H, Kong S, Pan Y, Zhang Z, Deng L. Microwave-assisted fabrication of strontium doped apatite coating on Ti6Al4V. Mater Sci Eng C. 2015 Nov;56:174–80.

269. Park J-W, Kang D-G, Hanawa T. New bone formation induced by surface strontium-modified ceramic bone graft substitute. Oral Dis. 2016 Jan;22(1):53–61.

270. Martin M. Cutadapt removes adapter sequences from high-throughput sequencing reads. EMBnet.journal. 2011 May 2;17(1):10.

271. Kim D, Langmead B, Salzberg SL. HISAT: a fast spliced aligner with low memory requirements. Nat Methods. 2015 Apr 9;12(4):357–60.

272. Trapnell C, Roberts A, Goff L, Pertea G, Kim D, Kelley DR, et al. Differential gene and transcript expression analysis of RNA-seq experiments with TopHat and Cufflinks. Nat Protoc. 2012 Mar 1;7(3):562–78.

273. Subramanian A, Tamayo P, Mootha VK, Mukherjee S, Ebert BL, Gillette MA, et al. Gene set enrichment analysis: A knowledge-based approach for interpreting genome-wide expression profiles. Proc Natl Acad Sci. 2005 Oct 25;102(43):15545–50.

274. Liberzon A, Birger C, Thorvaldsd??ttir H, Ghandi M, Mesirov JP, Tamayo P. The Molecular Signatures Database Hallmark Gene Set Collection. Cell Syst. 2015;1(6):417–25.

275. Toronen P, Ojala PJ, Marttinen P, Hol L. Robust Extraction of functional signals from gene set analysis using a generalized threshold free socring function. BMC Bioinformatics. 2009;10(307).

276. Löffler-Wirth H, Kalcher M, Binder H, Loffler-Wirth H, Kalcher M, Binder H. oposSOM: R-package for high-dimensional portraying of genome-wide expression landscapes on bioconductor: Fig. 1. Bioinformatics. 2015 Oct 1;31(19):3225–7.

277. Livak KJ, Schmittgen TD. Analysis of Relative Gene Expression Data Using Real-Time Quantitative PCR and the 2−ΔΔCT Method. Methods. 2001 Dec;25(4):402–8.

278. Weisz B, Giehl K, Gana-Weisz M, Egozi Y, Ben-Baruch G, Marciano D, et al. A new functional Ras antagonist inhibits human pancreatic tumor growth in nude mice. Oncogene. 1999;

279. Collins MA, Pasca di Magliano M. Kras as a key oncogene and therapeutic target in pancreatic cancer. Front Physiol. 2014;4.

280. Rotblat B, Ehrlich M, Haklai R, Kloog Y. The Ras Inhibitor Farnesylthiosalicylic Acid (Salirasib) Disrupts The Spatiotemporal Localization Of Active Ras: A Potential Treatment For Cancer. Methods Enzymol. 2008;439(07):467–89.

281. Laheru D, Shah P, Rajeshkumar N V., McAllister F, Taylor G, Goldsweig H, et al. Integrated preclinical and clinical development of S-trans, trans-farnesylthiosalicylic acid (FTS, Salirasib) in pancreatic cancer. Invest New Drugs. 2012;30(6):2391–9.

282. Heim MH. The Jak-STAT pathway: Specific signal transduction from the cell membrane to the nucleus. European Journal of Clinical

Investigation. 1996.

283. Rane SG, Reddy EP. Janus kinases: Components of multiple signaling pathways. Oncogene. 2000;

284. Zacharaki D, Ghazanfari R, Li H, Lim HC, Scheding S. Effects of JAK1/2 inhibition on bone marrow stromal cells of myeloproliferative neoplasm (MPN) patients and healthy individuals. Eur J Haematol. 2018 Jul;101(1):57–67.

285. Thomas SM, Brugge JS. CELLULAR FUNCTIONS REGULATED BY SRC FAMILY KINASES. Annu Rev Cell Dev Biol. 1997;

286. Curnock AP, Logan MK, Ward SG. Chemokine signalling: Pivoting around multiple phosphoinositide 3-kinases. Immunology. 2002;105(2):125–36.

287. Chen Z, Gibson TB, Robinson F, Silvestro L, Pearson G, Xu BE, et al. MAP kinases. Chem Rev. 2001;101(8):2449–76.

288. Id Boufker H, Lagneaux L, Najar M, Piccart M, Ghanem G, Body J-J, et al. The Src inhibitor dasatinib accelerates the differentiation of human bone marrow-derived mesenchymal stromal cells into osteoblasts. BMC Cancer. 2010 Dec 17;10(1):298.

289. Benson DA, Karsch-Mizrachi I, Lipman DJ, Ostell J, Wheeler DL. GenBank. Nucleic Acids Res. 2005;33(DATABASE ISS.):34–8.

290. Booth V, Keizer DW, Kamphuis MB, Clark-Lewis I, Sykes BD. The CXCR3 Binding Chemokine IP-10/CXCL10: Structure and Receptor Interactions †. Biochemistry. 2002 Aug;41(33):10418–25.

291. Wang Z, Gerstein M, Snyder M. RNA-Seq: a revolutionary tool for transcriptomics. Nat Rev Genet. 2009 Jan;10(1):57–63.

292. Choudhary S, Wadhwa S, Raisz LG, Alander C, Pilbeam CC. Extracellular calcium is a potent inducer of cyclo-oxygenase-2 in murine osteoblasts through an ERK signaling pathway. J Bone Miner Res. 2003;18:1813–24.

293. Ohgushi H, Dohi Y, Yoshikawa T, Tamai S, Tabata S, Okunaga K, et al. Osteogenic differentiation of cultured marrow stromal stem cells on

the surface of bioactive glass ceramics. J Biomed Mater Res. 1996;32(3):341–8.

294. Grassi F, Piacentini A, Cristino S, Toneguzzi S, Cavallo C, Facchini A, et al. Human osteoclasts express different CXC chemokines depending on cell culture substrate: Molecular and immunocytochemical evidence of high levels of CXCL10 and CXCL12. Histochem Cell Biol. 2003;120(5):391–400.

295. Kieswetter K, Schwartz Z, Hummert TW, Cochran DL, Simpson J, Dean DD, et al. Surface roughness modulates the local production of growth factors and cytokines by osteoblast-like MG-63 cells. J Biomed Mater Res. 1996 Sep;32(1):55–63.

296. Lincks J, Boyan BD, Blanchard CR, Lohmann CH, Liu Y, Cochran DL, et al. Response of MG63 osteoblast-like cells to titanium and titanium alloy is dependent on surface roughness and composition. Biomaterials. 1998 Dec;19(23):2219–32.

297. Martin JY, Schwartz Z, Hummert TW, Schraub DM, Simpson J, Lankford J, et al. Effect of titanium surface roughness on proliferation, differentiation, and protein synthesis of human osteoblast-like cells (MG63). J Biomed Mater Res. 1995;29(3):389–401.

298. Deligianni DD, Katsala ND, Koutsoukos PG, Missirlis YF. Effect of surface roughness of hydroxyapatite on human bone marrow cell adhesion, proliferation, differentiation and detachment strength. Biomaterials. 2000;22(1):87–96.

299. Samavedi S, Whittington AR, Goldstein AS. Calcium phosphate ceramics in bone tissue engineering: A review of properties and their influence on cell behavior. Acta Biomater. Acta Materialia Inc.; 2013;9(9):8037–45.

300. Uccelli A, Moretta L, Pistoia V. Mesenchymal stem cells in health and disease. Nat Rev Immunol. 2008 Sep;8(9):726–36.

301. Park CW, Kim K-S, Bae S, Son HK, Myung P-K, Hong HJ, et al. Cytokine Secretion Profiling of Human Mesenchymal Stem Cells by Antibody Array. Int J Stem Cells. 2009;2(1):59–68.

302. Shin SY, Nam J-S, Lim Y, Lee YH. TNFα-exposed Bone Marrow-derived Mesenchymal Stem Cells Promote Locomotion of MDA-MB-231 Breast Cancer Cells through Transcriptional Activation of CXCR3 Ligand Chemokines. J Biol Chem. 2010;285(40):30731–40.

303. Alves SM, Abreu SC, Lemos JC, Gomes FIF, Alves SM, do Val DR, et al. Anti-inflammatory and anti-nociceptive effects of strontium ranelate on the zymosan-induced temporomandibular joint inflammatory hypernociception in rats depend on TNF-α inhibition. Pharmacol Reports. Institute of Pharmacology, Polish Academy of Sciences; 2017;69(4):764–72.

304. Renaudin G, Laquerrière P, Filinchuk Y, Jallot E, Nedelec JM. Structural characterization of sol–gel derived Sr-substituted calcium phosphates with anti-osteoporotic and anti-inflammatory properties. J Mater Chem. 2008;18(30):3593.

305. Sun JS, Tsuang YH, Chang WHS, Li J, Liu HC, Lin FH. Effect of hydroxyapatite particle size on myoblasts and fibroblasts. Biomaterials. 1997;18(9):683–90.

306. Ninomiya JT, Struve JA, Stelloh CT, Toth JM, Crosby KE. Effects of hydroxyapatite particulate debris on the production of cytokines and proteases in human fibroblasts. J Orthop Res. 2001;19(4):621–8.

307. Anton K, Banerjee D, Glod J. Macrophage-associated mesenchymal stem cells assume an activated, migratory, pro-inflammatory phenotype with increased IL-6 and CXCL10 secretion. PLoS One. 2012;7(4):1–10.

308. Boyer B, Vallés AM, Edme N. Induction and regulation of epithelial–mesenchymal transitions. Biochem Pharmacol. 2000 Oct;60(8):1091–9.

309. Hugo H, Ackland ML, Blick T, Lawrence MG, Clements JA, Williams ED, et al. Epithelial—mesenchymal and mesenchymal—epithelial transitions in carcinoma progression. J Cell Physiol. 2007 Nov;213(2):374–83.

310. Trivanović D, Jauković A, Krstić J, Nikolić S, Okić Djordjević I, Kukolj

T, et al. Inflammatory cytokines prime adipose tissue mesenchymal stem cells to enhance malignancy of MCF-7 breast cancer cells via transforming growth factor-β1. IUBMB Life. 2016 Mar;68(3):190–200.

311. Mele V, Muraro MG, Calabrese D, Pfaff D, Amatruda N, Amicarella F, et al. Mesenchymal stromal cells induce epithelial-to-mesenchymal transition in human colorectal cancer cells through the expression of surface-bound TGF-β. Int J Cancer. 2014;134(11):2583–94.

312. Liao TT, Yang MH. Revisiting epithelial-mesenchymal transition in cancer metastasis: the connection between epithelial plasticity and stemness. Mol Oncol. 2017;11(7):792–804.

313. Sewell-Loftin MK, Chun YW, Khademhosseini A, Merryman WD. EMT-inducing biomaterials for heart valve engineering: taking cues from developmental biology. J Cardiovasc Transl Res. 2011 Oct;4(5):658–71.

314. Meyer N, Penn LZ. Reflecting on 25 years with MYC. Nat Rev Cancer. 2008;8(12):976–90.

315. Armesilla-Diaz A, Elvira G, Silva A. p53 regulates the proliferation, differentiation and spontaneous transformation of mesenchymal stem cells. Exp Cell Res. Elsevier Inc.; 2009 Dec;315(20):3598–610.

316. Miura M, Miura Y, Padilla-Nash HM, Molinolo AA, Fu B, Patel V, et al. Accumulated Chromosomal Instability in Murine Bone Marrow Mesenchymal Stem Cells Leads to Malignant Transformation. Stem Cells. 2006;24(4):1095–103.

317. Rubio D, Garcia S, Paz MF, de la Cueva T, Lopez-Fernandez LA, Lloyd AC, et al. Molecular characterization of spontaneous mesenchymal stem cell transformation. PLoS One. 2008;3(1).

318. Zindy F, Eischen CM, Randle DH, Kamijo T, Cleveland JL, Sherr CJ, et al. Myc signaling via the ARF tumor suppressor regulates p53-dependent apoptosis and immortalization. Genes Dev. 1998;12(15):2424–33.

319. Wagner AJ, Kokontis JM, Hay N. Myc-mediated apoptosis requires wild-type p53 in a manner independent of cell cycle arrest and the

ability of p53 to induce p21(waf1/cip1). Genes Dev. 1994;8(23):2817–30.

320. Piek E, Sleumer LS, van Someren EP, Heuver L, de Haan JR, de Grijs I, et al. Osteo-transcriptomics of human mesenchymal stem cells: Accelerated gene expression and osteoblast differentiation induced by vitamin D reveals c-MYC as an enhancer of BMP2-induced osteogenesis. Bone. Elsevier Inc.; 2010;46(3):613–27.

321. Brzostek-Racine S, Gordon C, Van Scoy S, Reich NC. The DNA damage response induces IFN. J Immunol. 2011 Nov 15;187(10):5336–45.

322. Oshimori N, Fuchs E. The Harmonies Played by TGF-β in Stem Cell Biology. Cell Stem Cell. 2012 Dec;11(6):751–64.

323. Kong Y, Guo Y, Zhang J, Zhao B, Wang J. Strontium Promotes Transforming Growth Factors β1 and β2 Expression in Rat Chondrocytes Cultured In Vitro. Biol Trace Elem Res. Biological Trace Element Research; 2017 Nov 23;1208–7.

324. Boanini E, Torricelli P, Gazzano M, Della Bella E, Fini M, Bigi A. Combined effect of strontium and zoledronate on hydroxyapatite structure and bone cell responses. Biomaterials. 2014 Jul;35(21):5619–26.

325. Bonewald LF, Dallas SL. Role of active and latent transforming growth factor β in bone formation. J Cell Biochem. 1994 Jul;55(3):350–7.

326. CENTRELLA M, HOROWITZ MC, WOZNEY JM, MCCARTHY TL. Transforming Growth Factor-β Gene Family Members and Bone*. Endocr Rev. 1994 Feb;15(1):27–39.

327. Alliston T, Choy L, Ducy P, Karsenty G, Derynck R. TGF-beta-induced repression of CBFA1 by Smad3 decreases cbfa1 and osteocalcin expression and inhibits osteoblast differentiation. EMBO J. 2001 May 1;20(9):2254–72.

328. Chen J, Crawford R, Chen C, Xiao Y. The key regulatory roles of the PI3K/Akt signalling pathway in the functionalities of mesenchymal stem cells and applications in tissue regeneration. Tissue Eng Part B

Rev. 2013;19(6):516–28.

329. Johnson CW, Reid D, Parker JA, Salter S, Knihtila R, Kuzmic P, et al. The small GTPases K-Ras, N-Ras, and H-Ras have distinct biochemical properties determined by allosteric effects. J Biol Chem. 2017 Aug 4;292(31):12981–93.

330. Saidak Z, Haÿ E, Marty C, Barbara A, Marie PJ. Strontium ranelate rebalances bone marrow adipogenesis and osteoblastogenesis in senescent osteopenic mice through NFATc/Maf and Wnt signaling. Aging Cell. 2012;11(3):467–74.

331. Ono K, Yamamuro T, Nakamura T, Kokubo T. Apatite Wollastonite Containing Glass Ceramic Granule Fibrin Mixture As a Bone-Graft Filler - Use With Low Granular Density. J Biomed Mater Res. 1990;24(1):11–20.

332. Sponer P, Urban K, Kucera T. Comparison of Apatite-Wollastonite Glass-Ceramic and β-tricalcium Phosphate used as Bone Graft Substitutes after Curettage of Bone Cysts. In: Sikalidis C, editor. Advances in Ceramics - Electric and Magnetic Ceramics, Bioceramics, Ceramics and Environment. InTech; 2011. p. 473–84.

333. Teramoto H, Kawai A, Sugihara S, Yoshida A, Inoue H. Resorption of Apatite-wollastonite containing glass-ceramic and ??-tricalcium phosphate in vivo. Acta Med Okayama. 2005 Oct;59(5):201–7.

334. Jones KS. Effects of biomaterial-induced inflammation on fibrosis and rejection. Semin Immunol. 2008;20(2):130–6.

335. Lovett M, Lee K, Edwards A, Kaplan DL. Vascularization Strategies for Tissue Engineering. Tissue Eng Part B Rev. 2009;15(3):353–70.

336. Franz S, Rammelt S, Scharnweber D, Simon JC. Immune responses to implants - A review of the implications for the design of immunomodulatory biomaterials. Biomaterials. 2011 Oct;32(28):6692–709.

337. Anderson JM, Rodriguez A, Chang DT. Foreign body reaction to biomaterials. Semin Immunol. 2008 Apr;20(2):86–100.

338. Xia Z, Triffitt JT. A review on macrophage responses to biomaterials. Biomed Mater. 2006;1(1).

339. Glowacki J, Mizuno S. Collagen scaffolds for tissue engineering. Biopolymers. 2008;89(5):338–44.

340. Parenteau-Bareil R, Gauvin R, Berthod F. Collagen-based biomaterials for tissue engineering applications. Materials (Basel). 2010;3(3):1863–87.

341. Chevallay B, Herbage D. Collagen-based biomaterials as 3D scaffold for cell cultures: applications for tissue engineering and gene therapy. Med Biol Eng Comput. 2000;38(2):211–8.

342. Sun B, Ma W, Su F, Wang Y, Liu J, Wang D, et al. The osteogenic differentiation of dog bone marrow mesenchymal stem cells in a thermo-sensitive injectable chitosan/collagen/ β-glycerophosphate hydrogel: in vitro and in vivo. J Mater Sci Mater Med. 2011;22(9):2111–8.

343. Hui TY, Cheung KMC, Cheung WL, Chan D, Chan BP. In vitro chondrogenic differentiation of human mesenchymal stem cells in collagen microspheres: Influence of cell seeding density and collagen concentration. Biomaterials. 2008;29(22):3201–12.

344. Kniazeva E, Kachgal S, Putnam AJ. Effects of Extracellular Matrix Density and Mesenchymal Stem Cells on Neovascularization *In Vivo*. Tissue Eng Part A. 2011;17(7–8):905–14.

345. Sevastianov VI, Dukhina GA, Ponomareva AS, Kirsanova LA, Perova N V, Skaletskiy NN. AND ENVIRONMENT PROTECTION A Biomedical Cell Product for the Regeneration of Articular Cartilage : Biocompatible and Histomorphological Properties ( an Experimental Model of Subcutaneous Implantation ). 2015;6(2):162–70.

346. Liu G, Wang X, Sun X, Deng C, Atala A, Zhang Y. The effect of urine-derived stem cells expressing VEGF loaded in collagen hydrogels on myogenesis and innervation following after subcutaneous implantation in nude mice. Biomaterials. Elsevier Ltd; 2013;34(34):8617–29.

347. Wong VW, Rustad KC, Galvez MG, Neofytou E, Glotzbach JP,

Januszyk M, et al. Engineered Pullulan-Collagen Composite Dermal Hydrogels Improve Early Cutaneous Wound Healing. Tissue Eng Part A. 2011;17(5 and 6).

348. Xynos ID, Hukkanen MVJ, Batten JJ, Buttery LD, Hench LL, Polak JM. Bioglass ®45S5 stimulates osteoblast turnover and enhances bone formation in vitro: Implications and applications for bone tissue engineering. Calcif Tissue Int. 2000;67(4):321–9.

349. Marie PJ. Strontium ranelate: New insights into its dual mode of action. Bone. 2007 May;40(5):S5–8.

350. Salman SM, Salama SN, Abo-Mosallam H a. The role of strontium and potassium on crystallization and bioactivity of Na2O–CaO–P2O5–SiO2 glasses. Ceram Int. 2012 Jan;38(1):55–63.

351. Brennan TC, Rybchyn MS, Green W, Atwa S, Conigrave AD, Mason RS. Osteoblasts play key roles in the mechanisms of action of strontium ranelate. Br J Pharmacol. 2009;157(7):1291–300.

352. Ter Brugge PJ, Wolke JGC, Jansen JA. Effect of calcium phosphate coating crystallinity and implant surface roughness on differentiation of rat bone marrow cells. J Biomed Mater Res. 2002;60(1):70–8.

353. Bosetti M, Hench L, Cannas M. Interaction of bioactive glasses with peritoneal macrophages and monocytes in vitro. J Biomed Mater Res. 2002;60(1):79–85.